Symmetry and its Signatures in Quantum Many-Body Dynamics

by

Olumakinde Ogunnaike

B.A. Physics and Mathematics, Harvard, 2017
MSt. Philosophy of Physics, Oxford, 2018

Submitted to the Department of Physics
in partial fulfillment of the requirements for the degree of

DOCTOR OF PHILOSOPHY IN PHYSICS

at the

MASSACHUSETTS INSTITUTE OF TECHNOLOGY

September 2024

Authored by:	Olumakinde Ogunnaike Department of Physics August 16th, 2024
Certified by:	Jong Yeon Lee Professor of Physics, UIUC, Thesis Supervisor
Certified by:	Leonid Levitov Professor of Physics, MIT, Thesis Supervisor
Accepted by:	Lindley Winslow Associate Department Head of Physics

Symmetry and its Signatures in Quantum Many-Body Dynamics

by

Olumakinde Ogunnaike

Submitted to the Department of Physics
on August 16th, 2024 in partial fulfillment of the requirements for the degree of

DOCTOR OF PHILOSOPHY IN PHYSICS

ABSTRACT

Symmetry has long been a defining feature in our understanding of statistical or many-body systems. By making appeals to universal properties associated with global symmetries and topology, one may describe universal properties of "typical" states and dynamics in equilibrium, even when keeping track of the precise dynamics of a particular many-body system is impossible. This challenge of tracking allowable states and dynamical transitions is only exacerbated for non-equilibrium systems, where one cannot rely on the same notions of typicality. Further, when driven out of equilibrium by external interactions, quantum orders constructed from highly sensitive correlations between states are liable to vanish. Despite these conceptual and practical difficulties, the rise of quantum technologies and accompanying theoretical developments has motivated a surge of interest in dynamical quantum phenomena. The recent developments in the field of quantum many-body dynamics provide satisfactory accounts of many interesting phenomena, including failures of the Eigenstate Thermalization Hypothesis, various dynamical and mixed-state phases of matter, and measurement-induced dynamics and phase transitions. Many of these results are explained for specific systems or within different conceptual frameworks, however these results rarely generalize. In this thesis, I attempt to unify many aspects of quantum many-body dynamics under the same conceptual framework through an investigation of the universal signatures of symmetry in quantum dynamical systems. This is accomplished via a mapping between the averaged dynamics and the low-energy spectrum of an effective Hamiltonian in a "doubled Hilbert space," comprised of two copies of the original space. This provides a general and versatile framework to qualitatively understand both familiar and novel universal properties of dynamical phenomena like charge diffusion, sub(super)-diffusion of multipole moments in systems with short and long-range interactions, charge and multipole, and even measurement-induced phase transitions. By expanding into a doubled Hilbert space, one may capture the subtleties of non-equilibrium physics, and particularly dynamical phases, within the framework of equilibrium physics and phases. In this work, we examine how to understand various symmetry-constrained dynamical phases and phase transitions using through a dual description of symmetry-constrained equilibrium phases and symmetry-breaking transitions in an enlarged Hilbert space.

Thesis supervisor: Jong Yeon Lee
Title: Professor of Physics, UIUC

Thesis supervisor: Leonid Levitov
Title: Professor of Physics, MIT

Acknowledgments

This work is, in many ways, a culmination of the work of many hands. I could not have reached this point without the support of a legion of advisors, teachers, friends, and family.

Before anyone, I would like to thank my late father, Dr. Babatunde Ogunnaike, who was the first to encourage my love of physics, to teach me infinite series, calculus, linear algebra, and so much more. He taught me to love God, my culture, and my family, and I could not have asked for a better example as a father. In addition to my father, I would like to thank my mother, Anna Ogunnaike; my eldest brother, sister-in-law, and their children, Oludamini, Naseemah, Jibril, and Sakinah; and my older brother, sister-in-law, and their children, Ayodeji, Stacy, Anu, and Tunde.

I would like to thank each of the members of my dissertation committee. My research advisor, Professor Leonid Levitov, who supported me though my shifting intellectual interests, many teaching and advising commitments, and encouraged me through my father's illness and after his passing. My co-advisor, and the one who has taught me nearly everything that I know about quantum many-body dynamics, Professor Jong Yeon Lee, who has functionally been acting as an advisor since he wsa a post-doc, and we began collaborating. Professor Max Metlitski, who was one of the first professors to welcome me to MIT, for whom I was briefly a TF, and who has been an inspiration, support, and source of boundless intuition on interesting problems. And last, but not least, Professor Lindley Winslow, who championed my efforts during this dissertation process and helped me structure my time and efforts while still leaving time for family.

Sincere thanks to my best friend and college roommate, Henry Lin, who has been carrying me through Physics problem sets and research since Physics 16 our freshman year, and who helped review this work at every stage.

I would also like to extend my deepest gratitude to Professor Soonwon Choi, who has been supporting and advising me since before he officially began his post as a Professor at MIT. He introduced me to Quantum dynamics, helped me find my first project, and has advised me as though I were his own student.

Finally, I would like to acknowledge the incredible support I have received from, and many wonderful conversations had with collaborators in the completion of this and many other works, Professor Ehud Altman, Johannes Feldmeier, Hasaan Shapourian, Michael DeMarco, Ali Fahimniya, Margarita Davydova, Zhiyu Dong, Zhihuan Dong, Seth Musser, Yimu Bao, Ethan Lake, Robert Jones, Shreya Vardhan, Arkya Chaterjee, Jamison Sloan, and Archisman Panigraih.

Contents

List of Figures

Chapter 1

Introduction to Quantum Many-Body Dynamics

Aristotle originally defined physics as dealing with the principles of natural or moving things, specifically, the principles and causes of their change and motion[1]. Although modern physics has a different definition of the natural world, it is still rooted in the concepts of matter and change. Many-body physics specializes in the study of the collective motion of many moving "things." For example, the waves on a lake of water are formed from a nearly-countless number of H_2O molecules, each with its own detailed dynamics. Yet, the collective motion that forms a wave is quite simple and can be seen in other mediums other than water. Likewise, water and most familiar substances can all exist in the three familiar states of matter: solid, liquid, and gas. One could never predict such phenomena from the dynamics of an individual water molecule, and yet, the addition of an overwhelming number of molecules ($\sim 10^{23}$) renders produces simple, yet novel behaviors. Many-body physics addresses this curious phenomenon by extracting universal collective behavior from complicated particular dynamics of many individual particles. This relies on two key aspects of matter: first, the collective behavior of a larger, composite object is often much simpler than the sum of its parts. Second, collective behavior is often not easily predicted from the behavior of individual components.

Many-body physics finds natural application in condensed matter systems. These huge collections of atoms or molecules in solid or liquid form provide fertile fields for asking questions about collective behavior. Further, because the atoms within these systems are fundamentally quantum mechanical, even these emergent, universal features can often be traced back to quantum mechanical origins. For example, one could study how the electrical conductivity of a material depends on temperature. For some materials, electrons will not be able to flow freely until they absorb a certain "quantum" of energy necessary. More exotic behaviors like superconductivity can only exist when certain quantum correlations are able to persist over sufficiently long distances and/or timescales.

Quantum many-body systems are inherently even more difficult to describe because uncertainty arises from both the outrageously large number of degrees of freedom involved and the inherent uncertainty of quantum observables and states. Rather than arising from definite trajectories of many particles, observable thermodynamic structures will depend on evolving quantum correlations between states. To keep track of all the different quantum

correlations that can entangle different particles, the Hilbert spaces used to define systems grow exponentially in the number of particles involved. For any kind of investigation into many-body phenomena to be feasible, one must, therefore, find some mechanism of restricting their description to a small sector of the full Hilbert space. This is often done by focusing on systems at equilibrium, at low temperatures, and/or with low degrees of quantum entanglement. For all of these reasons, understanding the phenomena associated with non-equilibrium dynamics, where entanglement can often spread extensively throughout the system, has proven a challenging affair. Still, recent advances in simulation platforms, computational tools, and theoretical connections to formal notions of quantum information have made such investigations more feasible than ever.

Experimentally, it is now possible to exercise fine control over local quantum degrees of freedom. This, in turn, means that previously inaccessible quantum non-equilibrium phenomena are now being explored in systems of ultracold-atoms [2–4], Rydberg arrays [5, 6], trapped ions [7–9], etc. These each provide insights into the out-of-equilibrium dynamics of closed and open quantum systems.

Advances in quantum technology are not the only tools at our disposal. An invaluable tool in the study of equilibrium matter is the investigation of universal properties associated with global symmetries and topology. As in the equilibrium setting, while it may still be an insurmountable task to track the exact dynamics of a particular many-body system, much can be said about "typical" dynamics and "typical" systems through the study of universal properties in dynamical phenomena associated with global symmetries and topology. In this dissertation, I will address many of the universal signatures of symmetry in quantum many-body dynamics and explore a novel way to relate said signatures to familiar paradigms of symmetry in equilibrium systems.

In particular, one of the most striking features of quantum systems is their ability to thermalize even in closed systems. Typical constructions of thermodynamics hold that, as a system comes to equilibrium, it loses memory of its initial state through the loss of information to an environment. Yet, for a closed, quantum system, the constraint of unitarity and the absence of classical chaos makes this straightforward interpretation impossible. Instead, in a quantum system, equilibration comes about via the dispersal of initially local quantum correlations into intricate, non-local structures that are effectively invisible to typical experiments with access to local quantities[3, 10]. For this reason, no discussion about quantum dynamics is complete without some consideration of the phenomenon of thermalization. This work will focus particularly on late-time dynamics of thermalizing systems, which will be shown to play a similar role to the low-energy modes in equilibrium condensed matter systems.

These questions of dynamics and thermalization are particularly pertinent for current quantum technologies, where imperfect isolation and control render the efficient realization of equilibrium quantum states nearly impossible.

1.1 Organization of Dissertation

In **chapter 1**, we will review notions of equilibriation and thermalization in classical and quantum physics, with particular emphasis on the Eigenstate Thermalization Hypothesis

(ETH), and particularly highlighting the manner in which symmetries modify these definitions. In closing, we will briefly review the relevant models and metrics used to understand dynamical phenomena in quantum many-body systems. In **chapter 2**, we will introduce symmetry into these dynamical models, review some established results on its effects and the limitations of these models, and then describe a novel way to understand and even generalize previous results. In **chapter 3**, we will extend this framework to include a wider class of symmetries, dynamical constraints, and interactions. Along the way, we will take time to explain how these constraints may pose serious issues to the ETH and thermalization in general. In **chapter 4**, we will extend this framework further to examine metrics that quantify correlations involving multiple powers of the density matrix and discuss the effects of repeated measurement on thermalization and dynamics.

1.2 Classical and Quantum Thermalization and Equilibriation

One of the great triumphs of physics is the derivation of thermodynamic properties and relations from an underlying understanding of statistical physics. This understanding does not come without a few key assumptions and caveats, however.

In a classical system, one needs to invoke some notion of chaotic dynamics and admit a degree of uncertainty in initial conditions or coarse grain phase space. A few, non-linear equations per particle can cause future states to be exponentially sensitive to initial conditions. Quantum theory is a bit more subtle, however. If a quantum system is open to the environment, then delicate internal quantum correlations will generically be lost due to interaction with an environment, and one can recover a similar dynamical framework as in the classical case. However, when a quantum system is closed, it will evolve according to linear dynamics acting on states without complete observable structure due to the non-commutativity of different observables. Instead of exact observables, one can examine correlations defined within a Hilbert space that grows exponentially with the number of particles. Linear dynamics on exponentially large Hilbert spaces can cause correlations to be extremely sensitive to initial conditions. As we shall see, there are many parallels to be drawn between the two notions of thermalization, however quantum thermalization will depend heavily on a type of correlation that is uniquely quantum: entanglement.

Due to their linear dynamics, quantum systems do not host states undergoing chaotic evolution. Rather, correlations between different local states can become increasingly non-local, resulting in mixed-state, typically approximately-thermal density matrices. This provides a nice intuition for the process of thermalization, particularly when the system open to a noisy environment, allowing information and coherences to "leak out." But in a closed environment, leaking of quantum entanglement can only occur through a novel process where one sector of a quantum system may act as a noisy environment to another. To make sense of this, one must partition the system into two distinct sets. Such partitions may be spatial (one geometric region to another), energetic (high energy to low-energy modes), or exist between distinct species (integrating out fermions); but whichever degrees of freedom are "traced out," those that remain are subject to generically noisy, stochastic evolution. This

stochasticity, arising from ignorance of certain degrees of freedom, allows for ensemble averages to replace more complicated temporal averages when certain ergodicity constraints are met.

As a classical analogue, consider a tracer, the original explanation of Brownian motion: a tracer particle bouncing off of a sea of larger species will appear to undergo random motion. Though the dynamics of all particles within the system is fully deterministic, when one ignores the dynamics of the large particles, the tracer dynamics are well-modeled by a Langevin equation[11]. This will be a particularly helpful analogy, as we will make heavy use of Brownian evolution in this work, however, rather than tracking particle positions, we will analyze the evolution of different correlations.

For the time being, let us specialize to the case of closed systems, where quantum dynamics are purely unitary. Assumptions allowing for the derivation of thermodynamics can roughly be classified into two categories: those allowing for equilibriation and those for thermalization.

- **Equilibriation** defines the approach to a steady state. The assumption of equilibriation amounts to the assertion that a system will relax into a steady state after a particular timescale.

- **Thermalization** is the approach to a thermal state. The assumption of thermalization amounts to the assertion that the steady state of a system is a distribution defined by a small number of conserved quantities. Further, every microstate of this system that has the same values for conserved quantities must be equally probable.

Together, these assumptions allow one to compute observable quantities as functions of a known distribution that is insensitive to most details of the system's initial configuration. In particular, the property of microstates within thermal configurations being equally probable when they share the same conserved quantities leads to a notion of the microcannonical ensemble. If the only conserved quantity is energy, this ensemble is classically defined by taking a uniform distribution, ρ_{mic}, over a small energy shell, Ω_E, defined as follows

$$\Omega_E = \{(q,p) \in \Omega_E : E - \Delta E \leq H(q,p) \leq E + \Delta E\}. \tag{1.1}$$

In quantum theory, this is accomplished by constructing a density matrix $\hat{\rho}_{\text{mic}} = \sum_E \frac{P_{E,\Delta E}}{\dim[\mathcal{H}_{E,\Delta E}]}$, where the Hilbert space considered in the denominator consists of all eigenstates within an energy window:

$$\mathcal{H}_{E,\Delta E} = \{|E_\alpha\rangle \in \mathcal{H}_{E,\Delta E} : \hat{H}|E_\alpha\rangle = E_\alpha|E_\alpha\rangle, E - \Delta E \leq E_\alpha \leq E + \Delta E\}, \tag{1.2}$$

and the numerator is a sum of projectors to said states

$$P_{E,\Delta E} = \sum_{E_\alpha \in \mathcal{H}_{E,\Delta E}} |E_\alpha\rangle\langle E_\alpha|. \tag{1.3}$$

Although these definitions are extraordinarily similar, the different dynamical frameworks in classical and quantum theory allow for diverging conceptions of equilibriation and thermalization within the two domains.

To be a bit more precise, we can note that thermodynamics and even thermalization happen with respect to a set of observable physical quantities, $O \in \mathcal{A}$, where $\mathcal{A}$ is a set of bounded, (typically local) observables. Specifically, for a particular class of observables, $O \in \mathcal{A}$, the notions of equilibriation and thermalization can be understood as follows:

- **Equilibriation**: $\overline{O}(t) \underset{t\to\infty}{\approx} \langle \hat{O} \rangle_{\text{stat}} = \mathbb{E}_{\rho_{\text{stat}}}[O]$
- **Thermalization**: $\langle \hat{O} \rangle_{\text{stat}} \approx \langle \hat{O} \rangle_{\text{mic}}$.

In other words, equilibrium is achieved when any observable quantity in the appropriate class has an approximately constant expectation at late times that can be calculated using some stationary distribution ρ_{stat}. Meanwhile, thermalization is achieved if the expectation of these observable quantities with the stationary distribution, ρ_{stat}, is well-approximated by the expectation using a thermal, microcanonical distribution, ρ_{mic}, described by a few conserved quantities. We will be more precise about these time-dependent expectations when we specialize to classical or quantum systems, however the relevant averages can be understood as either expectations over different times along the same "trajectory," or as expectations over possible states at a fixed time.

However, there are many ways for a system to avoid thermalizing. These will be important to bear in mind as we track various different dynamics in later chapters. First, if there are interactions with an external system, the stationary state need not be thermal. Energy can be constantly pumped into the system to produce highly non-thermal steady states. Alternatively, kinetic constraints can prevent certain non-thermal states from relaxing into the simple, thermal configurations.[1]

Still, in a sense, thermalization is a "typical" behavior. Justifying the assumptions required for thermalization from a physical standpoint is not a trivial matter. For one thing, the notion of equilibrium seems particularly strange given the fact that, in both quantum and classical systems, the underlying laws are time reversal invariant. Yet, the notion of equilibriation is clearly breaks time-reversal symmetry. Meanwhile, there is no *a priori* reason for each microstate within a certain energy window, ΔE, to be equally likely over time. To ensure thermal equilibrium, we will need to understand "typicality," and invoke concepts like ergodicity, chaos, and the like. Before expanding on the unique properties of the quantum setting, We review some salient features of the more familiar, classical picture.

1.2.1 Classical Thermalization

Evolving uncertainties seem to lie at the heart of thermalization. Thus, to get a handle on the spirit of classical thermalization, it will be useful to briefly review Boltzmann's H-theorem[12]. It states that

$$\frac{dH(t)}{dt} \geq 0 \quad \text{for} \quad H(t) = -\int d\vec{r} \int d\vec{v} f(\vec{r}, \vec{v}, t) \ln\left(f(\vec{r}, \vec{v}, t)\right), \tag{1.4}$$

[1] One may also come across notions of "prethermalization," where quasi-stationary states are reached before full thermalization, which may only occur on time-scales that are physically or experimentally inaccessible.

where $f(\vec{r}, \vec{v}, t)$ is a single-particle distribution function. This theorem was Boltzmann's attempt to prove the second law of thermodynamics, with the H-function playing the role of entropy. expressed in this manner, the issue of thermodynamic irreversibility is readily apparent. The laws describing the evolution of the position and momenta within $f(\vec{r}, \vec{v}, t)$ are time reversal invariant. So, one should expect that reversing the dynamics would not change anything. Yet, this means that the reverse dynamics should also lead to an increasing H, counter to the predictions of the 2nd law! Of course, this would be true if we were to track every position and velocity with exact precision, such that $f(\vec{r}, \vec{v}, t)$ became a sum of delta functions. However, once we admit some ignorance of the exact initial conditions by broadening $f(\vec{r}, \vec{v}, t)$, this is no longer the case, and the entropy of the system can plausibly grow over time *with high probability*. As such, the second law is not a dynamical "law" in the strict sense, but rather a *probabilistic claim*.

For a more intuitive picture, we might inisist that positions and velocities can only be measured to within some degrees of precision, Δr and Δv. Then, we can coarse grain phase space by some measure, $(\vec{r}', \vec{v}') = \int d\vec{r} \int d\vec{v} \mu(\vec{r}, \vec{v})(\vec{r}, \vec{v})$, where $\mu(\vec{r}, \vec{v})$ only has support in a limited to some local region of an initial point: $\vec{r} \in B_{\Delta r}(\vec{r})$ and $\vec{v} \in B_{\Delta v}(\vec{v})$ within the precision limits set by Δr and Δv. This coarse grained space gives us a notion of macrostates, given by averages of a large number of exact or microscopic configurations within the observable windows of Δr and Δv.

Thermalization, then, is related to the evolution of possible observable states. uncertainty in the exact degrees of freedom underlying these states can be set by limits on precision, which will allow the dynamics of the averages defining macrostate observables to be described in stochastic terms. Unless there is some special, rare constraint on the microscopic dynamics, these macrostates should spend most of their time in "typical" macroscopic configurations, namely those which host the greatest number of potential microstates. This should be true regardless of the direction of the system dynamics, leading to the concept of thermodynamic equilibrium as the macroscopically defined state of the system with maximum inhabited by the greatest number of microstates.

Classical Thermal Equilibrium

To make this definition of thermal equilibrium more precise, following [13], we define a classical system with N particles contained within a d-dimensional space $\Lambda \subset \mathbb{R}^d$ of volume V. The microstates of position and momentum are given by $\vec{q}^N = (\vec{q}_1, \dots \vec{q}_N)$ and $\vec{p}^N = (\vec{p}_1, \dots \vec{p}_N)$, so that a point in the phase space is $\Gamma = (\vec{q}^N, \vec{p}^N) \in \Lambda^N \times \mathbb{R}^{dN}$. Time evolution of the system can be represented as trajectories in phase space as a function of t, Γ_t. Finally, we define a Hamiltonian for the system, $H(\Gamma)$, insisting that the energy of a single trajectory remain constant $H(\Gamma_t) = E$. This allows us to partition phase space by trajectories that fall within the shells defined in Eq. 1.1:

$$\Omega_{E,N,\Lambda} = \{\Gamma \in \Lambda^N \times \mathbb{R}^{dN} : H(\Gamma) \in (E - \Delta E, E + \Delta E)\}. \tag{1.5}$$

Further, we can define a set of K macrovariables with definite configurations as functions of phase space,

$$\mathcal{M} = \{M_1(\Gamma), \dots, M_K(\Gamma)\}. \tag{1.6}$$

These will be macroscopic quantities averaged over many phase space points that specify a macrostate of the system. Familiar examples include energy, volume, or particle number. Similar to above, we can assume some finite interval of precision, ΔM_i. For this interval to be useful, the precision should be smaller than a typical amplitude of M_i, but large enough to host many different microstates. With this coarse graining of the macrovariable, we can define values ν_i with up to precision ΔM_i, and the full system can be characterized using the K different macrovariables with some set $\nu = (\nu_1, \ldots, \nu_K)$. Now, we can describe our system using these coarse grained subspaces for macrostate, ν, defined as

$$\Omega_\nu = \{\Lambda = (\vec{q}^N, \vec{p}^N) \in: \Lambda^N \times \mathbb{R}^{dN} : M_i(\Gamma) \in (\nu_1, \ldots, \nu_K), \quad \forall i \in (1, K)\}. \tag{1.7}$$

We say that Γ belongs to a macrostate ν if $\Gamma \in \Omega_\nu$. Since these macrostates are non-overlapping, $\Omega_\nu \bigcap \Omega_{\nu'} = \emptyset$, we can partition the energy shell with them such that

$$\Omega_{E,N,\Lambda} = \bigcup_{\{\nu\}} \Omega_\nu. \tag{1.8}$$

It is generally true that one of these macrostates, ν_{eq} will dominate the energy shell up to a remainder that is exponentially small in system size,

$$\frac{|\Omega_{\nu_{eq}}|}{|\Omega_{E,N,\Lambda}|} \approx 1 - e^{\mathcal{O}(V)}, \tag{1.9}$$

where $|\cdot|$ indicates the phase space volume. This macrostate corresponds to thermodynamic equilibrium, and Eq. 1.9 defines the notion of "typicality" of thermodynamic equilibrium. The overwhelming majority of phase space is occupied by an equilibrium configuration given by ν_{eq}.

This provides an explanation for the success of equilibrium statistical physics. One can calculate the expected value of a macrovariable in equilibrium, M_i^{eq} with confidence that it is approximately the same as that calculated with the microcannonical ensemble:

$$M_i^{eq} \equiv \frac{1}{|\Omega_{\nu_{eq}}|} \int_{\Omega_{\nu_{eq}}} d\Gamma M_i(\Gamma) \approx \frac{1}{|\Omega_{E,N,\Lambda}|} \int_{\Omega_{E,N,\Lambda}} d\Gamma M_i \equiv \langle M_i \rangle_{\text{mic}}. \tag{1.10}$$

This yields the expected notion of thermal equilibrium, effectively answering the question of thermalization. However, we still need to answer the question of equilibriation, or the approach to this steady state.

As mentioned before, thermal equilibrium is dependent on the set of observables being considered. Thus far, the only salient feature of these observables has been the existence of limits on precision. However, the scale of precision becomes far more important when considering the approach to equilibrium. If we restrict ourselves to macroscopic variables, then we will have a notion of *macroscopic thermal equilibrium* (MATE), that can be explained in classical mechanics with the assumption of the ergotic hypothesis. Beyond this, it will be possible to define a more stringent notion of *microscopic thermal equilibrium* (MITE), however, this will require additional assumptions about mixing[14].

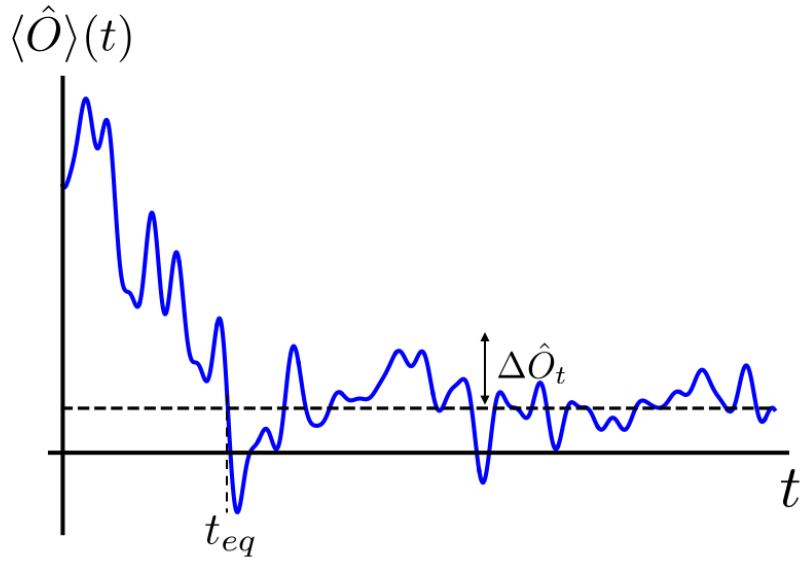

Figure 1.1: **Operator equilibriation**– A schematic representation of the equilibriation of an observable $\hat{O}$. After a timescale t_{eq}, the expectation fluctuates around its mean value with variance $\Delta \hat{O}$. Not shown is the rare recurrence that happens at late times for a very short period

Classical Thermalization

To understand equilibriation, we need to understand what observables "typically" look like over time. First, let us define some physical quantity over trajectories, $O(\Gamma)$. Now, we can define two different averages of this quantity, one over long times starting from Γ_0, and the other over trajectories drawn from the microcanonical ensemble:

$$\overline{O_{\Gamma_0}} = \lim_{T \to \infty} \int_0^T dt O(\Gamma_t) \tag{1.11}$$
$$\langle O \rangle_{\text{mic}} = \frac{1}{|\Omega_{E,N,\Lambda}|} \int_{\Omega_{E,N,\Lambda}} d\Gamma A(\Gamma)$$
$$.$$

The *ergodic hypothesis* states that, for an arbitrary Lebesgue integrable function $A(\Gamma)$, these two averages are equal: $\overline{A_{\Gamma_0}} = \langle A \rangle_{\text{mic}}$ for almost every initial state Γ_0[2]. Just as we might expect in thermal equilibrium, this equality only holds if the dynamics of $O(\Gamma_t)$ take it near to the equilibrium value, where it must stay for an overwhelming majority of the time. See Fig. 1.1

To complete this picture, we need the notion of typicality from Eq. 1.9. If our observable to simply be a projector to the equilibrium subspace: $O(\Gamma) = P_{\nu_{eq}}(\Gamma)$, the ergodic hypothesis

[2]Here, "almost" means that the set of points violating this equality has vanishing Lebesgue measure

implies

$$\overline{P_{\nu_{eq}}} = \langle P_{\nu_{eq}} \rangle = \frac{|\Omega_{\nu_{eq}}|}{|\Omega_{E,N,\Lambda}|} \approx 1. \tag{1.12}$$

As such, we know that $P(\Gamma_t) \approx 1$ for almost all t, and establishing MATE.

One can attempt to replicate this derivation with microscopic physical quantities by choose local, microspic observables $O \in \mathcal{A}_{\text{local}}$. However, if these local observables do not have sufficiently large macrostates, they can fluctuate arbitrarily far away from their equilibrium value. According to the ergodic hypothesis, the variance should be given by

$$\sigma_{\overline{O}}^2 = \overline{O^2} - \overline{O}^2 = \langle O^2 \rangle_{\text{mic}} - \langle O \rangle_{\text{mic}}^2. \tag{1.13}$$

While this final term tends to vanish with system size for macroscopic observables, generically, it does not for microscopic, local ones. This would imply that the presence of large fluctuations in the system do not vanish over time. Thus, $O(\Gamma_t)$ should never settle around its expected equilibrium value. Instead, we can ask whether these fluctuations follow a certain trend over time. We check this by looking at the time average over some finite interval, τ

$$O_\tau(\Gamma_0) \equiv \frac{1}{\tau} \int_0^\tau dt O(\Gamma_t). \tag{1.14}$$

We can redefine the variance for this time-average in terms of a concept that will be important later, the *autocorrelation function*, $C_{OO}(t_1 - t_2)$:

$$\sigma_{O_\tau} \equiv \overline{O_\tau^2} - \overline{O_\tau}^2 = \langle O_\tau^2 \rangle_{\text{mic}} - \langle O_\tau \rangle_{\text{mic}}^2 \tag{1.15}$$

$$= \frac{1}{\tau^2} \int_0^\tau \int_0^\tau dt_1 dt_2 C_{OO}(t_1 - t_2). \tag{1.16}$$

We can redefine the autocorrelation function using the ergodic hypothesis

$$C_{OO}(t) = \frac{1}{|\Omega_{E,N,\Lambda}|} \int_{\Omega_{E,N,\Lambda}} d\Gamma_0 (O(\Gamma_t) O(\Gamma_0) - \langle O_\tau^2 \rangle_{\text{mic}}). \tag{1.17}$$

If the system satisfies a quality beyond ergodicity called *mixing*[15], then $\lim_{t\to\infty} C_{OO}(t) = 0$, and there exists some finite time τ_0 for which $|C_{OO}(t)| \ll \langle O_\tau^2 \rangle_{\text{mic}}$ for all $t > \tau_0$ and thus, temporal fluctuations are small for all $\tau \gg \tau_0$[16]. We call τ_0 the correlation time. For most realistic physical systems, τ_0 is independent of system size[3] and the timescale of realistic observations or interaction is large, $\tau \gg \tau_0$, so that the time averaged observable should always reach its equilibrium value. As this shows, fluctuations in the microscopic values of observables mean that a classical notion of MITE depends on correlations, not just the equilibrium values themselves.[4]

[3]The decay rate of the correlation function is evaluated from the Ruelle-Pollicot resonance[17, 18], a quantity derived solely from the dynamics and is independent of the choice of $p_0(\Gamma)$ and O.

[4]It should be noted that one can define a dual notion of MITE starting from a distribution over possible initial states, $p_{\text{in}}(\Gamma_0)$, with averaged observables given by $\langle O(\Gamma_t) \rangle_{\text{in}} \equiv \int d\Gamma_0 p_{in}(\Gamma_0) O(\Gamma_0)$. Similar to the previous discussion, for sufficiently local observables, one requires a similar mixing constraint on correlations to show that $\lim_{t\to\infty} \langle O(\Gamma_t) \rangle_{in} = \langle O \rangle_{\text{mic}}$[13].

1.2.2 Quantum Thermalization

Quantum thermalization poses a number of different challenges to classical thermalization. Rather than representing states as points in a phase space, we now must represent them as rays in a Hilbert space $|\psi_i\rangle \in \mathcal{H}$. Further, because of the existence of conjugate observables like position and momentum that no longer commute in quantum theory, we can no longer define trajectories with both variables simultaneously well-defined. If we restrict attention to observables over large sections of the system, we can find sets of observables that *nearly* commute, allowing us to define a notion of MATE similar to the classical case. On the microscopic scale, large fluctuations in the expectation of observables, $\langle \hat{O}(t) \rangle$, necessitate the study of correlations between observables, much like the classical case. However, unlike in the classical setting, where the scale of these fluctuations could be tuned by arbitrarily adjusting the precision of measurements, in the quantum setting, nature has set a limit on the scale of quantum fluctuations for conjugate variables,

$$\sigma_X^2 \sigma_P^2 \geq \frac{\hbar^2}{4}, \tag{1.18}$$

where $\sigma^2_{X(P)}$ is nothing more than the variance of the position (momentum) for a particular state. This is nothing more than the Heisenberg uncertainty principle. Classically, we only needed to think of fluctuations describing the uncertainty in the value of definite observable states over time; however, quantum systems have the additional uncertainty from *quantum fluctuations*, which can be understood as the inherent uncertainty in the value of observables for a definite quantum state at a given time. Observable uncertainty is baked into the quantum state, and quantum thermalization is inexorably tied to this unique form of uncertainty. In like fashion, classical dynamics produced increasing uncertainty through chaotic dynamics, originating from the second-order dynamical laws. In contrast, quantum theory is driven by a linear Schrödinger equation:

$$H|\Psi(\vec{r}^N, t)\rangle = -\frac{d}{dt}|\Psi(\vec{r}^N, t)\rangle = \left(-\frac{\nabla^2}{2m} + V(\vec{r}^N) \right) |\Psi(\vec{r}^N, t)\rangle. \tag{1.19}$$

Although there is no proper notion of chaos, the states, $|\Psi(\vec{r}^N, t)\rangle$, will explore the Hilbert space, $\mathcal{H}$ in a manner that justifies similar notions of ergodicity and mixing to the classical case. In quantum thermodynamics, the structure of states themselves plays an integral role in the growing uncertainty within a system.

As an example, let us briefly examine the status of the second law of thermodynamics in quantum theory. First, we will need an appropriate notion of entropy. This notion must be able to account for probability distributions over different quantum states, capturing any uncertainty that may come from the quantum states themselves, and should be independent of the basis chosen.[5] All of this implies that this quantum entropy should be a function of the density matrix of a system, $\hat{\rho} = \sum_i p_i |\psi_i\rangle\langle\psi_i| \in \mathcal{H} \otimes \mathcal{H}$, where p_i are classical probabilities ($\sum_i p_i = 1$) for each state $|\psi_i\rangle$. The density matrix allows us to encode statistical mixtures of quantum states in a basis-independent fashion. When there exists a basis for which the

[5] This last condition arises because a particular choice of basis for a state, $|\psi\rangle = \sum_i c_i |\phi_i\rangle$, corresponds to a choice of observables that share the same basis, $\hat{O} = \sum_i o_{ii} |\phi_i\rangle\langle\phi_i|$.

density matrix can be represented by one single quantum state $\hat{\rho} = |\psi_j\rangle\langle\psi_j|$, we say that the density matrix is a *pure state*. When no such basis exists and the probability distribution over pure states is always non-trivial, we say the density matrix is a *mixed state*. These states can be distinguished by the trace of $\hat{\rho}^2$, called the *purity*. For a pure state, $\mathrm{Tr}[\hat{\rho}^2] = 1$, while, for a mixed state, $\mathrm{Tr}[\hat{\rho}^2] = \sum_i p_i^2 < 1$. Given the density matrix in any basis looks like a probability distribution over different pure states $\hat{\rho} = \sum_i p_i |\psi_i\rangle\langle\psi_i|$, a natural definition for entropy would be to calculate the Shannon or information theoretic entropy for these probabilities,

$$S(\hat{\rho}) = -\mathrm{Tr}[\hat{\rho}\log(\hat{\rho})]. \tag{1.20}$$

We term this the *entanglement entropy* or the *von Neumann entropy*. However, this choice of entropy seems to have an issue: it does not change with time. This can be seen if we note that the quantity inside the trace can be formally expanded into a power series in the density matrix, $\hat{\rho}$, but the trace of any polynomial in $\hat{\rho}$ does not change under unitary operations:

$$\mathrm{Tr}[\hat{\rho}^n(t)] = \mathrm{Tr}[\big(U(t)\hat{\rho}(0)U^\dagger(t)\big)^n] = \mathrm{Tr}[\hat{\rho}^n(0)]. \tag{1.21}$$

This is an immediate consequence of unitarity in quantum theory, where $U(t)U^\dagger(t) = 1$. So, how do we understand entropy in a manner that respects the 2nd law? Similar to the classical case, to observe growth of entropy, we need to partition different subsystems A and B. This partitioning is accomplished at the level of the density matrix by tracing out any degrees of freedom outside the subsystem of interest. We define these *reduced density matrices* for subsystems A and B as $\hat{\rho}_A = \mathrm{Tr}_B[\hat{\rho}]$ and $\hat{\rho}_B = \mathrm{Tr}_A[\hat{\rho}]$, where $\mathcal{H} = \mathcal{H}_A \otimes \mathcal{H}_B$. An important consequence of this formulation is that entropy is sub-additive and bounded by the entropy of its subsystems[19]:

$$S(\hat{\rho}) \leq S(\hat{\rho}_A) + S(\hat{\rho}_B) \tag{1.22}$$

For a clear example, consider a generic pure state, $|\psi\rangle$. Since the density matrix can be written in a form where only one entry on the diagonal will be 1, and all others entries zero, there will be no entanglement entropy, $S(\hat{\rho}) = 0$. However, generically, if we trace out some section of the space, the reduced density matrices, $\hat{\rho}_{A(B)}$ will be mixed, and $S(\hat{\rho}_{A(B)}) > 0$. This encodes the fact that quantum entanglement may exist between subsystems A and B. With this, we have a notion of entropy within subsystems that accounts for the correlations captured by entanglement and can grow over time.

Quantum Thermal Equilibrium

Now that we have a sense for the unique formalism of quantum thermal equilibrium, let us be a bit more precise. Following [13], we begin by considering a d-dimensional lattice with V total sites. We denote the set of positions of each site as $\Lambda = \{\vec{r}_1, \ldots, \vec{r}_V\}$ for $\vec{r}_i \in \mathbb{R}^d$. We will be interested in the dynamics of some state $|\psi(\vec{r}_1, \ldots, \vec{r}_V)\rangle \in \mathcal{H}$. We now restrict this state to within a certain energy shell as in Eq. 1.2:

$$\mathcal{H}_{E,\Lambda} = \{|E_\alpha\rangle \in \mathcal{H}_{E,\Delta E} : \hat{H}|E_\alpha\rangle = E_\alpha|E_\alpha\rangle, E - \Delta E \leq E_\alpha \leq E + \Delta E\}. \tag{1.23}$$

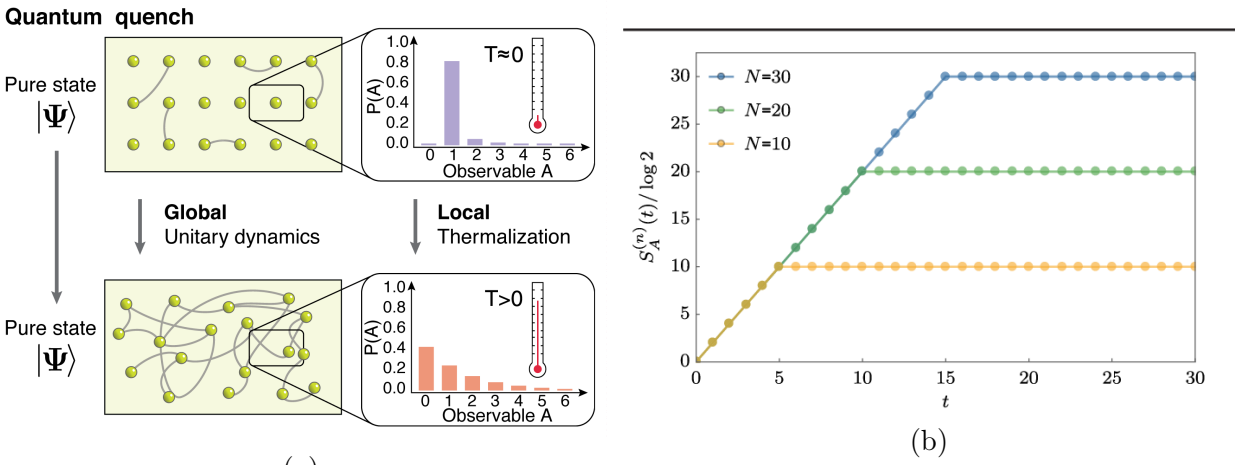

Figure 1.2: **Quantum Thermalization from Entanglement** – A look at quantum thermalization **a)** quantum thermalization occurs on a local scale, driven by entanglement between local sectors with the rest of the system. Figure originally from [10]. **b)** A diagram of entanglement spreading in a quantum chain for various lengths. Figure reproduced from [20].

We require that ΔE is macroscopically small, but microscopically large[6], and define the dimension of this Hilbert space as $D_{E,\Lambda} \equiv \dim \mathcal{H}_{E,\Lambda}$

Next, it will be important to have well-defined notions of this state and different operators restricted to different local sectors within this lattice system. We begin by decomposing our Hilbert space into a tensor product of local spaces, $\mathcal{H}_i$, associated with each site i, such that $\mathcal{H} = \bigotimes_{i=1}^{V} \mathcal{H}_i$. Next, we define a set of bounded linear operators on $\mathcal{H}_i$, denoted by $\mathcal{B}_i$ such that the set of all bounded operators is $\mathcal{B} = \bigotimes_{i=1}^{V} \mathcal{B}_i$. And finally, we can define the Hilbert space and set of bounded operators for some subset of our system $X \subset \{1, \ldots, V\}$ as $\mathcal{H}_X = \bigotimes_{i \in X} \mathcal{H}_i$ and $\mathcal{B}_X = \bigotimes_{i \in X} \mathcal{B}_i$ respectively.

We can define the support for an operator $\hat{O} \in \mathcal{B}$ as the minimal set $X \subset \{1, \ldots, V\}$ where one can apply the decomposition $\hat{O} = \hat{O}_X \otimes \mathbb{I}_{X^c}$. Here, $\hat{O}_X \in \mathcal{B}_X$ and the identity $\mathbb{I}_{X^c} \in \mathcal{H}_{X^c}$ lives in the space defined by the complement of X. There should be D_X^2 linearly independent operators with support in X, which we denote by the set $\mathcal{S}_X$. We can additionally define a notion of a *few-body operator*, or a *k-local* operator, as one that only has support on k sites. We denote the set of all such operators as $\mathcal{S}_{\text{few}}^{(k)} \equiv \bigcup_{X \in \{1,\ldots,V\}, |X|=k} \mathcal{S}_X$

We can now introduce a notion of locality. First, we take some length scale, l, and consider the set of all sites that are within a distance l, from an initial point, i, and the set of operators with support on this set,

$$\begin{aligned} X_i^{(l)} &\equiv \{j \in \{1, \ldots, V\} : |\vec{r}_i - \vec{r}_j| \leq l\} \\ \mathcal{S}_i^{(l)} &\equiv \mathcal{S}_{X_i^{(l)}}. \end{aligned} \tag{1.24}$$

This defines a notion of a local operator of length scale, l, if $\hat{O} \in \mathcal{S}_i^{(l)}$ for some i $i \in \{1, \ldots, V\}$.

[6]Formally, this requirement is that $\Delta E = o(V)$ and $\beta \Delta E \gg 1$, where $\beta = \frac{1}{k_B T}$, where k_B is the Boltzmann constant, and β is defined as the expected energy in a canonical ensemble, $\langle \hat{H} \rangle_{can} = \beta$

We denote the set of all local operators of length scale l by $\mathcal{S}^{(l)}_{loc} = \bigcup_{i=1}^{V} \mathcal{S}^{(l)}$.[7] An immediate consequence of this is that for any length l, local operators are k-local operators with k = l.

As in the classical case, we now have two different notions of thermal equilibrium. MATE and MITE. The definitions are as follows:

- **MATE**: $\langle\psi|\hat{P}_{\text{eq}}|\psi\rangle \approx 1$ for a projection to the equilibrium macrospace $\hat{P}_{\text{eq}}$, defined as the largest subspace after partitioning the Hilbert space $\mathcal{H}_{E,\Lambda}$ according to increments, $\Delta\tilde{M}_i$, of approximately commuting macroscopic observables, $\tilde{M}_i$.

- **MITE**: $\hat{\rho}_{\psi}^{X_i^{(l)}} \approx \hat{\rho}_{\text{mic}}^{X_i^{(l)}}$, when considering any (l-) local subset $X_i^{(l)}$ of the full system.

While the quantum version of macroscopic thermal equilibrium parallels the classical case by projecting onto a particular subspace, the microscopic version has a uniquely quantum flavor arising from the properties of reduced density matrices. Because of this, we shall focus on MITE in the quantum case.

Microscopic Thermal Equilibrium (MITE) – When considering MITE, we will rely on the structure of reduced density matrices within different partitions of the system. Specifically, we will focus on operators $\hat{O} \in \mathcal{S}_X$, that have support limited to a small region, X, of the full system. If we take the expectation of this operator with some pure state $|\psi\rangle \in \mathcal{H}$, we see

$$\langle\psi|O|\psi\rangle = \text{Tr}[\hat{O}\hat{\rho}] = \text{Tr}_X[\hat{O}_X\hat{\rho}_{\psi}^X], \tag{1.25}$$

where we have used the fact that $\hat{O} = \hat{O}_X \otimes \mathbb{I}_{X^c}$, and $\hat{\rho}_{\psi}^X = \text{Tr}_{X^c}|\psi\rangle\langle\psi|$. This reduced density matrix will be a mixed state if and only if quantum entanglement exists between X and X^c. There is no classical analogue for this, and so it will form the basis of an intrinsically quantum notion of typicality. Specifically, within an energy shell, a typical state, $|\psi\rangle \in \mathcal{H}_{E,\Lambda}$, will have a reduced density matrix over X that will be nearly identical to the microcannonical ensemble.

$$\hat{\rho}_{\psi}^X \approx \hat{\rho}_{\text{mic}}^X \equiv \text{Tr}_{X^c}[\hat{\rho}_{\text{mic}}], \tag{1.26}$$

for some measure 1 set over states $|\psi\rangle \in \mathcal{H}_{E,\Lambda}$[21–23]. This is known as *canonical typicality*, and gives rise to a wholly different notion of MITE. Namely, for operators that are local to within a length scale, l, a system is in thermal equilibrium when its state, ψ, is such that, for every $i \in \{1, \ldots, V\}$,

$$\hat{\rho}_{\psi}^{X_i^{(l)}} \approx \hat{\rho}_{\text{mic}}^{X_i^{(l)}} \tag{1.27}$$

. This implies that we may calculate operator expectations for operators $\hat{O} \in \mathcal{S}^{(l)}_{loc}$ using the microcanonical ensemble

$$\langle\psi|O|\psi\rangle = \text{Tr}[\hat{O}\hat{\rho}_{\psi}] = \text{Tr}_{X_i^{(l)}}[\hat{O}_{X_i^{(l)}}\hat{\rho}_{\psi}^{X_i^{(l)}}] \approx \text{Tr}_{X_i^{(l)}}[\hat{O}_{X_i^{(l)}}\hat{\rho}_{\text{mic}}^{X_i^{(l)}}] = \langle\hat{O}\rangle_{\text{mic}}. \tag{1.28}$$

In fact, this holds true for few-body operators even if the system is not spatially local, but only k-local.

[7] This discussion does not address the ambiguity in locality for fermions, which will be addressed elsewhere.

Quantum Thermalization

Eq. 1.26 defines a rough notion of typicality, but does not address the approach to equilibrium. For a time-dependent state, $|\psi(t)\rangle$, equilibration occurs if, for most $t > 0$,

$$\hat{\rho}_{\psi(t)}^{X_i^{(l)}} \approx \hat{\rho}_{\text{mic}}^{X_i^{(l)}}. \tag{1.29}$$

This can be formalized for expectations of arbitrary local operators, $\hat{O} \in \mathcal{S}_{loc}^{(l)}$, using the *operator norm*: $||\hat{O}|| \equiv \sup_{|\psi\rangle \in \mathcal{H}} \sqrt{\langle |\hat{O}^\dagger \hat{O}| \rangle}$:

$$\overline{\sup_{\hat{O} \in \mathcal{S}_{loc}^{(l)}: ||\hat{O}||=1} |\langle \psi(t)|\hat{O}|\psi(t)\rangle - \langle \hat{O}\rangle_{\text{mic}}|} \ll 1, \tag{1.30}$$

This enforces a fairly strict condition that the expectation of *all* local operators are approximately equal to their equilibrium value at almost all times.[8]

To understand the dynamics necessary to satisfy this condition, we should first consider the most generic time evolution of a quantum system. Given a Hamiltonian, $\hat{H}$, the dynamics in a closed system can be described in the energy basis as follows:

$$\hat{\rho}(t) \equiv e^{-it\hat{H}} \hat{\rho}_0 e^{it\hat{H}} = \sum_{\alpha,\beta} e^{it(E_\alpha - E_\beta)} \langle E_\beta|\hat{\rho}_0|E_\alpha\rangle \big(|E_\beta\rangle\langle E_\beta|\big). \tag{1.31}$$

This can be used to describe the generic evolution for an expectation of $\hat{O} \in \mathcal{S}_{loc}^{(l)}$,

$$\begin{aligned} \langle \hat{O}\rangle_\rho(t) \equiv \langle \psi(t)|\hat{O}|\psi(t)\rangle &= \sum_{\alpha,\beta} C_\beta^* C_\alpha e^{it(E_\alpha - E_\beta)} O_{\beta\alpha} \\ &= \sum_\alpha |C_\alpha|^2 O_{\alpha\alpha} + \sum_{\alpha \neq \beta} C_\beta^* C_\alpha e^{it(E_\alpha - E_\beta)} O_{\beta\alpha}, \end{aligned} \tag{1.32}$$

where we have defined $C_\alpha = \langle \psi(0)|E_\alpha\rangle$. For this system to thermalize, this expression must relax to $\langle \hat{O}\rangle_{\text{mic}}$, which is diagonal in this basis, and only admit small fluctuations around this value. Naively, this looks promising, as the diagonal component is a stationary, weighted average, and the off-diagonal terms should vanish from dephasing after some timescale on the order of the inverse spectral gap, assuming no degeneracies.

Unfortunately, these considerations are not sufficient, as there is no *a priori* reason why the diagonal sum $\sum_\alpha |C_\alpha|^2 O_{\alpha\alpha}$ should match the microcanonical expectation, $\langle \hat{O}\rangle_{\text{mic}}$. Further, for a many-body system, the smallest gap in energy values will generically be exponentially small in system size, meaning one would need to wait for unrealistically long timescales to witness thermalization. Since thermalization occurs in realistic situations under much faster timescales, something else must be at play.

[8] One can formulate weaker notions of microscopic thermalization, where only *most* of the local operators are approximately equal to their equilibrium value at almost all times, however, this is still a fairly stringent condition.

1.3 Eigenstate Thermalization Hypothesis (ETH)

Perhaps the most instructive attempt to identify sufficient criteria for thermalization is the conjecture known as the Eigenstate Thermalization Hypothesis (ETH). In this section, we will review this powerful conjecture. Not only will this conjecture help us understand the conditions necessary for quantum thermalization, it will also suggest clear ways in which thermalization can be affected by symmetry. It will even suggest ways in which symmetry and other dynamical constraints can prevent thermalization from taking place.

Although the ETH is a relatively recent conjecture[13], the search for sufficient conditions for quantum thermalization dates back to Von Neumann, only a few years after Schrödinger and Heisenberg proposed their dual formulations of quantum mechanics[24]. He proved a result called the *Quantum Ergodic Theorem*. This result states that, for an ensemble of Hamiltonians with the same set of eigenvalues within an energy shell of dimension D_E, the following condition is satisfied for most such Hamiltonians:

$$\max_n \left(\langle E_n | \hat{P}_\nu | E_n \rangle - \frac{D_\nu}{D_{E,\Lambda}} \right)^2 + \max_{n \neq m} |\langle E_n | \hat{P}_\nu | E_m \rangle|^2 \ll \frac{1}{N_\nu^2} \frac{D_\nu}{D_{E,\Lambda}}, \tag{1.33}$$

where N_ν is the number of macrostates, ν with dimension D_ν. The above defines a condition called *normality* [24], and is satisfied for almost any initial state so long as $\log D \ll D_\nu \ll D$ for all macrostates ν. This implies that any initial state in the energy shell thermalizes.

Although an impressive result, the Quantum Ergotic Theorem should always come with a note of caution. The derivation of this theorem involves the use of an ensemble of Hamiltonians that are generated from random unitary operators acting on the full Hilbert space. For many-body systems, typical interactions for these Hamiltonians are highly non-local and involve interactions with an extensive number of degrees of freedom. As such, most of these Hamiltonians are highly unphysical. This will be a recurring concern when modeling dynamical phenomena. Averaging over possible evolutions or interactions will simplify calculations, however, if one is not careful to include the appropriate dynamical constraints, like locality, the results will generically include highly unphysical contributions. This will be an important point when considering the role of random matrices in the next section and the role of Haar-random unitary circuits at the end of this chapter.

1.3.1 Random Matrices and the ETH

The ETH attempts to exploit the fact that energy eigenstates are stationary. Because of this, one should expect that any energy eigenstate located in an energy shell, $|E_n\rangle \in \mathcal{H}_{E,\Lambda}$, is already be in thermal equilibrium.[9] As with thermalization itself, we can break the ETH into two classes, MATE-ETH and MITE-ETH[13, 25]:

- **MATE-ETH**: $\langle E_n | \hat{P}_{eq} | E_n \rangle \approx 1$ for all $|E_n\rangle \in \mathcal{H}_{E,\Lambda}$.
- **MITE-ETH**: $\langle E_n | \hat{O} | E_n \rangle \approx \langle \hat{O} \rangle_{\text{mic}}$ for $\hat{O} \in \mathcal{S}_{loc}^{(l)}$ and $|E_n\rangle \in \mathcal{H}_{E,\Lambda}$.

[9] A weaker version, dubbed the *Weak ETH*, claims that a vanishing number of *rare eigenstates* are not in thermal equilibrium.

Macroscopic thermalization follows quickly from the definition of MATE-ETH. By assumption, $\langle E_n|\hat{P}_{eq}|E_n\rangle \approx 1$. However, this implies the same should be true for the temporal average for a given state, $\overline{\langle\psi(t)|\hat{P}_{eq}|\psi(t)\rangle} \approx 1$, whenever $|\psi(t)\rangle \in \mathcal{H}_{E,\Lambda}$. This follows from the fact that off-diagonal terms like $\langle E_n|\hat{P}_{eq}|E_m\rangle$ will dephase as $e^{it(E_m-E_n)}$. Since the expectation of any projector lies in the unit interval ($\langle\hat{P}_\nu\rangle \in [0,1]$), it must be true that $\langle\psi(t)|\hat{P}_{eq}|\psi(t)\rangle \approx 1$ at most times.

Establishing thermalization from MITE-ETH will be more involved, requiring the use of random matrices, however, it will highlight features that reveal more about the underlying quantum dynamics.

Random Matrix Theory (RMT)

Upon closer inspection, understanding quantum thermalization from the version of MITE-ETH written above seems like a intractable problem. While this description places a constraint on the diagonal elements of $\hat{O}$ as needed, it says nothing of the off-diagonal components.

Thankfully, a little physical insight can be employed to deduce a more defined version of MITE-ETH. These arguments originated from Wigner, who, while studying the spectra of atomic nuclei, realized how hopeless it was attempting to trace the exact eigenstates for such many-body systems. Instead, he noted that, if one looks at a sufficiently small energy window such that there is an approximately constant density of states, the Hamiltonian for the system will look like a random matrix in a *non fine-tuned* basis[26]. Thus, to understand a generic physical system subject to a small number of symmetries, one should study the ensemble behavior of random matrices subject to the same constraints.

It is worth pausing for a moment to consider the implications of the use of random matrices in this derivation. We will once again be employing an average over random Hamiltonians. This does not appear particularly physical, however, by limiting the support of the operators considered, we can avoid any issues of non-locality. In fact, this attention to local operators can provide another physical motivation for the use of such random matrices. Consider the basis of a particular many-body Hamiltonian. If we use this basis to describe the eigenstates of a similar Hamiltonian with a slight change (i.e. one where the couplings have been incrementally altered), we will have a notion of how sensitive the eigenstates are to small perturbations. Generically, non-integrable many-body Hamiltonians are highly sensitive, even to small perturbations[13]. If we only consider the local degrees of freedom, it will be impossible to extrapolate the eigenstates arising from the global system, but the generic behavior can still be understood with the appropriate distribution over random matrices.

These random matrix distributions have well-behaved statistics over their potential spectra that display important properties like level repulsion and Gaussian decay for large energy spacings[27].[10] In the absence of additional symmetries, and in the thermodynamic limit, RMT predicts that eigenstates are effectively uncorrelated random unit vectors drawn from the uniform measure.

[10]Specifically, one may define a distribution over potential Hamiltonians as $P(\hat{H}) \propto \exp\left\{\left(-\frac{\beta}{2a^2}\mathrm{Tr}[\hat{H}^2]\right)\right\}$ [27]. Here, a, is a normalization coefficient, and $\beta = 1(2)$ is a special value corresponding to the Gaussian orthogonal (unitary) ensemble, which preserves (breaks) time-reversal symmetry.

This property will allow us to define "typical" matrix elements using RMT. Consider an operator $\hat{O}$ in its eigenbasis: $\hat{O} = \sum_i O_i |i\rangle\langle i|$, where $\hat{O}|i\rangle = O_i|i\rangle$. Now, if we switch to the energy eigenbasis for a random Hamiltonian, $|E_m\rangle \in \mathcal{H}_{E,\Lambda}$, then we can express the matrix elements of this operator as

$$O_{mn} \equiv \sum_i O_i \langle E_m|i\rangle\langle i|E_n\rangle = \sum_i O_i (\psi_i^m)^* \psi_i^n. \tag{1.34}$$

For convenience, we have defined a wavefunction in the operator's eigenbasis, $\psi_i^n = \langle i|E_n\rangle$. Now, because the possible energy eigenstates are approximately uniformly distributed for any basis, the average over energy eigenstates is simple,

$$\mathbb{E}_{E_n}[(\psi_i^m)^* \psi_j^n] \approx \frac{1}{D_{E,\Lambda}} \delta_{mn}\delta_{ij}. \tag{1.35}$$

This has immediate and drastic consequences for the expected diagonal and off-diagonal elements of $\hat{O}$:

$$\begin{aligned} \mathbb{E}_{E_n}[O_{mm}] &\approx \frac{1}{D_{E,\Lambda}} \sum_i O_i \equiv \langle \hat{O}\rangle_{\text{mic}} \\ \mathbb{E}_{E_n}[O_{mn}] &\approx 0 \quad \text{for} \quad m \neq n. \end{aligned} \tag{1.36}$$

This establishes that a "typical" state will have the appropriate expectations for microscopic thermalization. However, we can also constrain the fluctuations around these values to see that they should vanish with the subsystem size:

$$\begin{aligned} \mathbb{E}_{E_n}[O_{mm}^2] - \mathbb{E}_{E_n}[O_{mm}]^2 &= \sum_{i,j} O_i O_j \left(\mathbb{E}_{E_n}[(\psi_i^m)^* \psi_i^m (\psi_j^m)^* \psi_i^m] - \mathbb{E}_{E_n}[(\psi_i^m)^* \psi_i^m] \mathbb{E}_{E_n}[(\psi_j^m)^* \psi_i^m] \right) \\ &= \sum_i O_i^2 \left(\mathbb{E}_{E_n}[|\psi_i^m|^2] - \mathbb{E}_{E_n}[|\psi_i^m|^2]^2 \right) = \frac{2}{D_{E,\Lambda}^2} \sum_i O_i^2 \\ &\approx \frac{2\langle \hat{O}^2\rangle_{\text{mic}}}{D_{E,\Lambda}} \\ \mathbb{E}_{E_n}[O_{mn}^2] - \mathbb{E}_{E_n}[O_{mn}]^2 &= \sum_i O_i^2 \mathbb{E}_{E_n}[|\psi_i^m|^2 |\psi_i^n|^2] = \frac{1}{D_{E,\Lambda}^2} \sum_i O_i^2 \\ &= \frac{\langle \hat{O}^2\rangle_{\text{mic}}}{D_{E,\Lambda}}. \end{aligned} \tag{1.37}$$

In deriving this, we have used the fact that the random unit vector, ψ_i^m has components that are Gaussian distributed. This implies that $\mathbb{E}_{E_n}[|\psi_i^m|^4] = 3\mathbb{E}_{E_n}[|\psi_i^m|^2]$. These fluctuations will vanish with $D_{E,\Lambda}^{-1/2}$. Since the size of an energy shell scales exponentially with the number of sites within the subsystem, L_X, these fluctuations will be suppressed by a term $D_{E,\Lambda} \sim e^{-L_X}$. Now it is clear that states within the energy shell will almost certainly thermalize, and the matrix elements for an operator at any time will approximately resemble the ensemble

$$O_{mn} \approx \langle \hat{O}\rangle_{\text{mic}} \delta_{mn} + \sqrt{\frac{\langle \hat{O}^2\rangle_{\text{mic}}}{D_{E,\Lambda}}} R_{mn}, \tag{1.38}$$

where R_{mn} is a random variable drawn from a distribution with zero mean and variance of 1 for diagonal components and 2 for off-diagonal ones.[11]

This is an incredible result. So long as the eigenvalues of $\hat{O}$ do not scale with the size of the energy shell, as expected for MITE, we should expect thermalization for generic operators. In fact, this seems like just the justification we needed in Eq. 1.31 for thermalization to occur. Recalling the form, we may now justify the diagonal average through the basis independence expected in RMT:

$$\sum_m |C_m|^2 O_{mm} \approx \mathbb{E}_{En}[\langle E_n|\hat{O}|E_n\rangle] \sum_m |C_m|^2 = \langle \hat{O}\rangle_{\text{mic}}. \tag{1.39}$$

This result can be generalized into a conjecture that is often taken to be synonymous with the MITE-ETH[13, 28]:

$$O_{mn} \underset{L\to\infty}{=} O(\overline{E})\delta_{mn} + e^{-S(\overline{E})/2} f_o(\overline{E}, \omega) R_{mn}, \tag{1.40}$$

where $S(\overline{E})$ is the thermodynamic entropy at the average energy $\overline{E} = \frac{E_n+E_m}{2}$, the energy difference, $\omega = E_m + E_n$ is sufficiently small such that both states are in the same energy window, $O(\overline{E})$ is a smooth function of $\overline{E}$ that approximates $\langle \hat{O}\rangle_{\text{mic}}$ within a sufficiently small energy window, $f_o(\overline{E}, \omega)$ is a smooth O(1)-valued function of its two variables, and R_{mn} is a pseudorandom variable with zero mean and unit variance. We see that this reduces to the result derived from RMT if we focus on a narrow energy window where $f_o(\overline{E}, \omega) \approx$ Const.

The ETH can be broken down into two pieces: the off-diagonal and diagonal that relate to equilibriation and the diagonal, relating to thermalization:

- **Diagonal ETH**: For some smooth function, $\overline{O}(\overline{E})$, it follows that

$$\sum_{E_\alpha \in \mathcal{H}_{E,\Lambda}} \langle E_\alpha|\hat{O}|E_\alpha\rangle \underset{V\to\infty}{=} \langle \hat{O}\rangle_{\text{mic}}$$

  .

- **Off-diagonal ETH**: $\langle E_\alpha|\hat{O}|E_\beta\rangle \underset{V\to\infty}{=} 0$. This follows from the entropic $e^{-S(\overline{E})/2}$ factor that should vanish as $\frac{1}{\sqrt{D_{E,\Lambda}}} \sim e^{-L_X}$ in the absence of symmetries. With symmetries present, the energy shell will need to be broken up in to additional sectors, but so long as these are still extensive in system size, in the thermodynamic limit, expectations of these operators rapidly settle to a stationary value, even when spectral gaps are exponentially small.

As mentioned before, there is a notion of *Weak ETH*, where all but a vanishingly small set of rare states satisfy MITE. The weak ETH has been proven for a wide class of translation-invariant short-range interacting spin systems [25, 29]. It ensures that initial states that do not have substantial overlap with these rare states thermalize. One must be particularly

[11] If we repeat this analysis for the GUE, where there is no time-reversal symmetry, $\mathbb{E}_{E_n}[|\psi_i^m|^4] = 2\mathbb{E}_{E_n}[|\psi_i^m|^2]$, because ψ_i^m can be complex, and the variance of $R_m n$ is 1 for both diagonal and off-diagonal components

careful of initial states that can be well-approximated with a small number of energy eigenstates. Such states are said to have a small effective dimension and will generally have slow relaxation times[13]. Thus, even if rare states form a small fraction of the total energy shell, if a state with small enough effective dimension has non-vanishing support on these rare states, MITE cannot be guaranteed. In fact, typical states prepared via quantum quench usually do not have sufficiently large effective dimension to microscopically thermalize due to non-trivial overlap with rare states. Another difficulty is that the ETH often holds for translation-invariant integrable systems, which often fail to thermalize [25, 30, 31].

There is a wide range of numerical evidence for each version of the ETH [3, 25, 32] and the strong version provides a sufficient condition for thermalization, however no formal proof exists for the conjecture. In fact, as we will see later on, there are a number of characteristic ways in which the ETH fails in specific systems, even for some familiar or less exotic dynamics. Some of the most well-studies examples include integrable systems[12] [25, 30, 31], many-body localized phases [33–35], and dynamics with Hilbert space fragmentation [36–38]. Each of these systems displays various forms of ergodicity breaking, where states are unable to explore the full Hilbert space under the system dynamics. However, as will be discussed below, this segmenting of the Hilbert space is not always an issue for thermalization, and can actually be an essential feature.

Timescale of thermalization

The ETH established conditions for thermalization to occur, however an equally pressing physical concern is the timescale under which thermalization occurs. We have ruled out certain mechanisms for thermalization that seemingly took place over times exponential in the system size, but it remains to provide an estimate for reasonable thermalization times for systems that are known to thermalize. This can be a difficult task in general because the timescale can depend on the initial state and observable of interest.

One can bound the thermalization time by averaging over random Hamiltonians once more. Specifically, we generate an ensemble of Hamiltonians with constant energy spectrum by considering equal weights for all possible Hamiltonians connected to an initial reference $\hat{H}_0$ by unitary transformations, $\hat{H}' = \hat{U}^\dagger \hat{H}_0 \hat{U}$. This is called the *Haar measure* on unitaries. We will return to this when we discuss random unitary circuits, as it is a powerful tool.

To bound thermalization time, we simply consider the ensemble (Haar-)average of the evolution of the expectation $\langle\psi(t)|\hat{O}|\psi(t)\rangle$ for a fixed observable $\hat{O}$. Under some realistic assumptions, it can be shown that this leads to a thermalization time corresponding to a thermal energy scale, called the Boltzmann time or Planckian thermalization time: $\tau_B \equiv \beta\hbar = \frac{\hbar}{k_B T}$, where we have restored $\hbar \approx 1.05 \times 10^{-34} Js$ and $k_B \approx 1.38 \times 10^{-23} J/K$ to emphasize the scale of this time [13]. This time has two particular features of note. First, it is incredibly fast. For a system at room temperature, where $T \sim 300K$, this would correspond to a timescale of 2.5×10^{-12} s. Second, this value does not depend on system size. The Haar-average above has no notion of locality, and so we have made use of a host of unphysical many-body, non-local Hamiltonians in deriving this result.

[12] Integrable systems prove difficult because they host an extensive number of conserved quantities (each trajectory yields one) and tend to relax into something called the general Gibbs ensemble (GGE) that depends strongly on initial conditions

To gain a more nuanced view, we return to the ETH. Eq. 1.40 suggests that the timescale for any dynamical phenomena in thermalization is determined by $f_o(\overline{E}, \omega)$[39]. In ergotic systems, the slowest timescale is typically diffusive, which can be seen by the fact that $f_o(\overline{E}, \omega)$ becomes constant for when considering energy shells with widths limited by the diffusion constant, D[39]:

$$\omega < E_T = \frac{D}{L^2}, \tag{1.41}$$

where E_T is called the Thouless time. As mentioned above, in order to have such diffusive dynamics, the system considered typically has some globally conserved quantities. Such conserved quantities are a generic feature of dynamics in closed systems, but they can also inhibit thermalization, as we will see below

1.3.2 Thermalization with Symmetry

Conceptually, symmetry plays an essential role in thermalization. Symmetries partition a system into different invariant sectors within which thermalization may occur. However, if the symmetry is too restrictive, these sectors may become so small as to prevent thermalization from being possible.

As an example, let us return to the definition of our energy shell. We have already seen how to restrict the Hilbert space into energy shells in Eq. 1.23. If we want to restrict our discussion into the subspace with a fixed value of another macroscopic conserved quantity besides energy, we will simply need another width for the new conserved quantity. For example, when the total number operator of bosons or fermions denoted by $\hat{N}$ is a conserved quantity, and we consider a fixed particle number N, then the energy shell $\mathcal{H}_{E,N,\Lambda}$ should be defined as the Hilbert subspace spanned by simultaneous eigenstates of both $\hat{H}$ and $\hat{N}$ given by $|E_\alpha, N_\beta\rangle$, where we now have both an energy width, ΔE, and a number width, ΔN This shell will have a size given by $D_{E,N,\Lambda} = \dim\mathcal{H}_{E,N,\Lambda}$. So long as $D_{E,N,\Lambda}$ is still extensive in system size, all the previous results about thermalization should still hold. This is rather trivial for most familiar global symmetries like parity, space group symmetries, or particle number conservation.

Before adding additional symmetries, let us consider how the microcannonical ensemble is altered by the presence of continuous conserved quantities. Let us start by considering the role of energy. The size of an energy shell can be defined by $D_{E,\Lambda} \equiv e^{S_{\text{mic}}(E)}$, If we consider sufficiently small energy windows, ΔE, we may consider the Taylor expansion of the microcanonical entropy in ΔE,

$$S_{\text{mic}}(E + \Delta E) \approx S_{\text{mic}}(E) + \frac{\partial S_{\text{mic}}(E)}{\partial E}\Delta E + \cdots \equiv S_{\text{mic}}(E) - \beta\Delta E + \ldots \tag{1.42}$$

Now, if we re-write the microcanonical ensemble within the energy shell,

$$\begin{aligned}\hat{\rho}_{\text{mic}}(E) &= \frac{1}{D_{E,\Lambda}} \sum_{E_n \in \mathcal{H}_{E,\Lambda}} |E_n\rangle\langle E_n| = e^{S_{\text{mic}}(E)} \sum_{E_n \in \mathcal{H}_{E,\Lambda}} |E_n\rangle\langle E_n| \\ &\approx \sum_{E_n \in \mathcal{H}_{E,\Lambda}} e^{S_{\text{mic}}(E) - \beta(\hat{H} - E)} |E_n\rangle\langle E_n|\end{aligned} \tag{1.43}$$

If we consider all of the different energy shells, we expect that $\hat{\rho}_{\text{mic}} \sim e^{-\beta \hat{H}}$. When properly normalized, this defines a *canonical ensemble*:

$$\hat{\rho}_{\text{mic}} \approx \frac{e^{-\beta \hat{H}}}{\text{Tr}[e^{-\beta \hat{H}}]} \equiv \hat{\rho}_{can}. \tag{1.44}$$

Applying the same logic, to the conserved charge, Q, we should be able to expand the entropy out as a function of small increments ΔQ,

$$S_{\text{mic}}(E + \Delta E, Q + \Delta Q) \approx S_{\text{mic}}(E, Q) - \beta \Delta E + \beta \mu \Delta Q + \ldots, \tag{1.45}$$

where we have defined $\mu = \left(\frac{\partial E}{\partial Q}\right)_{S,Q}$, as expected for a thermodynamics potential. Just as above, we arrive at a *grand canonical ensemble*:

$$\hat{\rho}_{\text{mic}} \approx \frac{e^{-\beta(\hat{H} - \mu \hat{Q})}}{\text{Tr}[e^{-\beta(\hat{H} - \mu \hat{Q})}]} \equiv \hat{\rho}_{g.can}. \tag{1.46}$$

Continuous symmetries also give rise to novel dynamics when inhomogeneities arise in the density of conserved charges. The total charge operator can be written as a uniform sum of local charge densities, $\hat{Q} = \sum_i \hat{q}_i$. By definition, the total charge does not change because of its commutation with the Hamiltonian, $[\hat{H}, \hat{Q}] = 0$. However, as mentioned above, inhomogeneities in the local charge density will are subject to the additional constraints compared to other operators. This results in slower dynamics for these charge density operators, and, in turn, generically sets the thermalization time for a system. In chapter 2, this notion will be made more precise.

However, the discussion above assumes the existence of large shells of approximately constant energy and charges. Conceptually, this can be understood as a constraint that a shell be large enough so that it may be partitioned into a small "system" subspace where local operators have support, and the rest of the shell, comprising a large effective bath or reservoir. Unlike in a heat bath, however, this reservoir will source entanglement from the small system. Should the shell under consideration be too small to absorb significant entanglement, or should the coupling between subspaces be too weak for entanglement to develop effectively, MITE is unlikely. We now explore the mechanisms by which the ETH may fail.

1.3.3 Failures of the ETH

The ETH can be violated in a number of different ways. however, each failure can be characterized as a certain failure to "forget" an initial state.

Perhaps the simplest case of this failure comes from integrability. Classically, these are the paradigmatic examples of systems that retain perfect memory of their initial conditions. These systems have an extensive number of conserved quantities that are typically associated with orbits in phase space. If a system has an extensive number of conserved quantities, $\{Q_k\}$, it follows that the system does not follow the MITE-ETH. This is because each charge defines an operator that does not thermalize $\langle E_n | \hat{Q}_k | E_n \rangle \neq \langle \hat{Q}_k \rangle_{\text{mic}}$ under the system

dynamics. Indeed, were we to examine the predicted matrix elements from the ETH for integrable systems, the justifications for both the diagonal and off-diagonal forms are called into question:

- **Diagonal ETH**: With an extensive number of conserved quantities, $\{Q_k\}$, it is no longer guaranteed that one can find a shell preserving energy and $\{Q_k\}$ with a sufficiently large number of energy eigenstates to define a smooth function $O(\overline{E}, \{Q_k\})$, leaving the diagonal average sensitive to initial conditions.
- **Off-diagonal ETH**: With an extensive number of conserved quantities, $\{Q_k\}$, the effective dimension of each shell, $D_{E,\{Q_k\}}$ is no longer guaranteed to scale exponentially with system size due to the $\sqrt{\frac{1}{D_{E,\{Q_k\}}}}$ suppression, and the off-diagonal components may have long-time fluctuations that decay as a power law in system size or even remain constant.

In effect, there is no longer a guarantee that each shell is large enough to act as a thermalizing reservoir for its own subsystems. There is a great deal of numerical evidence that integrable systems do not satisfy the strong MITE-ETH [3, 25, 32]. However, the weak MITE-ETH is satisfied for translation invariant integrable systems[25, 29]. Even when the weak MITE-ETH is satisfied, the relaxation dynamics in these systems can be highly non-trivial[29].

A similar violation can arise with non-commuting charges, $\{Q_k^{(nc)}\}$ that arise from non-Abelian symmetries, even for a sub-extensive number of charges[40]. In such systems, it is impossible to construct a shell that has all the charges simultaneously well-defined. As a result, one must construct these shells from a non-unique maximal number of co-commuting quantities, $\{\tilde{Q}_k\}$ that can be derived from the maximal Abelian subgroup of the original symmetry group. Because the choice of co commuting quantities, $\{\tilde{Q}_k\}\{\tilde{Q}_k\}$, is not unique, the system cannot relax to a distribution defined by a particular choice of such charges. This leaves the system and its evolution sensitive to initial conditions such that $O(\overline{E}, \{\tilde{Q}_k\})$ can no longer be a simple function of the commuting quantities used to define it. Because of this, the system retains some memory of the initial distribution of non-commuting charge through its dynamics.

The case of non-commuting charges presents an example of the notion of *ergodicity breaking*. This phenomenon occurs when the system dynamics do not allow states in a symmetry sector, $|\psi\rangle \in \mathcal{H}_Q$, to explore the full sector. In other words, $\text{Span}\{\hat{U}_\tau|\psi\rangle : \tau > 0\} \neq \mathcal{H}_Q$ for some states $|\psi\rangle \in \mathcal{H}_Q$. Instead, the system breaks up into many dynamically disconnected *Krylov* sectors, $\mathcal{K} \subset \mathcal{H}_Q$ defined as the smallest unit of connected dynamics. Each sector can be identified by a non-unique, characteristic element, $|\psi_n\rangle$ as

$$\mathcal{K}_n = \text{Span}\{\hat{U}_\tau|\psi_n\rangle : \tau > 0\}. \tag{1.47}$$

In the case of non-commuting charges, this ergodicity breaking occurrs due to the inability to simultaneously diagonalize all symmetry generators. Generically, this breakdown of ergodicity within a symmetry sector will lead to violations of the ETH for the reasons mentioned above.

There exist many other instances of ergodicity breaking besides non-commuting charges. Notable examples include many-body Localization (MBL)[33–35], quantum many-body Scars (QMBS)[31, 41], Hilbert-Space fragmentation[36–38].

In many-body localization, random fluctuations in some spatial potential, when sufficiently strong, cause the system to relax into equilibrium states that hold a local memory of initial conditions. Such configurations are generically non-thermal and can be described by a complete set of conserved quantities, each of which is defined as a quasi-local operator[34, 35]. Although MBL is one of the most famous examples of violations of the ETH, we do not discuss it in detail here, and the interested reader may find more complete treatments in Ref[33].

Quantum many-body Scars (QMBS) refer to a phenomenon where a a few sections of a full Hilbert space are dynamically disconnected from the rest of the space. These "scars" give rise to behaviors like short-time recurrence phenomena that demonstrate an enhanced memory of the initial state [41] and do not thermalize with the rest of the system. Due to the small size the space covered by these scars compared with the full Hilbert space, such systems satisfy the weak ETH. In contrast, Hilbert Space Fragmentation occurs when there are exponentially many disconnected sectors (not accounted for by traditional symmetries). In this case, we may distinguish two forms of fragmentation. Strong Hilbert space fragmentation occurs when the largest of the system's Krylov sector is exponentially small in system size. Weak Hilbert space fragmentation occurs when the largest Krylov sector is comensurate with the total system size.[13] Due to the small size of their Krylov sectors, systems displaying strong Hilbert space fragmentation generically violate even the weak ETH. Most states in the Hilbert space will have a significant overlap with exponentially many Krylov sectors, and thus retain significant information about initial conditions over time. In contrast, many systems with weak Hilbert space fragmentation actually satisfy the weak ETH because a generic initial state is likely to lie within the largest Krylov sector or have vanishing overlap with other sectors.

1.4 Characterizing Dynamic Phenomena

In this section, we will explore some of the many ways to diagnose different quantum dynamical phenomena. We will be particularly concerned with *universal* properties of dynamical systems that do not depend on the microscopic details of a particular system. In what follows, we will review some of the salient markers of thermalizing or entangling dynamics that will be pertinent to the rest of this dissertation. Following this, we will review a number of different, similarly relevant approaches to model dynamical systems of interest.

1.4.1 Metrics of Dynamics

There are many different ways to diagnose the approach to equilibrium for particular states and operators. In fact, a whole review could be written on the various metrics diagnosing different aspects of dynamical phenomena. However, when discussing thermalization, nearly all of the relevant metrics pertain in some way to the spread of entanglement across a system.

[13] Different definitions allow for the size of the largest Krylov sector to vanish as a power law in system size.

Entanglement Measures

Many-body quantum entanglement is essential in classifying different equilibrium states of matter, but hard to quantify. There are many different different measures, however, for the purposes of this work, we will focus on two of the simplest and their related quantities. First, we have the above-defined entanglement entropy in Eq. 1.20. This has a helpful form that mimics that of a quantity from classical information theory, the Shannon entropy:

$$S(p) \equiv -\sum_{x \in X} p(x) \log\left(p(x)\right), \tag{1.48}$$

where $p(x)$ is a classical probability distribution over a discrete random variable $x \in X$. This quantity codifies the amount of uncertainty in or unexpectedness of the distribution. The term $-\log\left(p(x)\right)$ can be interpreted as a measure of the surprise at witnessing an element x. Elements with lower probabilities $p(x)$ are less likely, and therefor generate more surprise. The Shannon entropy can then be interpreted as the expected surprise generated by a distribution. It is minimized when any element is certain ($p(x_0) = 1$), and maximized when all elements are equally probable ($p(x) = \frac{1}{|X|}$ for all $x \in X$). In similar fashion, $S(\hat{\rho})$ provides a basis independent measure of the uncertainty in the quantum state of a density matrix, $\hat{\rho}$. When $\hat{\rho}$ is a pure state, $|\psi\rangle$, it can be cast as a matrix whose only non-zero element is a 1 along the diagonal, corresponding to the state $|\psi\rangle\langle\psi|$. As expected, this minimizes the entanglement entropy, so that $S(\hat{\rho}) = 0$. If a state is described by the *maximally mixed* distribution that takes the form $\hat{\rho} = \frac{1}{D_{\mathcal{H}}}\mathbb{I}_{\mathcal{H}}$ in every basis, then the entanglement entropy is maximized so that $S(\hat{\rho}) = \log D_{\mathcal{H}}$.

As discussed above, even when the sate of a full system is pure, the density matrix for a particular subsystem may be mixed if it is entangled with other subsystems. To better understand this, let us consider a system of N spin 1/2 particles arranged in a one dimensional lattice of sites $i \in \{1, \ldots, N\}$. We can partition this lattice into a subsystem X and its compliment X^c, where $D_X = 2^{|X|}$, and likewise for X^c. The entanglement between regions X and X_c can be expressed as the entanglement entropy of the reduced density matrix on either subsystem:

$$S(\hat{\rho}_X) = -\mathrm{Tr}[\hat{\rho}_X \log\left(\hat{\rho}_X\right)] = -\mathrm{Tr}[\hat{\rho}_{X^c} \log\left(\hat{\rho}_{X^c}\right)] = S(\hat{\rho}_{X^c}). \tag{1.49}$$

If the full system is described by a pure state, $|\psi\rangle$, this entropy roughly corresponds to (the logarithm of) the number of terms needed to write this pure state as a superposition of product states between X and X^c. This can be seen by writing $|\psi\rangle$ in the non-unique Schmidt- form

$$|\psi\rangle = \sum_i \sqrt{\lambda_i} |\phi_{i,X}\rangle |\phi_{i,X^c}\rangle, \tag{1.50}$$

where λ_i are the eigenvalues of $\hat{\rho}_X$ or $\hat{\rho}_{X^c}$, which can be interpreted as probabilities for seeing the states $|\phi_{i,X(X^c)}\rangle \in \mathcal{H}_{X(X^c)}$. Entanglement entropy has a number of useful properties:

- $S(\hat{\rho}_X)$ is invariant under unitary transformations that act separately on X and X^c, such as a change of basis or dynamical evolution purely within the two subsystems. When unittary evolution couples X and X_c, entanglement generically grows.

- $S(\hat{\rho}_X) \in [0, D]$, where $D = \min(D_X, D_{X^c})$. It is minimized when the two one system is pure, and maximized when the smaller system can be written as the D x D matrix, $\frac{1}{D}\mathbb{I}_D$.
- When written as a probabilistic sum of orthonormal pure states, $\hat{\rho}_X = \sum_i p_i |\phi_{i,X}\rangle\langle\phi_{i,X}|$, the entanglement entropy is equal to the Shannon entropy, $S_X(p_i) = -\sum_i p_i \log(p_i)$ for this distribution.

We can add to this list the effects of measurement on entaanglement. Generically, measurements project to product states in the appropriate basis. If one measures local observables, this will reduce the entanglement that has developed across the full system. If one considers measuring a system in a local basis at some finite rate, there will be competition between the entangling dynamics of unitary evolution and the disentangling effects of measurements. The entanglement present in the steady state of such a dynamical setup will show a sharp transition at a finite measurement rate, known as measurement-induced phase transition (MIPT).

Unfortunately, entanglement entropy can prove computationally and experimentally unwieldy. Since it involves the trace of the logarithm of a matrix, calculating or observing the entanglement entropy generically requires incredibly precise knowledge of each of its matrix elements.

In place of this, one can study another entropy that shares many of the same properties. This *Rényi*-entropy is defined for any integer, n, as

$$S^{(n)}(\hat{\rho}) = \frac{1}{1-n} \log\left(\mathrm{Tr}[\hat{\rho}^n]\right), \tag{1.51}$$

and has the useful property that $\lim_{n\to 1} S^{(n)}(\hat{\rho}) = S(\hat{\rho})$. Calculating the trace of different powers of the density matrix is a much simpler task. Even when the entanglement entropy is a prefered metric, one will often see calculations of the entanglement entropy make use of the above limit by calculating $S^{(n)}(\hat{\rho})$ as a function of n, then taking a formal limit to n = 1. Each moment often shows qualitatively similar properties to the entanglement entropy, but caution must be taken when inferring details from any specific Rényi moment, as we will review in Chapter 4.

Because of their connection to information theory, there are a host of other quantum information theoretic measures that can be defined, including the quantum mutual information[42], negativity[42], Fisher information[43], etc. However, these will be discussed in other works.

Operator Dynamics

While discussing entanglement entropies, we have solely focused on the system's dynamics without considering any particular observable entities. To relate this dynamics to thermalization, we must relate it to a set of observables. If we are primarily concerned with the dynamics of operator expectations $\langle\psi(t)|\hat{O}|\psi(t)\rangle = \mathrm{Tr}[\hat{\rho}(t)\hat{O}]$, it can often help to switch to the heisenburg picture and focus on operator dynamics. In this picture, the spread of entanglement is replaced by the spread of initially localized operators, $\hat{O} \in \mathcal{S}_X$.

For such a setup, assuming $\hat{\rho}$ does not have any initial entanglement between the two regions, one can diagnose the onset of entanglement between a region, X and the rest of the system, X^c by the time it take for $\hat{O}(t)$ to develop support in X^c. Let us take a complete basis of bounded operators in the space, $\hat{O}_S \in \mathcal{B}$, where S is a particular string or product of local operators on each lattice site. We may define any operator in the hilbert space as [44, 45]

$$\hat{O}(t) = \sum_S c_S(t)\hat{O}_S. \tag{1.52}$$

Here, we have exploited the fact that each string operator satisfies the orthogonality constraint, $\mathrm{Tr}[\hat{O}_{S'}\hat{O}_S] = \delta_{S'S}$ under the trace norm for normalized operators, where $\mathrm{Tr}[\hat{O}^2] = 1$. By definition, we must have that $\sum_S |c_S(t)|^2 = 1$[14], and each amplitude and weight evolves as

$$\begin{aligned} c_S(\delta t) &= \sum_{S'} \mathrm{Tr}[U_{\delta t}\hat{O}_S U_{\delta t}^\dagger \hat{O}_{S'}]c_{S'} = \sum_{S'} W_{S,S'}(\delta t)c_{S'} \\ |c_S(\delta t)|^2 &= \sum_{S',S''} W_{S,S'}(\delta t)W_{S,S''}(\delta t)c_{S'}c^*_{S''}. \end{aligned} \tag{1.53}$$

We will return to these expressions when we address random unitary circuits, where calculating these quantities becomes feasible. However, qualitatively, one may notice that, the weight for any particular operator, $|c_S(t)|^2$ tends to decrease exponentially in time because there are exponentially many operators in the system size. Further, it is clear that thermalization times should be determined by the dynamics of these correlation functions, $W_{S,S'}$. Thus, if one wishes to understand thermalization via operator dynamics, it suffices to study two-point correlations, where one operator can be understood as an element of the density matrix, $\hat{\rho}$ [46]:[15],

$$C_{\hat{O}\hat{O}_S}(t) = \mathrm{Tr}[\hat{O}(t)\hat{O}_S(0)]. \tag{1.54}$$

There are a number of bounds on the dynamics of such correlators. The most famous of which is the *Lieb-Robinson bound* [47]. This bound was initially calculated for dynamics that were driven by short-range interactions, where one can show an emergent "soft" light cone limiting the propagation of quantum information. For such systems, the correlations outside the "soft" light cone are exponentially suppressed [47, 48]. More preciseley, the theorem states that for local operators $\hat{O}_X$ and $\hat{O}_Y$ with support on X and Y, there exists constants $\kappa > 0$, v, and c > 0 such that [47]

$$||[\hat{O}_X, \hat{O}_Y]|| \leq ce^{-\kappa(d(X,Y)-vt)}, \tag{1.55}$$

where $d(X,Y)$ is the minimum distance between regions X and Y. Although it is unclear whether a general form may be given for arbitrary interactions, the bound has been generalized for systems that have interactions whose strength decays algebraically with distance to some power, α [49]. We will return to this bound when considering long-range interactions in Ch. 3.

[14] Because of the hermiticity requirement for observables, the coefficients c_S are all real valued, so the absolute value is actually unnecessary.

[15] As we will discuss later, one also needs to take care about the weight of an initial state on the operator considered, $|c_{\hat{O}}|^2$

Out of Time Ordered Correlator (OTOC)

This discussion has focused on on operator spreading that mostly concerned itself with local support, but was largely insensitive to the scrambling of quantum information or entanglement between many different degrees of freedom. Much like in classical physics with initial conditions, a key aspect to thermalization comes in the chaotic scrambling of initial correlations. In the quantum setting, we can develop a parallel notion of scrambling, but since we do not have a proper phase space, it will be defined over (initially local) operators. Classically, the sensitivity of coordinates $\vec{r}(t)$ to initial conditions, $\vec{r}(0)$ can be defined as follows: $\frac{\partial \vec{r}(t)}{\partial \vec{r}(0)}$. In chaotic systems, this quantity grows exponentially in magnitude with a growth rate defined by a *Lyapunov exponent*, λ. A finite λ indicates an exponential dependence of the state of a system on its initial conditions.

If we wish to search for a quantum analogue to this chaotic dynamics, we first explicitly write out this term using the poisson bracket: $\frac{\partial \vec{r}(t)}{\partial \vec{r}(0)} = \{\vec{r}(t), \vec{p}(0)\}_{PB}$. The quantum analogue will simply replace the poisson bracket with a commutator of operators: $-i[\hat{X}(t), \hat{P}]$. However, this is still an operator valued quantity, so we will need to take the expectation withh respect to some state $\hat{\rho}$ that is often chosen to be the thermal equilibrium state: $-i\mathrm{Tr}[\hat{\rho}_{\mathrm{mic}}[\hat{X}(t), \hat{P}]]$. To avoid averaging away fluctuations, it is better to use the square of this commutator: $\mathrm{Tr}[\hat{\rho}_{\mathrm{mic}}[\hat{X}(t), \hat{P}]^2]$.

We can generalize this for two initially local operators $\hat{W}$, $\hat{V}$ and thermal state, $\hat{\rho}_{\mathrm{mic}}$ by defining an *Out of Time Ordered Correlator* (OTOC)[50, 51]:

$$C_{WV}(t) \equiv \mathrm{Tr}[[\hat{W}(t), V(0)]^\dagger [\hat{W}(t), V(0)]\hat{\rho}_{\mathrm{mic}}]. \tag{1.56}$$

Expanding out the commutators, this can be decomposed into a number of different parts, which includes the out-of-time ordered product:

$$\mathcal{F}_{WV}(t) \equiv \mathrm{Tr}[\hat{W}^\dagger(t)\hat{V}^\dagger(0)\hat{W}(t)\hat{V}(0)]. \tag{1.57}$$

As will be discussed in Ch. 4, this will be the most relevant term at late times. It has been shown that quantum systems with well-defined, chaotic, quasi-classic limits, at intermediate times, the OTOC scales exponentially, just as in the classical case, its spread is bounded by $\lambda_L \leq \frac{2\pi k_B T}{\hbar}$[51]. To see the exponential behavior, we can use the quantum-classical correspondence $\lim_{\hbar\to 0} \frac{1}{i\hbar}[\hat{W}, \hat{V}] = \{W, V\}$, where W and V are phase space quantities. If we chose some conjugate variables like $\hat{W} = \hat{X}$ and $\hat{V} = \hat{P}$, then much like classical systems, [52]

$$C^{(qc)}_{WV}(t) \sim (-i\hbar\{X(t), P(0)\}) = -\hbar^2 \left(\frac{\partial X(t)}{\partial X(0)}\right)^2 \sim \hbar^2 e^{-2\lambda t}. \tag{1.58}$$

The OTOC has a straightforward interpretation. It is the degree to which $\hat{W}(t)$ fails to commute with $\hat{V}(0)$. Yet there are additional, more physical interpretations available within the many-body setting. If we define $\hat{W}(0)$ and $\hat{V}(0)$ as operators living on the single sites i and j within a lattice with local Hilbert space dimension q, then it can be shown that the average of $\mathcal{F}_{WV}(t)$ over different choices of $\hat{V}$ yields the probability that the state $\hat{W}(t)$ does

not have support on j. More precisely [53],

$$\frac{1}{q^2}\sum_V \mathcal{F}_{WV}(t) = \sum_S |c_S(t)|^2 \delta_{\hat{S}_j,\mathbb{I}_j}, \tag{1.59}$$

where S is a string with local element $\hat{S}_i$ on site i. In another formulation, the out-of-time ordered product can even be cast as the mutual information between two time-slices of quantum dynamics[54].

Now that we have discussed a number of different measures characterizing the spread of entanglement through a system and across different degrees of freedom, we can turn to discuss the methods for calculating these quantities. Each of these measures nominally still requires one to keep track of a large number of degrees of freedom, meaning that calculating their explicit dynamics is next to impossible for all but a handful of toy systems. Instead, to make progress, one must resort to particular approximations, or else, search for universal trends through the use of phenomenological models. Even here, there are additional difficulties, as many of the above measures are non-linear in the density matrix, and naively may appear unobservable. We will address this issue more in Ch. 4, however, we now turn to the use of various dynamical models used to facilitate the calculation of relevant quantities.

1.4.2 Dynamical Models

Quantum Information theoretic quantities like those above describe the intricate correlation structure in many-body systems, however they also qualify the difficulty in simulating a quantum state or process classically. In what follows, we will explore a handful of models of dynamics that seek to address this by stripping down exact dynamical information to arrive at typical behavior.

We begin with mention of methods that are characteristic of first-principles investigations of non-equilibirum dynamics. If we assume that a system thermalizes to some Boltzmann steady state, we may calculate dynamics of thermal expectation values using Non-equilibrium Greens functions. These are accomplished by allowing time to flow along a very specific contour (See Fig. 1.3) in the complex plane such that [55]

$$\mathrm{Tr}[\hat{\rho}_{can,\beta}\hat{O}(t)] = \frac{\mathrm{Tr}[\hat{U}_{i\beta}\hat{U}_t^\dagger \hat{O}(0)\hat{U}_t]}{\mathrm{Tr}[\hat{U}_{i\beta}]}, \tag{1.60}$$

where we have used the fact that $U_t = e^{-i\hat{H}t}$ to define the canonical ensemble as the expectation of evolution in imaginary time. This technique is called the *Keldysh Formalism*. The non-equilibrium Green's functions employed allow one to construct exchange correlation potentials with memory by using diagrammatic techniques. More generally, this formalism allows one to perform calculations required for time-dependent density functional theory (TDDFT) that can be invaluable in descriptions of certain quantum transport or atoms in intense laser pulses.[55] However, these calculations are generically still quite involved and do not highlight the role of symmetries as directly as other formalisms. We will not discuss the Keldysh formalism in detail, however the interested reader may learn more through Ref. [55].

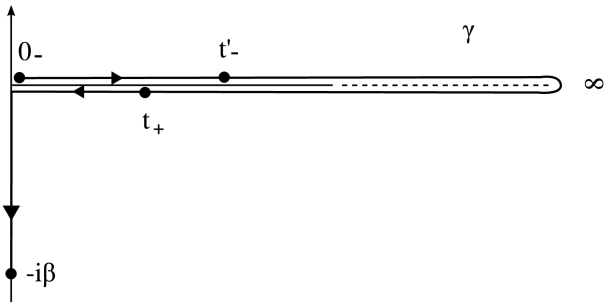

Figure 1.3: **Keldysh Contour**– The contour, γ, of time evolution in the complex time plane for the Keldysh formalism. Starting at $t = 0$, it winds round positive infinity, returns, and ends at $t = -i\beta$. Figure reproduced from [55].

Rather than assuming equilibrium distribution, one may attempt to render calculations more tractable by focusing on the degrees of freedom within a system of interest. This means that one can no longer track the full state of the system. However, under reasonable assumptions, the compliment of a small region of interest, X, should by typical in a way that enables one to calculate generic evolution within the region X. This is the driving intuition behind *Quantum Master Equations*, which hare the subject of the next section.

Quantum Master Equations

As mentioned above, quantum master equations operate by making assumptions about typical state and behavior of the environment surrounding a particular subsystem. Once we decompose degrees of freedom between the subsystem and environment, then the full dynamics of the system can be decomposed into three pieces:

$$\hat{H} = \hat{H}_S + \hat{H}_E + \hat{H}_{\text{int}}. \tag{1.61}$$

Written in this form, the dynamics of our subsystem of interest can be written as

$$\dot{\hat{\rho}}_S(t) = -i\text{Tr}_E[\hat{H}, \hat{\rho}(t)]. \tag{1.62}$$

The benefit of this decomposition is that one may ignore the the dynamics driven by $\hat{H}_E$ due to the trace. From this, one need only supply some assumptions about the strength of interactions $\hat{H}_{\text{int}}$, and the state of the environment $\hat{\rho}_E$ in order to develop equations detailing stochastic evolution over density matricies $\hat{\rho}_S$. Some master equations make use of generic interaction terms, $\hat{H}_{\text{int}}$ to establish expected means for correlation to develop between the system and environment. One example of this approach comes in the form of the Bloch-Redfield master equation [56]. However, we will focus on a more restrictive case, where our subsystem couples weakly to a Markovian or "memoryless" environment. With these assumptions, we arrive at the Lindblad equation[56].

$$\dot{\hat{\rho}}(t) = -i[\hat{H}, \hat{\rho}(t)] + \sum_n \gamma_n \left(\hat{L}_n \hat{\rho}(t) \hat{L}_n^\dagger - \{\hat{L}_n^\dagger \hat{L}_n, \hat{\rho}(t)\} \right), \tag{1.63}$$

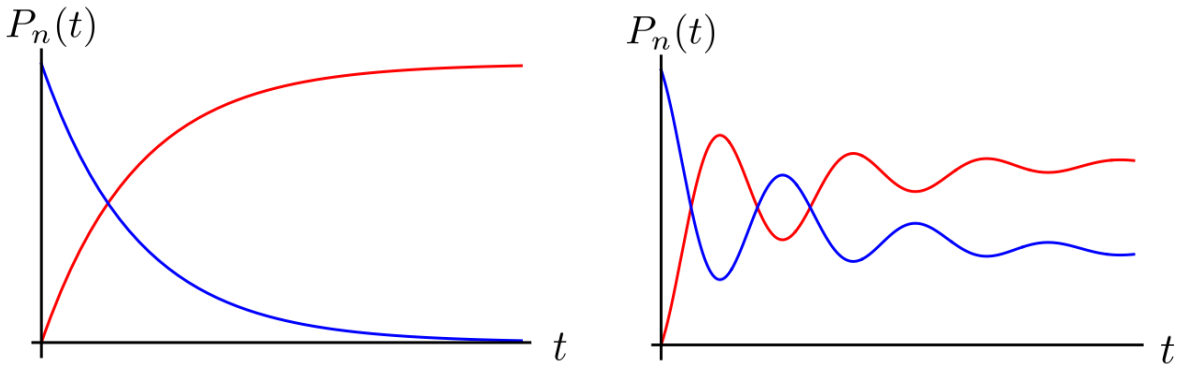

Figure 1.4: **Two-state system population dynamics** – The population dynamics of ρ_{11} (blue) and ρ_{00} (red) for **a)** incoherent dynamics ($\Omega = 0, \Delta E = 1, \Gamma = 0.5$) and **b)** coherent dynamics ($\Omega = 1, \Delta E = 1, \Gamma = 0.5$)

where $\hat{L}_n$ are called Lindblad or jump operators, and unlike terms in a Hamiltonian, need not be hermitian. In this form, we need not consider any of the degrees of freedom in the environment. The Lindblad equation is also the most general form of a completely positive and trace-preserving (CPTP), which effectively preserves the normalization of density matrix over time, map for $\hat{\rho}$ that is Markovian and time-independent[56].

As an example of how this equation can be used, let us consider a simple two-level system with spontaneous decay. We define the system Hamiltonian $\hat{H} = \frac{\Delta E}{2}\hat{\sigma}^z + \Omega\hat{\sigma}^x$ and relevant jump operator as $\hat{L} = \hat{\sigma}^-$, so that the Lindblad equation reads:

$$\dot{\hat{\rho}}(t) = -i\left[\frac{\Delta E}{2}\hat{\sigma}^z + \Omega\hat{\sigma}^x, \hat{\rho}(t)\right] + \Gamma\left(\hat{\sigma}^-\hat{\rho}(t)\hat{\sigma}^+ - \{\hat{\sigma}^+\hat{\sigma}^-, \hat{\rho}(t)\}\right), \tag{1.64}$$

where we have defined the spontaneous emission rate as Γ. This equation can be solved for the four components of $\hat{\rho}(t)$ to give

$$\begin{aligned}
\dot{\rho_{00}}(t) &= i\Omega\rho_{01} - i\Omega\rho_{10} + \Gamma\rho_{11} \\
\dot{\rho_{01}}(t) &= i\Omega\rho_{00} - \left(i\Delta E - \frac{\Gamma}{2}\right)\rho_{10} - i\Omega\rho_{11} \\
\dot{\rho_{10}}(t) &= -i\Omega\rho_{00} + \left(-i\Delta E - \frac{\Gamma}{2}\right)\rho_{10} + i\Omega\rho_{11} \\
\dot{\rho_{11}}(t) &= -i\Omega\rho_{01} + i\Omega\rho_{10} - \Gamma\rho_{11}.
\end{aligned} \tag{1.65}$$

From this, we can extract the full system dynamics, as shown in Figure 1.4.

The dynamics can be put in a more familiar form if we vectorize the density matrix as $\|\rho\rangle\rangle = (\rho_{00}, \rho_{01}, \rho_{10}, \rho_{11})^T$, so that the evolution of this vectorized form is given by the matrix,

$H_{\mathcal{L}}$,

$$H_{\mathcal{L}} = \begin{pmatrix} 0 & i\Omega & -i\Omega & \Gamma \\ i\Omega & i\Delta E - \frac{\Gamma}{2} & 0 & -i\Omega \\ -i\Omega & 0 & -i\Delta E - \frac{\Gamma}{2} & i\Omega \\ 0 & -i\Omega & i\Omega & -\Gamma \end{pmatrix}. \tag{1.66}$$

This matrix has a unique eigenstate with eigenvalue 0 for all values of the couplings, corresponding to the steady state. More generally, we may always characterize these dynamics using a *Louiville superoperator*, $\mathcal{L}$, such that $\dot{\hat{\rho}}(t) = \mathcal{L}[\hat{\rho}(t)]$. And if we vectorize the density matrix, this superoperator can be cast as an effective Hamiltonian for the system as $\frac{d}{dt}\|\rho\rangle\rangle = H_{\mathcal{L}}\|\rho(0)\rangle\rangle$, and one may find the steady state of the system as the eigenstate(s) with zero eigenvalue. We will make frequent use of this superoperator formalism in the following chapters.

As is apparent from the example above, these master equations are typically difficult to solve analytically and computationally quite demanding, even for small systems. One may explore toy models with characteristic symmetry constraints, however, it will often be more difficult to derive universal signatures from symmetry constraints compared to the equilibrium setting.

If one wishes to distill dynamics down the bare essentials expected for physically realistic model, they should turn to quantum circuits.

Random Unitary Circuits

Quantum circuits are simple, discrete-time models that distill dynamical models into their most basic building blocks. One may impose locality, unitarity, local system size, etc. while leaving all other details of the model to the side. Further, calculations are rendered feasible by averaging over some imposed notion of random operators within the appropriate circuit geometry.

More precisely, a quantum circuit is a lattice of spins where the state evolution is determined by sequential application of discrete-time unitary gates and measurements. This resembles the ttrotterization of continuous-time Hamiltonians, however the time steps need not be infinitiesmal and the the unitaries need not be constant over time. These features result in a generic absence of energy-conservation. Without such a constraint, and with no additional symmetry or special structure imposed, this implies that the long-time steady state of a generic circuit will be the featureless, maximally disordered state, which has he same form as the infinite temperature statistical ensemble, $\frac{1}{D_{\mathcal{H}}}\mathbb{I}_{\mathcal{H}}$

A key feature in these circuits is the use of randomness. Each operation in the circuit is assumed to be taken from some distribution of possible gates. This randomness allows one to observe these systems in a form that is quantum mechanically incoherent and can be homogeneous in time, if desired. In a similar vein to how RMT was used to average over Hamiltonians satisfying physical constraints to predict level statistics, averaging over different unitaries in the circuit geometries produces a classical statistical ensemble of possible Feynman trajectories. To better understand this, we will focus on the most familiar circuit geometry, called a brickwork circuit.

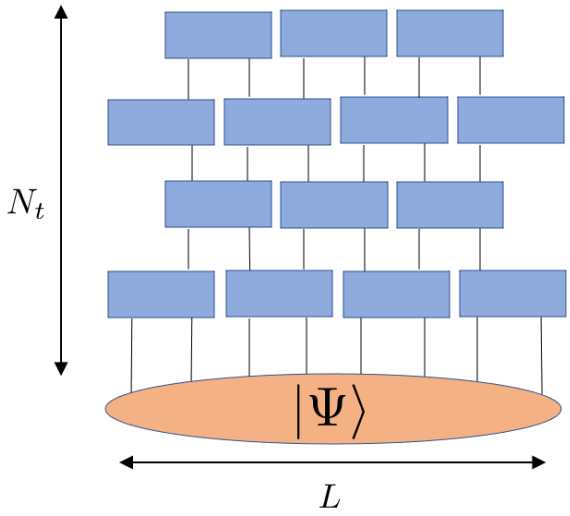

Figure 1.5: **Random Unitary Circuit**– An example of a Random Unitary Circuit. At each time step, random local unitaries, drawn from an appropriate distribution, are applied to neighboring sites

Brickwork RUC's

We now consider a one-dimensional system with N sites, each of which has a local Hilbert space dimension of q. The system is initialized at some initial time in a pure state within the q^N dimensional Hilbert space, $|\psi\rangle \in \mathcal{H}$. It is then evolved by a discrete increments $\Delta t = 1$ by a unitary that is defined as a tensor product of local gates acting on pairs of neighboring spins, with the alternating structure seen in Figure 1.5:

$$\hat{U}_t = \hat{U}_t \hat{U}_{t-1} \dots \hat{U}_1 \tag{1.67}$$
$$U_\tau = \begin{cases} \bigotimes_{i=1}^{N} u_{\tau,i,i+1}, & \text{if } \tau \text{ is even} \\ \bigotimes_{i=1}^{N} u_{\tau,i-1,i}, & \text{if } \tau \text{ is odd} \end{cases},$$

where we have defined $q \times q$, 2-local unitaries acting on sites i and i+1 at time τ by $u_{\tau,i,i+1}$. This representation has two immediate and dual interpretations. First, it is a space–time diagram detailing the specific local interactions that act during specific time steps. Second, it is a tensor network used in constructing the full many-body unitary $\hat{U}_t$ from local four-legged tensors $u_{\tau,i,i+1}$ by contracting indices specifying the local state on all of the bonds. If we contract these indicies with configurations $|\phi_1, \phi_2, \dots, \phi_N\rangle$ on the bottom and $|\chi_1, \chi_2, \dots, \chi_N\rangle$ on the bottom, we will have represented the amplitude $\langle \phi_1, \phi_2, \dots, \phi_N | U_t | \chi_1, \chi_2, \dots, \chi_N \rangle$. We can now interpret the sums over the various indicies at each contraction as a sum over he various branching of different Feynman trajectories through the spin-chain. In this regard, we have produced a circuit is as a discrete real-time path integral with fixed initial and final condiions. However, if we are to calculate anything in this geometry, we must have an appropriate distribuion from which to draw each local gates, $u_{\tau,i,i+1}$. Since each gate lies in the unitary group $U(q^2)$, the most common and minimally structured circuits have each unitary sampled randomly and independently from the uniform distribution on the unitary

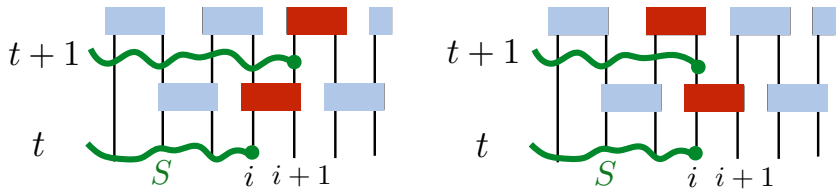

Figure 1.6: **Operator front dynamics**– An operator front in a random unitary circuit displays random walk dynamics. At each time step, application of a unitary gate can either extend or hold constant the length of the front with some probability p, leading to a random walk. Figure reproduced from [62].

group $U(q^2)$. This distribution, which has been mentioned before (see the discussion on RMT in sec 1.3), is called the Haar distribution. The generated random interactions produce a minimally structured imitation of dynamics non-integrable many-body systems.

This circuit can be enhanced in a number of ways. We can consider creating Floquet systems by imposing some periodicity in the unitaries, applying unitaries sparsely in random fashion rather that applying them at every spacetime point, intersperse measurements in the circuit, impose a space-time duality on the unitaries, relax the locality constraint, and more. In the following chapters, we will address many of these generalizations, with special attention paid to the imposition of global symmetries.

These simple 1+1D circuits without measuremrents are already increadibly useful models for the nonequilibrium dynamics present in thermalization of many-body systems [57–60]. One immediate consequence of the geometry presented is that operators can only spread ballistically, so that the Lieb-Robinson bound on operator spreading seems an almost-immediate consequence of the setup for this model. A more careful analysis can produce a particular maximum velocity and explain the exponential suppression for correlaions fallling outside the light cone through unlikely trajectories in the circuit[61]. Further, one can determine hydrodynamics in operator weight by noticing that the weight of operator strings from Eq. 1.53 must be conserved, so that $\sum_S |c_S(t)| = 1$, but at each time-step, an initially local operator will have a finite probability to spread further or move backwards as shown in Fig. 1.6. This leads to a random walk, describing a gaussian spreading of the front of operator weights that we will cover in more detail in the next chapter[62].

Replica Trick

As previously discussed, this tensor network descriptions to describe the average dynamics via a partition function enumerating weights for the various Feynman trajectories through the circuit. However, if we are to describe the evolution of a density matrix, $\hat{\rho}(t + \Delta t) = U_{\Delta t}\hat{\rho}(t)U_{\Delta t}^\dagger$, we must account for *two* simultaneous evolutions, one forwards in time, $U_{\delta t}$, and one backwards, $U_{\Delta t}^\dagger$. In the same fashion as above, we may calculate the quantity $\mathrm{Tr}[\hat{O}\hat{\rho}(t)]$ using a doubled circuit with U_t defining one layer, $U_t^\dagger$ the other, and the averaging is taken over both simultaneously so that the transfer matrix at each site, i, will the four component tensor $M_{ijkl} = (T_{\Delta t,i})_{ijkl} = \overline{(U_{\delta t,i}^\dagger)_{ij} \otimes (U_{\Delta t,i})_{kl}}$. Without any additional structure, averaging

over the Haar measure gives this transfer matrix a simple form:

$$M_{ijkl} = \int_{U(q^2)} dU U^{\dagger}_{ij} U_{kl} = \mathrm{Wg}(1,q)\delta_{ij}\delta_{kl} = \frac{\delta_{ij}\delta_{kl}}{q}, \tag{1.68}$$

where we have employed the Weingarten function $W(\sigma, q)$ that provides a weight for each potential paring of forwards and backwards unitaries[63]. To complete the calculation of $\mathrm{Tr}[\hat{O}\hat{\rho}(t)]$, we simply set the lower boundary to be $\hat{\rho}(0) = \sum_{\alpha} p_{\alpha} |\psi_1^{\alpha}, \psi_2^{\alpha}, \ldots, \psi_N^{\alpha}\rangle\langle\psi_1^{\alpha}, \psi_2^{\alpha}, \ldots, \psi_N^{\alpha}|$, and the upper boundary to be $\hat{O} = \sum_{\alpha,\beta} c_{\alpha\beta} |\phi_1^{\alpha}, \phi_2^{\alpha}, \ldots, \phi_N^{\alpha}\rangle\langle\phi_1^{\beta}, \phi_2^{\beta}, \ldots, \phi_N^{\beta}|$.

If we wish to calculate the evolution of higher powers of the density matrix, as is necessary for entanglement entropy, the OTOC, etc., we may do so by a clever pairing of multiple copies of the system using boundary conditions. When calculating the Feynman trajectories for n copies of the system, we will now have a transfer matrix of the form $T_{\Delta t} = \overline{\bigotimes_{i=1}^{n} \left[(U_{\Delta t}^{(i)})^{\dagger} \otimes U_{\Delta t}^{(i)} \right]}$, which will involve multiple different pairings of forwards and backwards unitaries with different weights given by the appropriate Weingerten function. These weights serve as transition probabilities, or be regarded as probabilities for particular spin configurations of a dual lattice. In this sense, one may treat the system evolution as a partition function, $\mathcal{Z}(\mathbf{m})$, over the different magnetic configurations, $\mathbf{m} = (m_1, \ldots, m_N)$, of this dual lattice as derived from these, N transition probabilities. This mapping will be made more precise in the Ch. 4, where additional symmetry constraints and measurements will be added to the circuit.

Nomenclature for Chapter 1

Selected Abbreviations

ETH Eigenstate Thermalization Hypothesis
MATE Macroscopic Thermal Equilibrium
MITE Microscopic Thermal Equilibrium
RMT Random Matrix Theory
OTOC Out-of-time-ordered correlator
MBL Many-Body Localization
RUC Random Unitary Circuit

Variables

Γ phase space point
$\mathcal{H}$ Hilbert Space
$\hat{\rho}$ density matrix $\hat{\rho} \in \mathcal{H}$
$\mathcal{H}_{E,N,\Lambda}$ the Hilbert space spanned by eigenstates of the Hamiltonian within a window ΔE, ΔN of the values E and N.
$D_{E,N,\Lambda}$ the dimension of the Hilbert space $\mathcal{H}_{E,N,\Lambda}$
$\mathcal{S}_X$ the set of all linearly independent, bounded operators with support on X
$\mathcal{S}_X^{(l)}$ the set of all linearly independent, l-local bounded operators with support on X

Chapter 2

Random Unitary Circuits with Symmetry

Haar-averaged random unitary circuits provide a fantastic toy model of chaotic systems with local interactions. However, most physical systems of interest are far from Haar-random, and instead have more structured on-site interactions. As a step towards understanding these more structured systems, we will now shift our focus to systems with symmetry present. We will begin by describing insights that have been gained from tractable calculations involving Haar-averaged RUC's with Abelian symmetries present. This has been the most common method of probing the effects of symmetry in dynamics. After this discussion, we will turn to an alternative averaging procedure that will prove strictly more general than Haar-averaging, and allow further insights. With it, one can establish a connection between random unitary circuits and quantum master equations. This framework can further be expanded to establish a duality between the dynamics described by this master equation and the spectral properties of a Hamiltonian in an equilibrium setting. This allows one to draw on the vast body of knowledge surrounding symmetry constraints in equilibrium to make predictions about dynamical phenomena. For convenience, moving forward, we will drop the hats added to operators unless there is a potential ambiguity of notation.

2.1 Haar-Averaged Random Unitary Circuits

In order for RUC's to be useful for calculations, one must employ a concrete measure over the space of random matrices in a circuit. By far the most practical measure is the Haar-measure, which, as mentioned above, is effectively the uniform measure over all matrices. Employing Haar-averaging, one can already establish a diffusive spread of operator weights in RUC's. This is diffusive spreading is the first effect of symmetry in the circuit framework and will provide insight into the effects of other symmetries when they are imposed. As such, let us trace the logic behind this aspect of operator dynamics in more detail.

2.1.1 Operator Hydrodynamics

Following [44], we will begin our investigation by decomposing an operator over a complete basis of exponentially many operator strings $O_S \in \mathcal{B}_{\mathcal{H}}$. For example, in a length L, spin-1/2 system $O_S = \sigma^{\mu_1} \otimes \sigma^{\mu_2} \otimes \cdots \otimes \sigma^{\mu_L}$ will be a string of Pauli matrices $S = (\mu_1, \mu_2, \ldots, \mu_L)$, with $\sigma^{\mu_i} = \{\mathbb{I}, \sigma^x, \sigma^y, \sigma^z\}$ for $\mu = 0, 1, 2, 3$. With such a complete basis, we may expand an arbitrary operator as in Eq. 1.52:

$$O(t) = \sum_S c_S(t) O_S. \tag{2.1}$$

Thus, the full dynamics can be described by examining the amplitudes and weights $c_S(t)$ and $|c_S(t)|^2$ in Eq. 1.53. Rather than attempt to calculate each individual term, however, we focus on a more coarse measure, given by the "right-weight" or "size distribution," $\rho_R(i,t)$. This is defined as the total weight of basis operators $O_S \in O(t)$ that have support ending at site, i, meaning that they act as the identity for all sites to the right of i. For concreteness, let us focus on the case of a spin chain of length, L, with local Hilbert space dimension, q, and local basis operators Σ^μ, where $\mu = 0, \ldots q^2 - 1$ indexes the different local basis operators and normalization follows from $\mathrm{Tr}[\Sigma^\mu \Sigma^n u]/q = \delta_{\mu\nu}$. Now, we may define $\rho_R(i,t)$ as the weight on all strings of the form $O_S \sim \left(\prod_{k<i+1} \Sigma^{\mu_i}\right) \mathbb{I}_{i+1} \ldots \mathbb{I}_L$:

$$\rho_R(i,t) = \sum_{\text{S terminating on site i}} |c_S|^2, \qquad \sum_i \rho_R(i,t) = 1. \tag{2.2}$$

Again, we have insisted on a normalization, such that $\mathrm{Tr}[O_S O_{S'}]/q^L = \delta_{SS'}$ and $c_S = \mathrm{Tr}[O(t) O_S]/q^L$. We recognize this second equality as nothing more than the unitarity constraint: $\sum_S |c_S(t)| = 1$. This allows us to treat $\rho_R(i,t)$ as a conserved density that can be shown to follow a biased diffusion equation[59, 64]. This can be understood if one considers the action of a 2-local random unitary gate, $U_{i,i+1}(\Delta t)$ acting on $\rho_R(i,t)$. First, we define the operator front on bonds such that the (right) front of an operator prior to unitary evolution as the position of the rightmost unitary gate that acts on non-identity states. From this, one can obtain the probabilities for the front to move forwards or backwards at each step. Under the Haar measure, the front gate will produce each of the $q^4 - 1$ non-identity 2-local operators with equal weight. This means that only $q^2 - 1$ of these states produced by $U_{i,i+1}(\Delta t)$ will include the identity on the rightmost site, $i + 1$. Since each of these results in the results in the front moving backwards by one step, we may define a probability for moving back as $p = \frac{1}{q^2+1}$. Due to the alternating layered structure of the brickwork circuit, this will appear as an operator front remaining on stationary when defined on lattice sites (See Figure 1.6).

Thus, we see that Haar averaging renders the dynamics of the operator front into a biased random walk with probability,p, for the front to retreat, and $1 - p$ to advance. From this, we can calculate the expected position of the front at time t, as $\langle x \rangle = (1 - 2p)t = v_B t$, where we define v_B as a *butterfly speed*. Similarly, the width of the front should grow diffusively as $\sim \sqrt{D_p t}$ with $D_p = \frac{1}{2}(1 - v_B^2) = 2p(1 - p)$ as the diffusivity of the biased random walk. Further, the front location can be described by some emergent biased random walk hydrodynamics [59, 64] with $\partial_t \rho_R(i,t) = v_B \partial_x \rho_R(i,t) + D_p \partial_x^2 \rho_R(i,t)$. In the scaling limit,

where $t, x \to \infty$, this means the density of the front should take the form:

$$\overline{\rho_R(x,t)} = \frac{1}{\sqrt{4\pi D_p t}} e^{\frac{(x-v_B t)^2}{4D_p t}}. \tag{2.3}$$

Note that if we take the limit $q \to \infty$, then we will reach a causal limit to the butterfly speed of $v_B \approx 1 - \frac{2}{q^2} \to 1$, and have a sharp front with vanishing diffusivity $D_p \approx \frac{2}{q^2} \to 0$. The central conservation law giving rise to diffusive dynamics comes from the unitarity constraint: $\sum_S |c_S(t)| = 1$. In other words, although a bare circuit has no conserved physical quantities, it must conserve probabilities over time. This large q limit will be useful in many circumstances to allow for analytical computations. In a sense, this limit renders the system more classical, as each local spin approximates a continuous parameter up to $1/q$ corrections.

The above discussion demonstrated how a notion of circuit locality paired with a local conserved quantity produced some notion of operator hydrodynamics in a random circuit. In fact, this diffusive broadening of the operator front is expected to be a generic feature of non-integrable quantum systems in one dimension. As we will see in the following sections, similar logic may be used to find another notion of operator hydrodynamics.

2.1.2 U(1)-Symmetric Dynamics

We may extend the framework above in a straightforward manner to systems that conserve an Abelian global symmetry. In keeping with [44], we will focus on the example of a U(1) symmetry for simplicity, as the following results will readily generalize. In order to implement this U(1) symmetry, we will adjoin a spin 1/2 particle to each lattice site. Now, with each site equipped with a qubit and a qudit of dimension q, we will label our local operators by $B_i^{\mu\nu} = \sigma_i^\mu \otimes \Sigma_i^\nu$, where σ^μ is lives in a space spanned by the Pauli matrices, $\sigma^\mu \in \{\mathbb{I}, \sigma^z, \sigma^+/\sqrt{2}, \sigma^-/\sqrt{2}\}$. Time evolution will be constrained to conserve the total z-component of the spin-1/2 particle. Now, each two-side unitary, $U_{i,i+1}(\Delta t)$ will be of size $4q^2 \times 4q^2$, and because of the symmetry, it will be broken up into block diagonal form.

$$U_{i,i+1}(\Delta t) = \begin{pmatrix} U^{\uparrow\uparrow}_{q^2\times q^2} & 0 & 0 \\ 0 & U^{(\uparrow\downarrow+\downarrow\uparrow)}_{2q^2\times 2q^2} & 0 \\ 0 & 0 & U^{\downarrow\downarrow}_{q^2\times q^2} \end{pmatrix}, \tag{2.4}$$

where the block $U^{\uparrow\uparrow}_{q^2\times q^2}$ preserves the with total z spin of +1. To complete the circuit, we simply treat each of these blocks independently as Haar-random matrices taken from U(q^4) or U($4q^2$). This has the pleasing physical interpretation of charge degrees of freedom interacting with a high-dimensional bath of randomly interacting degrees of freedom, as quantified by the local qudits. This is shown in Figure 2.1

The action of this circuit clearly acts differently on certain operators. For instance, by definition, if the total z-component of the spin-1/2 is conserved, then we may define an operator for this conserved total z-spin as

$$S^z_{tot} = \sum_i (\sigma^z \otimes \mathbb{I}_q)_i, \qquad U^\dagger(t) S^z_{tot} U(t) = S^z_{tot}. \tag{2.5}$$

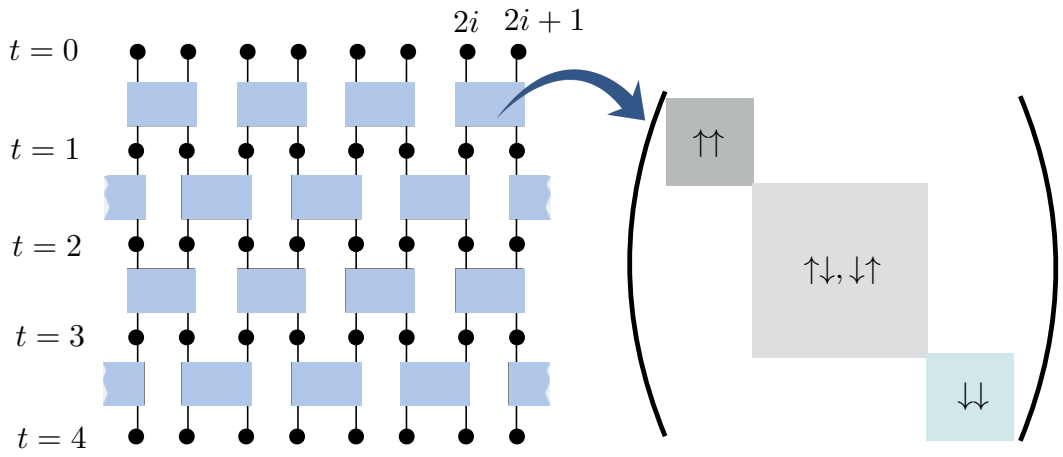

Figure 2.1: **Haar-averaged** U(1)**-circuit.** Left: a brickwork random unitary circuit. Each site (black dot) consists of the direct product of a two-state qubit and a q-state qudit. Each gate (blue box) locally conserves the total z-spin of the two qubits acted upon, S^z_{tot}. Right: the resultant block-diagonal form of the unitary, where each block within the gate chosen to be independently Haar-random. Original figure from [44]

.

We see that the local operators $(\mathbb{I}_2\otimes\mathbb{I}_q)_i(\mathbb{I}_2\otimes\mathbb{I}_q)_{i+1}$, $(\sigma^z\otimes\mathbb{I}_q)_i(\sigma^z\otimes\mathbb{I}_q)_{i+1}$, and $\Big[(\sigma^z\otimes\mathbb{I}_q)_i(\mathbb{I}_2\otimes\mathbb{I}_q)_{i+1}+(\mathbb{I}_2\otimes\mathbb{I}_q)_i(\sigma^z\otimes\mathbb{I}_q)_{i+1}\Big]/\sqrt{2}$ are also preserved by the dynamics.

Further still, the symmetry implies that the total z-spin should be conserved such, for an initially localized operator,$O(t)$,

$$\langle S^z_{tot}\rangle_{O(t)} = \frac{\mathrm{Tr}[O(t)S^z_{tot}]}{(2q)^L} = \frac{\mathrm{Tr}[O(0)S^z_{tot}]}{(2q)^L} = \langle S^z_{tot}\rangle_{O(0)}. \tag{2.6}$$

This implies a constant total charge throughout the system. If the charge is initially localized to some small region, then generically, we would expect it to diffuse to a uniform spread as $\langle(\sigma^z\otimes\mathbb{I}_q)_x\rangle \sim \frac{1}{\sqrt{t}}e^{x^2/(Dt)}$.

To make this more precise, we consider the amplitudes associated with local S^z_i operators, as these should play the role of localized charges. The amplitude for a single S^z_i operators is given by

$$c^c_i(t) \equiv \frac{\mathrm{Tr}[O(t)S^z_i]}{(2q)^L}. \tag{2.7}$$

With this definition, we see that we can decompose $O(t)$ into two components. The conserved sector, $O^c(t)$ is given by all of the overlap with local charge such that $O^c(t) = \sum_i c^c_i(t)(\sigma^z\otimes\mathbb{I}_q)_i$. And the non-conserved sector comprises the rest of the operator, $O^{nc}(t) = O(t) - O^c(t)$. From Eq. 2.6, we see that

$$\sum_i c^c_i(t) = \text{Const.} \tag{2.8}$$

The resultant operator dynamics will come from the interplay of charge conservation, placing a constraint on the dynamics of the L local operator *amplitudes* through Eq. 2.8. However, this will compete with the unitarity constraint that restricts a density of operator *weights* over all strings, as shown in Eq. 2.2.

At this stage, a brief note is in order. One must be cautious to realize that the charge transport described here is incoherent over all timescales. This is because we study slow transport at the level of operators, such that the behavior of single particle Green's functions like $\langle \sigma_r^- \sigma_0^+(t) \rangle$, where σ_r^+ creates a particle at position r, will not produce the same dynamics. In fact, under the dynamics considered, this term should vanish exponentially quickly, independent of the initial state of the system.

With this clarified, let us attempt to derive the expected hydrodynamics for these operator amplitudes. At each time step, unitaries equally distribute charges across their two site support such that

$$\overline{c_i^c(t+\Delta t)} = \overline{c_{i+1}^c(t+\Delta t)} = \frac{\overline{c_i^c(t)} + \overline{c_i^c(t)}}{2}. \tag{2.9}$$

This is an immediate consequence of the conservation law because the operator $\frac{1}{\sqrt{2}}\Big[(\sigma^z \otimes \mathbb{I}_q)_i(\mathbb{I}_2 \otimes \mathbb{I}_q)_{i+1} + (\mathbb{I}_2 \otimes \mathbb{I}_q)_i(\sigma^z \otimes \mathbb{I}_q)_{i+1}\Big]$ is left invariant, and has an amplitude given by $c_i^c(t) + c_{i+1}^c(t)$. In contrast, the operator $\frac{1}{\sqrt{2}}\Big[(\sigma^z \otimes \mathbb{I}_q)_i(\mathbb{I}_2 \otimes \mathbb{I}_q)_{i+1} - (\mathbb{I}_2 \otimes \mathbb{I}_q)_i(\sigma^z \otimes \mathbb{I}_q)_{i+1}\Big]$ does not have a conserved amplitude, and should rapidly vanish.[1]. This smoothing of charge over time results in a late time distribution of the form

$$\overline{c^c(x,t)} = \frac{1}{\sqrt{2\pi t}} e^{-x^2/2t}. \tag{2.10}$$

This is nothing more than simple charge diffusion with a diffusion coefficient of $D_c = 1/2$. Thus, we see that amplitudes of operators that are diagonal in the symmetry basis relax to a uniform equilibrium distribution with a timescale $t \sim L^{-2}$. In contrast, off-diagonal operators rapidly decay to small values and fluctuate around the average equilibrium value of 0. Thus, if we choose the symmetry basis, we recover relaxation behavior reminiscent of the ETH. Following this further, we see that the general form of the steady state should be that of a Gibbs ensemble of the form

$$\rho_\mu = \frac{e^{-\mu Q}}{\mathrm{Tr}[e^{-\mu Q}]}, \tag{2.11}$$

where μ will be determined by the initial charge distribution, and we have switched from a representation in terms of total charge, $Q_i = (\mathbb{I}_i - \sigma_i^z)/2$, so that total charge runs from 0 to $2L$. If we take the result from Eq. 2.10, then we can deduce a diffusion constant depending on the chemical potential, μ from

$$\mathbb{E}[\langle Q_x(0)Q_x(t)\rangle_\mu - \langle Q_x(t)\rangle_\mu^2] \underset{t\to\infty}{=} \frac{1}{\sqrt{\pi t}} \frac{1}{4\cosh^2(\mu/2)} = \frac{1}{\sqrt{\pi D(\mu) t}}. \tag{2.12}$$

[1] It is clear that this amplitude should vanish after one timestep in the $q \to \infty$ limit, and it can be shown that the resultant dynamics is exact for all q[44]

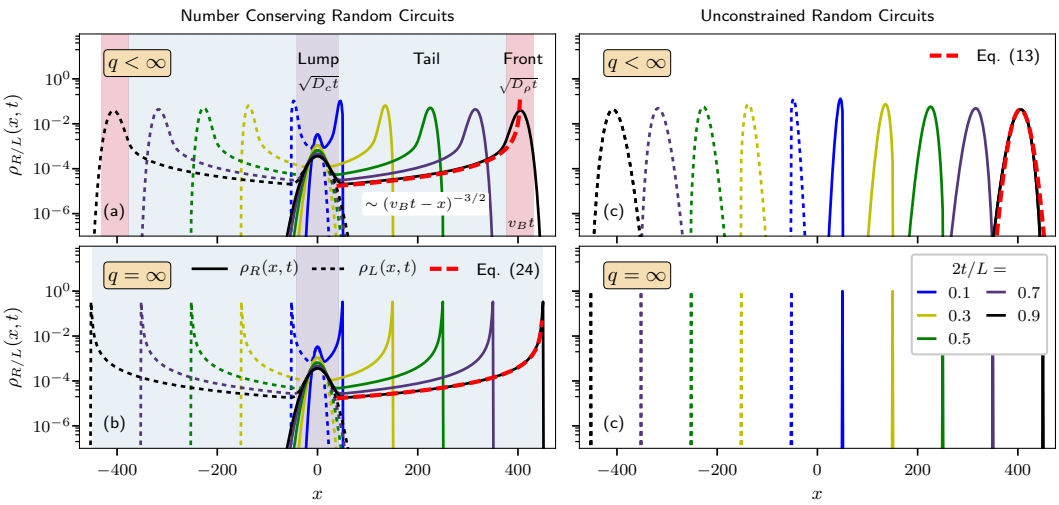

Figure 2.2: **Operator profiles at different times** Plots of $\rho_R(x,t)$ the distribution of operator weight for all operators that have right-most support on site x. Right: An unconstrained circuit, showing a ballistilally moving operator front whose profile diffuses over time. Left: A circuit with a U(1)-symmetry constraint demonstrating a lump of diffusing conserved charges, a ballistic front with diffusing profile, and a tail connecting the two. Original figure from [44]

This yields a notion of an effective diffusion constant $D(\mu) = 4\cosh^2(\mu/2)$[65]. Although there is no notion of conserved energy in these RUC's, the Gibbs form is reminiscent of the canonical distribution. By dimensional analysis or comparison with the grand canonical ensemble, we see that μ should scale with β, resulting in a prediction that this diffusion from incoherent charge transport should be faster at lower temperatures.

This diffusion of conserved amplitudes causes an interesting profile for operator spreading. If we initialize our system with a local operator mid-chain, $O(t=0) = \sigma^z_{x=L/2}$, there will now be a competition between the amplitude conservation, $\sum_x c^c_x(t) = 1$, from the spin/charge symmetry, and weight conservation, $\sum_x \rho_R(x,t) = 1$, from unitarity. Note that, while the sum of conserved amplitudes is constant. The sum of their weights, is not. In fact, from Eq. 2.10, it follows that $\sum_x |c^c(x,t)|^2 \sim \frac{1}{\sqrt{t}}$. Thus, we note there will be a transfer of weight from conserved operators to "non-conserved" operators over time. Recalling from section 2.1.1, these non-conserved operators should spread ballistically with a diffusing front profile. As such, we can identify three distinct regions in our operator spreading profile at late times with a U(1)-symmetry. As shown in Fig. 2.2, we will have a central region of diffusing conserved operators, a ballistic front whose profile is also diffusing, and a tail of non-conserved operators leaking from the lump of diffusing conserved ones in the center.

2.1.3 Discrete Symmetries and Limitations of Haar Averaging

The previous section demonstrated that Haar-averaged RUC's may effectively describe continuous Abelian symmetries. However, we seem to have skipped over the simpler case of

discrete symmetries. Before moving on to a different circuit framework, let us consider how these might be handled.

Naively, one might assume that we need only carry out the same procedure as above: decompose the local uniaries into block diagonal form and Haar-average within the different sectors. Yet, as we shall see, there is an obstruction to doing so.

Previously, we could decompose our unitary action by searching for the sectors that commuted with our symmetry generator. For the U(1) case above, this meant examining the commutation, $[U_{i,i+1}(\Delta t), S^z_{tot}] = 0$. however, because $S^z_{tot} = \sum_i \sigma^z_i$, we needed only consider the commutator with local terms $\sigma^z_i + \sigma^z_{i+1}$. Turning to the discrete case, if we have a simple $\mathbb{Z}_2$ symmetry defined by $P_2 = \bigotimes_i \sigma^z_i = \pm 1$, then we require that $[U_{\Delta t, P_2}] = 0$. However, in this case, we may no longer focus on the local terms from P_2. This discrete symmetry has imposed a highly non-local constraint on each individual unitary. Since this is a constraint of the full dynamics at a time-step, there is no clear way to enact this constraint on each unitary while leaving them to be independently drawn from the Haar-measure.

Setting aside the use of Haar-averaging, we can predict the effects of such a simple constraint on a generic random circuit. It will divide the full system into two, non-interacting symmetry sectors, and thus there will be two distinct steady states, $\mathbb{I}$ and P_2. If we impose a local $\mathbb{Z}_2$ symmetry on each bond, we will be able to make use of our Haar-averaging procedure as above, however, this will involve an extensive number of conserved quantities and will result in an exponential number of ground states. Such a system will generically be non-thermalizing, as discussed in Ch. 1.

However, this is not the only limitation of Haar-averaging. If, for example, we were aware of certain physically forbidden transitions, there is no straightforward way to incorporate this constraint into the Haar-averaged circuit. Below, we will discuss a different random circuit model that allows for just such additional structure.

2.2 Effective Hamiltonian via Brownian Averaging

Although Haar-averaging is powerful, as has been shown, it can be inflexible for certain applications. In particular, since it treats all potential interactions equally, it is a bit cumbersome when one wishes to input symmetries with non-local generators or other dynamical constraints. In contrast, in this section, we will introduce the notion of Brownian Hamiltonian Evolution (BHE).

Brownian Circuits

To begin with, we will remain in the quantum circuit formalism. Again, each unitary operator will be drawn randomly, however, we will focus on cases of infinitesimal evolution such that we may expand the unitary, $U_{\delta t} = e^{-iH_t \delta t} = \mathbb{I} + iH_t \delta t + \dots$. We introduce randomness into this Brownian circuit via random variables, $\{dB_i\}$ for the time-slice $[t, t + \Delta t)$ such that the first moment $\mathbb{E}[dB_i] = 0$ and the second moment $\mathbb{E}[dB_i dB_j] = \frac{\delta_{ij}}{\Delta t}$. Using these variables, the Hamiltonian at time slice $[t, t + \Delta)$ is defined as

$$H_t \equiv \sum_i h_i \, dB_{i,t}, \tag{2.13}$$

defined via interaction terms h_i and Brownian random variables $dB_{t,i}$ at each time slice $[t, t+\Delta t)$. Here, the label $i = (\boldsymbol{x}, \lambda)$ encodes both the spatial support and operator type of h_i. Under this time evolution, a density matrix $\rho(t)$ evolves as

$$\begin{aligned} e^{-iH_t\Delta t}\rho_t e^{iH_t\Delta t} &= \rho_t - i\Delta t \sum_i [h_i, \rho_t] dB_i \\ &\quad - \frac{(\Delta t)^2}{2} \sum_{i,j} [h_i, [h_j, \rho_t]] dB_i \, dB_j + \cdots . \end{aligned} \tag{2.14}$$

This allows one to characterize the expected continuous-time dynamics of ρ_t by averaging the infinitesimal time evolution over the random variables. The leading order operator evolution becomes

$$\begin{aligned} \mathbb{E}[\partial_\tau \rho] &\equiv \lim_{\Delta t \to 0} \frac{\mathbb{E}[\rho_{t+\Delta t} - \rho_t]}{\Delta t} \\ &= -\frac{1}{2} \sum_i [h_i, [h_i, \rho]] \\ &= -\frac{1}{2} \sum_i (h_i^2 \rho - 2 h_i \rho h_i + \rho h_i^2) = \mathcal{L}[\rho], \end{aligned} \tag{2.15}$$

where $\mathcal{L}$ is a superoperator called the Lindblandian. We now have a connection between the flexibility of the continuous-time master equation formalism and the computational benefits of the random circuits.

Before moving on, we note that we can easily recover the notion of Haar-averaging by simply insisting that there is only one interaction term that includes all 2-local operators, $h_i = h_{\mathbf{x}} = \sum_\lambda O_{\mathbf{x},\lambda}$, and thus, only one local $dB_i = dB_{\mathbf{x}}$. The resultant dynamics simply includes all allowable transitions. Thus, we see that Brownian averaging is strictly more general that he Haar-averaged case. In fact, the Brownian framework allows us to address some cases that were impossible to describe with Haar averaging. Let us return to the issue of discrete symmetries. This time, we will consider the $\mathbb{Z}_2 \times \mathbb{Z}_2$ symmetry on a spin-1/2 chain generated by $P_2^{(x)} = \bigotimes_i \sigma_i^x$ and $P_2^{(z)} = \bigotimes_i \sigma_i^x$. We will assume an even number of sites so that these symmetries commute. In this case, we can impose the constraints on the unitaries by restricting the form of h_i as follows

$$[U_{i,i+1}(\Delta t), P_2^{(x/z)}] = 0 \quad \Rightarrow \quad h_i \in \{\sigma_i^x \sigma_{i+1}^x, \sigma_i^y \sigma_{i+1}^y, \sigma_i^z \sigma_{i+1}^z\}. \tag{2.16}$$

From this, one may perform a similar calculation to describe the dynamics of $\rho_R(i,t)$, revealing biased random walk behavior parallel to that of circuits without discrete symmetries. If we consider an operator with support on site i, it must be some linear combination of the Pauli matrices: $\sigma_i^\mu \mathbb{I}_{i+1}$, where two of the three interactions terms can cause the operator to grow.[2]

[2]Note that one need be a bit careful to include superpositions when selecting the interactions to generate this biased random walk. Only interaction terms that are a superposition of these three terms will cause growth. If $h_i = \sigma_i^\mu \sigma_{i+1}^\mu$ for fixed $\mu = \{0, x, y, z\}$, the dynamics will be trivial.

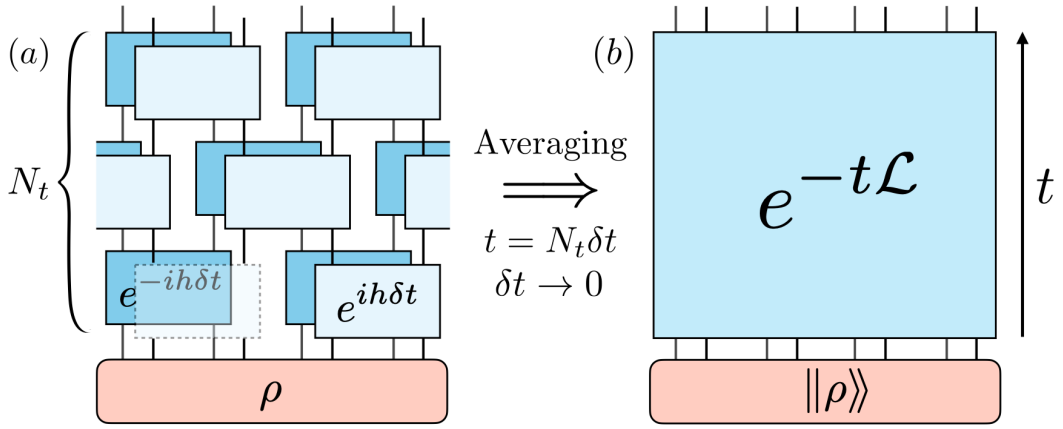

Figure 2.3: **Brownian circuit and effective Hamiltonian.** Mapping (a) random operator dynamics to (b) imaginary-time evolution by an effective Hamiltonian $\mathcal{L}$ in a doubled Hilbert space. On the left, an operator ρ is evolved by a local Hamiltonian $H_t \equiv \sum_i h_i dB_{i,t}$ with Brownian random variable dB. Overlapping blocks for forward/backward evolution (dark/light) share the same Brownian variable, but all other Brownian variables are independently drawn from Gaussian distributions. On the right, we average over random variables while taking time-steps to zero; this produces imaginary-time Schrödinger evolution by a Lindbladian operator. Figure reproduced from [44].

2.2.1 Brownian Hamiltonian Evolution and Effective Hamiltonians

As shown above, using Brownian Hamiltonian Evolution, we will have more control over the types of interactions available to be considered within a dynamical system. In addition, this new framing will allow a novel interpretation of the averaged dynamics. When examined in a doubled Hilbert space, once can cast the averaged Heisenberg evolution of a density operator, as determined by the Lindbladian superoperator, into a deterministic Schrödinger evolution dictated by an effective Hamiltonian. We briefly alluded to this fact in Sec. 1.4.2, while discussing the Lindblad equation, but now we treat this mapping more formally.

Choi Isomorphism and the Doubled Hilbert Space Formalism

We begin by constructing an alternative description of the operator dynamics from Eq. 2.15. This is accomplished by employing the Choi isomorphism, a mapping from an operator acting on the Hilbert space $\mathcal{H}$ to a state defined on the doubled Hilbert space $\mathcal{H}_u \otimes \mathcal{H}_l$, where subscripts u, l are introduced to distinguish two copies of $\mathcal{H}$. For a given Hermitian operator $O = \sum_j \lambda_j |\psi_j\rangle\langle\psi_j|$ acting on the Hilbert space $\mathcal{H}$ (such as a physical observable or density matrix), the Choi state $\|O\rangle\rangle$ [66, 67] is defined in a doubled Hilbert space $\mathcal{H}_d = \mathcal{H}_u \otimes \mathcal{H}_l$ as

follows:

$$\begin{aligned}\|\mathbb{I}\rangle\rangle &:= \sum_i |i\rangle_u \otimes |i\rangle_l \\ \|O\rangle\rangle &:= (\mathbb{I}\otimes O)\|\mathbb{I}\rangle\rangle = \sum_i |i\rangle_u \otimes O|i\rangle_l \\ &= \sum_f \lambda_j |\psi_j^*\rangle_u \otimes |\psi_j\rangle_l = (O^T\otimes\mathbb{I})\|\mathbb{I}\rangle\rangle. \end{aligned} \tag{2.17}$$

Note that it immediately follows that $(A\otimes B)\|\mathbb{I}\rangle\rangle = (AB^T\otimes\mathbb{I})\|\mathbb{I}\rangle\rangle = (\mathbb{I}\otimes BA^T)\|\mathbb{I}\rangle\rangle$. Therefore, under Choi Isomorphism, $AOB \mapsto (B^T\otimes A)\|O\rangle\rangle$. Now, for a given Choi state $\|O\rangle\rangle$, its operator form can then be obtained by taking an overlap with states $\|i,j\rangle\rangle \equiv |i\rangle\otimes|j\rangle \in \mathcal{H}_d$:

$$\langle\langle i,j\|O\rangle\rangle = \langle j|O|i\rangle. \tag{2.18}$$

The Choi state automatically respects the following symmetry:

$$\mathrm{SWAP}^* \equiv \mathcal{C}\circ\mathrm{SWAP}, \tag{2.19}$$

where the SWAP symmetry exchanges $\mathcal{H}_u$ and $\mathcal{H}_l$, and $\mathcal{C}$ is the complex-conjugation symmetry. This operation corresponds to Hermitian conjugation in the operator language.

Similarly, under the Choi isomorphism, a quantum channel acting on the space of linear operators defined on $\mathcal{H}$ would map into a linear operator (not necessarily Hermitian) defined on $\mathcal{H}_d$, namely the *Choi operator*. For a generic quantum channel $\mathcal{E}$ with Kraus representation $\{K_i\}$ ($\mathcal{E}:\rho\mapsto\sum_i K_i\rho K_i^\dagger$), its Choi operator form is defined as the following:

$$\mathcal{E}\mapsto\hat{\mathcal{E}} \equiv \sum_i K_i^*\otimes K_i. \tag{2.20}$$

For example, the averaged action of the Brownian time evolution in Eq. 2.15, the Lindbladian superoperator $\mathcal{L}$ maps to a linear operator $\hat{H}_\mathcal{L}$ acting on the doubled Hilbert space:

$$\hat{H}_\mathcal{L} = \frac{1}{2}\sum_i \left|h_i^T\otimes\mathbb{I}-\mathbb{I}\otimes h_i\right|^2 \equiv \frac{1}{2}\sum_{\boldsymbol{x},\lambda}\mathcal{O}_{\boldsymbol{x},\lambda}^\dagger\mathcal{O}_{\boldsymbol{x},\lambda}. \tag{2.21}$$

where $|\dots|^2$ should be understood as $(\dots)^\dagger(\dots)$, and we have defined an operator, $\mathcal{O}_{\boldsymbol{x},\lambda} = (h_{\boldsymbol{x},\lambda}^T\otimes\mathbb{I}-\mathbb{I}\otimes h_{\boldsymbol{x},\lambda})$, that we will henceforth refer to as a *commutor* (because it represents the operation of commutation with $h_{\boldsymbol{x},\lambda}$). The average dynamics in Eq. (2.15) can then be recast into an imaginary time evolution generated by the effective Hamiltonian $\hat{H}_\mathcal{L}$:

$$\partial_t\|O\rangle\rangle = -\hat{H}_\mathcal{L}\|O\rangle\rangle \quad\Rightarrow\quad \|O(t)\rangle\rangle = e^{-t\hat{H}_\mathcal{L}}\|O_0\rangle\rangle. \tag{2.22}$$

With this, we now have a generic map from a problem in a non-equilibrium setting using a quantum master equation to an equilibrium problem described by an imaginary-time Hamiltonian. In fact, the time evolution now resembles a Boltzmann weight with the time playing the role of β. With this analogy in mind, we turn to the familiar realm of low-temperature physics, corresponding to late times.

2.3 Late-Time Dynamics and Low-Energy Modes

More precisely, we are interested in the dynamics of a local operator O under Brownian evolution, which we characterize by the averaged auto-correlation function $\mathbb{E}\langle O_{\boldsymbol{y}}(0)O_{\boldsymbol{x}}(t)\rangle_\rho$ [3] with respect to the maximally mixed state $\rho = \frac{1}{D}\mathbb{I}$, where D is the dimension of the many-body Hilbert space.

Note that Eq. (2.21) is translation invariant, since if $T_{\boldsymbol{a}}$ is the translation operator by $\boldsymbol{a}$ in the original Hilbert space, $\tilde{T}_{\boldsymbol{a}} = T_{\boldsymbol{a}} \otimes T_{\boldsymbol{a}}$ leaves $\hat{H}_{\mathcal{L}}$ invariant. Therefore, we can label the eigenstates of $\hat{H}_{\mathcal{L}}$ by their momentum; let $\|\boldsymbol{k},\nu\rangle\!\rangle$ be the eigenstates of $\hat{H}_{\mathcal{L}}$ with energy $E_{\boldsymbol{k},\nu}$, carrying momentum $\boldsymbol{k}$ and an additional label ν. Inserting a completeness relation, we obtain

$$\begin{aligned}\mathbb{E}\langle O_{\boldsymbol{y}}(0)O_{\boldsymbol{x}}(t)\rangle_\rho &= \frac{1}{D}\langle\!\langle O_{\boldsymbol{y}}(0)\|e^{-t\hat{H}_{\mathcal{L}}}\|O_{\boldsymbol{x}}(0)\rangle\!\rangle \\ &= \frac{1}{D}\sum_{\boldsymbol{k},\nu} e^{-tE_{\boldsymbol{k},\nu}} e^{i\boldsymbol{k}\cdot(\boldsymbol{y}-\boldsymbol{x})} |\langle\!\langle \boldsymbol{k},\nu\|O_{\boldsymbol{x}}\rangle\!\rangle|^2. \end{aligned} \tag{2.23}$$

This form has some immediate consequences. Consider a d-dimensional system. In general, with no constraints other than translation invariance, one should expect a gapped spectrum with a ground state at zero momentum. The steady state, corresponding to the ground state of $\hat{H}_{\mathcal{L}}$, will determine the infinite time behavior of this autocorrelation, this (mass) gap, ΔE will result in an exponential decay of all non-steady states since,

$$\begin{aligned}\mathbb{E}\langle O_{\boldsymbol{y}}(0)O_{\boldsymbol{x}}(t)\rangle_\rho &= \frac{1}{D}\left(|\langle\!\langle \Omega\|O_{\boldsymbol{x}}\rangle\!\rangle|^2 + \sum_{\boldsymbol{k},\nu\neq\Omega} e^{-tE_{\boldsymbol{k},\nu}} e^{i\boldsymbol{k}\cdot(\boldsymbol{y}-\boldsymbol{x})} |\langle\!\langle \boldsymbol{k},\nu\|O_{\boldsymbol{x}}\rangle\!\rangle|^2\right) \\ &= \frac{1}{D}\left(|\langle\!\langle \Omega\|O_{\boldsymbol{x}}\rangle\!\rangle|^2 + e^{-t\Delta E}\sum_{\boldsymbol{k},\nu\neq\Omega} e^{-t(E_{\boldsymbol{k},\nu}-\Delta E)} e^{i\boldsymbol{k}\cdot(\boldsymbol{y}-\boldsymbol{x})} |\langle\!\langle \boldsymbol{k},\nu\|O_{\boldsymbol{x}}\rangle\!\rangle|^2\right) \end{aligned} \tag{2.24}$$

where we have defined $\|\Omega\rangle\!\rangle$ as the ground state of the system, for which $\mathbf{k} = 0$ and $E_\Omega = 0$. Further, the second term should be bounded by the product of an exponential and polynomial scaling with t: $e^{-t\Delta E}\mathrm{Poly}(t)$.

The situation changes drastically if one assumes a gapless spectrum. Let us consider a gapless dispersion $\min_\nu\{E_{\boldsymbol{k},\nu}\} \sim k^n$ at low momentum $\boldsymbol{k}\to 0$. Since the other states are no longer exponentially suppressed, we now have to be careful about the other terms in Eq. 2.23. Since $O_{\boldsymbol{x}}$ is local, the overlap $\langle\!\langle \boldsymbol{k},\nu\|O\rangle\!\rangle = \mathrm{tr}(OX_{k,\nu})$ should be near constant for small k, where $X_{k,\nu}$ is the operator corresponding to the Choi state $\|\boldsymbol{k},\nu\rangle\!\rangle$. Given this, the autocorrelation at $x = y$ decays algebraically as

$$\mathbb{E}\langle O_{\boldsymbol{x}}(t)O_{\boldsymbol{x}}(0)\rangle_\rho \underset{t\to\infty}{\sim} \int_k e^{-tk^n}\,\mathrm{d}^d\boldsymbol{k} \sim t^{-d/n}, \tag{2.25}$$

implying that the autocorrelation function can now be characterized by a dynamical exponent $z = n$. Therefore, the study of non-trivial late-time operator dynamics in the Brownian

[3] It measures the spreading of an operator O located at $\mathbf{x}$ at time t by measuring its overlap with an operator at $\mathbf{y}$.

evolution reduces to the identification of gapless dispersing states in the effective Hamiltonian $\hat{\mathcal{H}}_{\mathcal{L}}$.

Where might this gappless spectrum come from? An immediately apparent mechanism for the appearance of such gapless modes comes in the form of *spontaneous symmetry breaking* (SSB). However, as we will discuss at the end of the chapter, this will be a slightly different form of SSB than in generic physical systems

Symmetry Breaking and the Goldstone Theorem

We will take a small digression to describe the phenomenon of spontaneous symmetry breaking and its relation to goldstone modes. for the purposes of this work, we will limit ourselves to the case of continuous, global, internal symmetries.

Spontaneous symmetry breaking is a familiar concept from classical physics. There, in the thermodynamic limit, the ground state of a system no longer satisfies the same symmetry as the system itself. In quantum theory, this cannot happen. The true ground state will always satisfy the full system symmetry, however, when SSB does occur, there will be a degenerate manifold of exponentially close states that are locally distinct and related by the symmetry transformation.

Let us be a bit more precise. Let us consider a symmetry group for our system, G. The action of each element, $g \in G$ is represented by a unitary transformation $U(g) \in \mathcal{H}$. Conceptually, we expect that the symmetry of a physical ground state $|\Omega\rangle$ can be lower than G, and when this is the case, we say G is *spontaneously broken*. An element $h_b \in G$ will be called broken if $\hat{h}_b|\Omega\rangle$ does not equal the ground state itself. i.e.

$$\hat{h}_b|\Omega\rangle = e^{-\theta Q_{h_b}}|\Omega\rangle \neq |\Omega\rangle, \tag{2.26}$$

where Q_{h_b} is the symmetry generator corresponding to h_b. Now, if we consider the set of unbroken symmetries, $h_u \in G$ ($e^{-\theta Q_{h_u}}|\Omega\rangle = |\Omega\rangle$), these symmetries forms a subgroup H_u of G. The broken elements of G will be the subset defined by G $\setminus H_u$. Spontaneous breaking of the symmetry G down to $H_u \subset G$ produces a degeneracy in the ground state, that is defined by the coset space, G/H. We can then count the number of broken generators as $n_{BG} = \dim[G/H] = \dim[G] - \dim[H]$

The existence of SSB can also be detected by the emergence of a finite order parameter. This will be a quantity arising from the commutation of the symmetry generator with a local field $\Phi(x)$, such that $\langle\Omega|[Q_\alpha, \Phi]|\Omega\rangle \neq 0$. Here, when an order parameter arises from a commutation with the generator Q_α, we say that this generator is broken.

If we consider the action of a continuous symmetry (i.e. G is a Lie Group), Noether's theorem, will define a notion of a conserved current for local charges defined by the order parameter: $\partial q^\alpha(x,t) + \nabla \cdot \mathbf{j}^\alpha(x,t)$. The long-wavelength fluctuations in the order parameter result in gapless modes called *Nambu–Goldstone modes* (NGMs), or Goldstone modes. The number of modes and their dispersion will be a function of the number of symmetry generators broken. These modes can be classified as Type A, which typically have a linear dispersion ($E_k \sim |\mathbf{k}|$), or type B, which typically have a quadratic dispersion ($E_k \sim \mathbf{k}^2$). Further, the number of these modes follows a simple pattern[68]:

$$n_A = n_{BG} - 2n_B. \tag{2.27}$$

The number of each can further be identified with a number of broken symmetry generators. The number of Type B modes is obtained from the rank of a real, antisymmetric matrix[68]

$$\rho_{ij} \equiv -i\frac{1}{V}\langle\Omega|[Q_i, Q_j]|\Omega\rangle = \sum_k f_{ij}^k \frac{\langle\Omega|Q_k|\Omega\rangle}{V}, \tag{2.28}$$

where V is the volume of the system, $|\Omega\rangle$ is the system ground state, and we have employed structural constants in using The relation $[Q_i, Q_j] = i\sum_k f_{ij}^k Q_k$. As can be seen from the form of ρ_{ij}, Type B modes arise from pairs of broken generators, and their number should be given by $\frac{1}{2}\text{rank}\rho_{ij}$. All other broken generators will then give rise to type A goldstone modes.

As an example, let us consider the symmetry breaking present in the spin-1/2 Heisenberg chains:

$$H = J\sum_x \vec{\sigma}_x \cdot \vec{\sigma}_{x+1}. \tag{2.29}$$

This model has a full spin rotation symmetry, where $G = SO(3)$ is generated the three total spin operators $S_{tot}^i = \sum_x \sigma_x^i$ with $(i = x, y, z)$.

When $J < 0$, the ground state has a ferromagnetic order, which can be seen with the order parameter of magnetization in a given direction that we arbitrarily align with the z-axis: $\langle\vec{\sigma}_i\rangle = (0, 0, m_z)^T$ with $m_z > 0$. The antisymmetric matrix has the simple structure that $\rho_{xy} = -\rho_{yx} = m_z$, with all other entries zero, so that $\text{rank}\rho_{ij} = 2$. We see that both S_{tot}^x and S_{tot}^y are spontaneously broken, so we have that $n_{BG} = 2$ and the unbroken symmetry is $H_u = SO(2)$ generated by S_{tot}^z, which could point anywhere on the two-sphere S^2. According to Eq. 2.27, we should expect one type B mode with quadratic dispersion. Indeed, linearized spin-wave theory predicts just that. [69]

When $J > 0$, the ground state has a anti-ferromagnetic order, described by a vanishing magnetization, but a finite Néel order again defined arbitrarily to align with the z-axis: $\langle\vec{\sigma}_x\rangle = (-1)^x(0, 0, m_z)^T$ with $m_z > 0$. Just as before, both S_{tot}^x and S_{tot}^y are spontaneously broken ($n_{BG} = 2$), leaving the unbroken symmetry is $H_u = SO(2)$ generated by S_{tot}^z. However, due to the opposite magnetization of neighboring spins in the ground states, all the entries of ρ_{ij} are zero. According to Eq. 2.27, we should then expect two type A modes with linear dispersion. And again, this matches the prediction from linearized spin-wave theory. [69]

We now return to the symmetries present in our effective Hamiltonian, $\hat{H}_{\mathcal{L}}$.

2.3.1 Symmetries of the effective Hamiltonian and its ground state

Because of the doubled Hilbert space, $\hat{H}_{\mathcal{L}}$ seemingly can can host twice as many symmetries as a Hamiltonian living in the original Hilbert space, $\mathcal{H}$. When the symmetry is doubled, or acts independently on each Hilbert space, it is called a *Strong Symmetry*. When the symmetry for dynamics is not doubled and is shared between the two spaces instead, it is called a *Weak Symmetry*. As we shall see, strong symmetries of the original dynamics will appear as distinct ground states of $H_{\mathcal{L}}$ because they form a commutant algebra.

Let us be a bit more precise. Let G be the symmetry group acting on the original Hilbert space $\mathcal{H}$. Then, the Choi state can host a doubled symmetry group $G_u \times G_l$. We remark that the symmetry representation of $g \in G$ in the upper Hilbert space, $\mathcal{H}_u$, is defined as a complex-conjugated version of the original representation, $U^*(g)$. Accordingly,

$$|\Psi\rangle \mapsto (U^*(g_u) \otimes U(g_l))|\Psi\rangle \quad \forall g_u \cdot g_l \in G_u \times G_l. \tag{2.30}$$

For concreteness, let us discuss the two cases of strong and weak symmetry in our setup.

Strong Symmetry

First, we consider the case of strong symmetry. Here, we assume that each h_i in the original Hamiltonian exhibits a U(1) charge conservation symmetry. In the doubled Hilbert space, the symmetry is doubled as above, and the effective Hamiltonian $\hat{H}_{\mathcal{L}}$ in Eq. (2.21) must be symmetric under $G = \mathrm{U}(1)_u \times \mathrm{U}(1)_l$. We denote by G_{diag} and G_{off} the diagonal and off-diagonal subgroups of G, generated by $g_{\text{diag/off}} = (\hat{Q}_u \otimes \mathbb{I} \mp \mathbb{I} \otimes \hat{Q}_l)/2$, where $\hat{Q}$ is the total charge operator.

First, we examine the ground states of $\hat{H}_{\mathcal{L}}$. From the form of Eq. 2.21, we know that $\hat{H}_{\mathcal{L}}$ is positive semidefinite because it is the sum of squared operators. Thus, if we find any state with zero eigenvalue, it will automatically be a ground state of the effective Hamiltonian. This can be done quickly if we recall that the commutors defined in Eq. 2.21 enact a commutation with interaction terms, $h_{\mathbf{x},\lambda}$. There is a clear choice of operator that commutes with any other: the identity. The Choi state of the identity operator $\|\mathbb{I}\rangle\rangle$ then satisfies $\hat{H}_{\mathcal{L}}\|\mathbb{I}\rangle\rangle = 0$ and is thus a ground state of $\hat{H}_{\mathcal{L}}$.

However, it is not the only ground state. By definition, the operator representing the total charge should be invariant under the system dynamics, and thus commute with any interaction terms and be a ground state of this effective Hamiltonian. Indeed, we note that any operator O that commutes with all of the interaction terms, $h_{\mathbf{x},\lambda}$, should be a ground state. The set of all such operators is known as a commutant algebra. With no other constraints on the dynamics, this algebra is comprised of the identity and the U(1) symmetry generator for the original system. As such, we see that

$$\hat{H}_{\mathcal{L}}\|\hat{Q}\rangle\rangle = \hat{H}_{\mathcal{L}}(g_{\text{off}}\|\mathbb{I}\rangle\rangle) = 0. \tag{2.31}$$

This appears to be nothing more than a uniform charge density of the symmetry generator, as represented by G_{off}-charge. Due to the off-diagonal U(1) symmetry, $\mathbb{I}$ decomposes into the summation over projectors onto different charge sectors: $\mathbb{I} = \sum_m \mathcal{P}_m$, where $\mathcal{P}_m$ is the projector onto an off-diagonal U(1) sector of charge m. For a system with $N = L^d$ sites and local Hilbert space dimension M, $m \in \{0, 1, ..., ML^d\}$. We denote $\|m\rangle\rangle$ as the Choi state of $\mathcal{P}_m$. As such, $\|m\rangle\rangle$ is also a ground state of $\hat{H}_{\mathcal{L}}$ with vanishing G_{diag} charge and a G_{off}-charge of $2m$. Note that $\langle\langle m\|m\rangle\rangle = \dim[\mathcal{H}_m]$, the dimensionality of the charge-m sector. Moving forward, we renormalize $\|m\rangle\rangle$ to $\langle\langle m\|m\rangle\rangle = 1$. Now we move onto the case of weak symmetry.

Weak Symmetry

Here, we can no longer assume that each h_i in the original Hamiltonian individually exhibits a U(1) charge conservation symmetry. Instead, we can only assume that their collective

action will preserve the symmetry. Thus, if G is the symmetry group acting on the original Hilbert space, $\mathcal{H}$, we will have

$$|\Psi\rangle \mapsto (U^*(g) \otimes U(g))|\Psi\rangle \quad \forall g \in G. \tag{2.32}$$

Since the symmetry arises from the collective action of $U^* \otimes U$, in the doubled Hilbert space, the effective Hamiltonian $\hat{H}_{\mathcal{L}}$ in Eq. (2.21) would only be symmetric under the diagonal subgroup of $G = \mathrm{U}(1)_u \times \mathrm{U}(1)_l$. We now only have the one total charge operator G_{diag}, generated by $g_{\mathrm{diag}} = (\hat{Q}_u \otimes \mathbb{I} - \mathbb{I} \otimes \hat{Q}_l)/2$.

We note that the identity is now the only element guaranteed in the commutant algebra. In contrast to the case of strong symmetry, we cannot define a uniform charge of g_{diag} over the identity because the action of this charge kills the identity state: $g_{\mathrm{off}}\|\mathbb{I}\rangle\rangle = 0$. Consequently, we cannot decompose the ground state to different charge sectors of the diagonal U(1) charge, as in the case of strong symmetry. Generically, systems with weak symmetry will have an additional non-trivial ground state that is diagonal in the symmetry basis, however it will not be related to other ground states via rotation by G_{diag} generator, $e^{i\theta g_{\mathrm{diag}}}$. As such, we do not expect that weak symmetries will host any notion of SSB. If we hope to see any gappless modes emerge, then we must focus on the case of strong symmetries. Thankfully, if we insist on considering hermitian interactions, so that $\mathcal{O}_{\boldsymbol{x},\lambda} = \mathcal{O}^\dagger_{\boldsymbol{x},\lambda}$, a weak symmetry typically implies the presence of a strong symmetry. Consider the condition for a weak symmetry:

$$0 = [\hat{H}_{\mathcal{L}}, g_{\mathrm{diag}}] = \sum_{\boldsymbol{x},\lambda} [\mathcal{O}^\dagger_{\boldsymbol{x},\lambda}\mathcal{O}_{\boldsymbol{x},\lambda}, g_{\mathrm{diag}}] = \sum_{\boldsymbol{x},\lambda} \Big(\mathcal{O}_{\boldsymbol{x},\lambda}[\mathcal{O}_{\boldsymbol{x},\lambda}, g_{\mathrm{diag}}] - [\mathcal{O}_{\boldsymbol{x},\lambda}, g_{\mathrm{diag}}]\mathcal{O}_{\boldsymbol{x},\lambda} \Big), \tag{2.33}$$

where we have used the hermiticity of $\mathcal{O}_{\boldsymbol{x},\lambda} = h_{\boldsymbol{x},\lambda} \otimes \mathbb{I} - id \otimes h_{\boldsymbol{x},\lambda}$ in the last equality. Unless we choose a very restricted class of interactions, for this to be satisfied for all interactions, $h_{\boldsymbol{x},\lambda}$, it must be true that $[h_{\boldsymbol{x},\lambda}, \hat{Q}] = 0$, which is exactly the condition for a strong symmetry to be present.

Now that we have a sense for the different properties of strong and weak symmetry constraints, let us return to the generic and more promising case of strong symmetries to better understand the particular symmetry breaking phenomena that we expect to produce gapless excitations in our effective Hamiltonian's spectrum.

2.3.2 Approximate Symmetries as Goldstone Modes

Following the discussion from the previous section, we should expect that a system with strong symmetry constraints hosts gapless modes in the spectrum of $\hat{\mathcal{H}}_{\mathcal{L}}$. In this section, we will demonstrate how these gappless modes correspond to approximate symmetries of the system dynamics.

If we return to the original system defined by $\hat{\mathcal{H}}_{\mathcal{L}}$, we have a degenerate ground state manifold with different G_{off}-charges. This implies that the Hamiltonian of the form in Eq. (2.21) necessarily hosts the spontaneous symmetry breaking of G_{off}. This can be shown explicitly by constructing a ground state $\|\alpha\rangle\rangle \equiv \sum_m e^{im\alpha}\|m\rangle\rangle$ such that under the rotation by G_{off} generator, $e^{i\theta g_{\mathrm{off}}}\|\alpha\rangle\rangle = \|\alpha+\theta\rangle\rangle \neq \|\alpha\rangle\rangle$. Accordingly, the low-energy excitations of $\hat{\mathcal{H}}_{\mathcal{L}}$ must be given by the Nambu-Goldstone modes for the broken continuous symmetry. A standard

approach for constructing such Goldstone modes is to apply G_{off} density modulations with momentum k on the ground state $\|m\rangle\!\rangle$. The variational ansatz for such a state is defined as

$$\|m_{\boldsymbol{k}}\rangle\!\rangle \equiv \frac{1}{\sqrt{\mathcal{N}_{\boldsymbol{k}}}}\hat{\rho}_{\boldsymbol{k}}\|m\rangle\!\rangle, \quad \hat{\rho}_{\boldsymbol{k}} \equiv \sum_{\boldsymbol{x}} \frac{e^{i\boldsymbol{k}\cdot\boldsymbol{x}}}{L^{d/2}}(\hat{\rho}_{\boldsymbol{x},u} + \hat{\rho}_{\boldsymbol{x},l}), \tag{2.34}$$

where $\hat{\rho}_{\boldsymbol{x},u/l}$ measures U(1) charge in the layer u or l at position $\boldsymbol{x}$, and $\mathcal{N}_{\boldsymbol{k}} \equiv \langle\!\langle m\|\hat{\rho}^\dagger_{\boldsymbol{k}}\hat{\rho}_{\boldsymbol{k}}\|m\rangle\!\rangle$ is a static structural factor with $\hat{\rho}^\dagger_{\boldsymbol{k}} = \hat{\rho}_{-\boldsymbol{k}}$. It straightforward to show that $\|m_{\boldsymbol{k}}\rangle\!\rangle$ carries a well-defined momentum $\boldsymbol{k}$ and thus $\langle\!\langle m_{\boldsymbol{k}}\|m_{\boldsymbol{k}'}\rangle\!\rangle = \delta_{\boldsymbol{k},\boldsymbol{k}'}$. We will explicitly check this later, however this will be an important criterion to allow our variational modes to bound the true spectrum. We remark that since $(\hat{\rho}_{\boldsymbol{x},u} + \hat{\rho}_{\boldsymbol{x},l})$ measures a local G_{off}-charge, the constructed mode corresponds to the density fluctuations of the G_{off}-charge.

Feynman-Bijl Formula

The collective excitations described in the body of this paper closely mirror variational density fluctuation modes in bosonic systems, as described by the Feynman-Bijl formula [70–72].

The Feyman-Bijl formula is particularly useful in describing systems in which the system's ground state, ϕ_0 is comprised of a uniform distribution of charge. In this case, the variational states constructed as density modulations over the ground state, $\psi_{\mathbf{k}}$ are momentum eigenstates for which $\langle\psi_c|\psi_{\mathbf{k}'}\rangle \sim \delta_{\mathbf{k}\mathbf{k}'}$. If this is true, only energy eigenstates states with the same momentum may contribute to the construction of $\psi_{\mathbf{k}}$, and the variational energy, ϵ_k, will provide a proper variational bound on the true spectrum, $E_k \leq \epsilon_k$

In this literature, low-lying modes are described by the variational wavefunction in the first quantized form,

$$\psi_{\boldsymbol{k}} = \frac{1}{L^{d/2}}\hat{\rho}_{\boldsymbol{k}}\phi_0 = \frac{1}{L^{d/2}}\sum_{\boldsymbol{x}} e^{i\boldsymbol{k}\cdot\boldsymbol{x}}\phi_0, \tag{2.35}$$

where ϕ_0 is the exact ground state wavefunction. The difference between this original formulation and our construction is that our dispersing mode is written in second quantized form, where $\hat{\rho}_{\boldsymbol{k}} = \frac{1}{L^{d/2}}\sum_{\boldsymbol{x}} e^{i\boldsymbol{k}\cdot\boldsymbol{x}}\hat{\rho}_{\boldsymbol{x}}$. In addition, we chose to describe excitations over a specific ground state of fixed charge $\|m\rangle\!\rangle$. Carrying on with the Feynman-Bijl derivation, the variational estimate for the energy of density fluctuation excitations is given by

$$\epsilon_{\boldsymbol{k}} = \frac{\langle\psi_{\boldsymbol{k}}|H - E_0|\psi_{\boldsymbol{k}}\rangle}{\langle\psi_{\boldsymbol{k}}|\psi_{\boldsymbol{k}}\rangle} = \frac{f(\boldsymbol{k})}{s(\boldsymbol{k})}, \tag{2.36}$$

where E_0 is the exact ground state energy (which we set to zero). $f(\boldsymbol{k})$ is called the oscillator strength, which can be evaluated as

$$f(\boldsymbol{k}) = \frac{1}{2L^d}\langle\phi_0|\left[\hat{\rho}^\dagger_{\boldsymbol{k}}, [H, \hat{\rho}_{\boldsymbol{k}}]\right]|\phi_0\rangle, \tag{2.37}$$

and $s(\boldsymbol{k})$ is the static structure factor:

$$s(\boldsymbol{k}) = \langle\psi_{\boldsymbol{k}}|\psi_{\boldsymbol{k}}\rangle = \frac{1}{L^d}\langle\phi_0|\hat{\rho}^\dagger_{\boldsymbol{k}}\hat{\rho}_{\boldsymbol{k}}|\phi_0\rangle. \tag{2.38}$$

In the context of superfluid Helium [70, 71], the oscillator strength $f(\boldsymbol{k}) \sim k^2$ while the structural factor $s(\boldsymbol{k}) \sim k$, giving rise to the linear dispersion of the density fluctuation modes $E_{\boldsymbol{k}} \sim k$. For our problems of interest, we also expect an oscillator strength given as $f(\boldsymbol{k}) \sim k^2$, however, as we will show below, the static structural factor is generically constant.

Spectral Scaling

Returning to the spectral estimates from our original variational state, how will this characterize the original spectrum? With orthogonality between $\|m_{\boldsymbol{k}}\rangle\rangle$ for different momenta, the variational expected energy provides an upper bound for the low-energy dispersion of Eq. (2.21):

$$\begin{aligned}\langle\langle m_{\boldsymbol{k}}\|\hat{H}_{\mathcal{L}}\|m_{\boldsymbol{k}}\rangle\rangle &= \frac{1}{\mathcal{N}_{\boldsymbol{k}}}\langle\langle m\| \left[\hat{\rho}^\dagger_{\boldsymbol{k}}, [\hat{H}_{\mathcal{L}}, \hat{\rho}_{\boldsymbol{k}}]\right] \|m\rangle\rangle \\ &= \frac{1}{\mathcal{N}_{\boldsymbol{k}}}\sum_{\boldsymbol{x},\lambda}\langle\langle m\|[\mathcal{O}_{\boldsymbol{x},\lambda}, \hat{\rho}_{\boldsymbol{k}}]^\dagger[\mathcal{O}_{\boldsymbol{x},\lambda}, \hat{\rho}_{\boldsymbol{k}}]\|m\rangle\rangle,\end{aligned} \tag{2.39}$$

where we used $\mathcal{O}_{\boldsymbol{x},\lambda}\|m\rangle\rangle = 0$ to convert from the double commutator form. By using U(1) symmetry, the commutator in Eq. (2.39) can be recast as

$$[\mathcal{O}_{\boldsymbol{x},\lambda}, \hat{\rho}_{\boldsymbol{k}}] = e^{i\boldsymbol{k}\cdot\boldsymbol{x}}\sum_{\boldsymbol{y}\in\mathcal{S}_{\boldsymbol{x}}}\sum_{n=1}^{\infty}[\mathcal{O}_{\boldsymbol{x},\lambda}, \frac{[i\boldsymbol{k}\cdot(\boldsymbol{y}-\boldsymbol{x})]^n}{n!}\hat{\rho}_{\boldsymbol{y}}], \tag{2.40}$$

where we used $[\mathcal{O}_{\boldsymbol{x},\lambda}, \sum_{\boldsymbol{y}}\hat{\rho}_{\boldsymbol{y}}] = 0$, and $\mathcal{S}_{\boldsymbol{x}}$ is the *local* support of the operator $\mathcal{O}_{\boldsymbol{x},\lambda}$ (thus warranting the expansion of $e^{i\boldsymbol{k}\cdot(\boldsymbol{y}-\boldsymbol{x})}$ for small $\boldsymbol{k}$). Generally, assuming a finite expectation value of the local dipole fluctuations $\langle\langle m\|\left|[\mathcal{O}_{\boldsymbol{x},\lambda}, \sum_{\boldsymbol{y}} y_i\,\hat{\rho}_{\boldsymbol{y}}]\right|^2\|m\rangle\rangle$, the expansion Eq. (2.40) does not vanish at $n = 1$, giving rise to a leading order contribution proportional to k:

$$[\mathcal{O}_{\boldsymbol{x},\lambda}, \hat{\rho}_{\boldsymbol{k}}] \propto k \quad \Rightarrow \quad \langle\langle m_{\boldsymbol{k}}\|\hat{H}_{\mathcal{L}}\|m_{\boldsymbol{k}}\rangle\rangle \propto k^2. \tag{2.41}$$

Here, we focus on isotropic systems for simplicity; however, dynamical exponents can be obtained similarly for non-isotropic systems. Additionally, there is a nice physical interpretation for these gapless modes. Recall that the commutor, $\mathcal{O}_{\boldsymbol{x},\lambda}$ represents the action of a commutation with $h_{\boldsymbol{x},\lambda}$. The ground state$\|\hat{Q}\rangle\rangle$, is a symmetry of the system because $[h_{\boldsymbol{x},\lambda}, \hat{Q}] = 0$. And these gapless modes, $\|m_{\boldsymbol{k}}\rangle\rangle$, corresponding to operators $\mathcal{P}_{m_{\boldsymbol{k}}} = \sum_{\boldsymbol{x}} e^{i\boldsymbol{k}\cdot\boldsymbol{x}}\mathcal{P}_m$ can be interpreted as approximate symmetries in the sense that

$$\langle\langle m_{\boldsymbol{k}}\|\hat{H}_{\mathcal{L}}\|m_{\boldsymbol{k}}\rangle\rangle = \mathrm{Tr}[|[h_{\boldsymbol{x},\lambda}, \mathcal{P}_{m_{\boldsymbol{k}}}]|^2] \sim \frac{1}{L^2}. \tag{2.42}$$

In the thermodynamic limit, this quantity vanishing implies that the operator $\mathcal{P}_{m_{\boldsymbol{k}}}$ is an approximate symmetry of the system.

To complete this estimate, we must first check that $\mathcal{N}_{\boldsymbol{k}}$ is a constant, independent of k, and verify orthogonality of our variational states. In general, explicitly calculating $\mathcal{N}_{\boldsymbol{k}}$ may

be difficult; however, in a charge conserving system, it can be done directly as

$$\begin{aligned}\mathcal{N}_{\boldsymbol{k}} &= \sum_{\boldsymbol{x},\boldsymbol{x}'} \frac{e^{i\boldsymbol{k}\cdot(\boldsymbol{x}'-\boldsymbol{x})}}{L^d} \langle\langle m\|\hat{\rho}_{\boldsymbol{x}}\hat{\rho}_{\boldsymbol{x}'}\|m\rangle\rangle \\ &= \sum_{\boldsymbol{x}=\boldsymbol{x}'} \frac{\langle\langle m\|\hat{\rho}_{\boldsymbol{x}}^2\|m\rangle\rangle}{L^d} + \sum_{\boldsymbol{x}\neq\boldsymbol{x}'} \frac{e^{i\boldsymbol{k}\cdot(\boldsymbol{x}'-\boldsymbol{x})}}{L^d} \langle\langle m\|\hat{\rho}_{\boldsymbol{x}}\hat{\rho}_{\boldsymbol{x}'}\|m\rangle\rangle \\ &= \langle\langle m\|\hat{\rho}_{\boldsymbol{x}_0}^2\|m\rangle\rangle - \langle\langle m\|\hat{\rho}_{\boldsymbol{x}_0}\hat{\rho}_{\boldsymbol{x}_0+\boldsymbol{a}}\|m\rangle\rangle, \end{aligned} \tag{2.43}$$

where $\boldsymbol{x}_0$ and $\boldsymbol{a} \neq 0$ are arbitrary vectors. Here, we employ the fact that $\|m\rangle\rangle$ is the projection onto the sector of total charge m, and $\|m\rangle\rangle$ has no notion of distance. More precisely, it is invariant under the permutation of local sites. Accordingly, correlations between charges at different sites are the same for any two sites that are distinct. Thus, for a charge conserving system, the static structure factor, as given above, is a constant, independent of $\boldsymbol{k}$.

As a final check, we must ensure orthogonality of our variational states. To do so, we repeat the analysis above, allowing one of the states to be at a different momentum:

$$\begin{aligned}\langle\langle m|\hat{\rho}_k^\dagger\hat{\rho}_{k'}|m\rangle\rangle &= \sum_{x,x'} \frac{e^{i(k'x'-kx)}}{L} \langle\langle m|\hat{\rho}_x\hat{\rho}_{x'}|m\rangle\rangle \\ &= \sum_{x^+,x^-} \frac{e^{-i(k^+x^-+k^-x^+)}}{2L} \langle\langle m|\hat{\rho}_{x^++x^-}\hat{\rho}_{x^+-x^-}|m\rangle\rangle \\ &= \sum_{x^+,x^-} \frac{e^{-i(k^+x^-+k^-x^+)}}{2L} \langle\langle m|T_{x^+}\hat{\rho}_{x^-}\hat{\rho}_{-x^-}T_{-x^+}|m\rangle\rangle \\ &= \sum_{x^+,x^-} \frac{e^{-i(k^+x^-+k^-x^+)}}{2L} \langle\langle m|\hat{\rho}_{x^-}\hat{\rho}_{-x^-}|m\rangle\rangle \\ &= \delta_{k^-,0} \sum_{x^-} e^{-ik^+x^-} \langle\langle m|\hat{\rho}_{x^-}\hat{\rho}_{-x^-}|m\rangle\rangle \\ &= \delta_{k,k'} f(k+k') \end{aligned} \tag{2.44}$$

Where we use the coordinates $x^\pm = \frac{x\pm x'}{2}$ and $k^\pm = k \pm k'$ to simplify calculations. In the third line, we exploit the translation invariance of the ground state so that $T_{x^+}\|m\rangle\rangle = \|m\rangle\rangle$. In the fourth line, we sum over x^- to produce the delta function in $\delta_{k^-,0}$, which is equivalent to the delta function $\delta_{k,k'}$, completing the result. Finally, we note that when k = k', $f(k+k) = \mathcal{N}_k = \sum_{x^-} e^{-2ikx^-} \langle\langle m|\hat{\rho}_{x^-}\hat{\rho}_{-x^-}|m\rangle\rangle$.

Therefore, the constructed state with momentum k generically exhibits a quadratic dispersion, regardless of the details of the effective Hamiltonian. As these state provide a variational bound on the true spectrum, E_k, we have

$$E_k \leq \epsilon_{\boldsymbol{k}} \propto k^2 \tag{2.45}$$

Again, we note the similarity of our approach to the single mode approximation in superfluid or quantum Hall states [70–72], where the Feynman-Bijl ansatz also provides excellent variational states that capture the dispersion of density fluctuation excitations.

Following from Eq. 2.25, we now have the main result of this chapter. If one imposes a strong U(1) symmetry constraint on a thermalizing system, then, just as expected from the Haar-averaged calculation of the dynamics of conserved amplitudes, one should expect autocorrelations of conserved operators, S^z_x, to decay as

$$\mathbb{E}\langle S^z_{\boldsymbol{x}}(t)S^z_{\boldsymbol{x}}(0)\rangle_\rho \underset{t\to\infty}{\sim} \int_k e^{-tk^2}\mathrm{d}^d\boldsymbol{k} \sim t^{-d/2}. \tag{2.46}$$

For a system to fully thermalize, we will have to wait for these charges to reach a uniform density $\sim L^{-d}$. Thus, we expect thermalization to occur on a timescale $t_T \sim L^2$, as might be expected from a system with diffusion.

2.3.3 Discussion

We have shown that the Brownian Hamiltonian framework is strictly more general than a Haar-averaging description. Further, in the case of dynamics preserving a U(1) symmetry, this model seems to allow one to derive all the same properties and more. We note that the use of adjoined qudits was not necessary, even as a calculation convenience. Further, since we did not need to put a unitary in block diagonal form to complete our analysis, and thus, the results here should translate to non-Abelian symmetries just as readily as Abelian ones. In the next chapter, we will explore the differences that arise between the Abelian and non-Abelian case due to the structure of the ground state of $\hat{H}_{\mathcal{L}}$.

As has been seen, using this framework, the dynamics of an autocorrelation function can be well modeled by an imaginary-time Schrödinger evolution governed by an effective Hamiltonian. The late-time behavior of such autocorrelation functions then reduce to spectral properties of an effective Hamiltonian $\hat{H}_{\mathcal{L}}$. These properties can further be classified by the symmetry constraints on $\hat{H}_{\mathcal{L}}$. In the case of weak symmetries, there will generically be a gap in the spectrum, resulting in exponentially decaying correlations and a finite thermalization time. When a strong symmetry is present, however, spontaneous symmetry breaking produces goldstone modes, and the spectrum develops gappless modes with a dispersion that is quadratic (or weaker). This results in correlations decaying algebraically, and thermalization times that scale like $t_L \sim L^2$ or longer.

These gapless modes that arise from breaking the strong symmetry have an interesting quality. Typically, for SSB of a U(1) charge, one would expect a linear dispersion. This is because of the difference between type A and Type B goldstone modes. Generically, one must break two generators to produce a quadratically dispersing type-B mode. However, in the above example, we have only broken one of the two U(1) generators, yet we expect a quadratic spectrum. Why might this be? It has be shown that frustration-free Hamiltonians like $\hat{H}_{\mathcal{L}}$ display anomalous symmetry breaking phenomena. To be more precise, let us define a frustration-free, translation invariant Hamiltonian, $\hat{H} = \sum_{i=1}^{L}\hat{H}_i$, with ground state energy 0. We look at a subsystem of length, l, where $(3 \leq l \leq L/2)$, and define a subsystem Hamiltonian as $H^{OBC}_{l,x_0} \equiv \sum_{i=0}^{l-2} H_{x_0+i}$. Now, we define the first excitation energies ϵ^{PBC} and ϵ^{OBC} for $\hat{H}$ and H^{OBC}_{l,x_0}, respectively. Now, it has been shown that, if $\hat{H}$ is gappless, then there exists a constant C > 0 such that $0 < \epsilon^{OBP} < C(l^2+l)^{-2}$. [73–75] The specific mechanism for this SSB has been discussed in [76]. Here, it has been shown that all Hamiltonians

that take the same form as $\hat{H}_{\mathcal{L}}$ display SSB with nematic order parameters that do not commute with the system Hamiltonian and are rotated into one another by the symmetry generator. This parallels the case of the spin-1/2 ferromagnetic Heisenberg chain, where the generators doubled as order parameters that could be rotated into one another. In this case, however, these two order parameters producing the quadratic mode, are not symmetry generators themselves, and thus, do not commute with the Hamiltonian[76]. Further, these modes appear to be related to the type B diffusion modes referenced in [77], which explicitly discusses the goldstone theorem in open quantum systems.

However, before we conclude, there are a number of caveats that must be made. First, as explained in Ch. 1, thermalization depends on the operators chosen. The above analysis shows that overlap with the operator Q_{tot} will result in diffusive dynamics, however, if there is no overlap, then operators should still reach steady state in a finite time. Further, we should note that the procedure above can only bound the scaling of the full spectrum. Because it lives in a doubled Hilbert space, calculating the explicit spectrum of $\hat{H}_{\mathcal{L}}$ will generically computationally infeasible. However, one can tighten the bounds and look for approximate coefficients by focusing on the diagonal sector of the doubled Hilbert space, reducing the complexity of the problem enormously. In fact, all effective Hamiltonians projected into the diagonal subspace become *RK-type* Hamiltonians that can be classically simulated as generators of classical Markovian processes[78].

Nomenclature for Chapter 2

Selected Abbreviations

BHE Brownian Hamiltonian Evolution

SSB Spontaneous Symmetry Breaking

Variables

$\hat{H}_{\mathcal{L}}$ Effective Hamiltonian and vectorization of Lindbladian Superoperator, $\mathcal{L}$

E_k Spectrum of the effective Hamiltonian $\hat{H}_{\mathcal{L}}$

ϵ_k variational esimate of E_k given by $\epsilon_k = \langle\langle m_{\boldsymbol{k}} \| \hat{H}_{\mathcal{L}} \| m_{\boldsymbol{k}} \rangle\rangle$

Chapter 3

Generalizations to other Symmetries and Lindbladian Dynamics

The previous chapter demonstrated that Brownian Hamiltonian Evolution could provide a more complete understanding of local random circuits with global symmetries than the standard Haar-averaging procedure. Yet, global symmetries on local interactions still only addresses a small fraction of the possible structure allowable in chaotic quantum systems. As such, we will now focus our discussion on dynamics with more complicated symmetries and interactions to demonstrate how the framework developed in the previous chapter can be applied to more generic dynamic models. As will be noted in the chapter, a number of the results presented here have been obtained in limited fashion through previous analysis involving subtle use of Haar-averaging. These studies are typically detailed analysis of a particular toy model, and lack the degree of generality that we will demonstrate with BHE.

Before addressing any particular new symmetry or interaction, however, it behooves us to review the connection between symmetries of physical systems and the ground states of our effective Hamiltonian, $\hat{H}_{\mathcal{L}}$.

3.1 Ground States and Commutant Algebras

The most familiar symmetries considered in physical systems are usually on-site symmetries. These come in the form of global unitary operators formed from tensor products of single-site unitaries that are representations of a corresponding group. Examples of such unitary symmetries with nice group structures are lattice symmetries like translation, rotation, and reflection. However, not all symmetries take this familiar form, and many "unconventional" symmetries have proven essential to understand the dynamical phenomena known as weak ergodicity breaking, where conventional symmetry sectors are no longer dynamically connected[79–82]. This occurs in systems that display novel or non-thermalizing behavior such as systems exhibiting Hilbert Space Fragmentation, where the number of connected sectors grows exponentially with system size [83], and systems with Quantum Many-Body Scars that include non-local symmetries like projectors onto particular pure states[84]. In order to understand the dynamical behavior of such systems, it would be useful to have a straightforward way to generalize beyond the familiar on-site symmetries.

With this in mind, we turn to the role that on-site symmetries played in the previous chapter. There, when dealing with the generic case of strong symmetries, we noted that the generators of such symmetries, $\hat{Q}_\alpha \in \mathcal{H}$, corresponded to ground states of $\hat{H}_\mathcal{L}$, as could be seen by the vanishing action of a commutor:

$$\mathcal{O}_{\boldsymbol{x},\lambda}\|\hat{Q}_\alpha\rangle\rangle = 0 \quad \Rightarrow \quad [h_{\boldsymbol{x},\lambda}, \hat{Q}_\alpha] = 0. \tag{3.1}$$

By definition, this commutation is satisfied for all $\mathcal{O}_{\boldsymbol{x},\lambda}$. This, in turn, implies that the state $\|\hat{Q}_\alpha\rangle$ will be a ground state of the effective Hamiltonian, $\hat{H}_\mathcal{L} = \frac{1}{2}\sum_{\mathbf{x},\lambda} \mathcal{O}^\dagger_{\boldsymbol{x},\lambda}\mathcal{O}_{\boldsymbol{x},\lambda}$. Yet, this did not require that the operator $\hat{Q}_\alpha$ be local, correspond to any group element, or otherwise be related to any conventional symmetry. In fact, we may take this as a definition for the symmetries present in a system. I.e, we define symmetry algebras as *Commutant algebras*, $\mathcal{C}$ - the associative algebra of operators that commute with a given set of local operators corresponding to the allowable interactions, $h_{\boldsymbol{x},\lambda} \in \mathcal{A}$, that we define as *Bond algebras*. In other words, the commutant algebra, $\mathcal{C}$, is the centralizer of the bond algebra. This definition allows us to attempt to characterize the properties of generic Hamiltonians of the form $H = \sum_\alpha J_\alpha h_\alpha$. The BHE framework matches this exactly, but takes the interactions J_α to be Brownian variables.

As such, given a set of interactions, $h_{\boldsymbol{x},\lambda} \in \mathcal{A}$, we can immediately identify the ground state subspace to correspond to the commutant algebra for $\mathcal{A}$. And the degeneracy of the ground state subspace for the effective Hamiltonian generated from these interactions will be

$$d = \dim[\mathcal{C}]. \tag{3.2}$$

In addition to this, we further decompose the ground state subspace into connected sectors. Specifically, we may systematically count the number and the sizes of Krylov subspaces, the dynamically disconnected blocks mentioned in Ch. 1, in terms of the dimensions the irreducible representations of the bond algebra and the commutant[85].

3.2 Non-Abelian Symmetries and Non-Unique Krylov Sectors

To better understand this perspective, let us return to the issue of non-Abelian symmetries. Specifically, we will pay close attention to the Krylov sectors that define the ground state. As mentioned in Ch. 1, the presence of non-Abelian symmetries will generically prevent thermalization, however, we should still expect steady states described by the Generalized Gibbs Ensemble [40]. Let us attempt to understand how this could come to be.

When a system is constrained by an Abelian symmetry, like a U(1) symmetry, there will be a well-defined symmetry basis, and each Krylov sector will simply correspond to the various charge sectors of the symmetry. As discussed in the previous chapter, we may then examine dynamics within particular charge-m sectors by projecting to the state $\|m\rangle\rangle$, then examining excitations within this sector, $\|m_{\boldsymbol{k}}\rangle\rangle$. In particular, the steady state within a charge sector will have no structure other than the weight determined by the initial overlap, $\mathrm{Tr}[\hat{\rho}(0)\hat{Q}]$.

If a system is constrained by a non-Abelian symmetry, G, then, by definition, there does not exist a basis where each of the non-commuting charges $\{Q_\alpha\}$ is well-defined. In other words, if we block diagonalize the system's density matrix, each block or irreducible representation will represent some non-unique Abelian subgroup $H \subset G$. In the case of an SU(2) symmetry, this is apparent in that each irreducible representation is defined by S^2_{tot} and S^i_{tot} for one of the three generators of rotations (or a single linear combination of them), $S^i_{\text{tot}} \in \{S^x_{\text{tot}}, S^y_{\text{tot}}, S^z_{\text{tot}}\}$. Now, if we wish to characterize the steady state within a charge sector defined by $S^2_{\text{tot}} = s$, $S^z_{\text{tot}} = m$), there will be additional constraints on the structure from the initial overlap with the other non-commuting charges, $\text{Tr}[\hat{\rho}(0)S^x_{\text{tot}}]$, and $\text{Tr}[\hat{\rho}(0)S^x_{\text{tot}}]$. This will result in a generalized Gibbs ensemble where the charges, where one must account for initial averages of each of the non-commuting charges [40][1].

$$\hat{\rho}_S = e^{-\beta(H-\sum_\alpha \mu_\alpha Q^\alpha)}, \tag{3.3}$$

where β and the chemical potentials, μ_α are all functions of the charge expectation values $E = \text{Tr}[\hat{H}\hat{\rho}_S]$ and $Q^\alpha = \text{Tr}[\hat{Q}^\alpha\hat{\rho}_S]$.

Beyond the failure to thermalize, we can also understand the additional consequence that the late-time dynamics of systems obeying a non-Abelian symmetry cannot be easily simulated with classic algorithms. This is due to the fact the low-energy theory of an effective Hamiltonian cannot be fully restricted to the diagonal subspace of any set of commuting symmetry generators. As such, we will not be able to describe the late-time dynamics via an RK-type Hamiltonian that can be modeled with a classical Markovian process.

We thus have an immediate understanding of steady-state properties for a given system from the symmetries it obeys. Turning from internal symmetries, in the next section, we will discuss both steady state and late-time properties of systems involving spatial degrees of freedom in their symmetries.

3.3 Multipole Symmetries

In the previous section, we noted how the non-unique partitioning of the ground state of our effective Hamiltonian lead to issues with thermalization for systems involving non-Abelian symmetries. However, none of the discussion changed the nature of the excited states above the ground state, and thus, the late-time dynamics of non-commuting charges should display diffusion just as commuting ones do. In this section, we will attempt to characterize if and how the addition of constraints involving spatial degrees of freedom can change the equilibriation timescale. As a paradigmatic example, we will consider the case of multipole moments of internal symmetries. We will see that the methods of the previous chapter can be readily generalized to systems conserving multipole moments of a particular charge. Further, these multipole symmetries will prove to have unique ground state structures that pose different challenges to thermalization than do non-Abelian symmetries. For the sake of clarity, we will focus on multipole moments of U(1) charges, although, as explained, the dynamics obtained for non-commuting charges should mirror those of their commuting counterparts at late times.

[1] In [40], the ensemble is referred to by the name "non-Abelian thermal state" - ρ_{NATS}

3.3.1 Naive Generalization

The method outlined in Ch.2 also applies to systems with conserved quantities beyond $U(1)$ charges. Let us focus on one-dimensional models with charge multipole symmetries, as relevant to fracton systems [86–94], generated by

$$Q^{(n)} \equiv \sum_x x^n \hat{\rho}_x = \sum_x x^n (\hat{\rho}_{x,u} + \hat{\rho}_{x,l}). \tag{3.4}$$

For concreteness, we consider Brownian time evolution conserving the first two multipole moments $n = 0$ and $n = 1$, i.e. $[h_i, Q^{(0)}] = [h_i, Q^{(1)}] = 0$.

In the presence of both charge and dipole conservation symmetries, the commutator in Eq. (2.40) now vanishes at $n = 1$, and takes a finite value only at order $n \geq 2$.

$$[\mathcal{O}_{\boldsymbol{x},\lambda}, \hat{\rho}_{\boldsymbol{k}}] = e^{i\boldsymbol{k}\cdot\boldsymbol{x}} \sum_{\boldsymbol{y}\in\mathcal{S}_{\boldsymbol{x}}} \sum_{n=2}^{\infty} [\mathcal{O}_{\boldsymbol{x},\lambda}, \frac{[i\boldsymbol{k}\cdot(\boldsymbol{y}-\boldsymbol{x})]^n}{n!} \hat{\rho}_{\boldsymbol{y}}]. \tag{3.5}$$

Accordingly, the excited modes $\|m_k\rangle\rangle$ carry an energy proportional to the square of this commutator,

$$E_k = \langle\langle m_k \| \hat{\mathcal{H}}_{\mathcal{L}} \| m_k \rangle\rangle \propto \frac{1}{\mathcal{N}_k} k^4. \tag{3.6}$$

If we focus on a single charge sector, we can repeat the same argument from Ch.2 to see that the static structure factor $\mathcal{N}_k$ remains finite as $k \to 0$. We thus obtain subdiffusive relaxation with dynamical exponent $z = 4$.

The generalization of this result to systems conserving $\{Q^{(0)}, ..., Q^{(m)}\}$ multipoles is straightforward: The commutator in Eq. (2.40) now vanishes up to order $n = m$, giving rise to a dispersion proportional to $k^{2(m+1)}$ and dynamical exponent $z = 2(m+1)$, in accordance with previous results [95–100].

As before, the diffusion of conserved amplitudes causes an interesting profile for operator spreading. Now, if our system is initialized with a local operator, there will be competition between the unitary weight conservation, $\sum_x \rho_R(x,t) = 1$, the charge amplitude charge $\sum_x c_x^{Q^{(0)}}(t) = 1$, and the dipole amplitude conservation, $\sum_x c_x^{Q^{(1)}}(t) = 1$.This will produce a spreading profile much like Fig. 2.2, however, the additional subiffusion of dipole-conserving operators will concentrate the central lump further, these operators will, in turn, leak to both non-conserved operators and diffusing charge-conserving operators. Meanwhile, the diffusion of the operator front and the tail connecting it to the central lump will remain largely unaffected.

As we explain below, we have been a bit too quick in this analysis. Just as before, we need to take care when defining our ground state structure. Since charge is not the only conserved quantity, we should really be looking at the sectors with fixed charge *and* dipole moment. Similarly to the non-Abelian case, we shall see that this attempt to project into a sector conserving all symmetries present will be frustrated, resulting in additional dynamical structure.

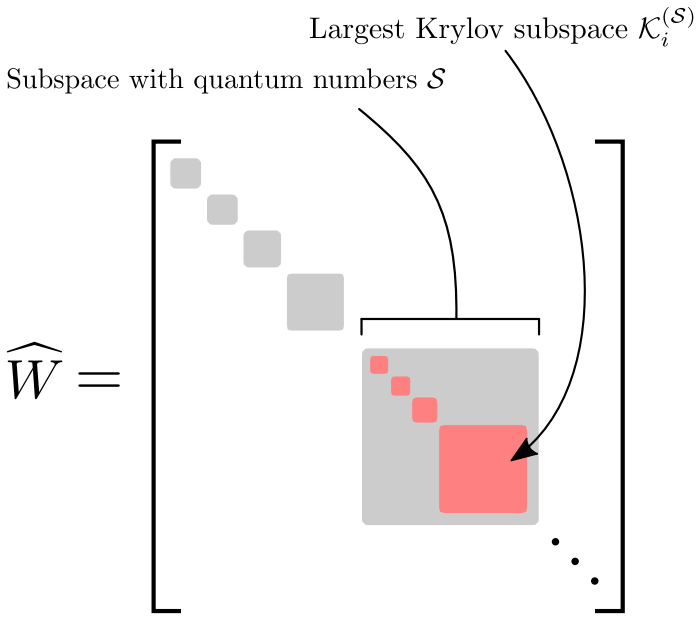

Figure 3.1: **Example of an effective Hamiltonian exhibiting Hilbert Space Fragmentation.** Specifically, a Floquet operator, $\hat{W}$, exhibiting Hilbert space fragmentation in the Z-basis, with symmetry sectors denoted by $\mathcal{S}$, and individual Krylov subspaces within symmetry sectors are denoted by $\mathcal{K}_i^{(S)}$. Figure reproduced from [103].

3.3.2 Hilbert Space Fragmentation and Krylov-Resolved Dynamics

One needs to be a bit more careful, as these additional constraints can have drastic effects on the dynamics. Rather than focusing on the charge-resolved symmetry sectors, we should rather focus on Krylov-space-resolved dynamics.

In the case of non-Abelian symmetries, these Krylov sectors, or the dynamically disconnected sectors, were defined by a non-unique, maximal set of commuting charges. However, the above combination of charge and dipole symmetries generally leads to something more complicated: Hilbert space fragmentation [83, 101, 102]: For a given symmetry sector $Q^{(0)}, Q^{(1)}$ labeled by the different charge and dipole values, there are numerous distinct Krylov sectors, $\mathcal{K}$, connected by the Hamiltonian evolution. The origin of this fragmentation, comes from the non-commutativity of the dipole charge and the generator of momentum, $[T_{\boldsymbol{x}}, Q^{(1)}] \neq 0$. However, even with these commuting generators, there will still be an exponential number of Krylov sectors in any sector with well-defined charge and dipole moment.

Krylov-Space-Resolved Hydrodynamics

As we have mentioned, if we truly want to understand the dynamics in a system conserving both charge and dipole moment, we must take care to account for the differences present in the various Krylov sectors present. Thus, our goal is to understand the associated *Krylov-space-resolved hydrodynamics* in such systems. For this purpose, we introduce the operator $\mathcal{P}_{\mathcal{K}}$ projecting onto an individual Krylov sector, $\mathcal{K}$, and its vectorized Choi state $\|\mathcal{K}\rangle\rangle$, which we define to be normalized. In the doubled Hilbert space formalism, we thus define new

excited states,

$$\|\mathcal{K}_{\boldsymbol{k}}\rangle\rangle \equiv \frac{1}{\sqrt{\mathcal{N}_{\boldsymbol{k}}^{\mathcal{K}}}}\hat{\rho}_{\boldsymbol{k}}\|\mathcal{K}\rangle\rangle, \tag{3.7}$$

where $\hat{\mathcal{H}}_{\mathcal{L}}\|\mathcal{K}\rangle\rangle = 0$ and $\mathcal{N}_k^{\mathcal{K}} \equiv \langle\langle\mathcal{K}\|\hat{\rho}_k^\dagger\hat{\rho}_k\|\mathcal{K}\rangle\rangle$ is the Krylov-resolved structure factor.

Orthonormal Basis States

These Krylov sectors can be markedly different from charge symmetry sectors in ways that could invalidate our previous construction. First, we recall that orthonormality as calculated in Eq. 2.44 was a key component in the application of the Feynman-Bijl formula used for our spectral estimates

Orthonormality plays an essential role in the construction of our variational modes in two respects. First, if orthogonality breaks down such that $\|\mathcal{K}_{\boldsymbol{k}}\rangle\rangle$ has significant overlap with the ground state, our variational modes may display a gapless dispersion even when the spectrum of our effective Hamiltonian, $\hat{\mathcal{H}}_{\mathcal{L}}$, is gapped. Next, as was the case for He-4 in Feynman's famous application of his formula, the dispersion of $\|\mathcal{K}_{\boldsymbol{k}}\rangle\rangle$ may depend on the normalization by its static structure factor, $\mathcal{N}_{\boldsymbol{k}}^{\mathcal{K}}$

We begin by discussing a concrete example where a failure in orthonormality would result in incorrectly predicted relaxation times. Consider a charge conserving effective Hamiltonian that has a gapped spectrum. Due to the finite spectral gap, ΔE, the relaxation should occur in $\mathcal{O}(1)$ time. However, it is possible for the expected energy of our collective modes to still yield a gapless, quadratic dispersion: $\langle\langle m_{\boldsymbol{k}}\|\hat{\mathcal{H}}_{\mathcal{L}}\|m_{\boldsymbol{k}}\rangle\rangle \underset{k\to 0}{\sim} k^2$, which would predict diffusive transport.

This situation can arise if $\|m_{\boldsymbol{k}}\rangle\rangle$ is formed from the superposition of the ground state and a small portion of a gapped excitation, $\|e_1\rangle\rangle$. For example, we can consider the following imagined decomposition at small k:

$$\|m_{\boldsymbol{k}}\rangle\rangle \underset{k\to 0}{=} \sqrt{1-|c\boldsymbol{k}|^2}\|m\rangle\rangle + c|\boldsymbol{k}|\|e_1\rangle\rangle \tag{3.8}$$

$$\langle\langle m_{\boldsymbol{k}}\|m_{\boldsymbol{k}'}\rangle\rangle \underset{k\to 0}{\approx} 1 - \frac{|c|^2}{2}|\boldsymbol{k}-\boldsymbol{k}'|^2 \tag{3.9}$$

$$\langle\langle m_{\boldsymbol{k}}\|\hat{\mathcal{H}}_{\mathcal{L}}\|m_{\boldsymbol{k}}\rangle\rangle \underset{k\to 0}{\propto} k^2\langle\langle e_1\|\hat{\mathcal{H}}_{\mathcal{L}}\|e_1\rangle\rangle \propto k^2\Delta E. \tag{3.10}$$

Where c is some $\mathcal{O}(1)$ constant, and ΔE is the energy gap associated with $\|e_1\rangle\rangle$. In this example, a strong violation of orthogonality in the variational modes, $\|m_{\boldsymbol{k}}\rangle\rangle$, caused the variational bound on the spectrum to fail.

Additionally, we must be careful of the size of the Krylov sectors being considered. we remark that all Krylov spaces considered so far have exhibited hydrodynamic relaxation. However, in constrained models, there may exist Krylov subspaces with localized dynamics due to Hilbert space fragmentation, thus precluding hydrodynamic relaxation. Such a situation holds e.g. for most of the Krylov subspaces associated with a strongly fragmented $S = 1$ dipole-conserving spin model considered below, as demonstrated in Refs. [101, 104]. In this case, the system decomposes into extensively many disjoint regions of finite size, separated

by frozen configuration segments [97, 104]. Each of these independent regions exhibits a discrete – and thus gapped – spectrum. Accordingly, the spectrum of the effective Hamiltonian will be *gapped* as well, implying relaxation on a finite timescale. On a technical level, the gapless single mode approximation utilized throughout this work breaks down, as the states $\|\mathcal{K}_k\rangle\rangle$ acquire a large overlap with the ground state $\|\mathcal{K}\rangle\rangle$ as $k \to 0$.

However, overlap with the ground state is not the only way for orthogonality to fail. When considering individual Krylov sectors, if $\mathcal{K}$ is translation invariant and its dimension is at least extensive in system size, momentum is well-defined, and orthogonality of variational states $\|\mathcal{K}_{\boldsymbol{k}}\rangle\rangle$ follows directly. However, in general, a Krylov subspace, $\mathcal{K}$, may not be translation symmetric, i.e., $T_{\boldsymbol{x}}\mathcal{K}T_{\boldsymbol{x}}^\dagger \neq \mathcal{K}$ because multipole conservation and translation symmetries do not commute. In this case, our variational mode $\|\mathcal{K}_{\boldsymbol{k}}\rangle\rangle$ will not be a momentum eigenstate, and orthogonality does not follow. In order to circumvent this issue, we consider the *symmetrized* Krylov subspace, $\mathcal{K}^{\mathrm{s}}$, as the following:

$$\mathcal{K}^{\mathrm{s}} \equiv \bigoplus_{\boldsymbol{x}} T_{\boldsymbol{x}}\mathcal{K}T_{\boldsymbol{x}}^\dagger. \tag{3.11}$$

We can thus define a new momentum eigenmode $\|\mathcal{K}^{\mathrm{s}}_{\boldsymbol{k}}\rangle\rangle = \sum_{\boldsymbol{x}} T_{\boldsymbol{r}}\|\mathcal{K}_{\boldsymbol{k}}\rangle\rangle/L^{d/2}$. The translation invariance of the effective Hamiltonian, $\hat{H}_{\mathcal{L}}$, ensures that the modes $\|\mathcal{K}_{\boldsymbol{k}}\rangle\rangle$ have the same energy expectation value as that of the symmetrized space:

$$\langle\langle\mathcal{K}^s_{\boldsymbol{k}}\|\hat{H}_{\mathcal{L}}\|\mathcal{K}^s_{\boldsymbol{k}}\rangle\rangle = \sum_{\boldsymbol{x}} \frac{\langle\langle\mathcal{K}_{\boldsymbol{k}}\|T_{\boldsymbol{x}}^\dagger\hat{H}_{\mathcal{L}}T_{\boldsymbol{x}}\|\mathcal{K}_{\boldsymbol{k}}\rangle\rangle}{L^d} = \langle\langle\mathcal{K}_{\boldsymbol{k}}\|\hat{H}_{\mathcal{L}}\|\mathcal{K}_{\boldsymbol{k}}\rangle\rangle, \tag{3.12}$$

where we use the fact that Krylov sectors are preserved under the action of $\mathcal{L}$, but not translation, so that $\langle\langle\mathcal{K}_{\boldsymbol{k}}\|T_{\boldsymbol{r}}^\dagger\hat{H}_{\mathcal{L}}T_{\boldsymbol{r}'}\|\mathcal{K}_{\boldsymbol{k}}\rangle\rangle \sim \delta_{\boldsymbol{r},\boldsymbol{r}'}$. As such, we must now interpret $\boldsymbol{k}$ in $\|\mathcal{K}_{\boldsymbol{k}}\rangle\rangle$ as a label for an eigenstate that is distinct from the momentum. However, since $\|\mathcal{K}_{\boldsymbol{k}}\rangle\rangle$ shares the same spectral properties as $\|\mathcal{K}^{\mathrm{s}}_{\boldsymbol{k}}\rangle\rangle$, we may exploit the translation invariance of $\|\mathcal{K}^{\mathrm{s}}_{\boldsymbol{k}}\rangle\rangle$ to derive the compact form of Eq.2.23. Still, a similar expression should exist for $\|\mathcal{K}_{\boldsymbol{k}}\rangle\rangle$, with $\boldsymbol{k}$ effectively entering as a mere integration variable.

Bounded Fluctuations

For generic dipole-conserving systems featuring *weak* fragmentation, the largest Krylov sector $\mathcal{K}_0$ makes up a finite portion of the full Hilbert space (up to a prefactor algebraic in system size) in the symmetry sector. As a consequence, its static structure factor $\mathcal{N}_k^{\mathcal{K}_0} \to \mathcal{O}(1)$ remains finite as $k \to 0$. We thus obtain some subdiffusive relaxation with dynamical exponent $z = 4$.

However, this does not address whether any relaxation differing from the subdiffusive behavior $z = 4$ can emerge in specific Krylov sectors. First, let us observe that the structure factor $\mathcal{N}_k^{\mathcal{K}}$ quantifies the magnitude of charge fluctuations within a Krylov sector $\mathcal{K}$. This suggests unconventional hydrodynamics may emerge in Krylov sectors where charge fluctuations follow a *sub-volume* law with vanishing $\lim_{k\to 0}\mathcal{N}_k^{\mathcal{K}} = 0$ at small momenta, speeding up the subdiffusive relaxation. We demonstrate this effect in several concrete examples below.

Let us first consider a one-dimensional chain with charge and dipole conservation and introduce bond variables $\hat{e}_x$ defined via

$$\hat{\rho}_x = \hat{e}_x - \hat{e}_{x-1} \;\Leftrightarrow\; \hat{e}_x = \sum_{i=0}^{x} \hat{\rho}_i. \tag{3.13}$$

For convenience, we define the charge density $\hat{\rho}_x$ relative to its average value within $\mathcal{K}$, i.e. $\sum_x \langle \hat{\rho}_x \rangle_{\mathcal{K}} = 0$. We note that the $\hat{e}_i$ can be understood as a local dipole density, with $\sum_x \hat{e}_x = Q^{(1)}$ [105–107]. Let us now assume that a sector $\mathcal{K}$ exhibits *bounded* fluctuations of these bond variables. Formally,

$$\lim_{L\to\infty} \langle \hat{e}_k \hat{e}_{-k} \rangle_{\mathcal{K}} \xrightarrow{k\to 0} \sigma_1^2 < \infty, \tag{3.14}$$

where $\hat{e}_k = \frac{1}{\sqrt{L}} \sum_x e^{ikx} \hat{e}_x$ and σ_1 corresponds to the average fluctuation of the local dipole density. Since $\hat{e}_x = \sum_{i=0}^{x} \hat{\rho}_i$, the finiteness of $\hat{e}_x$ implies area-law fluctuations (i.e. an $\mathcal{O}(1)$ value in 1D) of the total charge within any given region. Using that $\hat{\rho}_k = (1 - e^{-ik})\hat{e}_k$ for $k \neq 0$, the structure factor for small k becomes

$$\mathcal{N}_k^{\mathcal{K}} = \langle \hat{\rho}_k \hat{\rho}_{-k} \rangle_{\mathcal{K}} = k^2 \langle \hat{e}_k \hat{e}_{-k} \rangle \to \sigma_1^2 \, k^2. \tag{3.15}$$

Therefore, for Krylov sectors satisfying Eq. (3.15), the energy of the excited mode $\|\mathcal{K}_k\rangle\!\rangle$ scales as

$$E_k \leq \langle\!\langle \mathcal{K}_{\boldsymbol{k}}^s \| \hat{H}_{\mathcal{L}} \| \mathcal{K}_{\boldsymbol{k}}^s \rangle\!\rangle \propto \frac{k^4}{\mathcal{N}_k^{\mathcal{K}}} \propto k^2, \tag{3.16}$$

and we expect *diffusive* relaxation, despite the presence of dipole-conservation. To interpret this result, note that the $\hat{e}_x$ constitute a conserved local density with an effectively finite local state space due to their bounded fluctuations. If $\hat{e}_x$ is bounded, these local dipoles move without additional kinetic constraints and are thus expected to relax diffusively (see also Ref. [106]). We emphasize that this argument requires the fluctuations of $\hat{e}_x$ to be finite; for volume-like charge fluctuations, transport behavior returns to being subdiffusive.

Generalization to systems conserving $\{Q^{(0)}, ..., Q^{(m)}\}$ is again straightforward. To see this, we assume that $\hat{\rho}_{\boldsymbol{x}}$ can be written as a m^{th}-order derivative, $\hat{\rho}_{\boldsymbol{x}} = \partial_{\boldsymbol{x}}^m \hat{e}_{\boldsymbol{m},\boldsymbol{x}}$, the structure factor becomes

$$\begin{aligned}
\mathcal{N}_{\boldsymbol{k}} &= \sum_{\boldsymbol{x},\boldsymbol{x}'} \frac{e^{i\boldsymbol{k}\cdot(\boldsymbol{x}'-\boldsymbol{x})}}{L^d} \langle\!\langle m \| \partial_{\boldsymbol{x}}^m \hat{e}_{\boldsymbol{m},\boldsymbol{x}} \partial_{\boldsymbol{x}'}^m \hat{e}_{\boldsymbol{m},\boldsymbol{x}'} \| m \rangle\!\rangle \\
&\propto k^{2p} \sum_{\boldsymbol{x},\boldsymbol{x}'} \frac{e^{i\boldsymbol{k}\cdot(\boldsymbol{x}'-\boldsymbol{x})}}{L^d} \langle\!\langle m \| \hat{e}_{\boldsymbol{m},\boldsymbol{x}} \hat{e}_{\boldsymbol{m},\boldsymbol{x}'} \| m \rangle\!\rangle \\
&= k^{2p} \langle\!\langle m \| \hat{e}_{\boldsymbol{m},\boldsymbol{k}} \hat{e}_{\boldsymbol{m},-\boldsymbol{k}} \| m \rangle\!\rangle.
\end{aligned} \tag{3.17}$$

Thus, if a system has bounded fluctuations of p^{th} order moments, as described by variables, $\hat{e}_{\boldsymbol{m},\boldsymbol{k}}$, the structure factor will scale as $\mathcal{N}_{\boldsymbol{k}} \sim k^{2p}$. Thus, Krylov sectors with bounded multipole densities up to order $p \leq m$ have $\mathcal{N}_k \to \sigma_p^2 \, k^{2p}$, leading to a dispersion,

$$E_k \leq \langle\!\langle \mathcal{K}_{\boldsymbol{k}}^s \| \hat{H}_{\mathcal{L}} \| \mathcal{K}_{\boldsymbol{k}}^s \rangle\!\rangle \propto \frac{k^4}{\mathcal{N}_k^{\mathcal{K}}} \propto k^{2(m-p+1)}. \tag{3.18}$$

S = 1 Example

As mentioned before, so long as we do not consider non-Abelian symmetry groups, we can consider our system to be constrained by "classical" symmetries, where the super-Hamiltonians map onto RK-type Hamiltonians[108]. This has been helpful because such systems are easily simulatable by mapping the evolution of diagonal elements of the density matrix to a classical Markovian process.

In order to verify the prediction in Eq. 3.16, we numerically evaluate the relaxation of classical systems exhibiting these constraints under discrete random time evolution. We emphasize that due to the universality of hydrodynamic transport, the same qualitative relaxation behavior is expected in thermalizing quantum many-body systems, see also Refs. [96, 97, 99, 109] for related approaches.

As a concrete example of Eq. (3.15), we consider random Brownian evolution in a $S = 1$ spin chain with local dipole-conserving terms $h_i = \hat{S}_i^+(\hat{S}_{i+1}^-)^2\hat{S}_{i+2}^+ + \text{h.c.}$. Although these terms induce a strong fragmentation of the Hilbert space, there exist exponentially large, delocalized Krylov sectors [101, 104]. We label the local charge density by $\hat{\rho}_x = S_x^z \in \{0, \pm\}$ and consider the Krylov sector containing the initial state $|\psi_0\rangle = |...00 + 00...\rangle$. In terms of the variables $\hat{e}_x$ introduced above, $|\psi_0\rangle = |...00111...\rangle$ corresponds to a domain wall, and the $\hat{e}_x \in \{0, 1\}$ can be shown to take values in a bounded range [101], thus satisfying our condition Eq. (3.15). Diffusive relaxation of this state has indeed been found in Ref. [106], and as we shall see, $\mathbb{E}\langle S^z_{x=L/2}(t)\rangle \sim t^{-1/2}$ can be verified numerically using random classical time evolution.

This time evolution is performed by applying local three-site updates that conserve both the charge $\sum_x \hat{\rho}_x$ and dipole moment $\sum_x x\,\hat{\rho}_x$ of the local three-site configuration. These updates are arranged in a brick wall pattern, as depicted in Fig. 3.2a. Furthermore, the updates are random, i.e. the updated charge configuration on the three sites is chosen randomly from all configurations within the same three-site charge and dipole sector. In Fig. 3.2b, we show the time evolution of $\mathbb{E}\left\langle\hat{\rho}_{x=L/2}(t)\right\rangle \sim t^{-1/2}$, confirming diffusive behavior. This is contrasted with the generic, subdiffusive decay $\sim t^{-1/4}$ seen when evolving the same initial state with similar local *four-site* updates, for which the associated Krylov sector no longer follows a charge area law. In Fig. 3.2e, we provide a scaling collapse of the full spatial profile of $\mathbb{E}\left\langle\hat{\rho}_x(t)\right\rangle$, again in agreement with diffusion. We note that the diffusive behavior in this Krylov sector has previously been reported in Ref. [106]. Within the framework developed in our work, the emergence of diffusion in dipole conserving systems is explained as a consequence of the more general charge area-law constraint given in Eq. (3.15).

2D Dimer-Vacancy Example

To further illustrate the generality of this result, we extend our analysis to systems beyond one spatial dimension. As a concrete example, we study the dynamics of a two-dimensional dimer-vacancy model, subject to the hard-core constraint of maximally one dimer attached to each lattice site, see Fig. 3.3a. Vacancies, i.e. sites without an attached dimer, carry a charge $\hat{\rho}(\boldsymbol{x}) = (-1)^{x_1+x_2}$. The constraint of either zero or one dimer on each bond of the lattice is equivalent to a finite electric field state space in a $U(1)$ link model formulation of this system [110, 111], ensuring area law charge fluctuations. We then explicitly demand the

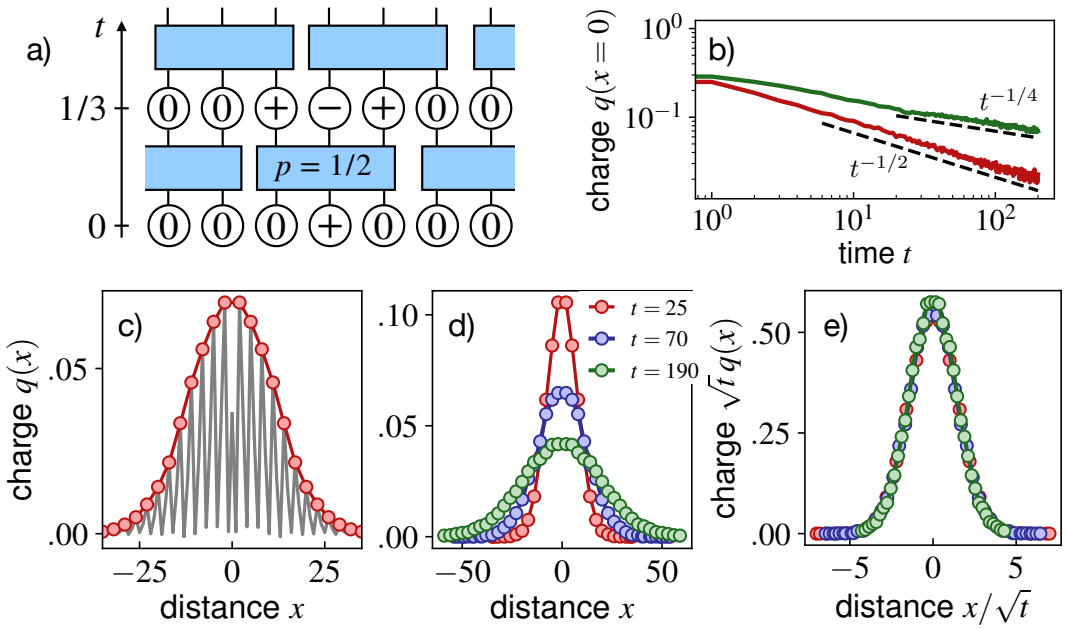

Figure 3.2: **Numerical simulation of dipole-conserving dynamics. a)** We simulate the relaxation dynamics of a classical, discrete random time evolution, in which dipole-conserving updates of a given spatial range are performed randomly. **b)** For evolution with 3-site updates, the charge excitation of the initial state shown in a) decays diffusively as $t^{-1/2}$ (red curve). In contrast, dynamics under 4-site updates lead to subdiffusive decay $t^{-1/4}$ expected for generic systems (green curve). **c)** Profile $\hat{\rho}(x,t)$ of the charge density at time $t = 60$ of the evolution defined in a) with 3-site updates. The red curve corresponds to an enveloping function. **d)** Enveloping functions of the charge density at different times. **e)** Diffusive scaling collapse of the enveloping functions shown in b). Numerical results were averaged over 2×10^5 runs of the random time evolution in a chain of length $L = 1000$.

conservation of both the total charge and dipole moment under time evolution.

More precisely, in analogy to $d = 1$, for $d > 1$ we write $\hat{\rho}(\boldsymbol{x}) = \boldsymbol{\nabla} \cdot \hat{\boldsymbol{e}}(\boldsymbol{x})$, where $\hat{\boldsymbol{e}}(\boldsymbol{x}) = (\hat{e}_1(\boldsymbol{x}), ..., \hat{e}_d(\boldsymbol{x}))$ is now a d-component vector. We recognize that $\hat{\boldsymbol{e}}(\boldsymbol{x})$ is not uniquely determined by the charge configuration $\hat{\rho}(\boldsymbol{x})$, and the relation between these variables takes the form of a $U(1)$ Gauss law, where the $\hat{\boldsymbol{e}}(\boldsymbol{x})$ constitute electric field degrees of freedom. Indeed, area-law charge fluctuations arise in $U(1)$ gauge theories if fluctuations of the electric fields $\hat{\boldsymbol{e}}(\boldsymbol{x})$ are bounded, as $\int_V dV \hat{\rho}(\boldsymbol{x}) = \int_{\partial V} d\boldsymbol{A} \cdot \hat{\boldsymbol{e}}(\boldsymbol{x})$. Thus, imposing global dipole conservation on $U(1)$ link models [112–114] with a finite electric field state space gives rise to diffusive behavior through Eq. (3.15). To verify this prediction, we numerically simulate classical, discrete random time evolution in a hard-core dimer model on a square lattice (see Fig. 3.3a), which can be mapped to a $U(1)$ link model [110, 111]. Under this mapping, a site $\boldsymbol{x}$ without any attached dimer carries a charge $\hat{\rho}(\boldsymbol{x}) = (-1)^{x_1+x_2}$ at $\boldsymbol{x} = (x_1, x_2)$, while a site with an attached dimer carries no charge.

To verify the emergence of diffusive relaxation in this setup, we implement a random, discrete classical time evolution similar to the previous example. Here, as depicted schematically in Fig. 3.3a), we first apply plaquette updates which randomly update the state of elementary

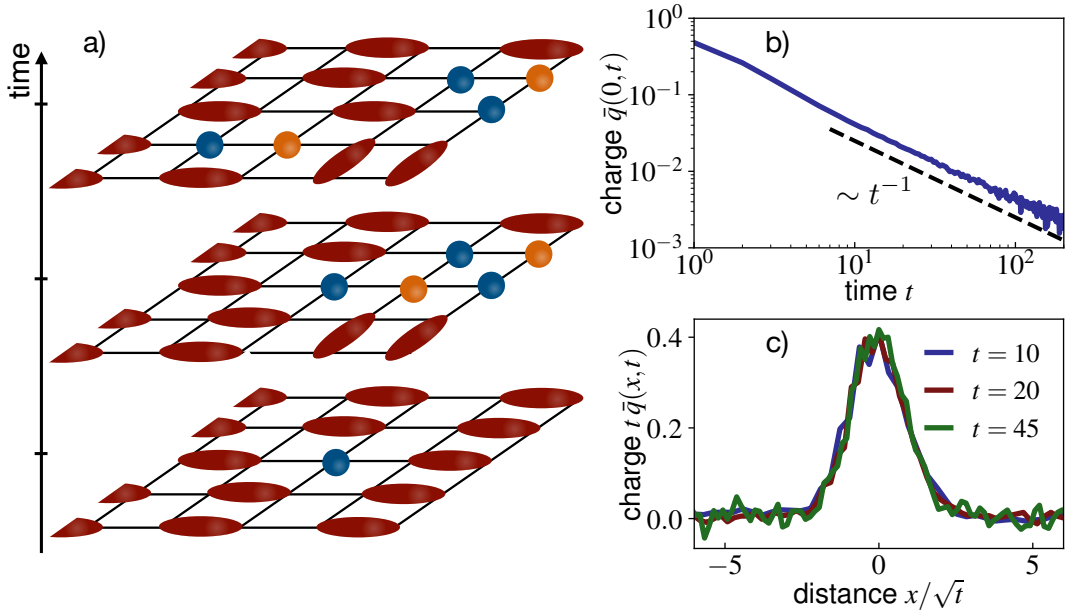

Figure 3.3: **Relaxation dynamics in a dipole-conserving dimer model. a)** We numerically consider a classical, discrete random time evolution in a dimer model with hard-core constraint, i.e. maximally one dimer attached to each site in the square lattice. This model can be mapped onto a $U(1)$ link model following Refs. [112–114]. Under this mapping, vacancies, i.e. sites without attached dimer, carry positive (blue spheres) or negative charge (orange spheres), depending on their sublattice. We explicitly incorporate preservation of the hard-core constraint, the total charge, and the dipole moment associated with these charges in the time evolution. **b)** Decay of the charge density $\bar{\rho}(0,t)$ for an isolated positive charge initially placed at $\boldsymbol{x} = 0$ in the bulk of the system: see a). The decay is consistent with diffusion in two dimensions. **c)** Scaling collapse of the charge distribution at different times along $\bar{\rho}(\boldsymbol{x} = (x,0),t)$, indicating Gaussian diffusion. Numerical results were averaged over 3×10^6 runs of the random time evolution.

square plaquettes that contain either a horizontal or vertical pair of parallel dimers, or four charges. This process conserves the total charge and dipole moment. Then, we apply random dipole hoppings of neighboring ±-charge pairs. Note that due to the sublattice structure of the local charge density $\hat{\rho}_x$, conservation of the dipole moment implies that these charge pairs may only hop along displacement vectors $\boldsymbol{r} = (r_x, r_y)$ that satisfy $(r_x + r_y) \mod 2 = 0$. In our numerical implementation, we take into account $(|r_x| = 2, r_y = 0)$, $(r_x = 0, |r_y| = 2)$, and $(|r_x| = 1, |r_y| = 1)$.

In the dynamics carried out numerically (see also Refs. [96, 97, 99, 109] for related approaches), we then explicitly incorporate conservation of the dipole moment associated to $\hat{\rho}(\boldsymbol{x})$. Starting from an initial state with an isolated positive charge in the bulk of the system $\hat{\rho}(\boldsymbol{x}, t = 0) = \delta_{x_1,0}\,\delta_{x_2,0}$ (see Fig. 3.3a), we numerically find a diffusive broadening of the resulting charge distribution at late times. As the overall charge density in the system vanishes, and positive and negative charges occupy different sublattices, we consider the quantity $\bar{\rho}(x_1, t) \equiv \hat{\rho}((x_1, 0), t) + \hat{\rho}((x_1 - 1, 0), t)$. We show in Fig. 3.3c that $t\,\bar{\rho}(x_1, t)$ exhibits a scaling collapse when plotted against $x_1/\sqrt{t}$, in agreement with diffusive relaxation in two dimensions.

3.4 Long-Range Interactions

While it is useful to consider short range interactions, many familiar forces and interactions involve long-ranged contributions. Such interactions can have profound effects in equilibrium systems, and thus, naturally, one might expect the same to be true in the non-equilibrium setting as well. To demonstrate this, we will begin our investigation by generalizing charge-conserving dynamics, then build on this by examining long-range interactions conserving various multipole moments.

3.4.1 Charge-conserving Interactions

We extend our preceding analysis to charge-conserving systems with long-range interactions, similarly to how we extended the analysis to multipole conserving systems. We will examine the effect of the symmetry on the commutor, $\mathcal{O}_{\boldsymbol{x},\lambda}$, which will reveal the scaling of the full effective Hamiltonian. Specifically, we consider the effects of long-range terms in our Hamiltonian of the following form[2]:

$$h_{\boldsymbol{x},\boldsymbol{x}'} = \frac{\hat{S}^+_{\boldsymbol{x}}\hat{S}^-_{\boldsymbol{x}'} + \text{h.c.}}{|\boldsymbol{x} - \boldsymbol{x}'|^\alpha} = \mathcal{O}_{\boldsymbol{x},\boldsymbol{x}'}, \tag{3.19}$$

where $\hat{S}^\pm_{\boldsymbol{x}}$ are raising and lowering operators for the charge $\hat{\rho}_{\boldsymbol{x}}$ at site $\boldsymbol{x}$ and $\hat{Q} = \sum_x \hat{\rho}_{\boldsymbol{x}}$ is conserved. The effective Hamiltonian reads $\hat{H}_{\mathcal{L}} = \sum_{\boldsymbol{x},\boldsymbol{x}'} \mathcal{O}^\dagger_{\boldsymbol{x},\boldsymbol{x}'}\mathcal{O}_{\boldsymbol{x},\boldsymbol{x}'}$ and the commutator

[2]These interactions are chosen in order to demonstrate non-trivial dynamics. Interactions that are diagonal in the symmetry basis will result in a trivial effective Hamiltonian, and all other operators can be built from raising and lowering operators combined with local commutation with $\hat{S}^z_{\boldsymbol{x}}$

entering Eq. (2.39) becomes

$$[\mathcal{O}_{\boldsymbol{x},\boldsymbol{x}'},\hat{\rho}_{\boldsymbol{k}}] = e^{i\boldsymbol{k}\cdot\boldsymbol{x}}\frac{(1-e^{i\boldsymbol{k}\cdot(\boldsymbol{x}'-\boldsymbol{x})})}{|\boldsymbol{x}-\boldsymbol{x}'|^{\alpha}}\left[\tilde{\mathcal{O}}_{\boldsymbol{x},\boldsymbol{x}'},\hat{\rho}_{\boldsymbol{x}}\right], \tag{3.20}$$

where $\tilde{\mathcal{O}}_{\boldsymbol{x},\boldsymbol{x}'} \equiv \mathcal{O}_{\boldsymbol{x},\boldsymbol{x}'}|\boldsymbol{x}-\boldsymbol{x}'|^{\alpha}$ is now distance-independent. Squaring each term yields the variational energy

$$\begin{aligned}
\langle\langle m_{\boldsymbol{k}}\|\hat{\mathcal{H}}_{\mathcal{L}}\|m_{\boldsymbol{k}}\rangle\rangle &\propto \sum_{\boldsymbol{x},\boldsymbol{x}'}\frac{(1-\cos\boldsymbol{k}\cdot(\boldsymbol{x}'-\boldsymbol{x}))}{|\boldsymbol{x}-\boldsymbol{x}'|^{2\alpha}} \\
&\quad\times\langle\langle m_{\boldsymbol{k}}\|\left[\tilde{\mathcal{O}}_{\boldsymbol{x},\boldsymbol{x}'},\hat{\rho}_{\boldsymbol{x}}\right]^{\dagger}\left[\tilde{\mathcal{O}}_{\boldsymbol{x},\boldsymbol{x}'},\hat{\rho}_{\boldsymbol{x}}\right]\|m_{\boldsymbol{k}}\rangle\rangle \\
&\quad\propto\int d^{d}\boldsymbol{r}\frac{(1-\cos\boldsymbol{k}\cdot\boldsymbol{r})}{|\boldsymbol{r}|^{2\alpha}} \\
&\propto\int d\Omega_{d-2}\int_{1}^{\infty}dr\int_{1}^{-1}du\frac{(1-\cos(ukr))}{|r|^{2\alpha-d+1}} \\
&\propto\int_{1}^{\infty}\frac{dr}{|r|^{2\alpha-d+1}}\left(2-\frac{\sin kr}{kr}\right) \\
&=\frac{{}_1F_2\left(\frac{d}{2}-\alpha;\frac{3}{2},\frac{d}{2}+1-\alpha;-\frac{k^2}{4}\right)-2}{2\alpha-d} \\
&\quad+\Gamma(-1-2\alpha+d)\cos\left(\pi\alpha-\frac{d\pi}{2}\right)|k|^{2\alpha-d} \\
&\underset{k\to 0}{\propto}\left(C_1(\alpha)|k|^{2\alpha-d}+C_2(\alpha)k^2\right),
\end{aligned} \tag{3.21}$$

where we have performed the spatial integral for $d\geq 3$ and $\alpha>\frac{d}{2}$, making use of the form of the angular integral. However, the asymptotic scaling form in the last line of Eq. (3.21) also holds for $d=1,2$. Above, we used the substitution $u=\cos\theta$ with θ the angle between $\boldsymbol{k}$ and $\boldsymbol{r}$, expanded out the hypergeometric function ,${}_1F_2(a;b_1,b_2;z)$, and defined $C_1(\alpha)$ and $C_2(\alpha)$ as $\mathcal{O}(1)$ coefficients obtained from this expansion that are smooth except at $\alpha=d/2$ and $1+d/2$. At $\alpha\leq d/2$, the spatial integral above exhibits IR divergences scaling with $\log L$ at $\alpha=d/2$ and with $L^{(d-2\alpha)}$ at $\alpha<d/2$, where L is the linear system size. Such a divergence of the single mode dispersion would lead to ultra-fast relaxation in the thermodynamic limit. However, for physical systems, we should renormalize the resulting dispersion to be bounded. In order to do so, we have to rescale the interaction strength with the diverging expression, which we label by $C_0(\alpha\leq\frac{d}{2},L)=\int_{|\boldsymbol{r}|<L}d^{d}\boldsymbol{r}\frac{(1-\cos\boldsymbol{k}\cdot\boldsymbol{r})}{|\boldsymbol{r}|^{2\alpha}}$. This rescaling leads to a finite energy gap at low k, and thus, relaxation within an $\mathcal{O}(1)$ time when $\alpha<d/2$.

Additionally, in this derivation, we assumed that the expectation $\langle\langle m_{\boldsymbol{k}}\|\left[\tilde{\mathcal{O}}_{\boldsymbol{x},\boldsymbol{x}'},\hat{\rho}_{\boldsymbol{x}}\right]^{\dagger}\left[\tilde{\mathcal{O}}_{\boldsymbol{x},\boldsymbol{x}'},\hat{\rho}_{\boldsymbol{x}}\right]\|m_{\boldsymbol{k}}\rangle\rangle$ did not depend on the distance, $\boldsymbol{x}-\boldsymbol{x}'$. This is true due to the same special property of the position-space representation of the $\|m\rangle\rangle$ state that allowed us to simplify Eq. (2.43): The correlation of two local operators acting on $\|m\rangle\rangle$ only depends on whether the operators are at the same or distinct sites because the state $\|m\rangle\rangle$ is invariant under the permutation of local sites. This is the case for $\langle\langle m_{\boldsymbol{k}}\|\left[\tilde{\mathcal{O}}_{\boldsymbol{x},\boldsymbol{x}'},\hat{\rho}_{\boldsymbol{x}}\right]^{\dagger}\left[\tilde{\mathcal{O}}_{\boldsymbol{x},\boldsymbol{x}'},\hat{\rho}_{\boldsymbol{x}}\right]\|m_{\boldsymbol{k}}\rangle\rangle$, and the quantity is independent of the distance $\boldsymbol{x}-\boldsymbol{x}'$.

Assuming a finite expectation value for the square of the commutator on the RHS of Eq. (3.20), the variational energy of $\|m_{\boldsymbol{k}}\rangle\rangle$ is

$$\langle\langle m_{\boldsymbol{k}}\|\hat{H}_{\mathcal{L}}\|m_{\boldsymbol{k}}\rangle\rangle \underset{k\to 0}{\propto} \begin{cases} C_0(\alpha, L) & \alpha \leq \frac{d}{2} \\ C_1(\alpha)|k|^{2\alpha-d} & \frac{d}{2} < \alpha < \frac{d}{2}+1 \\ C_2(\alpha)k^2 & \alpha \geq 1+\frac{d}{2}. \end{cases} \tag{3.22}$$

Thus, there will be three different dynamical regimes depending on the locality of interactions. When $\alpha > 1 + \frac{d}{2}$, interactions are sufficiently local as to reproduce the diffusion seen in the previous chapter. For $\frac{d}{2} < \alpha < 1 + d/2$, the system relaxes superdiffusively with $z = 2\alpha - d$, successfully reproducing previous works on long-range interacting systems [115–117]. On the other hand, for $\alpha \leq d/2$ the prefactors $C_1(\alpha)$ and $C_2(\alpha)$ exhibit divergences and the associated modes become gapped; accordingly, the operator decays exponentially fast [115], entering an effectively non-local "all-to-all" interacting regime.

3.4.2 Multipole-conserving Interactions

The previous section can now be straightforwardly extended to include higher multipole moment conservation. For clarity, we will always assume that we are describing dynamics within a system with weak HSF, whose largest Krylov sector, $\mathcal{K}$ does not have bounded charge or multipole fluctuations. Adding in these constraints will follow in the same fashion as outlined above.

Dipole Conservation

Similar to the charge-conserving case, these results can be extended to long-range interacting systems in arbitrary dimensions. First, we turn to the concrete case of dipole conservation. Here, we look at generic dipole hoppings of the form

$$h_{\boldsymbol{x},\boldsymbol{x}',\boldsymbol{n}} = \frac{(\hat{S}^+_{\boldsymbol{x}}\hat{S}^-_{\boldsymbol{x}+\boldsymbol{n}})(\hat{S}^-_{\boldsymbol{x}'}\hat{S}^+_{\boldsymbol{x}'+\boldsymbol{n}}) + \text{h.c.}}{|\boldsymbol{x}-\boldsymbol{x}'|^{\alpha_0}|\boldsymbol{n}|^{\alpha_1}}, \tag{3.23}$$

where $(\hat{S}^+_{\boldsymbol{x}}\hat{S}^-_{\boldsymbol{x}+\boldsymbol{n}})$ defines a dipole operator, $D_{\boldsymbol{x},\boldsymbol{n}}$, whose locality is controlled by the power, $\alpha_1 > \alpha_0$. Accordingly, our effective Hamiltonian will be of the form $\hat{H}_{\mathcal{L}} = \sum_{\boldsymbol{x},\boldsymbol{x}',\boldsymbol{n}} \mathcal{O}_{\boldsymbol{x},\boldsymbol{x}'}\mathcal{O}^\dagger_{\boldsymbol{x},\boldsymbol{x}',\boldsymbol{n}}$. With this, we return to calculate the commutator as above

$$\begin{aligned} [\mathcal{O}_{\boldsymbol{x},\boldsymbol{x}',\boldsymbol{n}}, \hat{\rho}_{\boldsymbol{k}}] &= \sum_{\boldsymbol{y}\in\mathcal{S}_{\boldsymbol{x}}} e^{i\boldsymbol{k}\cdot\boldsymbol{x}}[\mathcal{O}_{\boldsymbol{x},\boldsymbol{x}',\boldsymbol{n}}, e^{i\boldsymbol{k}\cdot(\boldsymbol{y}-\boldsymbol{x})}\hat{\rho}_{\boldsymbol{y}}] \\ &= e^{i\boldsymbol{k}\cdot\boldsymbol{x}}\frac{(1-e^{i\boldsymbol{k}\boldsymbol{n}})(1-e^{i\boldsymbol{k}\cdot(\boldsymbol{x}'-\boldsymbol{x})})}{|\boldsymbol{x}-\boldsymbol{x}'|^{\alpha_0}|\boldsymbol{n}|^{\alpha_1}}\left[\tilde{\mathcal{O}}_{\boldsymbol{x},\boldsymbol{x}',\boldsymbol{n}}, \hat{\rho}_{\boldsymbol{x}}\right], \end{aligned} \tag{3.24}$$

where $\tilde{\mathcal{O}}_{\boldsymbol{x},\boldsymbol{x}',\boldsymbol{n}} = \mathcal{O}_{\boldsymbol{x},\boldsymbol{x}',\boldsymbol{n}}|\boldsymbol{x}-\boldsymbol{x}'|^{\alpha_0}|\boldsymbol{n}|^{\alpha_1}$ moves the power-law displacement dependence to the commutator prefactor. Note that this prefactor now carries the dependence on the displacement, $\boldsymbol{r} = \boldsymbol{x} - \boldsymbol{x}'$, *and* an effective dipole size, $\boldsymbol{n}$. Repeating the same analysis as in

the charge conserving case,

$$\langle\langle \mathcal{K}_{\boldsymbol{k}} \| \hat{\mathcal{H}}_{\mathcal{L}} \| \mathcal{K}_{\boldsymbol{k}} \rangle\rangle \propto \sum_{\boldsymbol{r}} \frac{(1-\cos \boldsymbol{k}\cdot(\boldsymbol{r}))}{|\boldsymbol{r}|^{2\alpha_0}} \sum_{\boldsymbol{n}} \frac{(1-\cos \boldsymbol{k}\cdot \boldsymbol{n})}{|\boldsymbol{n}|^{2\alpha_1}}$$
$$\propto \begin{cases} C_0(\alpha_0, L) \int_{\boldsymbol{n}} \frac{(1-\cos \boldsymbol{k}\cdot \boldsymbol{n})}{|\boldsymbol{n}|^{2\alpha_1}}, & \alpha_0 \leq \frac{d}{2} \\ \int_{\boldsymbol{r}} \frac{(1-\cos \boldsymbol{k}\cdot \boldsymbol{r})}{|\boldsymbol{r}|^{2\alpha_0}} \int_{\boldsymbol{n}} \frac{(1-\cos \boldsymbol{k}\cdot \boldsymbol{n})}{|\boldsymbol{n}|^{2\alpha_1}} & \alpha_0 > \frac{d}{2}, \end{cases} \tag{3.25}$$

where $C_0(\alpha, L)$ is a constant diverging with system size as discussed below Eq. (3.21). Now, we proceed with the above integration for each range of α_0:

$$\begin{aligned} (\alpha_0 \leq d/2): \quad & E_{\boldsymbol{k}} \propto C_0(\alpha_0) \left(C_1(\alpha_1)|k|^{2\alpha_1 - d} + C_2(\alpha_1)k^2 \right) \underset{\alpha_1 \to \infty}{\propto} k^2 \\ (\alpha_0 > d/2): \quad & E_{\boldsymbol{k}} \propto \left(C_1(\alpha_0)|k|^{2\alpha_0 - d} + C_2(\alpha_0)k^2 \right) \left(C_1(\alpha_1)|k|^{2\alpha_1 - d} + C_2(\alpha_1)k^2 \right), \\ & \underset{\alpha_1 \to \infty}{\propto} \left(C_1(\alpha_0)|k|^{2\alpha_0 + 2 - d} + C_1(\alpha_0)k^4 \right), \end{aligned} \tag{3.26}$$

where $C_1(\alpha_{0/1})$ and $C_2(\alpha_{0/1})$ are the same as before, and we have taken the limit $\alpha_1 \to \infty$ in order to understand the behavior of local dipole dynamics.When $\alpha_1 \to \infty$, the effective Hamiltonian can be understood as describing long-ranged hopping of 2-local dipoles, $D_{\boldsymbol{x}} \equiv S^+_{\boldsymbol{x}} S^-_{\boldsymbol{x}+\mathbf{1}}$, where $\mathbf{1}$ is a unit vector. In this case, we once more obtain three dynamical regimes:

$$\langle\langle m_{\boldsymbol{k}} \| \hat{H}_{\mathcal{L}} \| m_{\boldsymbol{k}} \rangle\rangle \underset{k \to 0}{\propto} \begin{cases} C_0(\alpha, L)k^2 & \alpha \leq \frac{d}{2} \\ C_1(\alpha)|k|^{2\alpha + 2 - d} & \frac{d}{2} < \alpha < \frac{d}{2} + 1 \\ C_2(\alpha)k^4 & \alpha \geq 1 + \frac{d}{2}. \end{cases} \tag{3.27}$$

However, this does not exhaust all possibilities. For example, if both $\alpha_{1/0} \leq \frac{d}{2}$, we have diverging integrals for both $\boldsymbol{r}$ and $\boldsymbol{n}$, which results in finite-time relaxation after renormalizing the divergence. Aside from this fast relaxation, we identify five distinct regimes (note that the physics is symmetric under the exchange of $\alpha_0 \leftrightarrow \alpha_1$):

1. $\alpha_0, \alpha_1 > \frac{d}{2} + 1$:

   This regime contains the limiting case $\alpha_{0/1} \to \infty$, corresponding to local dipoles with nearest neighbor hoppings, and yields a dispersion $E_{\boldsymbol{k}} \sim k^4$.

2. $\alpha_1 > \frac{d}{2} + 1$ and $\frac{d}{2} < \alpha_0 < \frac{d}{2} + 1$:

   Local dipoles with long-range hoppings result in a dispersion $E_{\boldsymbol{k}} \sim k^{2(\alpha_0+1)-d}$

3. $\alpha_1 > \frac{d}{2} + 1$ and $\alpha_0 < \frac{d}{2}$:

   Hoppings of local dipoles becomes so long-ranged that they are nearly perfectly non-local and local charge transport arises from individual dipole creation/annihilation terms, $D_{\boldsymbol{x}} \equiv S^+_{\boldsymbol{x}} S^-_{\boldsymbol{x}+\mathbf{1}}$. This is equivalent to conventional charge conservation, and yields a dispersion $E_{\boldsymbol{k}} \sim k^2$.

4. $\frac{d}{2} < \alpha_0, \alpha_1 < \frac{d}{2} + 1$,

   Large dipoles with long-range hoppings yield a dispersion of $E_{\boldsymbol{k}} \sim k^{(2\alpha_0 - d) + (2\alpha_1 - d)}$. This gives rise to a dynamical exponent $z \in (0, 4)$.

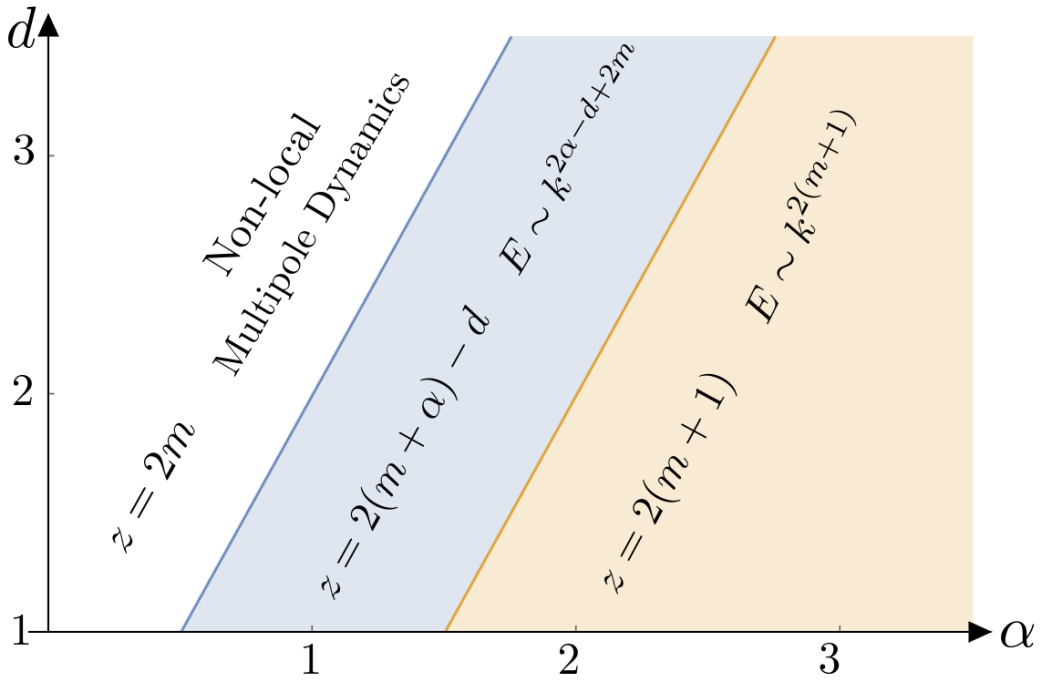

Figure 3.4: **Relaxation dynamics in multipole-conserving systems with long-range interactions.** Systems with $\frac{1}{r^\alpha}$ power-law decaying hopping of local multipoles of order m exhibit three distinct dynamical regimes. When $\alpha > \frac{d}{2} + 1$ (orange), the dynamics is (sub)diffusive with dynamical exponent $z = 2(m+1)$. For $\frac{d}{2}+1 > \alpha > \frac{d}{2}$ (blue), the dynamics is faster, with dynamical exponent $z = 2(m+\alpha) - d$. When $\alpha \leq \frac{d}{2}$, the system is effectively non-local, thus, relaxation occurs from individual m-th multipole creation/annihilation operators, which are hoppings of $(m-1)$-th multipole charges. This results in (sub)diffusive transport with $z = 2(m-1) + 2 = 2m$.

5. $\frac{d}{2} < \alpha_1 < \frac{d}{2} + 1$, $\alpha_0 < \frac{d}{2}$,

   Hoppings of large dipoles becomes so long-ranged that they are nearly perfectly non-local and local charge transport arises from the long individual dipole creation/annihilation terms, $D_{\boldsymbol{x},\boldsymbol{n}} \equiv S^+_{\boldsymbol{x}} S^-_{\boldsymbol{x}+\boldsymbol{n}}$. This yields a dispersion $E_{\boldsymbol{k}} \sim k^{(2\alpha_1 - d)}$, giving rise to a dynamical exponent $z \in (0, 2)$.

And we see that, depending on the internal locality of the dipole terms, $D_{\boldsymbol{x},\boldsymbol{n}} \equiv S^+_{\boldsymbol{x}} S^-_{\boldsymbol{x}+\boldsymbol{n}}$, and the hopping between such terms, one may develop dynamics that are superdiffusive, diffusive, or subdiffusive. This immediately generalizes to arbitrary multipole moments.

Multipole Conservation

The extension of this to systems conserving $\{Q^{(0)}, ..., Q^{(m)}\}$ multipoles is straightforward. A summary of the dynamical exponents emerging in multipole-conserving systems with such long-range hopping of local moments can be found in Fig. 3.4.

In the general case, however, interactions are composed of hoppings that scale as $\prod_{p=0}^{m} \frac{1}{|\boldsymbol{r}_p|^{\alpha_p}}$, where r_p indicates the hopping distance between $(m-p)$-th moment charges. Therefore, $\alpha_0, \ldots, \alpha_{m-2}, \alpha_{m-1}, \alpha_m$ control the locality of m-th moment hoppings ($(m+1)$-th moment sizes), ..., quadrupole hoppings (octopole size), dipole hoppings (quadrupole size), and charge hoppings (dipole lengths), respectively. From the above derivation, when all $\alpha_p > \frac{d}{2}$, our variational modes produce a dispersion of

$$\langle\langle \mathcal{K}_{\boldsymbol{k}} \| \hat{\mathcal{H}}_{\mathcal{L}} \| \mathcal{K}_{\boldsymbol{k}} \rangle\rangle \underset{k\to 0}{\propto} \prod_{p=0}^{m} \left(C_1(\alpha_p)|k|^{2\alpha_p - d} + C_2(\alpha_p)k^2 \right). \tag{3.28}$$

Whenever $\alpha_p < \frac{d}{2}$, the p-th term in this product is replaced by $C_0(\alpha_p, L)$, effectively acting as a constant upon renormalization of the divergence. As in the previous case, we enumerate four regimes:

1. $\alpha_0, \ldots, \alpha_m > \frac{d}{2} + 1$

   Local m-th moment charges with nearest neighbor hoppings yield a dispersion of $E_{\boldsymbol{k}} \sim k^{2(m+1)}$

2. $\alpha_1, \ldots, \alpha_m > \frac{d}{2} + 1$ and $\frac{d}{2} < \alpha_0 < \frac{d}{2} + 1$,

   Local m-th moment charges with long-range hoppings yield a dispersion of $E_{\boldsymbol{k}} \sim k^{2(\alpha_0+m)-d}$

3. $\alpha_1, \ldots, \alpha_m > \frac{d}{2} + 1$ and $\alpha_0 < \frac{d}{2}$,

   Local m-th moment charges with extensive hoppings yield a dispersion of $E_{\boldsymbol{k}} \sim k^{2m}$

4. $\frac{d}{2} < \alpha_0, \ldots, \alpha_m < \frac{d}{2} + 1$,

   Extended m-th moment charges with long-range hoppings yield a dispersion $E_{\boldsymbol{k}} \sim k^{\sum_{p=0}^{m}(2\alpha_p - d)}$. Since $0 < 2\alpha_i - d < 2$, the dynamical exponent $z = \sum_p (2\alpha_p - d) \in (0, 2(m+1))$ covers the entire range between finite-time relaxation and conventional multipole subdiffusion.

In [118], we focus on cases 1-3, where transport can be accounted for by local excitations, however, our method accounts for dynamics for all ranges of different α_p, where case 4 corresponds to a particular example.

3.5 Lindbladian Dynamics

Thus far, we have expanded the applicability of our model by including both short and long-range interactions that obey non-Abelian symmetries and symmetries with spatial components. We have already come a long way from the Haar-random dynamics of unstructured quantum circuits. Yet, there remains two major elements missing from this framework: discrete-time evolution and coherent dynamics. The former will prove to be little trouble. However, as will be explained below, describing coherent and incoherent dynamics simultaneously will prove difficult for general systems; yet, with some additional constraints, much of the above analysis may still be employed.

Discrete Evolution

Addressing discrete time-evolution will follow naturally now that we have a notion of the continuous case. First, we remark that the averaged dynamics in the doubled Hilbert space can be expressed as

$$e^{-\hat{\mathcal{H}}_{\mathcal{L}}dt} := \int dB_t p(dB_t)\big(e^{-ih^T(dB_t)dt} \otimes e^{-ih(dB_t)dt}\big) \tag{3.29}$$

where $p(dB_t)$ is the probability distribution for the Brownian random variable dB_t. The above expression can be immediately extended to any random local-unitary ensemble $\mathcal{U} = \{(p(U), U)\}$ where each U conserves a desired symmetry (e.g. U(1)) by replacing a continuous time evolution by a discrete-time evolution, where its averaged dynamics for each time step is captured as

$$e^{-\mathcal{H}} = \int dU p(U)\big(U^T \otimes U\big). \tag{3.30}$$

Note that the RHS is really a completely positive trace preserving (CPTP) map with eigenvalue magnitudes always equal or smaller than 1, implying that $\mathcal{H} \succcurlyeq 0$. Now, the late-time averaged dynamics of this random ensemble $\mathcal{U}$ is captured by the low energy spectrum of the effective Hamiltonian $\mathcal{H}$, since after the application of this random unitary circuit layers $T \gg 1$ times, the Choi states with small eigenvalues against $\mathcal{H}$ would survive.

3.5.1 Non-Hermitian Effective Hamiltonian

Now we return to the question of coherent dynamics. Before, we analyzed the vectorized form of a Markovian quantum master equation generated from a Brownian random circuit. This resulted in a Hermitian effective Hamiltonian whose low-energy modes describe late-time dynamics. However, as we will see, a generic effective Hamiltonian for Lindbladian evolution will result in a non-Hermitian Hamiltonian with a complex spectrum as shown in Fig. 3.5

Let us now attempt to extend our perspective to encompass the full Lindblad equation, the most general Markovian QME, and its corresponding effective Hamiltonian. If we recall the definition of the full Lindblad equation from Eq. 1.63, the time evolution of the density matrix (or operator) is given as

$$\dot{\rho} = -i[H, \rho] + \sum_i \gamma_i \left(L_i \rho L_i^\dagger - \frac{1}{2}\{L_i^\dagger L_i, \rho\} \right). \tag{3.31}$$

Under the Choi isomorphism, it can be expressed as the action of the following non-Hermitian linear operator $\hat{\mathcal{H}}_{\mathcal{L}}$ on $\|\rho\rangle\rangle$:

$$\begin{aligned} \hat{\mathcal{H}}_{\mathcal{L}} = &-i\big(H^T \otimes \mathbb{I} - \mathbb{I} \otimes H\big) \\ &- \sum_i \frac{\gamma_i}{2}\Big(2L_i^* \otimes L_i - (L_i^\dagger L_i)^T \otimes \mathbb{I} - \mathbb{I} \otimes L_i^\dagger L_i\Big), \end{aligned} \tag{3.32}$$

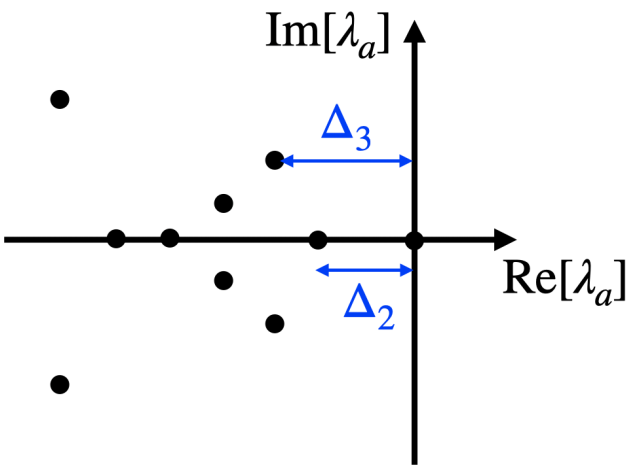

Figure 3.5: **Complex Spectra for a generic effective Hamiltonian,** $\hat{H}_{\mathcal{L}}$: There will always be at least one ground state with $\lambda = 0$, hermiticity will ensure a pairing of conjugate excited states with imaginary components, and generic decay of correlations often is determined by the spectral gap, Δ_2. Figure reproduced from [119].

where H is the system Hamiltonian, L_i are the jump operators, and $\gamma_i \geq 0$ are the damping weights. When the jump operators are Hermitian up to a phase, i.e. $L_i^\dagger = e^{i\theta} L_i$, and we set $H = 0$, we see a familiar form:

$$\hat{\mathcal{H}}_{\mathcal{L}} = \sum_i \frac{\gamma_i}{2} |L_i^T \otimes \mathbb{I} - \mathbb{I} \otimes L_i|^2 = \frac{1}{2} \sum_{\boldsymbol{x},\nu} \tilde{\mathcal{O}}_{\boldsymbol{x},\nu}^\dagger \tilde{\mathcal{O}}_{\boldsymbol{x},\nu}, \tag{3.33}$$

where $\tilde{O}_{i=(\boldsymbol{x},\nu)} = L_i^T \otimes \mathbb{I} - \mathbb{I} \otimes L_i$. Thus, in a system obeying Lindbladian dynamics governed by hermitian jump operators, our previous results should all hold. The intuition for this is as follows: a system whose interaction with the environment can be well approximated by hermitian operators implies that the thermalization timescale for the environment is so rapid that interactions take the form $H_{\text{int}} = L_i \otimes \mathbb{I}_{\text{env}}$. For this to hold generally, these thermalizing dynamics must be shorter than any timescale in the system, implying that the Boltzmann time of the environment $\tau_\beta \to 0$, and $T \to \infty$ in the thermodynamic limit. Thus, interaction with an infinite temperature bath imitates the steady state for random Brownian evolution with Hermitian interactions.

This form can also be derived from the Brownian circuit formalism used in the previous chapter. In Ch.2, we chose a specific type of Brownian circuit in order to demonstrate charge transport in a clear manner. Now, we will derive the Choi operator for the averaged dynamics of a general Brownian circuit.

The most general Brownian circuit employs random variables $\{dB_i\}$ for the time slice $[t, t + \Delta t)$ such that the first moment $\mathbb{E}[dB_i] = \mu_i$ and the second moment $\mathbb{E}[dB_i dB_j] = \mu_i \mu_j + \frac{\delta_{ij}}{\Delta t}$. Using these variables, the Hamiltonian at time slice $[t, t + \Delta t)$ is defined as

$H_t \equiv \sum_i h_i dB_{i,t}$, so that a density matrix ρ_t evolves as

$$e^{-iH_t\Delta t}\rho_t e^{iH_t\Delta t} = \rho_t - i\Delta t\sum_i [h_i,\rho_t]dB_i \\ - \frac{(\Delta t)^2}{2}\sum_{i,j}[h_i,[h_j,\rho_t]]dB_i\,dB_j + \cdots . \tag{3.34}$$

This allows one to characterize the expected continuous-time dynamics of ρ_t as

$$\begin{aligned}\mathbb{E}[\partial_\tau \rho] &\equiv \lim_{\Delta t\to 0}\frac{\mathbb{E}[\rho_{t+\Delta t}-\rho_t]}{\Delta t} \\ &= \sum_i \Big(-i\mu_i[h_i,\rho] - \frac{1}{2}[h_i,[h_i,\rho]]\Big) \\ &= \sum_i \Big(-i\mu_i(h_i\rho-\rho h_i) - \frac{1}{2}(h_i^2\rho - 2h_i\rho h_i + \rho h_i^2)\Big).\end{aligned} \tag{3.35}$$

Employing the Choi isomorphism explained in the previous section, we can recast the operator ρ_t as a state vector in a doubled Hilbert space, $\|\rho_t\rangle\rangle$. Similarly, the above action of averaged time evolution, which can be understood as a quantum channel, can be recast into a linear operator $\hat{\mathcal{H}}_{\mathcal{L}}$ acting on the doubled state as $\partial_\tau\|\rho\rangle\rangle = -\hat{\mathcal{H}}_{\mathcal{L}}\|\rho\rangle\rangle$ where

$$\begin{aligned}\hat{\mathcal{H}}_{\mathcal{L}} &= \sum_i i\mu_i\big(h_i^T\otimes\mathbb{I} - \mathbb{I}\otimes h_i\big) + \big(h_i^T\otimes\mathbb{I}-\mathbb{I}\otimes h_i\big)^2 \\ &= \sum_i \big(i\mu_i\mathcal{O}_i + \mathcal{O}_i^\dagger\mathcal{O}_i\big),\end{aligned} \tag{3.36}$$

where $\mathcal{O}_i \equiv h_i^T\otimes\mathbb{I} - \mathbb{I}\otimes h_i$. At $\mu_i = 0$, we recover the sum of squares form from Eq.2.21. Note that this is not quite as general as Eq. 3.32 because the first and second terms are still linked so that there cannot be any coherent dynamics without an incoherent counterpart. This is due to the structure imposed in the Brownian evolution, and is not a fundamental constraint, therefore we will continue on with the more general expression from Eq. 3.32.

In all the work above, we have discussed the Brownian dynamics essentially captured by Eq. (3.31) with $H = 0$ and $L = e^{i\theta}L^\dagger$. However, our formalism is capable of describing random unitary evolution as well as more general Lindbladian evolution.

Quantum Coherent Terms

For more generic Lindbladian evolution, we loosen the restrictions imposed by Brownian evolution and add quantum-coherent terms to our Lindbladian to examine the effects on our dynamics. To do so, we return to Eq. (3.36) with $\mu_i \neq 0$ or Eq. (3.31) with $H \neq 0$. Treating each term separately, we get

$$\begin{aligned}\hat{H}_{\mathcal{L}} &= iH_1 + H_2 \\ H_1 &= -\big(H^T\otimes\mathbb{I} - \mathbb{I}\otimes H\big) \\ H_2 &= \sum_i \frac{\gamma_i}{2}\left(L_i^T\otimes\mathbb{I}-\mathbb{I}\otimes L_i\right)^\dagger\left(L_i^T\otimes\mathbb{I}-\mathbb{I}\otimes L_i\right)\end{aligned} \tag{3.37}$$

where H_1 and H_2 are Hermitian operators. Note that H_2 is positive semi-definite and $\|\mathbb{I}\rangle\rangle$ is the ground state with zero energy, i.e., $H_1\|\mathbb{I}\rangle\rangle = H_2\|\mathbb{I}\rangle\rangle = 0$. This is because

$$(O \otimes \mathbb{I})\|\mathbb{I}\rangle\rangle = (\mathbb{I} \otimes O^T)\|\mathbb{I}\rangle\rangle. \tag{3.38}$$

From this decomposition, one might expect that iH_1 contributes to the coherent evolution of the density matrix, creating oscillations in the diffusive profile or adding a ballistically moving center of diffusion, while H_2 causes diffusion of the wavepacket.

Let us see how this intuition carries through. Take the above effective Hamiltonian and further assume that each component is independently symmetry preserving: $[H_{1,2}, Q_{\text{diag}}] = 0$ (this condition is equivalent to $[H, Q] = [L_i, Q] = 0$). These two components may not commute; however, due to translation invariance, they should still have a spectrum parameterized by momentum eigenstates as $E_{\boldsymbol{k},\nu} = if_1(\boldsymbol{k},\nu) + f_2(\boldsymbol{k},\nu)$. As such, the autocorrelation function should take the form:

$$\begin{aligned}&\mathbb{E}\langle O_{\boldsymbol{y}}(t)O_{\boldsymbol{x}}(0)\rangle_\rho \\ &\quad\propto \sum_{\boldsymbol{k},\nu} e^{i\boldsymbol{k}\cdot\Delta\boldsymbol{x} - if_1(\boldsymbol{k},\nu)t} e^{-tf_2(\boldsymbol{k},\nu)} |\langle\langle \boldsymbol{k},\nu\|O_{\boldsymbol{x}}\rangle\rangle|^2\end{aligned} \tag{3.39}$$

where $\Delta x = y - x$. Now if we assume that $f_1(\boldsymbol{k},\nu) \approx c_\nu \boldsymbol{k} + \ldots$ is approximately linear for small k, and $f_2(\boldsymbol{k},\nu) \sim k^\beta$, then we obtain just what we might expect: a decay determined by the real part, yielding an expected decay, but with one operator in the autocorrelation shifted by distance $\Delta x = c_\nu t$

$$\mathbb{E}\langle O_{\boldsymbol{x}-\boldsymbol{c_\nu t}}(t)O_{\boldsymbol{x}}(0)\rangle_\rho \underset{t\to\infty}{\sim} \int_k e^{-t(E_0+k^\beta)} \mathrm{d}^d\boldsymbol{k} \sim \frac{e^{-tE_0}}{|t|^{d/\beta}}. \tag{3.40}$$

Now, let us derive these real and imaginary components for charge conserving dynamics. Using the variational states defined in the main text, the variational energy is

$$\begin{aligned}\langle\langle m_{\boldsymbol{k}}\|\hat{H}_{\mathcal{L}}\|m_{\boldsymbol{k}}\rangle\rangle &= i\langle\langle m_{\boldsymbol{k}}\|H_1\|m_{\boldsymbol{k}}\rangle\rangle + \langle\langle m_{\boldsymbol{k}}\|H_2\|m_{\boldsymbol{k}}\rangle\rangle \\ &= i\langle\langle m\|\rho_{-k}[H_1,\rho_k]\|m\rangle\rangle \\ &\quad + \sum_{i,\lambda}\langle\langle m\|[\mathcal{O}_{i,\lambda},\rho_k]^\dagger[\mathcal{O}_{i,\lambda},\rho_k]\|m\rangle\rangle \\ &\underset{k\to 0}{\approx} iC_1k + C_2k^2.\end{aligned} \tag{3.41}$$

The first term is linear in k for a generic H_1 because $[H_1,\rho_k] = \sum_{n,x}\frac{(ikx)^n}{n!}[H_1,\rho_x]$, and the $n = 0$ term vanishes due to symmetry. Naively, this would seem to give the appropriate scaling for a ballistically spreading front; however, we have to be careful when applying our variational estimate. While it is still true that our variational modes may bound the real spectrum arising from H_2, the imaginary component coming from H_1 should not have any such bound. Instead, the imaginary component of the spectrum will generically either be gapped or have a linear dispersion. Expanding to the lowest order, we have $f_1(\boldsymbol{k},\nu) \approx c_{0,\nu} + c_\nu\boldsymbol{k} + \ldots$, where $c_{0,\nu}$ can be zero.

Thus, we cannot prove the imaginary component of the true complex-valued spectrum will scale with the gapless expected energy of our variational modes. Instead, one will generically expect a non-zero $c_{0,\nu}$, resulting in diffusion with some form of oscillating amplitude.

$$\mathbb{E}\langle O_{\boldsymbol{y}}(t)O_{\boldsymbol{x}}(0)\rangle_\rho \underset{t\to\infty}{\sim} \int_k e^{i(k\Delta x - C_1 t)} e^{-tC_2 k^2} dk \tag{3.42}$$
$$\sim e^{-iC_1 t} \frac{e^{-\frac{(\Delta x)^2}{4C_2 t}}}{\sqrt{C_2 t}}.$$

To make this more precise, we need to bring up an important fact about Lindbladians. Because they preserve hermiticity (as encoded by the SWAP symmetry in Sec. A, which is complex-conjugation symmetry in the operator formalism), any complex-valued eigenstates of our effective Hamiltonian, $\hat{\mathcal{H}}_{\mathcal{L}}$, must come in conjugate pairs. As such, there will always exist an index ν' such that, at lowest order, the spectrum is $E_{\boldsymbol{k},\nu'} = iC_{1,\nu'} + C_{2,\nu'}k^2$, where $C_{1,\nu'} = -C_{1,\nu}$, $C_{2,\nu'} = C_{2,\nu}$. Thus, we obtain multiple spreading fronts, so that, summing over these pairs

$$\mathbb{E}\langle O_{\boldsymbol{y}}(t)O_{\boldsymbol{x}}(0)\rangle_\rho \underset{t\to\infty}{\sim} \sum_{\nu\neq\nu'} \frac{\cos\left(C_{1,\nu}t\right) e^{-\frac{(\Delta x)^2}{4C_{2,\nu}t}}}{\sqrt{C_{2,\nu}t}}, \tag{3.43}$$

and we see that a typical system will be defined by simultaneous oscillating correlations and diffusive decay.

If one can confirm $c_{0,\nu} = 0$, we recover exactly the form needed for a ballistic front. This spectrum will produce diffusion from a ballistically moving front as captured by the autocorrelation function:

$$\mathbb{E}\langle O_{\boldsymbol{y}}(t)O_{\boldsymbol{x}}(0)\rangle_\rho \underset{t\to\infty}{\sim} \int_k e^{ik(\Delta x - C_1 t)} e^{-tC_2 k^2} dk \tag{3.44}$$
$$\sim \frac{e^{-\frac{(\Delta x - C_1 t)^2}{4C_2 t}}}{\sqrt{C_2 t}}.$$

Further, an important fact about Lindbladians allows us to capture the dynamics of multiple fronts. Because they preserve hermiticity (as encoded by the SWAP symmetry in Sec.2.2.1, which is complex-conjugation symmetry in the operator formalism), any complex-valued eigenstates of our effective Hamiltonian, $\hat{H}_{\mathcal{L}}$, must come in conjugate pairs. As such, there will always exist an index ν' such that $E_{\boldsymbol{k},\nu'} = iC_{1,\nu'}k + C_{2,\nu'}k^2$, where $C_{1,\nu'} = -C_{1,\nu}$, $C_{2,\nu'} = C_{2,\nu}$. Thus, we obtain multiple spreading fronts, so that, summing over these pairs

$$\mathbb{E}\langle O_{\boldsymbol{y}}(t)O_{\boldsymbol{x}}(0)\rangle_\rho \underset{t\to\infty}{\sim} \sum_{\nu\neq\nu'} \frac{e^{-\frac{(\Delta x - C_{1,\nu}t)^2}{4C_{2,\nu}t}} + e^{-\frac{(\Delta x + C_{1,\nu}t)^2}{4C_{2,\nu}t}}}{\sqrt{C_{2,\nu}t}}, \tag{3.45}$$

and we would expect that such a system will have at least two counter-propagating fronts with the expected diffusion.

We now address the complications that arise for the most general form of this non-Hermitian effective Hamiltonian.

Non-Hermitian Jump terms

As a non-Hermitian Hamiltonian, $\hat{H_{\mathcal{L}}}$ will generically have different left and right eigenvectors $\langle\langle L_\alpha\|$ and $\|R_\alpha\rangle\rangle$ for the shared eigenvalue ϵ_α. Although generically right (left) eigenvectors are not orthogonal to each other, they satisfy a biorthonormality:

$$\langle\langle L_\alpha\|R_\beta\rangle\rangle = \delta_{\alpha\beta}. \tag{3.46}$$

Thus, if we wish to describe to the evolution of an operator $\langle O(t)\rangle = \mathrm{tr}(O\rho(t)) = \langle\langle O\|e^{-t\hat{\mathcal{H}_{\mathcal{L}}}}\|\rho\rangle\rangle$, we may choose to study late-time dynamics in the Schrödinger picture by focusing on right eigenvectors with ground state $\|\rho_{eq}\rangle\rangle$, or in the Heisenberg picture by focusing on left eigenvectors with ground state $\langle\langle\mathbb{I}\|$.

To carry out further analysis, we switch from density matrix evolution to operator evolution. This is because the steady state for density matrix evolution is generically not the maximally mixed state $\mathbb{I}$, yet that of operator evolution always is due to the trace-preserving nature of the Lindbladian dynamics.

$$\begin{aligned} &\mathrm{tr}(\rho(t)) = \langle\langle\mathbb{I}\|\rho(t)\rangle\rangle = 1 \\ \Rightarrow\quad &\partial_t\langle\langle\mathbb{I}\|\rho\rangle\rangle = \langle\langle\mathbb{I}\|\hat{\mathcal{H}_{\mathcal{L}}}\|\rho\rangle\rangle = 0 \end{aligned} \tag{3.47}$$

Since this holds for any density matrix, $\|\rho\rangle\rangle$, it is clear that $\langle\langle\mathbb{I}\|$ is a left-ground state. This ground state structure greatly simplifies our analysis, and since we care about the rates of decay, not the exact form of the equilibrium density matrix, we focus on operator evolution.

The operator evolution is given as

$$\begin{aligned} \dot{O} &= i[H,O] + \sum_i \gamma_i\left(L_i^\dagger O L_i - \frac{1}{2}\{L_i^\dagger L_i, O\}\right) \\ &= i[H,O] + \sum_i \frac{\gamma_i}{2}\left(\{L_i^h,[O,L_i^a]\} - \{L_i^a,[O,L_i^h]\}\right) \\ &+ \sum_i \frac{\gamma_i}{2}\left([L_i^h,[O,L_i^h]] + [L_i^a,[O,L_i^a]]\right) \end{aligned} \tag{3.48}$$

Where we have split the jump operator into hermitian and antihermitian components, $L_i = L_i^h + iL_i^a$, where both L^h and L^a are hermitian. Using the Choi-Isomorphism, this can be translated into an effective Hamiltonian of the form

$$\begin{aligned} \hat{\mathcal{H}_{\mathcal{L}}} &= iH_1 + H_2 \\ H_1 &= \left(H^T\otimes\mathbb{I} - \mathbb{I}\otimes H\right) \\ &+ \sum_i \frac{\gamma_i}{2}\left((L_i^h)^T\otimes\mathbb{I} + \mathbb{I}\otimes L_i^h\right)\left(\mathbb{I}\otimes(L_i^a)^T - L_i^a\otimes\mathbb{I}\right) \\ &- \sum_i \frac{\gamma_i}{2}\left((L_i^a)^T\otimes\mathbb{I} + \mathbb{I}\otimes L_i^a\right)\left(\mathbb{I}\otimes(L_i^h)^T - L_i^h\otimes\mathbb{I}\right) \\ H_2 &= \sum_i \frac{\gamma_i}{2}\left((L_i^h)^T\otimes\mathbb{I} - \mathbb{I}\otimes L_i^h\right)^2 \\ &+ \sum_i \frac{\gamma_i}{2}\left((L_i^a)^T\otimes\mathbb{I} - \mathbb{I}\otimes L_i^a\right)^2, \end{aligned} \tag{3.49}$$

where H_1 and H_2 are both Hermitian.Using (3.38), it quickly follows that $H_1\|\mathbb{I}\rangle\rangle = H_2\|\mathbb{I}\rangle\rangle = 0$. Given this, using the same logic as above, we see that the new iH_1 will has the potential to contribute to ballistic spreading, now with additional influence from the jump operators L_i. Further, H_2, now the sum of two locally squared operators, will once more result in diffusion.

Liouvillian Gap

Before closing this chapter, we must address one final assumption that underlies our analysis. That is the correspondence between the *Liouvillian Gap*, or spectral gap, of our effective Hamiltonian and the thermalization time for our system. To understand this point, we must return to Eq. 2.23:

$$\begin{aligned}\mathbb{E}\langle O_{\boldsymbol{y}}(0)O_{\boldsymbol{x}}(t)\rangle_\rho &= \frac{1}{D}\langle\langle O_{\boldsymbol{y}}(0)\|e^{-t\hat{H}_{\mathcal{L}}}\|O_{\boldsymbol{x}}(0)\rangle\rangle \\ &= \frac{1}{D}\sum_{\boldsymbol{k},\nu} e^{-tE_{\boldsymbol{k},\nu}}e^{i\boldsymbol{k}\cdot(\boldsymbol{y}-\boldsymbol{x})}|\langle\langle \boldsymbol{k},\nu\|O_{\boldsymbol{x}}\rangle\rangle|^2. \end{aligned} \tag{3.50}$$

From this, we see that calculating late-time dynamics are requires an understanding of the spectrum, given by $E_{\boldsymbol{k},\nu}$ *and* the initial conditions, given by the expansion coefficients, $|c_{\boldsymbol{k},\nu}|^2 = |\langle\langle \boldsymbol{k},\nu\|O_{\boldsymbol{x}}\rangle\rangle|^2$. If the effective Hamiltonian, $\hat{H}_{\mathcal{L}}$ is translation invariant and Hermitian, then for a local $O_{\boldsymbol{x}}$, the expansion coefficients are approximately evenly distributed over low momenta. As such, we have only focused on the spectral gap, $\Delta_{\mathcal{L}}$.

Naively, the time of equilibration is related to this spectral gap as $\tau_{\mathcal{L}} \sim \frac{1}{\Delta_{\mathcal{L}}}$, however, one must be careful to account for the initial weights on slow decaying modes to ensure $c_{\boldsymbol{k},\nu}e^{-E_{\boldsymbol{k},\nu}t} \ll 1$ for $t > \tau_{\mathcal{L}}$. Non-Hermitian Hamiltonians, in particular, are prone to produce non-uniform spatial distributions of charges. These non-uniform expansion coefficients cause the equilibration time, often referred to as the *mixing time*, to deviate from $\tau_{\mathcal{L}}$[119–122]. Because of this, we provide a more general definition of the equilibration time, $\tau_m(\epsilon)$:

$$\tau_m(\epsilon) \equiv \min(t): \quad d(t) \leq \epsilon, \tag{3.51}$$

for a cutoff $\epsilon > 0$, and a distance defined as $d(t) = \max[||\hat{\rho}(t) - \hat{\rho}_{\text{SS}}||_1]$. Where we have, again, employed the trace norm. The exact choice of ϵ matters very little, as typical transitions occur relatively rapidly due to the cutoff phenomenon, where $\lim_{L\to\infty} \frac{\Delta\tau_m(\epsilon)}{\tau_{\epsilon_c}} = 0$[123, 124]. (See Fig. 3.6)

Thus, when considering combinations of coherent and incoherent dynamics that produce a non-Hermitian $\hat{H}_{\mathcal{L}}$, one must pay special attention to the initial states present and analyze their effect in relaxation to a steady state.[3]

As we can see, the doubled Hilbert space formalism is powerful enough to capture a vast array of chaotic unitary dynamics, however caution must be taken when including coherent and incoherent evolution simultaneously. In the next chapter, we will attempt to characterize

[3]Recently, a different perspective has emerged that the decay following the Louiviliian gap follows when initial states are sufficiently "close" to the steady state of a system, as defined by some operator norm, but diverge otherwise. This results in a condition of validity for using the Louivillian gap, dubbed "uniformity."[125]

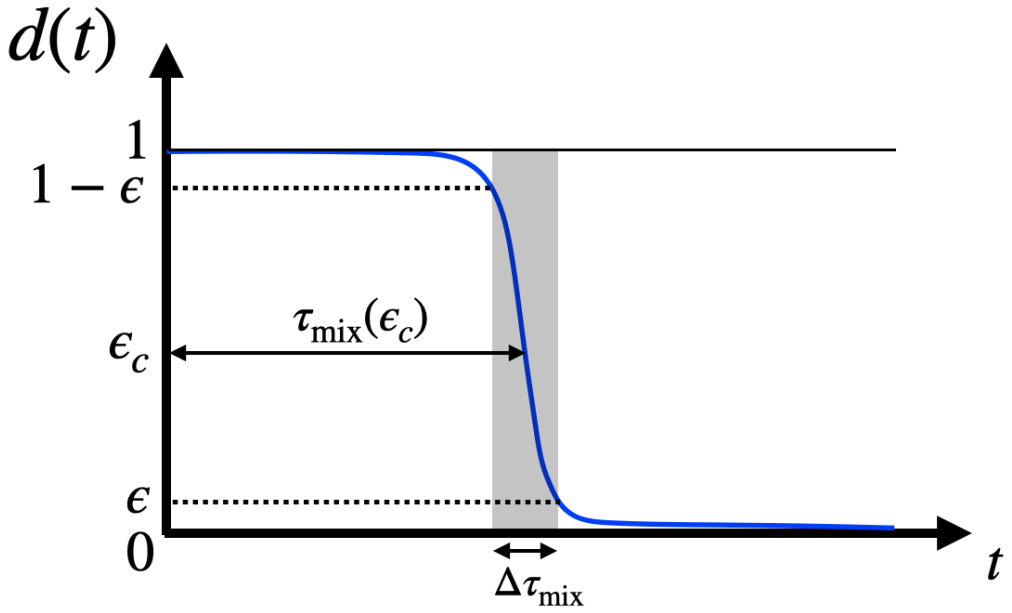

Figure 3.6: **Cutoff phenomena for mixing times**: At times $t \sim \tau_{\text{mix}}(\epsilon_c)$, the distance from the steady state, $d(t)$ rapidly drops from 1 to 0 in the thermodynamic limit, where $\frac{\Delta\tau_m(\epsilon)}{\tau_{\epsilon_c}} \to 0$. Figure reproduced from [119].

some more subtle aspects of dynamics captured by multiple copies of a system, including the dynamical effects arising from monitored quantum circuits.

Nomenclature for Chapter 3

Selected Abbreviations

HSF Hilbert Space Fragmentation

QME Quantum Master Equation

Variables

$\mathcal{K}$ Krylov secctor

$D_{\boldsymbol{x}}$ Local dipole operator of a form similar to $D_{\boldsymbol{x}} = S^+_{\boldsymbol{x}} S^-_{\boldsymbol{x}+\boldsymbol{a}}$ + h.c.

Chapter 4

Higher Moments and Measurement

In this chapter, we will expand the above formalism to address measures involving higher moments of the density matrix. As mentioned in the introduction, these will be particularly important in quantifying the dynamics of entanglement and allow for investigations of the effects of measurement in dynamical systems. Before addressing the role of symmetry, we will need to acquaint ourselves with the expected measurement dynamics with and without measurement. With no measurement present, we will show how it is possible to track the dynamics of quantities like the entanglement entropy and OTOC for a better understanding of thermalization than simple autocorrelation functions could afford. As we shall see, much of the intuition from previous chapters may be applied to understand entanglement dynamics with no measurement present. Generic states will evolve towards a steady-state configuration of maximal entanglement, and late-time behavior may be interpreted via perturbations away from this state or excitations over the ground state of an effective Hamiltonian. In contrast, with a finite measurement rate, all initial states may become *purified* after sufficiently long times, resulting in stationary states that are pure (not necessarily product) states[126, 127]. If measurement rates are low, purification may take a long time and the eventual pure state may retain a great deal of entanglement. If measurements are taken in the appropriate basis, then sufficiently high measurement rates will rapidly extract a great deal of information and produce a purified state that has low entanglement[127–129]. Finally, when we impose a continuous symmetry constraint to both unitary dynamics and measurements, it will produce a whole new dynamical phenomenon called *charge sharpening*, wherein an initial state is resolved to a particular charge sector long before it is fully purified[130, 131].

To understand these effects quantitatively, we should first understand how to calculate quantities involving multiple density matrices within the framework of random unitary circuits.

4.1 Haar-Averaged Higher Moments

Consider an ensemble of quantum states. When can we say the ensemble is random, or taking further, thermalized enough? Two different ensembles of quantum states can have the same density matrix: For a single qubit, one may imagine an ensemble with spin-up and spin-down, each of which appears with a probability 1/2, and the other ensemble with quantum

states uniformly distributed on the Bloch sphere, i.e., Haar random ensemble. Although their statistical properties are drastically different, they would look the same when it comes to the density matrix, thus physical observables. Therefore, in order to quantify the degree of randomness in a given ensemble of quantum states, one has to examine *higher moments* of the density matrix. For a given ensemble $\mathcal{E} = \{(p_\psi, |\psi\rangle)\}$, k-th moment of the density matrix is defined as

$$\rho^{(k)} := \sum_\psi p_\psi (|\psi\rangle\langle\psi|)^{\otimes k} \tag{4.1}$$

where $\sum_\psi p_\psi = 1$. It is straightforward to check that the aforementioned ensemble of spin-up and spin-down states would be distinguished from the Haar random ensemble at the second moment of the density matrix. More generally, any distribution of states that is indistinguishable from the first k moments of the Haar random ensemble will be called a *k-design*.

One can model the dynamics of a density matrix with a random unitary circuit with two, "layers," each of which describes the evolution of the ket's (bra's) of $\hat{\rho} = \sum_i p_i |\psi_i\rangle\langle\psi_i|$ by forwards (backwards) evolution via U_t ($U_t^\dagger$). One may generalize the evolution of multiple copies of the density matrix by including $2n$ layers evolved with the same circuits. By employing clever boundary conditions to the initial and final states, one may then calculate quantities that depend on multiple system copies. This technique is known as the *replica trick*

4.1.1 Rényi Entropies and the OTOC

To better understand the application of the replica trick, we will demonstrate its use in calculating two useful quantities in entanglement dynamics involving multiple system copies: the Rényi entanglement entropy and the OTOC. These were briefly described in the Introduction, however, we review the relevant properties here.

Rényi Entanglement Entropy

When looking to study the dynamics of entanglement, one might first think to look at the entanglement entropy, $S(\rho) = -\mathrm{Tr}[\rho \log \rho]$. However, because of the logarithm of the density matrix, this quantity can be computationally intractable when calculated directly. Instead, one can focus on the various moments of Rényi entropy, defined as

$$S^{(n)}(\rho) \equiv \frac{1}{1-n} \log \rho^n, \tag{4.2}$$

which shares many of the same properties as the entanglement entropy. Further, if one can find an analytical expression for these moments, the entanglement entropy can be calculated by the analytic continuation of these moments to n = 1: $S(\rho) = \lim_{n\to 1} S^{(n)}(\rho)$. Thus, we can infer a great deal of information about the entanglement content of a density matrix, $\rho(t)$, by examining the trace of its various moments, $\mathrm{Tr}[\rho^n(t)]$.

We demonstrate how to calculate the Rényi entanglement entropy by focussing on the case of $n = 2$, where we will calculate the quantity, $\mathrm{Tr}[\rho^2(t)]$ or the purity. As such, we will require

two copies of our system, as described by the density matrix, $\rho = \sum_i \sum_i p_i |\psi_i(t)\rangle\langle\psi(t)|$. The evolution of each state, $|\psi_i(t)\rangle$ can be represented as a tensor network. Since each density matrix involves a bra and a ket, we will need four copies of the single circuit to describe unitary evolution of this quantity. Finally, calculating the trace of the reduced density matrix for a region, A, can be accomplished by contracting tensor indices on the boundary as in Fig. 4.1. This produces an effective path integral of four different trajectories, two forward and two backwards, with fixed boundary conditions. To obtain the purity, the initial state should correspond to the identity in each sector, while the will include the boundary permutation T_2 acting on region A:

$$\begin{aligned} \mathrm{Tr}[\rho_A^2(t)] &= \langle\langle \mathbb{I}_{ij} \otimes \mathbb{I}_{kl} \| T_2^A \| (\rho_{ij}^A \otimes \rho_{ij}^B) \otimes (\rho_{kl}^A \otimes \rho_{kl}^B) \rangle\rangle \\ &= \langle\langle \mathbb{I}_{ij} \otimes \mathbb{I}_{kl} \| (\rho_{li}^A \otimes \rho_{ij}^B) \otimes (\rho_{jk}^A \otimes \rho_{kl}^B) \rangle\rangle \\ &= \mathrm{Tr}[\rho_A^2]\mathrm{Tr}[\rho_B]^2 = \mathrm{Tr}[\rho_A^2]. \end{aligned} \tag{4.3}$$

If evolution in one copy with local Hilbert space dimension, q, is defined by some unitary, U_t, then this four-fold evolution is governed by a gate $U_t \otimes U_t^\dagger \otimes U_t \otimes U_t^\dagger$ acting on a Hilbert space of local dimension, q^4. If we wish to calculate the average properties of the purity, $\overline{\mathrm{Tr}[\rho^2(t)]}$, we may average over each of these gates independently using the Haar-measure. To simplify matters, we will restrict to unitaries acting on single sites rather than two-local gates[1]. As such, we may calculate the transfer matrix for this averaged evolution at each site,

$$M_{\Delta t} = \overline{U_{\Delta t} \otimes U_{\Delta t}^\dagger \otimes U_{\Delta t} \otimes U_{\Delta t}^\dagger} = P_+ + P_- = \sum_{\sigma=\pm} P_\sigma. \tag{4.4}$$

This transfer matrix reduces to the sum of projections onto the two non-orthogonal states, $\|+\rangle\rangle$ and $|-\rangle\rangle$. These states have a very clear physical meaning, defining the pairing between different copies:

$$\|+\rangle\rangle \equiv \sum_{q_a,q_b} |q_a\rangle\langle q_a| \otimes |q_b\rangle\langle q_b|, \qquad \|-\rangle\rangle \equiv \sum_{q_a,q_b} |q_a\rangle\langle q_b| \otimes |q_b\rangle\langle q_a|, \tag{4.5}$$

where $q_{a(b)} \in \{0, 1, \ldots q-1\}$. This is nothing more than the two different possible pairings between forwards and backwards trajectories, where the paired trajectories form maximally entangled pairs. These configurations survive the Feynman trajectories because each forwards and backwards configuration contribute equal and opposite phases to the path integral.

Thus, each unitary can be represented as the sum of weighted projections to definite configurations. In the case above, we have an Ising-like projection to configurations $\sigma = \pm$. If we do this for every unitary in the circuit, we will map the $1+1d$ circuit for $\overline{\mathrm{Tr}[\rho_A^2(t)]}$ to a partition function for a classical 2d Ising-model with one spin at each unitary. The weights for the various configurations can be calculated by contracting tensor the indices for different configurations.

[1] This will not fundamentally change the mapping to a statistical mechanics model, however, it will exclude trajectories with genuine entanglement spreading. These will be explicitly addressed in later sections.

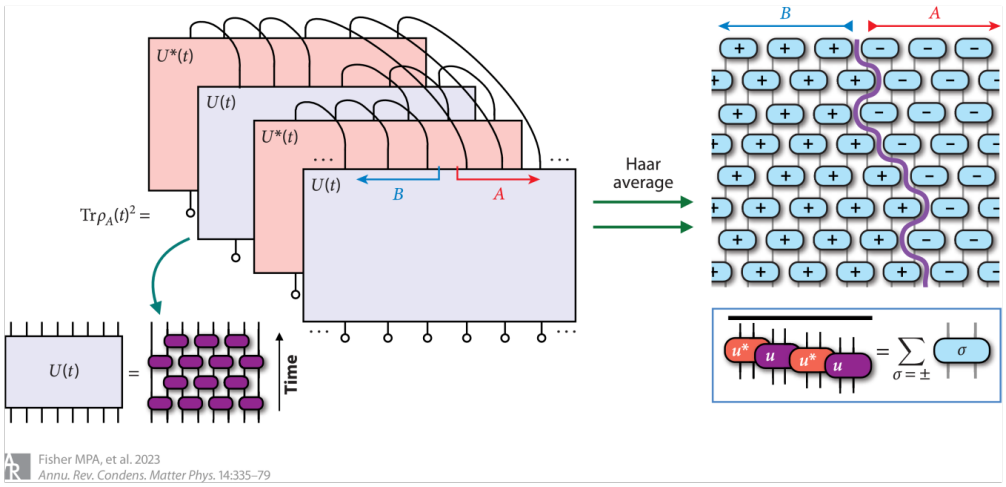

Figure 4.1: **Haar-averaged purity via Ising model partition function** – By averaging each local unitary over the Haar measure in the circuit, one can map the path-integral-like calculation of $\mathrm{Tr}[\rho_A^2(t)]$ into the partition function of a two-dimensional classical Ising model. In this configuration, there is one single Ising spin for each two-site quantum gate. Figure reproduced from [61].

This picture will become essential when we consider the effect of measurements below. For the simple case of single-site unitaries, this operation is trivial and only pairs like configurations. For two-site unitaries, this operation is more complicated, arising from contractions of two-site projectors. These describe the local interactions of the σ configurations. These interactions are anisotropic and impose strict constraints on the possible dynamics to ensure that they match with the unitary evolution of observables in the original space. Using this, one can calculate that unconstrained circuits have entanglement entropies that grow linearly, $S_A(t) \sim t$ until they saturate to some constant value, cL_A. Recalling from the introduction that unconstrained circuits cause operator fronts to spread ballistically, one might have intuited this result, as operators at a distance deep within region A will spread ballistically until they have support in regions A and B, leading to entanglement between the two region.

This story changes if we consider the effects of charge conservation. Here, we must be careful to note the presence of diffusing modes. While these are effectively a classical phenomenon (at least for Abelian charges), and therefore do not directly contribute to the transport of entanglement, diffusing charge amplitudes release a tail of non-conserved operators as shown in Fig. 2.2. As such, there will always be a substantial operator weight emerging from these diffusing conserved charges, giving rise to entanglement scaling as $S_A(t) \sim \sqrt{t}$.

Out-of-time-ordered correlator (OTOC)

We can extend this story to the OTOC in a straightforward manner. We recall the definition of the OTOC:

$$C_{WV}(t) \equiv \mathrm{Tr}[[\hat{W}(t), \hat{V}(0)]^\dagger [\hat{W}(t), \hat{V}(0)]\hat{\rho}_{mic}]. \tag{4.6}$$

Since we will consider RUC's, we set the equilibrium configuration to its infinite temperature realization: $\hat{\rho}_{mic} = \mathbb{I}$[2]. Assuming that W and V are Hermitian, this commutator can be decomposed into two distinct terms.[3] Expanding out the commutators, we obtain the time-ordered, $\mathcal{I}_{WV}(t)$ and the out-of-time ordered product, $\mathcal{F}_{WV}(t)$:

$$\begin{aligned} C_{WV}(t) &= 2\big(\mathcal{F}_{WV}(t) - \mathcal{I}_{WV}(t)\big) \\ \mathcal{F}_{WV}(t) &\equiv \mathrm{Tr}[\hat{W}^\dagger(t)\hat{V}^\dagger(0)\hat{W}(t)\hat{V}(0)] \\ \mathcal{I}_{WV}(t) &\equiv \mathrm{Tr}[\hat{W}^2(t)\hat{V}^2(0)]. \end{aligned} \tag{4.7}$$

The time-ordered product has the same form as the correlators calculated in the previous chapter, requiring only one system copy to describe the dynamics of $W^2(t)$. However, the out-of-time ordered product, $\mathcal{F}_{WV}(t)$ requires two system copies. As before, we can average over a single realization of two-site unitaries to obtain a transfer matrix. Unlike the case of single-site unitaries, however, this transfer matrix involves more complicated projectors. In the case of spin-1/2 particles with charge conservation [65]:

$$\begin{aligned} M_{\Delta t} = \overline{U_{\Delta t} \otimes U_{\Delta t}^\dagger \otimes U_{\Delta t} \otimes U_{\Delta t}^\dagger} &= \sum_{s=\pm} \sum_{Q_1 \neq Q_2} \frac{1}{d_{Q_1} d_{Q_2}} |\mathcal{I}^s_{Q_1Q_2}\rangle\langle\mathcal{I}^s_{Q_1Q_2}| \\ + \sum_{s=\pm} \sum_{Q_1=Q_2} \frac{1}{d_Q^2 - 1} &\left[|\mathcal{I}^s_{QQ}\rangle\langle\mathcal{I}^s_{QQ}| - \frac{1}{d_Q} |\mathcal{I}^s_{QQ}\rangle\langle\mathcal{I}^{-s}_{QQ}| \right], \end{aligned} \tag{4.8}$$

where we have defined the projector states $|\mathcal{I}^\pm_{Q_1Q_2}\rangle$ on the four-copy, two-site Hilbert space as follows:

$$|\mathcal{I}^+_{Q_1Q_2}\rangle \equiv \sum_{\alpha\in\mathcal{H}_{Q_1},\beta\in\mathcal{H}_{Q_2}} |\alpha\rangle\langle\alpha| \otimes |\beta\rangle\langle\beta|, \qquad |\mathcal{I}^-_{Q_1Q_2}\rangle \equiv \sum_{\alpha\in\mathcal{H}_{Q_1},\beta\in\mathcal{H}_{Q_2}} |\alpha\rangle\langle\beta| \otimes |\beta\rangle\langle\alpha|, \tag{4.9}$$

and we have defined $\mathcal{H}_Q$ as the two-site Hilbert space with total charge Q. These configurations are spanned by six total basis states. Thus, as before, we can recover a classical partition function by contracting the indices between unitaries via these projection operators. We will return to this basis in a later section, however, we complete this calculation of the out-of-time product by adding the boundary conditions to the evolution, M_t, in our doubled formalism as follows:

$$\begin{aligned} \overline{\mathcal{F}_{WV}}(t) &= \overline{\mathrm{Tr}[\hat{W}^\dagger(t)\hat{V}^\dagger(0)\hat{W}(t)\hat{V}(0)]} \\ &= \langle\langle V \otimes V \| T_2 M_t \| W \otimes W \rangle\rangle. \end{aligned} \tag{4.10}$$

Here, we have used states $\|W \otimes W\rangle\rangle = W_{\alpha\beta}W_{\gamma\delta}|\alpha\rangle\langle\beta| \otimes |\gamma\rangle\langle\delta|$, and a shift operator that permutes indices, $T_2\|V\otimes V\rangle\rangle = V_{\delta\alpha}V_{\beta\gamma}|\alpha\rangle\langle\beta|\otimes|\gamma\rangle\langle\delta|$. Contracting boundary indices recovers the proper form in the first line. In this form, each time step acts as a transfer matrix in the

[2] We will relax this constraint slightly when calculating a chemical potential-dependent diffusion constant below. To see a more detailed treatment on finite temperature/chemical potential calculations of the OTOC, see [62, 65].

[3] The case where W and V is conceptually the same, but required more care in the explicit calculation of each term.

2d classical spin problem. Analytically evaluating this partition function is highly non-trivial, however, the functional form allows for efficient numerical computations using techniques for evolving matrix product states[65].

As with the purity, we can also understand the qualitative behavior of the OTOC by examining the profile of its operator spreading, as described in Ch. 2.

While time-ordered correlators are sensitive to the diffusive dynamics of charged operators so that, $\mathrm{Tr}[S^z(r,t)S^z(0,0)] \sim \frac{1}{\sqrt{t}}e^{-r^2/Dt}$, they are largely insensitive to the operator front, spreading with butterfly velocity, v_B[61]. In contrast, with the appropriate choice of operators, the OTOC is sensitive the full profile of operator trajectories as shown in Fig. 2.2.

It can be shown that an initially local operator in a U(1) conserving system behaves differently in various regimes at late times. For example, consider a 1+1d circuit of qubits, where we consider an OTOC, $C_{OO}(x,t) \equiv \mathrm{Tr}[[O(x,t),O(0)]^\dagger[O(x,t),O(0)]]$. If we have a charge diffusion coefficient of D_c and a diffusion coefficient for the operator front of D_ρ, then we can enumerate 5 relevant regimes, as represented in Fig. 4.2:

1. *Outside the light cone* ($|x| > t$) – This regime is too far for any operators to have reached, even at the maximum causal speed of $v = 1$. As such, $C_{OO}(x,t)$.

2. *Beyond the leading operator front* ($t > |x| \gg v_B t + \sqrt{D_\rho t}$) – This regime is outside the diffusive spreading of the operator front, so any operators present have an exponentially suppressed weight in t. Thus, we see an exponential increase in $C_{OO}(x,t)$ over time.

3. *Within the leading operator front* ($|x| \sim v_B t + \sqrt{D_\rho t}$) – Within this regime, the operator weight grows as the diffusing front passes by, resulting in an error function accumulation of $C_{OO}(x,t)$ to first order and at early times.

4. *Within the tails* ($\sqrt{D_c t} < |x| \ll v_B t - \sqrt{D_\rho t}$) – Within this regime, the operators passing by are typically non-conserved operators leaking from the central diffusion of conserved operators. These contributions come from operators emitted before time $t' = t - |x|/v_B$. Due to the decrease in operator weight, the OTOC will scale as $1 - C_{OO}(x,t) \sim \frac{1}{\sqrt{(t-|x|/v_B)}}$.

5. *Within diffusive regime.* ($|x| \sim \sqrt{D_c t}$) – Within this regime, there are $\sim 1/t$ corrections to the OTOC that smoothly connect the values at $x > 0$ and $x < 0$.

It should be noted that these regimes are only visible to the OTOC if either W or V have overlap with conserved operators. If neither do, corrections arising from the diffusing conserved operators, like the presence of tails, are absent. If both overlap with conserved operators, then these OTOC contribution are doubled[44].

Permutation Symmetry

So far, we have only considered the case of two system copies. However, this replica paradigm can easily be generalized to n replicas for integer $n > 1$ to allow calculation of higher Rényi moments and other quantities. In the most general setting, this will require n layers of

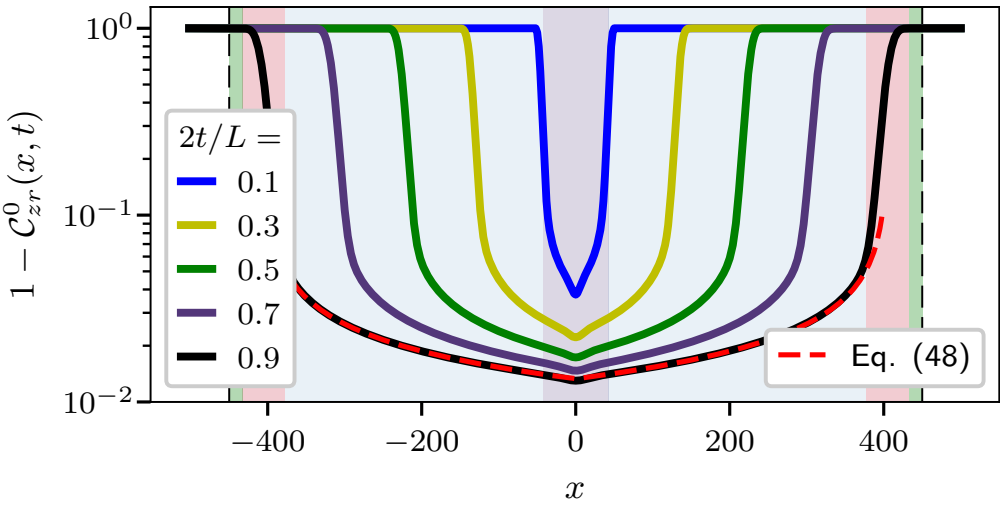

Figure 4.2: **OTOC in different regimes** - One minus the out-of-time-order commutator (OTOC) between $\sigma_0^z(t)$ (z) and σ_0^+ (r), plotted at zero chemical potential with C^0_{zr}, plotted against x for a length L = 1000 chain at various times. The different regimes above are represented with 1 (white), 2(green), 3(red), 4(light blue), and 5(gray). Figure reproduced from [44].

forward evolution from U_t and n layers of backwards evolution from $U_t^\dagger$. Haar-averaging these 2n layers will generically result in transfer matrices to "spin" configurations, σ that describe the different pairing configurations between forwards and backwards trajectories. Here, each spin, $\|\sigma\rangle\rangle$, will be a different element of the permutation group, $\sigma \in S_n$[132, 133], $\sigma \in S_k$, as follows:

$$\|\sigma\rangle\rangle = \bigotimes_n^k \sum_{\mathbf{i_n}} |\mathbf{i}_{\sigma(\mathbf{n})}\rangle\langle \mathbf{i_n}|, \tag{4.11}$$

where $\mathbf{i_n}$ indicates basis configurations for the n'th replica[4]. This allows us to define a transfer matrix for these configurations that will take the form [63]

$$T_{ij} = \mathbb{E}[U^{\otimes n} \otimes (U^\dagger)^{\otimes n}] = \sum_{\sigma,\tau \in S_n} W_D(\sigma^{-1}\tau)\|\sigma\rangle\rangle\langle\langle\tau\|, \tag{4.12}$$

where, for two-site unitaries, $D = d^2$ for local Hilbert space dimension, d, and $W_D(\sigma^{-1}\tau) = \langle\langle\sigma\|\tau\rangle\rangle$ is a Weingarten function that decays polynomially in D when σ and τ are not each other's inverse ($\sigma^{-1}\tau = \mathbb{I}$)[5]. Contracting all possible tensor indices produces the following statistical mechanical model as a function of these weights:

$$\mathcal{Z} = \sum_{g_i \in S_n} \prod_{\langle ij \rangle} W_D(g_i^{-1} g_j). \tag{4.13}$$

[4]We employ standard cycle notation to denote permutations, such that (123)4 refers to the cyclic permutation 1234 → 2314

[5]This implies that, in the limit of infinite local Hilbert space dimension, $d \to \infty$, the statistical physics model describes a system with perfect ferromagnetism, matching all states to the same permutation configuration, $\|\sigma\rangle\rangle$.

This partition function will generally have a minimal symmetry group given by[133, 134]

$$\mathcal{G} \equiv (S_n \times S_n) \rtimes \mathbb{Z}_2, \tag{4.14}$$

where the $\mathbb{Z}_2$ generator describes the exchange of forward with backward trajectories, taking a spin $\sigma \to \sigma^{-1}$. The two copies of S_n come from the symmetry under permutations of the forward and backward trajectories and act on spin $\sigma \to g_F \sigma g_B^{-1}$ for $g_F \in S_n$ and $g_B \in S_n$. As such, these models often resemble Potts models. If we add in non-unitary processes like measurement, then we can add another parameter to these statistical mechanical models, opening the door to potential phase transitions. Let us now turn our attention to these measurement-induced-phase-transitions (MIPT's).

4.1.2 Measurement Induced Phase Transitions (MIPT)

Up until this point, we have primarily been concerned with unitary dynamics. To better describe thermalization, we have focused on ideal, closed systems, where certain degrees of freedom act as a bath, and may be integrated out to understand general dynamics. In this, we have modeled an effective, intra-system decoherence. However, no system is truly isolated, thus we cannot understand quantum dynamical phenomena without addressing the role of environmental decoherence. This environmental decoherence can be approximated by a model of the environment 'monitoring' or measuring the system, then forgetting the result. This will effectively remove internal entanglement, rendering the system density matrix a classical average over the different pure states that emerge from continued measurement. The combination of various forms of measurements and unitary operations has opened up a whole swath of new states of matter[129, 135–139]. We will only review a handful of such phases to highlight their nature.

Entanglement Transitions

Before characterizing any particular transition, let us first consider how system dynamics are affected by measurement. For concreteness, we consider a system of $M \geq 1$ local measurements, taking place at various locations and times during the evolution of a pure state $|\psi\rangle$. Let these be projective measurements of individual spins in the z-basis. If spin i is measured, the state will undergoes the stochastic evolution

$$|\psi\rangle \mapsto \begin{cases} P_{i\uparrow}|\psi\rangle/\sqrt{p_\uparrow} & (\text{for } p_\uparrow = \langle\psi|P_{i\uparrow}|\psi\rangle) \\ P_{i\downarrow}|\psi\rangle/\sqrt{p_\downarrow} & (\text{for } p_\uparrow = \langle\psi|P_{i\downarrow}|\psi\rangle) \end{cases}, \tag{4.15}$$

where the probabilities arise from Born's rule, and $P_{i\mathbf{m}}$ projects spin i onto states with $Z_i = m$. For a single evolution, one will obtain a random sequence of measurement outcomes $\mathbf{m} = (m_1, ..., m_M)$ of measurement outcomes, with $m_\alpha = \{\uparrow, \downarrow\}$. These will generically not be the same even when employing the same unitary evolution. Thus, a complete description of the system evolution must include a particular measurement record $\mathbf{m}$, and the associated evolving state $|\psi_{\mathbf{m}}(t)\rangle$, which we label a *trajectory*.

To model hybrid dynamics involving both measurement and unitary evolution, we may construct a quantum circuit where measurements are interspersed throughout the circuit

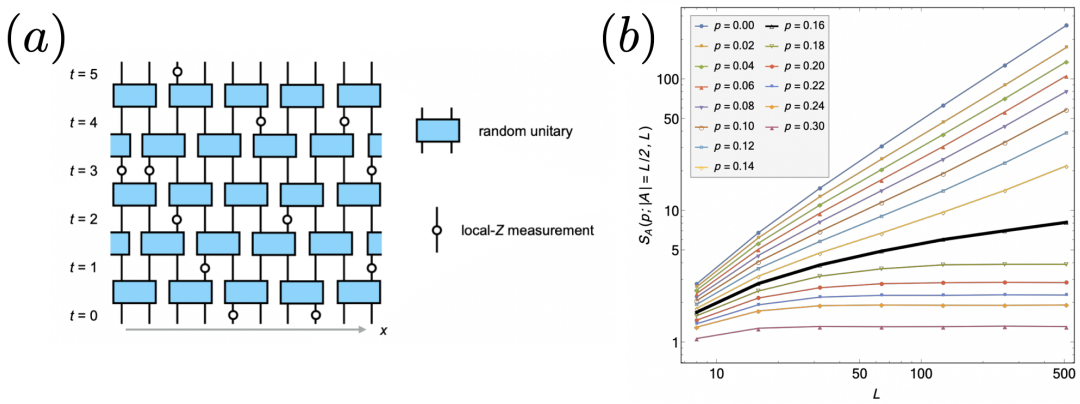

Figure 4.3: **Measurement-Induced Entanglement Transition** – By including local measurements in a quantum circuit to produce a hybrid or monitored random circuit (MRC), one may observe two different regimes distinguished by the entanglement present in the system's steady state after purification. **a)** an example of a MRC with two-site unitaries and local z-measurements occurring at random space-time locations with probability, p. **b)** Finite-size scaling of trajectory averaged entanglement entropy, S_A for a region of size $|A| = L/2$ using random Clifford circuits. Late time scaling shows a continuous phase transition at critical measurement rate $p_c \approx 0.16$, from volume-law entanglement, where $S_A \sim L_A$ for $p < p_c$, and area-law entanglement $S_A \sim$ Const. for $p > p_c$. At criticality, late-time entanglement grows logarithmically in L. Figure reproduced from [140].

with some probability, p, as shown in Fig. 4.3. This reduces to random circuit dynamics for in the case where $p = 0$. However, in the other limit, $p = 1$, the system state is repeatedly collapsed to an unentangled product state. Specifically, these circuits will be used to calculate the *trajectory*-averaged Rényi entanglement entropies for some region, A, as

$$\begin{aligned} \overline{S_A^{(n)}(\rho_A)}(t) &\equiv \mathbb{E}_{U,\mathbf{m}}\left[\frac{1}{1-n}\log\left(\mathrm{Tr}[\rho_{A,\mathbf{m}}^n(t)]\right)\right] \\ &= \mathbb{E}_U\left[\sum_{\mathrm{m}} p_{\mathbf{m}}\frac{1}{1-n}\log\left(\frac{\mathrm{Tr}[\rho_{A,\mathbf{m}}^n(t)]}{\mathrm{Tr}[\rho_{\mathbf{m}}(t)]^n}\right)\right]. \end{aligned} \tag{4.16}$$

When including measurement, it will be practically difficult to maintain normalization after specific measurement outcomes throughout the evolution. To account for normalization this necessary normalization, we include factors of $\mathrm{Tr}[\rho_A]$ in the denominator to explicitly enforce normalization of the density matrix when computing observables.

This difference can be understood as a qualitative change in the nature of the typical trajectories as a function of the measurement rate, p. [141] For frequent measurements, single-spin measurements trap the stochastically evolving wavefunction within the subspace of area-law states ($\overline{S^{(n)}(\rho_A)} \sim |\partial A|$). Entanglement cannot develop fast enough between neighboring states to become extensive in system size before measurements decouple entangled regions. But, below a critical threshold p_c, $|\psi\rangle$ escapes into the volume-law part of

Hilbert space ($\overline{S^{(n)}(\rho_A)} \sim |A|$). At the transition itself, the evolving state has a random but scale-invariant entanglement structure [141].

The average entanglement can be calculated by casting the evolution into the form of a partition function where

$$\begin{aligned} \mathcal{Z} &= \sum_{g_i \in S_n} \prod_{\langle ij \rangle \in G_p} W_p(g_i^{-1}, g_j) \prod_{\langle ij \rangle \in G_U} W_D(g_i^{-1}, g_j) \\ \mathcal{Z}_0 &= \mathbb{E}_{U\mathbf{m}}[\mathrm{Tr}[\rho_{,\mathbf{m}}^{\otimes n}]], \end{aligned} \tag{4.17}$$

where we define $W_p(g_i^{-1}, g_j)$ as the modified Weingarten functions that arise from contracting indices where measurement takes place with probability, p. This shifts the amplitude of $W_D(g_i^{-1}, g_j)$ when all copies are projected to the same state with probability, p.

$$\begin{aligned} \overline{S_A^{(n)}(\rho_A)}(t) &\equiv \mathbb{E}_U \left[\sum_{\mathrm{m}} \frac{p_{\mathrm{m}}}{1-n} \left(\mathcal{Z}_A - \mathcal{Z}_0 \right) \right] \\ \mathcal{Z}_A &= \mathbb{E}_{U,\mathbf{m}}[\mathrm{Tr}[\mathcal{S}_{A,n} \rho_{\mathbf{m}}^{\otimes n}]] \\ \mathcal{Z}_0 &= \mathbb{E}_{U,\mathbf{m}}[\mathrm{Tr}[\rho_{\mathbf{m}}^{\otimes n}]], \end{aligned} \tag{4.18}$$

where $\mathcal{S}_{A,n}$ is a permutation "Swap" operator that implements the partial trace in the subregion A, acting on each of the n replica states as follows,

$$\mathcal{S}_{A,n} = \prod_{\sigma \in S_n} P_\sigma, \qquad \sigma = \begin{cases} (12 \dots n), & (x \in A) \\ id, & (x \notin A) \end{cases} \tag{4.19}$$

Here, the operator, $P_\sigma = \|\sigma\rangle\rangle\langle\langle\sigma\|$ represents a projection onto an element of the permutation group acting on the indices for system copies and forwards or backwards evolution.

As seen above, the various weights relevant to these partition functions will now arise from contractions in a tensor net comprised of interactions from both Haar-averaged unitaries and averaged measurement occurrences. The particular manner in which measurement is incorporated into this tensor net formalism can depend heavily on the model employed, however, the weights corresponding to contractions of different tensor indices between vertices will generically depend on a probability of measurement or measurement rate, p. When averaging over n system copies, the resultant partition function often resembles that of a modified Potts model where the coupling to different spin states $\|\sigma\rangle\rangle$, depend on the measurement rate in such a fashion that for infrequent measurement, the model is in a symmetry breaking phase with all spins polarized along some direction fixed by the operator $\S_{A,n}$, at the boundary; whereas for rapid measurements, the model is in a symmetric state with no preferred orientation.

This transition is called an *entanglement transition,* as it has to do with the degree of entanglement in the steady state. As such, it can be understood by looking at the steady state properties of the entanglement entropy, or qualitatively by examining various Rényi moments. Although the system will purify into a pure state at infinite times, sufficiently low measurement rates will ensure that the system scrambles information fast enough to leave encode an extensive amount of entanglement in this state. In contrast, for high measurement

rates, this pure state will have entanglement that will be limited to system boundaries. Numerical evidence for this transition has by now been seen in a wide range of different microscopic models[126–128, 140, 142, 143].

The above transition occurs for simple, single-site measurements interspersed between unstructured unitaries; however, more complex states can be achieved by imposing symmetry constraints on system dynamics or interspersing non-commuting, multi-site measurements.

4.1.3 Symmetry-Enriched Hybrid Circuits

Nature is often more complex than the idealized featureless Haar-random circuits above that involve only with two-qubit gates and single-site measurements. There are a host of variations that can be made on the allowed interactions and measurements. We have already discussed how symmetries have a profound effect on pure unitary dynamics, and one should expect that appropriate multi-site measurements will "collapse" a system into interesting entangled states rather than featureless product states, even at high measurement rates.

These new elements immediately suggest two questions:

1. Are the universal properties of the entanglement transition modified by the inclusion of system symmetries. And if so, how?

2. Are there additional measurement-induced orders that beyond the trivial area and volume law phases?

The first question does not have an analytic answer, however, there is significant evidence that discrete and Abelian symmetries do not fundamentally alter the transition from volume to area law phases [129, 130]. If both measurements and unitaries respect the same non-Abelian symmetries, a system may no longer host any area-law phase, instead remaining in a critical phase through to the measurement-only limit[144]. Our second question does have a clear and positive answer. There are a host of different transitions both in the area-law and volume-law phases that have been constructed and numerically observed to follow a wide range of universality classes[129, 130, 135, 136]. In the case of discrete symmetries, these states can be distinguished in an analogous manner to how symmetry distinguishes symmetry-broken and symmetry protected topological (SPT) or symmetry-enriched topological (SET) phases in equilibrium systems. For continuous U(1) symmetries, we expect an altogether novel transition in the volume law phase, dubbed a *charge-sharpening* transition. Notably, this is distinguished from the entanglement transition, which occurs in a regime where the charge degrees of freedom are frozen by measurements and do not affect the entanglement transition bulk criticality[130].

To better understand the structure of these transitions, let us review the symmetry properties of a dynamical system. If we impose a symmetry on the measurements and unitary evolution of states, this will induce an enhanced symmetry for the full system dynamics. If the state evolution is invariant under a symmetry, G, The full dynamical symmetry will be[136]

$$\mathcal{G} \equiv \left[(G^{\otimes n} \rtimes S_n) \times (G^{\otimes n} \rtimes S_n)\right] \rtimes \mathbb{Z}_2^{\mathbb{H}}, \tag{4.20}$$

where each system copy in the circuit hosts an independent symmetry G for both its forward and backwards evolutions. Each of these forward(backwards) copies can be permuted into each other, giving rise to the invariance with respect to $G \rtimes S_n$. Finally, the system evolution must preserve the Hermiticity of the density matrix, which induces an anti-linear (anti-unitary) symmetry of order 2 that we label $\mathbb{Z}_2^{\mathbb{H}}$.

With the appropriate choice of measurements and interactions, one can recover a cascade of symmetric, symmetry-breaking, SPT states, and even intrinsic topological or SET order, and fracton orders[135, 136]. In fact, because of the enlarged dynamical symmetry group, $\mathcal{G}$, steady states of hybrid dynamical systems with symmetry constraints, G display a richer phase structure than equilibrium systems constrained by the same symmetry group, G. [136]

Discrete Symmetry and Topology

As discussed in Ch. 2, Haar-averaging does not handle discrete symmetries well. As such, other techniques must be employed when analyzing systems with these constraints.

One approach to doing so involves analytical description of the measurement-only regime, followed by numerical exploration of behavior with weak unitary dynamics[129, 135]. Within the measurement only regime, the entanglement structure is all short-ranged, mirroring that of ground-states of local Hamiltonians. Thus, it is natural to guess that phases of hybrid circuits in the area-law regime with symmetry G should align with equilibrium phases with the same symmetry. This should include potentially paramagnetic, spontaneous symmetry-broken, SPT, or even SET phases with the same symmetry.

Let us attempt to understand how to produce such states in the measurement regime. First, consider the simple example of a system whose dynamics respect a $\mathbb{Z}_2$ symmetry. We construct measurements from local generators of some stabilizer group $\mathcal{S}t$.[6] If there is no unitary evolution, these measurements constantly project into state-specified eigenvalues of $s = \pm 1$ for each configuration $s \in \mathcal{S}t$. These stabilizer states allow for the emergence of a wide variety of many-body orders, and depending on the structure and locality of the stabilized state, these orders may include discrete symmetry breaking and symmetry-protected topological (SPT) orders, and non-chiral- topological- or fracton- orders[135]. See Fig. 4.4 for an examples phase diagrams that can arise from such analysis and the hybrid circuits used to generate them.

Alternatively, different orders can be predicted and diagnosed via recourse to effective Hamiltonians over Choi states, similar to our own analysis[136]. We will return to this in the next section when we discuss the effective Hamiltonian for evolving hybrid circuits.

Continuous Symmetry and charge sharpening

As shown in Ch. 2, Haar-averaging can be carried out with Abelian, local, continuous symmetries. In fact, much like the case without this symmetry, one can construct a partition function with a U(1)-symmetry imposed. This model has an analytic expression in the limit of infinite local Hilbert space dimension, $d \to \infty$. In addition to the degrees of freedom identified with different replica permutations, this partition function includes spin-1/2 (qubit) components specifically constrained by the U(1) symmetry. This model displays two separate

[6] For a spin-1/2 system, these would be a group of mutually-commuting Pauli strings

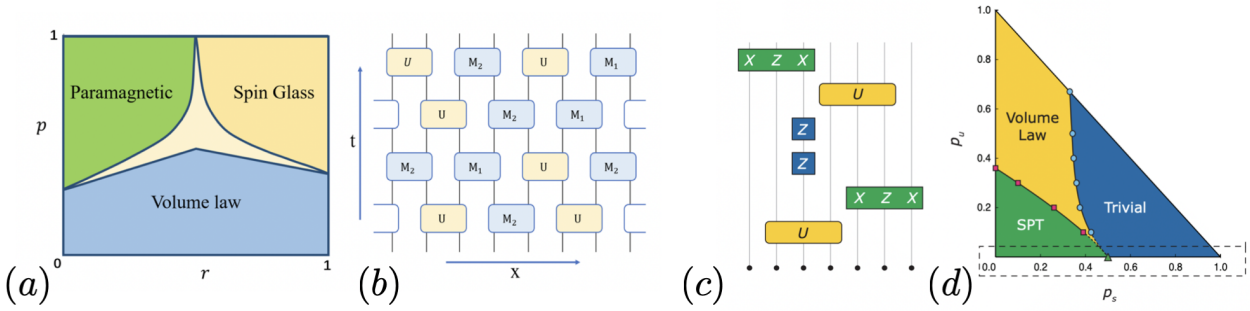

Figure 4.4: **Measurement induced stabilizer orders.** – **a)** Phase diagram and **b)** circuit model of Ising symmetric MRC's exhibiting area-law phases both with- and without- order. Figures taken from [145]. The circuit in b) is comprised of measurements occurring with probability p and unitary evolution via two-site Clifford gates with probability $1-p$. Measurements will either be two-site measurements of $Z \otimes Z$ with probability r, or single-site measurements of either $\mathbb{I} \otimes X$ or $Z \otimes \mathbb{I}$ with probability $1-r$. The phase diagram in a) involves a fan region in the middle that shrinks to a sharp phase boundary in the thermodynamic limit. Next, **c)** the circuit model and **d)** phase diagram of a symmetric MRC's exhibiting both SPT and trivial area-law phases. Figures taken from [129]. The circuit in c) includes measurements of stabalizers for $X \otimes Z \otimes X$ states, producing a cluster state protected by two $\mathbb{Z}_2$ symmetries, single site Z measurements, unitaries from Clifford gates with probabilities p_t, p_s, p_u respectively. In the measurement-only regime shown in the dashed box, p_s tunes between phases with trivial or SPT order in the area-law regime.

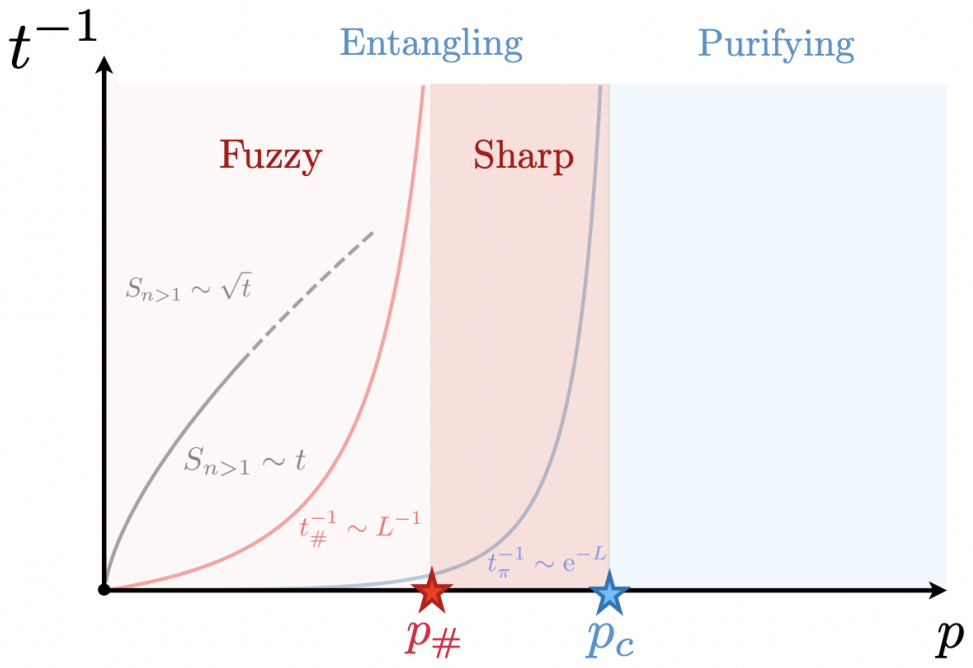

Figure 4.5: **Phase Diagram for U(1)-conserving MRC in 1+1d** – A circuit respects an Abelian symmetry will host at least two phase transitions as a function of measurement rate. First, there will be an entanglement transition from area-law (blue) to volume law (red) phases at critical measurement rate $p = p_c$, and charge sharpening transition within the volume-law phase at measurement rate, $p = p_{\#}$, Entanglement and Charge sharpening transitions. Rényi entanglement moments, $S^{(n)}$ convert from diffusive to ballistic growth for any finite measurement rate, $p > 0$. in a system of size, L, these regimes are characterized by transitions in the scaling of $t_{\#}$, the time taken for measurement to collapse an state with a superposition of states with different charge sectors into one with definite charge, and t_{π}, the time taken to purify an initially mixed state. Figure reproduced from [130].

transitions, as shown in Fig. 4.5. First, within the volume law regime, there is a transition at measurement rate, $p_{\#}$ between a *charge fuzzy* and a *charge-sharp* phase; then, there is the entanglement transition at measurement rate, p_c between the *charge sharp* phase and a *purifying* phase[130].

The three different regimes can be explained from multiple perspectives; however, one clear way to distinguish the three regimes is by a comparison of the timescales taken to purify and the time to resolve the total charge of a system with the timescale for entanglement spreading.

As discussed above, the rate of entanglement spreading is linear $S^{(n)}(t) \sim t$ for all finite measurement rates. Thus, the time taken to saturate the entanglement for a region of length L scales approximately with the length, $t_S \sim L$.

We can understand the entanglement transition as a competition between the purification and entanglement spreading. When a system purifies before entanglement can spread to long distances, it will have area-law correlations. In contrast, if this purification is much

slower than the rate of entanglement spreading, the final pure state will have volume-law correlations.

If we start with an initially mixed state, we can clearly distinguish timescales for its purification as a function of measurement rate, p. When $p < p_c$ a mixed state for a system of size L will evolve into a pure state on a timescale of $t_\pi \sim e^L$, but when $p > p_c$, it will evolve to a pure state on a timescale that is sublinear in L: $t_\pi \sim L^\alpha$ for $\alpha < 1$. Thus, comparing these timescales to that of entanglement spreading, $t_S \sim L$, we see there is a clear transition.[7][130]

For charge sharpening, we must examine a different parameter. Specifically, we look at the variance of the total charge, Q, witnessed over a single trajectory, then averaged across trajectories and samples:

$$[\delta Q^2] = [\langle Q^2 \rangle_{\mathbf{m}} - \langle Q \rangle_{\mathbf{m}}^2]. \tag{4.21}$$

When the charge variance is zero, it means that all trajectories reside in the same charge sector. If a system resolves to a single charge sector on a timescale faster than entanglement to other sectors can spread, the resultant pure state will be restricted to a unique charge sector. In contrast, if this charge resolution is much slower than the rate of entanglement spreading, the final pure state will generically involve entanglement between charge sectors.

If we start with an initially mixed state for a system of size L with overlap on multiple charge sectors, we can clearly distinguish timescales for the charge variance as a function of measurement rate, p. When $p < p_\#$ $[\delta Q^2(t)]$ will evolve into a pure state on a timescale of $t_\# \sim L$, but when $p > p_c$, it will evolve to a pure state on a timescale that is sublinear in L: $t_\# \sim \log(L)$[131]. Again, comparing these timescales to that of entanglement spreading, $t_S \sim L$, we see there is a clear transition. Note that this takes place in the volume-law regime, so entanglement still persists, but it has now been restricted to within a particular charge sector.[8][130] One can also understand these different phases by examining the charge fluctuations in their steady states, described by

$$C(r) = \mathbb{E}_{U,\mathrm{m}}[\langle \sigma_r^z \sigma_0 \rangle - \langle \sigma_r^z \rangle \langle \sigma_0^z \rangle] \sim \begin{cases} 1/r^2 & (\text{for } p < p_\#) \\ e^{-r/\xi} & (\text{for } p > p_\#) \end{cases}, \tag{4.22}$$

where $\xi \ll L$ is some length constant, and the power law scaling for $p < p_\#$ is expected to yield to true long-range order ($\lim_{r\to\infty} C(r) \sim$ Const.) in higher dimensions in the case of discrete Abelian symmetries. The nature of this transition has been studied using field theory techniques and is expected to mimic a superfluid to Mott transition[131].

4.2 Brownian-Averaged Higher Moments

Many of the properties above can be captured using the doubled Hilbert space formalism developed in previous chapters. For clarity, we will focus on the case of Hermitian interactions,

[7] This can be made more precise by defining the system in the limit where $t/L =$ Const. and $L \to \infty$. In this limit, the purity of a mixed state is effectively constant for $p < p_c$, but vanishes for $p > p_c$.

[8] This can be made more precise by using the limit defined in the previous footnote, where $t/L =$ Const. and $L \to \infty$. In this limit, $[\delta Q^2]$ is non-zero for $p < p_c$, but vanishes for $p > p_c$.

$h_i = h_i^\dagger$, leading to Hermitian effective Hamiltonians from unitary dynamics. Before incorporating measurement, let us address how to generalize our formalism to multiple system copies.

4.2.1 Higher Moments and Replica Symmetry

To begin, consider a Brownian random circuit described by the unitary transformation U_t:

$$U_t := e^{-idt(\sum_i h_{t,i} dB_{t,i})} \tag{4.23}$$

where $dB_{t,i}$ is a Brownian random variable with $\mathbb{E}[dB] = 0$ and $\mathbb{E}[dB^2] = 1/dt$. Under the evolution by this random circuit, the k-th moment of the density matrix evolves as

$$\rho^{(k)}(t+dt) \equiv \int dB \cdot p(dB) U_t^{\otimes k}(dB) \rho^{(k)}(t) [U_t^{\otimes k}(dB)]^\dagger \tag{4.24}$$

where the Choi Isomorphism for this k-th moment is defined as

$$\|\rho^{(k)}\rangle\rangle \equiv \sum_{i \in \mathcal{H}^{\otimes k}} |i\rangle \otimes (\rho^{(k)}|i\rangle). \tag{4.25}$$

Expanding out the above Brownian circuit, it can be shown that

$$\begin{aligned}\mathbb{E}[\partial_t \rho^{(k)}] = -\frac{1}{2} \sum_i \sum_{n,m} \Big(& h_i^{(n)} h_i^{(m)} \rho^{(k)} + \rho^{(k)} h_i^{(n)} h_i^{(m)} \\ & - 2 h_i^{(n)} \rho^{(k)} h_i^{(m)} \Big),\end{aligned} \tag{4.26}$$

where $h_i^{(n)} \equiv \mathbb{I}_1 \otimes \cdots \otimes \mathbb{I}_{n-1} \otimes h_i \otimes ... \otimes \mathbb{I}_k$ with $1 \leq n \leq k$. With this derivation, the effective Hamiltonian that captures the imaginary evolution of the Choi state for the k-th moment is given as

$$\begin{aligned} H_{\mathcal{L}}^{(k)} &\equiv \frac{1}{2} \sum_i \Big(\sum_{n=1}^k \big[(h_i^{(n)})^T \otimes \mathbb{I} - \mathbb{I} \otimes h_i^{(n)} \big] \Big)^2 \\ &= \frac{1}{2} \sum_{\boldsymbol{x}, \lambda} (\mathcal{O}_{\boldsymbol{x},\lambda}^{(k)})^\dagger \mathcal{O}_{\boldsymbol{x},\lambda}^{(k)} \end{aligned} \tag{4.27}$$

where $\|\partial_t \rho^{(k)}\rangle\rangle = -H_{\mathcal{L}}^{(k)} \|\partial_t \rho^{(k)}\rangle\rangle$, and we once again define commutors, $\mathcal{O}_{\boldsymbol{x},\lambda}^{(k)} = \sum_{n=1}^k \big[(h_i^{(n)})^T \otimes \mathbb{I} - \mathbb{I} \otimes h_i^{(n)} \big]$. First, note that this Hamiltonian has multiple symmetries. $\mathcal{H}_{\mathcal{L}}^{(k)}$ is invariant under $\mathbb{Z}_2^{\mathbb{H}}$ symmetry that exchanges upper and lower Hilbert spaces with complex conjugation. Second, $H_{\mathcal{L}}^{(k)}$ is invariant under permutation among k copies within left or right Hilbert spaces, respectively. For a generator $\sigma \in S_k$, $\sigma h_i^{(n)} \sigma^{-1} = h_i^{(\sigma(n))}$. Finally, as each h_i is U(1) symmetric, so is the Hamiltonian. Therefore, the full symmetry is given as

$$G = \big[(\mathrm{U}(1)^{\otimes k} \rtimes S_k) \times (\mathrm{U}(1)^{\otimes k} \rtimes S_k) \big] \rtimes \mathbb{Z}_2^{\mathbb{H}} \tag{4.28}$$

The full symmetry of the effective Hamiltonian should also be present in the ground state. In fact, we can characterize the ground state by its commutant algebra[108]. This allows us to present explicit expressions for states in the ground state manifold. They are given by the representation of permutation operators and the various charge sectors representing elements in each of the 2k U(1) symmetries.

Recalling the states defined in Eq. 4.11, the states representing elements $\sigma \in S_k$ of the permutation group can be expressed as follows[146]:

$$\|\sigma\rangle\rangle = \bigotimes_n^k \sum_{\mathbf{i_n}} |\mathbf{i_n}\rangle \otimes |\mathbf{i}_{\sigma(\mathbf{n})}\rangle, \tag{4.29}$$

where $\mathbf{i_n}$ indicates basis configurations for the n'th replica. With this definition, we can identify the states for the identity permutation and the Choi state of $\mathbb{I}^{\otimes k}$: $\|id\rangle\rangle = |\mathbb{I}^{\otimes k}\rangle$. Further, each of these permutation states, $\|\sigma\rangle\rangle$, can be further decomposed by the into M symmetry sectors for each replica, so that a ground state with charges, $(m^{(1)}, m^{(2)}, \ldots, m^{(n)}) = \mathbf{m}$ can be expressed as the projection

$$\|\sigma_{\mathbf{m}}\rangle\rangle = \bigotimes_n P^{(n)}_{m^{(n)}} \otimes P^{(\sigma(n))}_{m^{(\sigma(n))}} \sum_{\mathbf{i_n}} |\mathbf{i_n}\rangle \otimes |\mathbf{i}_{\sigma(\mathbf{n})}\rangle, \tag{4.30}$$

Written in this form, one can read off the ground state degeneracy of this system: $k!M^k$, where M is the total number of charge sectors in a single replica.

Further, we can repeat the analysis from Ch. 2 to demonstrate the same bound on the spectrum. By constructing variational states of momentum $\mathbf{k}$ (for clarity, momentum will always be in bold, $\boldsymbol{k}$, compared to the replica number, k), $\|\sigma_{\mathbf{m}}(\mathbf{k})\rangle\rangle$, we can show that the spectrum, $E_{\boldsymbol{k}}$ is bounded by a quadratic scaling given by the expected energy of these states $\epsilon_{\boldsymbol{k}} \sim \mathbf{k}^2$, regardless of the details of the effective Hamiltonian

$$\begin{aligned}\langle\langle \sigma_{\mathbf{m}}(\mathbf{k}) \| H_{\mathcal{L}} \| \sigma_{\mathbf{m}}(\mathbf{k}) \rangle\rangle &= \frac{1}{\mathcal{N}_{\boldsymbol{k}}} \langle\langle \sigma_{\mathbf{m}} \| \left[\hat{\rho}^\dagger_{\boldsymbol{k}}, [H^{(k)}_{\mathcal{L}}, \hat{\rho}_{\boldsymbol{k}}]\right] \| \sigma_{\mathbf{m}} \rangle\rangle \\ &= \frac{1}{\mathcal{N}_{\boldsymbol{k}}} \sum_{\boldsymbol{x},\lambda} \langle\langle \sigma_{\mathbf{m}} \| [\mathcal{O}^{(k)}_{\boldsymbol{x},\lambda}, \hat{\rho}_{\boldsymbol{k}}]^\dagger [\mathcal{O}^{(k)}_{\boldsymbol{x},\lambda}, \hat{\rho}_{\boldsymbol{k}}] \| \sigma_{\mathbf{m}} \rangle\rangle,\end{aligned} \tag{4.31}$$

where we employ the symmetric density over k-copies, $\hat{\rho}_{\boldsymbol{k}} \equiv \sum_{\boldsymbol{x},n} \frac{e^{i\boldsymbol{k}\cdot\boldsymbol{x}}}{L^{d/2}} (\hat{\rho}^{(n)}_{\boldsymbol{x},u} + \hat{\rho}^{(n)}_{\boldsymbol{x},l})$. As before, we exploit the effects of charge symmetry in isotropic systems, $[h_{\boldsymbol{x},\lambda}, \sum_{\boldsymbol{y}} \hat{\rho}_{\boldsymbol{y}}] = 0 \Rightarrow [\mathcal{O}^{(k)}_{\boldsymbol{x},\lambda}, \sum_{\boldsymbol{y}} \hat{\rho}_{\boldsymbol{y}}] = 0$, to demonstrate a leading order contribution proportional to k:

$$[\mathcal{O}^{(k)}_{\boldsymbol{x},\lambda}, \hat{\rho}_{\boldsymbol{k}}] \propto k \quad \Rightarrow \quad \epsilon_{\boldsymbol{k}} = \langle\langle \sigma_{\mathbf{m}}(\mathbf{k}) \| H^{(k)}_{\mathcal{L}} \| \sigma_{\mathbf{m}}(\mathbf{k}) \rangle\rangle \propto k^2. \tag{4.32}$$

The presence of these diffusion modes in higher moments will be important for a number of phenomena. Below, we will demonstrate a case where these additional copies allow us to take a circuit average of a trace raised to a power, $\mathbb{E}[\mathrm{Tr}[Q(t)]^n]$, rather than raising the circuit average of a single trace to a higher power, $\mathbb{E}[\mathrm{Tr}[Q(t)]]^n$. One of the simplest examples of this comes from the calculation of a chemical potential-dependent diffusion coefficient $D(\mu)$ from Eq. 2.12.

Finite Chemical Potential

As discussed in Ch. 3, any random unitary circuit with a Hermitian effective Hamiltonian will be driven to an equilibrium ensemble at infinite temperature. However, when conserved charges, Q_i are present, we may still understand more structured thermal states through the use of finite chemical potentials, μ_i. For these states, we expect the thermal state to mirror a Gibbs ensemble, $\rho_{eq} = \frac{e^{-\sum_i \mu_i Q_i}}{\mathcal{Z}}$.[9]. As such, the expected charge variance for a system with chemical potential, μ, will be

$$\begin{aligned}
\langle Q_r^2(0)\rangle_\mu - \langle Q_r(0)\rangle_\mu^2 &= \frac{\prod_{i\neq r}\mathrm{Tr}[e^{-\mu Q_i}]\mathrm{Tr}[Q_r^2 e^{-\mu Q_r}]}{\prod_i \mathrm{Tr}[e^{-\mu Q_i}]} \\
&\quad - \left(\frac{\prod_{i\neq r}\mathrm{Tr}[e^{-\mu Q_i}]\mathrm{Tr}[Q_r e^{-\mu Q_r}]}{\prod_i \mathrm{Tr}[e^{-\mu Q_i}]}\right)^2 \\
&= \frac{e^{-\mu}}{1+e^{-\mu}} - \left(\frac{e^{-\mu}}{1+e^{-\mu}}\right)^2 \\
&= \frac{1}{4\cosh\left(\frac{\mu}{2}\right)}.
\end{aligned} \tag{4.33}$$

This is nothing more than the initial value of the autocorrelation at finite μ in Eq. 2.12. We can calculate the full autocorrelation function, however, we will need to employ two system copies to calculate one of the two terms. We begin with the simpler of the two:

$$\begin{aligned}
\mathbb{E}[\langle Q_x(0)Q_x(t)\rangle_\mu] &= \frac{\mathrm{Tr}[Q_x(0)e^{-\mu Q}Q_x(t)]}{\mathrm{Tr}[e^{-\mu\hat{Q}}]} \\
&= \frac{1}{\mathcal{Z}}\sum_N |\langle\langle Q_x(0)\|(\|N\rangle\rangle\langle\langle N\|e^{-\mu N})e^{-H_{\mathcal{L}}t}\|Q_x(0)\rangle\rangle| \\
&= \frac{1}{\mathcal{Z}}\sum_{k,N} e^{-E(k)t-\mu N}|\langle\langle k,N\|Q_x(0)\rangle\rangle|^2 \\
&= \sum_k e^{-E(k)t}|c_k|^2 \\
&\approx \frac{\sum_N e^{-\mu N}|\langle\langle N\|Q_x(0)\rangle\rangle|^2}{\sum_N e^{-\mu N}}\sum_k e^{-E(k)t} \\
&= \langle Q_x(0)^2\rangle_\mu \sum_k e^{-E(k)t} \\
&\underset{t\to\infty}{\sim} \left(\frac{e^{-\mu}}{1+e^{-\mu}}\right)\frac{1}{\sqrt{t}}
\end{aligned} \tag{4.34}$$

We note that, as above, $\mathcal{Z} = \prod_i \mathrm{Tr}[e^{-\mu Q_i}] = \sum_N e^{-\mu N}$. And, we have used the fact that the $|c_k|^2$ are approximately constant for long wavelength states to move this coeffi-

[9] Recall from Sec. 3.2 that, in the case of non-commuting charges, this will be replaced by a Generalized Gibbs Ensemble or Non-Abelian thermal state (see Eq. 3.3), $\rho_{GGE} = \frac{e^{-\sum_i \mu_i \tilde{Q}_i}}{\mathcal{Z}}$, where the $\tilde{Q}_i$ are expected values of the non-commuting charges that depend on the initial state of the system.

cient out of the momentum sum. We note that the numerator equivalent to $\mathrm{Tr}[Q_x^2 e^{-\mu Q}] = \sum_N e^{-\mu N} |\langle\langle N \| Q_x(0)\rangle\rangle|^2$, thus this momentum-independent constant should be $\langle Q_x(0)^2\rangle_\mu$.

We must be careful to take the circuit average after the square in the next calculation because $\mathbb{E}[\langle Q_x(t)\rangle_\mu^2] \neq \mathbb{E}[\langle Q_x(t)\rangle_\mu]^2$. Thus, we cannot simply square the result of evolving a single copy of the system, as this would already involve a circuit average. To take the appropriate average, we require two system copies so that

$$\begin{aligned}
\mathbb{E}[\langle Q_x(t)\rangle_\mu^2] &= \frac{\mathrm{Tr}[e^{-\mu Q} Q_x(t)]^2}{\mathrm{Tr}[e^{-\mu \hat{Q}}]^2} \\
&= \frac{1}{\mathcal{Z}^2} \sum_{N_1,N_2} |\langle\langle \mathbb{I},\mathbb{I} \| (\| N_1,N_2\rangle\rangle\langle\langle N_1,N_2 \| e^{-\mu(N_1+N_2)}) \\
&\times e^{-H_{\mathcal{L}}^{(2)} t} \| Q_x(0), Q_x(0)\rangle\rangle| \\
&= \frac{1}{\mathcal{Z}^2} \sum_{k,N_1,N_2} e^{-E_2(k)t - \mu(N_1+N_2)} \langle\langle k, N_1 \| Q_x(0)\rangle\rangle\langle\langle Q_x(0) \| k, N_2\rangle\rangle \\
&= \sum_k e^{-E_2(k)t} |c_k|^2 \\
&\approx \left| \frac{\sum_{N_1} e^{-\mu(N)} \langle\langle N \| Q_x(0)\rangle\rangle}{\sum_N e^{-\mu N}} \right|^2 \sum_k e^{-E(k)t} \\
&= \langle Q_x(0)\rangle_\mu^2 \sum_k e^{-E(k)t} |c_k|^2 \\
&\underset{t\to\infty}{\sim} \left(\frac{e^{-\mu}}{1+e^{-\mu}} \right)^2 \frac{1}{\sqrt{t}}
\end{aligned} \tag{4.35}$$

, where we have made use of the fact that $\mathrm{Tr}[Q_x e^{-\mu Q}] = \sum_N e^{-\mu N} \langle\langle N \| Q_x(0)\rangle\rangle$ similar to the previous calculation. If we combine these, then we have the result

$$\mathbb{E}[\langle Q_x(0) Q_x(t)\rangle_\mu - \langle Q_x\rangle_\mu^2(t)] = \frac{1}{\sqrt{t}} \frac{1}{4\cosh^2(\mu/2)} = \frac{1}{\sqrt{D(\mu)t}}. \tag{4.36}$$

It should be noted that we exploited a conjectured equality between the low-energy spectrum for effective Hamiltonian for two copies and one copy: $E_2(k) = E(k)$[10]. Further, had we reversed the order of averaging and squaring by calculating $\langle Q_x(t)\rangle$ with one copy and squared the result, the second term would scale with $1/t$, and there would be a mismatch in the two terms' late-time scaling. This underscores the need for multiple system copies when calculating the expectation of higher moments quantities. We now turn our attention to the calculation of Rényi moments and the OTOC in this formalism

4.2.2 Rényi Entropy and the OTOC

Given the structure laid down above, we can easily write down what the OTOC and various Rényi moments are by employing the appropriate boundary states. Recalling the form of

[10]This equality has been demonstrated for Haar-averaged spin-1/2 systems in [146]

Eq. 4.7, we see that we can calculate the OTOC as the difference of a two-copy and a one copy transition amplitude,

$$\begin{aligned}\overline{C_{WV}}(t) &= \mathrm{Tr}[[\hat{W}(t),\hat{V}(0)]^\dagger[\hat{W}(t),\hat{V}(0)]] \\ &= 2(\overline{\mathrm{Tr}[\hat{W}^\dagger(t)\hat{V}^\dagger(0)\hat{W}(t)\hat{V}(0)]} - \overline{\mathrm{Tr}[\hat{W}^2(t)\hat{V}^2(0)]}) \\ &= 2\left(\langle\langle V\otimes V\|\mathcal{S}_2 e^{-tH_{\mathcal{L}}^{(2)}}\|W\otimes W\rangle\rangle - \langle\langle V^2\|e^{-tH_{\mathcal{L}}^{(1)}}\|W^2\rangle\rangle\right),\end{aligned} \tag{4.37}$$

where $\mathcal{S}_2$ is the Swap operator defined in Eq. 4.19 for two copies on the entire system. If either W or V have any overlap with conserved charges, the OTOC will be sensitive to their diffusion. For more detailed information, we can explicitly calculate the OTOC using MPS methods as in [65], but with more fine control over the evolution.

Likewise, we can define the purity, $\rho^2(t)$ with an even simpler amplitude:

$$\overline{\rho^2}(t) = \langle\langle \mathbb{I}\otimes\mathbb{I}\|\mathcal{S}_{A,n}e^{-tH_{\mathcal{L}}^{(2)}}\|\rho\otimes\rho\rangle\rangle. \tag{4.38}$$

If the density matrix has any initial overlap with conserved charges, $\mathrm{Tr}[\rho S^z_{\mathrm{tot}}]$, then it immediately follows that the rate of entanglement spreading is limited by these diffusive modes so that $S^{(n)}(t)\sim\sqrt{t}$ until it saturates. It should be noted that this entanglement does not come from the charged operators, $S^z_{\boldsymbol{x}}$, as they are classical configurations that carry no entanglement, however, as these operators diffuse and the total weight of conserved operators decreases as $1/\sqrt{t}$, they release non-conserved operators that produce entanglement as they cross the system boundary. A more careful derivation of the exact scaling involves bounding the purity and thus $S_2(t)$ with the largest Schmidt coefficient[130]. This situation changes drastically once we include the effects of measurement.

4.3 Measurement

While studying unitary dynamics, we discovered that symmetry-breaking could be used to explain the late-time diffusive dynamics through goldstone modes of an effective Hamiltonian. Drawing on this intuition, we hope to use similar techniques to understand the late-time behavior of systems involving both measurement and unitary dynamics. Three natural questions emerge:

1. Can the entanglement transition be cast as a form of replica symmetry breaking in the ground state of an effective Hamiltonian, H_{eff}?

2. If so, can we establish whether this symmetry-breaking transition is affected by the presence of other symmetries?

3. Can we describe additional measurement-induced orders by examining the excitation spectrum of H_{eff}?

These questions have already been partially answered, albeit in disjointed fashion. In [136], the ground state structure of a restricted effective Hamiltonian H_{eff} was used to show how

the entanglement transition could be cast as a replica symmetry breaking transition in the ground state structure of H_{eff}. Further, it was shown that the addition of multiple discrete system symmetries resulted in the emergence of symmetric and symmetry-breaking phases in both the area and volume law regimes, with an additional SPT phase emerging in the area-law regime, among other potential phases[136]. Yet, even with the addition of continuous symmetries, there is numerical evidence that the character of the entanglement transition does not change [130].

Further, with the introduction of continuous symmetries, it was shown that late-time behavior was an important feature in distinguishing charge sharpening regimes[130]. This strongly suggests that a knowledge of the low-energy structure of H_{eff} could act as a diagnostic for the various allowable phases of a system due to symmetry. In what follows, we will attempt to extend our analysis to include measurement. As before, we will focus on the case of U(1) system symmetry.

To begin, let us assume that we are measuring U(1) charge at a rate Γ_p. This corresponds to adding the following term in the effective Hamiltonian,

$$H_{\text{eff}} = H_{\mathcal{L}}^{(k)} + H_{\mathcal{M}} \tag{4.39}$$

$$H_{\mathcal{M}} = \Gamma_p \left[\mathbb{I} - \sum_i \sum_m (\mathcal{P}_i^m \otimes \mathcal{P}_i^m)^{\otimes k} \right] \tag{4.40}$$

where $\mathcal{P}_i^m$ is the projection onto the charge-m state for a site i. Going forward, we will omit the constant shift in $H_{\mathcal{M}}$.

Before advancing further, let us try to put some constraints on the types of measurements allowed by our U(1) symmetry. We know that any (1-)local projections should be polynomials of powers of S^z. More precisely, for a spin-s system, the local projection to a charge m state, $\mathcal{P}^{(s,m)}$ can be expressed as

$$\mathcal{P}^{(s,m)} = \sum_{n=0}^{2s} a_n^{(s,m)} (S^z)^n, \tag{4.41}$$

where $a_n^{(s,m)}$ are the coefficients of n'th powers of S^z. We note that inverting the spin index flips the sign of S^z: $m \leftrightarrow -m$ takes $S^z \leftrightarrow -S^z$, yielding a constraint:

$$a_n^{(s,m)} = \pm a_n^{(s,-m)}, \tag{4.42}$$

where the sign is positive(negative) if n is even(odd). With all of this in mind, we see that the most general effective Hamiltonian for measurement will involve some ferromagnetic interaction with even powers of S^z between different copies and layers:

$$H_{\mathcal{M}} = -\Gamma_p \sum_{i,m} \left(\sum_{n_L=0}^{2s} a_{n_L}^{(s,m)} (S_i^z)^{n_L}) \otimes (\sum_{n_R=0}^{2s} a_{n_R}^{(s,m)} (S_i^z)^{n_R}) \right)^{\otimes k}, \tag{4.43}$$

where the sum $n_R + n_L$ must be even.

We can readily describe the ground state of $H_{\mathcal{M}}$. It is clear from the ferromagnetic form that $H_{\mathcal{M}}$ locks all replicas together in the ground state so that each charge sector has a

ground state manifold comprised of all local charge configurations with fixed total charge, m:

$$\|\Omega_{\mathbf{m}}\rangle\rangle = \sum_{\mathbf{i_x}, \sum_{i_x}=m} \bigotimes_x (|i_x\rangle \otimes |i_x\rangle)^{\otimes k}. \tag{4.44}$$

Before carrying on further, let us check to see if there are any shared elements of the ground state subspaces of the effective Hamiltonians for unitary and measurement dynamics. In fact, for any measurement strength, Γ_m, there will be at least two elements: the states of maximal charge, where each site and each replica have the same charge. For other charge sectors, there will be some amount of frustration present.

4.3.1 Effective Hamiltonian and Frustration

We may now combine the effective Hamiltonian for unitary evolution with that for measurement. The combination of these two Hamiltonians now presents a level of frustration that allows for transitions depending on the measurement rate. Since the ground states of the two Hamiltonians, $H_{\mathcal{L}}$ and $H_{\mathcal{M}}$, have different effective symmetries, this suggests that we will have at least one symmetry-breaking transition. This concept has already been applied to distinguish different steady state phases in hybrid circuits with discrete symmetries[136].

Let us focus on the simplest example to gain some intuition on the possible transitions. We will start with a spin-1/2 system with single-site z-measurements given by $\mathcal{P}_{\pm,i} = (\mathbb{I} \pm \sigma_i^z)/2$. As such, we see the measurement contribution will be

$$H_{\mathcal{M}} = -\frac{\Gamma_p}{2} \sum_{i,\pm} \left((\mathbb{I} \pm \sigma_i^z) \otimes (\mathbb{I} \pm \sigma_i^z) \right)^{\otimes 2} \tag{4.45}$$

$$\begin{aligned} &= -\Gamma_p \sum_i \big(\mathbb{I}^{\otimes 4} + \sigma^z \otimes \sigma^z \otimes \mathbb{I} \otimes \mathbb{I} + \sigma^z \otimes \mathbb{I} \otimes \sigma^z \otimes \mathbb{I} + \sigma^z \otimes \mathbb{I} \otimes \mathbb{I} \otimes \sigma^z \\ &\quad + \mathbb{I} \otimes \sigma^z \otimes \sigma^z \otimes \mathbb{I} + \mathbb{I} \otimes \sigma^z \otimes \mathbb{I} \otimes \sigma^z + \mathbb{I} \otimes \mathbb{I} \otimes \sigma^z \otimes \sigma^z + \sigma^z \otimes \sigma^z \otimes \sigma^z \otimes \sigma^z \big)_i. \end{aligned} \tag{4.46}$$

This Hamiltonian has a clear ground state. As above, if we simply lock the z-configurations of all copies, we obtain $\|\Omega_{\mathbf{m}}\rangle\rangle = |0000\rangle + |1111\rangle$.

Next, we consider the contribution arising from unitary dynamics. Specifically, we consider the U(1)-symmetric contributions from the interaction terms, $h_i^z = \sigma_i^z \sigma_{i+1}^z$ and $h_i^{\pm} = \sigma_i^+ \sigma_{i+1}^- + h.c.$. These will produce a contribution of

$$H_{\mathcal{L}}^{(2)} \equiv \frac{1}{2} \sum_{i, r \in \{z,\pm\}} \left(\left[(h_i^r)^T \otimes \mathbb{I} \otimes \mathbb{I} \otimes \mathbb{I} - \mathbb{I} \otimes h_i^r \otimes \mathbb{I} \otimes \mathbb{I} + \mathbb{I} \otimes \mathbb{I} \otimes (h_i^r)^T \otimes \mathbb{I} - \mathbb{I} \otimes \mathbb{I} \otimes \mathbb{I} \otimes h_i^r \right] \right)^2 \tag{4.47}$$

$$= \frac{1}{2} \sum_{\boldsymbol{x},\lambda} (\mathcal{O}_{\boldsymbol{x},\lambda}^{(k)})^\dagger \mathcal{O}_{\boldsymbol{x},\lambda}^{(k)}.$$

Again, we can check the ground states for this contribution, however, this effective Hamiltonian is still a bit cumbersome, and so we will attempt to simplify it by projecting to a sector including the low-energy degrees of freedom for our theory.

Low-energy Basis

We draw inspiration from the projection to the diagonal sector in single-copy systems. As mentioned in Ch. 2, the relevant late-time dynamics of single copy systems can be captured by the classically simulatable dynamics of the diagonal sector of the density matrix that includes the ground state of the vectorized identity matrix and total charge, $\|\mathbb{I}\rangle\rangle$ and $\|Q_{\text{tot}}\rangle\rangle$. For a qubit system, we can restrict to this subspace by applying a dephasing operation to each local component of the density matrix:

$$D_z[\rho_i] = \mathbb{E}_{\theta_u,\theta_l}[e^{-i\theta_u\sigma_u^z}\rho_i e^{i\theta_l\sigma_l^z}] = \begin{pmatrix}\rho_{00} & 0\\ 0 & \rho_{11}\end{pmatrix}. \tag{4.48}$$

When generalizing to multiple system copies, we must go beyond the diagonal sector of one copy to include the various permutation states, $\|\sigma\rangle\rangle$ in the ground state of $H_{\mathcal{L}}^{(2)}$. We can restrict to a sector containing these elements by applying a similar dephasing operation. If we dephase in our doubled Hilbert space with z rotations of the form

$$D_z = \overline{e^{-i\theta_u^1\sigma_{u,1}^z}\otimes e^{i\theta_l^1\sigma_{l,1}^z}\otimes e^{-i\theta_u^2\sigma_{u,2}^z}\otimes e^{i\theta_l^2\sigma_{l,2}^z}}. \tag{4.49}$$

With two copies, this reduces our total Hilbert space down to 6 allowable states from the original 16. For two copies, these exactly correspond to the non-orthogonal permutation states we expect in our low-energy theory.[11] These elements can be cast into an orthogonal basis using a tensor product of a spin 1 and spin 1/2 chain as follows:

$$\begin{aligned}
|1,+\rangle &= |1\rangle\langle 1|\otimes|0\rangle\langle 0| \\
|1,-\rangle &= |0\rangle\langle 0|\otimes|1\rangle\langle 1| \\
|0,+\rangle &= |1\rangle\langle 1|\otimes|1\rangle\langle 1| \\
|0,-\rangle &= |0\rangle\langle 0|\otimes|0\rangle\langle 0| \\
|-1,+\rangle &= |1\rangle\langle 0|\otimes|0\rangle\langle 1| \\
|-1,-\rangle &= |0\rangle\langle 1|\otimes|1\rangle\langle 0|
\end{aligned} \tag{4.50}$$

This basis will prove particularly useful in decomposing the different transitions present for different measurement rate. We note one useful feature immediately: left permutation (swap) symmetry $\mathcal{S}_2$ has a simple action on the basis:

$$C^l : |m, s_i\rangle \leftrightarrow |-m, s_i\rangle. \tag{4.51}$$

Thus, spontaneous breaking of the $\mathcal{S}_2$ permutation symmetry will appear as onset of a spontaneous z-magnetization of the spin-1 degrees of freedom. Meanwhile, the spin-1/2 component is assigned by the z-component of the leftmost state in the original basis. As we shall see, this basis will separate out sectors respecting the replica and U(1) symmetries.[12]

[11] Note that this is the same basis used in Eq. 4.9, as utilized in [65].

[12] This basis can be generalized by reducing to the minimal Hilbert space containing all independent permutations states and charge configurations on a single state. For example, with two copies of a system with local Hilbert space dimension, d, both the id and $\sigma_{12} \in S_2$ should contain d^2 independent two-site basis states, however, they will overlap on the d states that have the same spin on all four local states ($|s\rangle\langle s|\otimes|s\rangle\langle s|$). Thus, we will have a reduced basis of two-site dimension $d(2d-1)$ which can always be decomposed into a sector of local dimension (2d-1) that is inverted under the action of $\mathcal{S}_2$, and a sector of local dimension d, that respects the U(1) symmetry.

Now, we move on to explicitly write out the Hamiltonian from unitary evolution projected into this basis :

$$\begin{aligned} H_{\mathcal{L},\text{deph}} = &\sum_x P_{1,x}P_{-1,x+1} + P_{-1,x}P_{1,x+1} \otimes \mathbb{I} \\ &- \frac{1}{2}(SWAP_{x,x+1} - (\frac{1}{2}(S_x^+)^2(S_{x+1}^-)^2 + h.c)) \otimes (\sigma_x^\mu \cdot \sigma_{x+1}^\mu) \\ &+ \frac{3}{2}P_{m,x} \otimes (\sigma_x^\mu \cdot \sigma_{x+1}^\mu - 2\sigma_x^z\sigma_{x+1}^z) + \mathbb{I}_9 \otimes \mathbb{I}_4, \end{aligned} \tag{4.52}$$

where $P_{\pm 1,x}$ and $P_{m,x}$ are projectors onto local spin states $|\pm 1\rangle$ and $|m\rangle = \frac{1}{\sqrt{3}}(|11\rangle - |00\rangle + |-1-1\rangle)$, respectively. Additionally, $SWAP_{x,x+1}$ is the $S = 1$ swap operator that exchanges states at sites x and x+1, and $\sigma_x^\mu \cdot \sigma_{x+1}^\mu = \mathbb{I} + \vec{\sigma}_x \cdot \vec{\sigma}_{x+1}$. As we shall see, the gapless modes present without measurement derive their form from the action in the spin-1/2 sector.

The same dephasing procedure produces a simple form for the measurement contribution:

$$H_{\mathcal{M},\text{deph}} = \Gamma_p \sum_x (S_x^z)^2. \tag{4.53}$$

We expect the ground states of these two contributions to have different orders, just like before dephasing. The ground state of $H_{\mathcal{M},\text{deph}}$ is simple enough and includes any state where all of the spin-1 components are 0:

$$\|\Omega_{\mathbf{m}}\rangle\rangle = \bigotimes_i \sum_{s_i \in \{+,-\}} |0, s_i\rangle_i. \tag{4.54}$$

This state has a massive degeneracy, occupying 1/3 of the new, restricted Hilbert space.

Now we turn to $H_{\mathcal{L},\text{deph}}$. To ensure the states chosen are ground states, we can check that they have exactly zero energy. Since we have only restricted the Hilbert space, $H_{\mathcal{L},\text{deph}}$ should still be positive semi-definite, and by construction, the ground states of $H_{\mathcal{L},\text{deph}}$, which have zero energy, should exist within this subspace. This allows us to pick out four ground states:

1. The diagonal identity

$$\|id\rangle\rangle = \bigotimes_{i=1}^{L} \left(\sum_{s_i} |s_i\rangle|s_i\rangle \right) \otimes \left(\sum_{s_i'} |s_i'\rangle|s_i'\rangle \right)$$

$$\|id\rangle\rangle = \bigotimes_{i=1}^{L} (|1\rangle_i + |0\rangle_i)| + x\rangle_i$$

2. The exchange identity

$$\|\sigma_{12}\rangle\rangle = \bigotimes_{i=1}^{L} \left(\sum_{s_i} \sum_{s_i'} |s_i'\rangle|s_i\rangle \otimes |s_i'\rangle|s_i\rangle \right)$$

$$\|\sigma_{12}\rangle\rangle = \bigotimes_{i=1}^{L} (|-1\rangle_i + |0\rangle_i)| + x\rangle_i$$

3. The single diagonal S^z

$$\|S^z_{tot,id}\rangle\rangle = \sum_{j=1}^{L}(\sigma^z \otimes \mathbb{I} \otimes \mathbb{I} \otimes \mathbb{I})_j \bigotimes_{i=1}^{L}\left(\sum_{s_i}|s_i\rangle|s_i\rangle\right) \otimes \left(\sum_{s'_i}|s'_i\rangle|s'_i\rangle\right)$$

$$\|S^z_{tot,id}\rangle\rangle = \sum_{j=1}^{L}(\mathbb{I}_3 \otimes \sigma^z)_j \bigotimes_{i=1}^{L}(|1\rangle_i + |0\rangle_i)| + x\rangle_i = \sum_{j=1}^{L}(\mathbb{I}_3 \otimes \sigma^z)_j \|id\rangle\rangle$$

4. The single exchange S^z

$$\|S^z_{tot,\sigma_{12}}\rangle\rangle = \sum_{j=1}^{L}(\sigma^z \otimes \mathbb{I} \otimes \mathbb{I} \otimes \mathbb{I})_j \bigotimes_{i=1}^{L}\left(\sum_{s_i}\sum_{s'_i}|s'_i\rangle|s_i\rangle \otimes |s'_i\rangle|s_i\rangle\right)$$

$$\|S^z_{tot,\sigma_{12}}\rangle\rangle = \sum_{j=1}^{L}(\mathbb{I}_3 \otimes \sigma^z)_j \bigotimes_{i=1}^{L}(|-1\rangle_i + |0\rangle_i)| + x\rangle_i = \sum_{j=1}^{L}(\mathbb{I}_3 \otimes \sigma^z)_j \|\sigma_{12}\rangle\rangle$$

Here, $|\pm x\rangle = |+\rangle \pm |-\rangle$. Let us double-check that these are, in fact, ground states. This is relatively straightforward because the spin-1 state $|\psi\rangle = |\pm 1\rangle + |0\rangle$ is orthogonal to $|m\rangle$, and only activates the SWAP term, which clearly has eigenvalue 1. Next, the ferromagnetic spin-1/2 state produces an eigenstate of 2 from $\sigma^\mu_x\sigma^\mu_{x+1}$. Pairing these two together, the second term in H_{deph} produces an eigenvalue of -1, which cancels out the contribution from the identity term, $\mathbb{I}_9 \otimes \mathbb{I}_4$ for a zero eigenvalue. Since we know the original Hamiltonian was positive semi-definite, these are all, indeed, ground states. In the absence of measurement, we immediately see that our gapless modes simply come from magnons in the spin-1/2 Heisenberg term.

The different spin-1/2 sectors correspond to different fillings in the first element of the first copy. The fillings in other elements can then be deduced from the spin-1 information.

4.3.2 Replica and U(1) symmetry breaking

Let us explore the various forms of transitions that can occur in this particular example. The original effective Hamiltonian has a large symmetry group:

$$\Big[(\mathrm{U}(1)^{\otimes 2} \rtimes \mathcal{S}_2)_L \times (\mathrm{U}(1)^{\otimes 2} \rtimes \mathcal{S}_2)_R\Big] \rtimes \mathbb{Z}_2^{\mathbb{H}}. \tag{4.55}$$

After the projection to our new basis, we are left with a reduced symmetry group:

$$(\mathrm{U}(1)^{\otimes 3} \rtimes \mathcal{S}_2) \rtimes \mathbb{Z}_2^{\mathbb{H}}. \tag{4.56}$$

Unsurprisingly, after a dephasing operation, that effectively fixes one charge sector, $Q_{2,\text{deph}} = \sum_i \Big((S^z_{u,1} - S^z_{d,1}) + (S^z_{u,2} - S^z_{d,2})\Big)_i = 0$, we note that there are three remaining U(1) symmetries generated by the following in the new basis:

1. $Q_1 = \sum_i \left[1 + (P_0 \otimes \sigma^z)_i\right]$ (fully diagonal sector)
2. $Q_2 = \sum_i (P_1 \otimes \sigma^z)_i$ (first inter-replica charge difference)
3. $Q_3 = \sum_i (P_{-1} \otimes \sigma^z)_i$. (second inter-replica charge difference)

Note that Q_1, the sum of off-diagonal U(1) charge for copy-1 and copy-2, due to its projection into the spin-0 supspace of the spin-1 chain, is unaffected by measurement, and the spectrum of excitations assocciated with this charge remains quadratic regardless of measurement. Additionally, there exist two remaining discrete symmetries. We can trace the action of the original discrete symmetries in the new basis as follows:

- $\mathcal{S}_2$ (flipping spin-1): $|m, s\rangle \ \mapsto \ |-m, s\rangle$
- $\mathbb{Z}_2^{\mathbb{H}}$ (flipping spin-1/2): $|m, s\rangle \ \mapsto \ |m, -s\rangle$

We label the symmetry acting on the spin-1 degrees of freedom that is associated with the SWAP operation as $\mathcal{S}_2$. We distinguish this from the spin 1/2 symmetry, which arises partially from the Hermitticity restriction. We label this symmetry with the same $\mathbb{Z}_2^{\mathbb{H}}$ $s^z_{tot} = \sum_x \mathbb{I}_3 \otimes \sigma^z_x$.

From the discussion above, we recognize that the entanglement transition originates from a form of replica symmetry breaking, with the volume-law phase corresponding to the symmetry-broken phase, and the area-law to the symmetric phase. Similarly, the goldstone modes that formed the subject of the previous chapters were the result of SSB of a U(1) symmetry.

With this in mind, We can already identify two different orders in the unitary evolution and measurement-only limits. In the limit of no measurement, we should see both replica and U(1) symmetry breaking. However, in the measurement-only limit, we see that $[\delta Q]$ is identically zero, and both the replica and U(1) symmetries should be restored.

We might hope to see another order at some intermediate measurement rate, corresponding to the charge-sharp regime above. This would break replica symmetry, but not the U(1) symmetry. Thus, there would be no freely dispersing charge modes; instead, at the timescale considered $t \sim L$, the interactions in $H_{\text{eff,deph}}$ will force charges to be approximately frozen in place like a Mott insulator.

As explained above, the decomposition on display in our new basis (Eq. 4.50) shows that these transitions affect non-overlapping, and thus commuting, orders. This supports the conjecture that the addition of system symmetries should not affect the qualitative features of the entanglement transition.

However, we must be a bit careful in our analysis of these different phases. Rather than looking at ground state (steady state) order, we may wish to examine the order present after evolution by a timescale that scales linearly with system size, as this is the timescale for entanglement to spread through our system. Doing so will require a knowledge of the low-energy spectrum of $H_{\text{eff,deph}}$ and its scaling with system size, L, but it may provide a robust, computationally accessible characterization of the various phases.

Entanglement Dynamics

Since we have different ground states for the measurement and unitary operations, we expect at least one transition by varying the measurement rate, Γ_p. The clearest difference in these ground states is that one describes a volume-law entangled phase, while the other, area-law entangled phase. Let us try to understand this in the doubled Hilbert space formalism.

For a generic system with measurements occurring at spacetime locations, $\{M\}$, with outcomes, $\mathbf{m}$, in a system with k copies, we can define a concept related to the measurement and circuit averaged Rényi moment can as follows[136, 147]:

$$\tilde{S}^{(k)} \equiv \frac{1}{1-k} \log \left| \frac{\sum_{\{M\}} p_M d^{|M|(k-1)} \overline{\sum_{\mathbf{m}} p_{\mathbf{m}}^k \mathrm{Tr}[\rho_{\mathbf{m}}^k]^k}}{\sum_{\{M\}} p_M d^{|M|(k-1)} \overline{\sum_{\mathbf{m}} p_{\mathbf{m}}^k}} \right|, \tag{4.57}$$

where, d, is the local Hilbert space dimension, and the factor, $d^{|M|(k-1)}$ is used to normalize measurements. We will be particularly concerned with the second moment, so we examine the circuit-averaged purity of a region A of the length L chain, defined as

$$\begin{aligned} \overline{\rho_A^2(t)} &= \frac{\langle\langle id \| \mathcal{S}_A \| \rho(t) \rangle\rangle}{\langle\langle id \| \rho(t) \rangle\rangle} \\ &= \frac{\langle\langle (\sigma_{12})_A \otimes \mathbb{I}_{\overline{A}} \| e^{-tH_{\text{eff,deph}}} \| \rho(0) \rangle\rangle}{\langle\langle id \| e^{-tH_{\text{eff,deph}}} \| \rho(0) \rangle\rangle}, \end{aligned} \tag{4.58}$$

where the swap operator, $\mathcal{S}_A$, acts to the left creates a state with domain walls at the boundary of region A. The relaxation of this quantity to its equilibrium value will determine the timescale of purification for a particular initial configuration $\|\rho(0)\rangle\rangle$. However, for now, we will focus on the infinite time limit, where $\|\rho(t)\rangle\rangle \underset{t\to\infty}{=} \|\rho_{GS}\rangle\rangle$ is the ground state for our effective Hamiltonian. In this limit,

$$\overline{\rho_{A,(GS)}^2} \equiv e^{-\overline{\tilde{S}^{(2)}(A)}} = \frac{\langle\langle id \| \mathcal{S}_A \| \rho_{GS} \rangle\rangle}{\langle\langle id \| \rho_{GS} \rangle\rangle} = \frac{\langle\langle (\sigma_{12})_A \otimes \mathbb{I}_{\overline{A}} \| \rho_{GS} \rangle\rangle}{\langle\langle id \| \rho_{GS} \rangle\rangle}, \tag{4.59}$$

In the absence of measurements, the ground state will simply be a symmetric superposition over swap-conjugate ground states: $\|\rho_{GS}\rangle\rangle \propto \|id\rangle\rangle + \|\sigma_{12}\rangle\rangle + \|S^z_{tot,id}\rangle\rangle + \|S^z_{tot,\sigma_{12}}\rangle\rangle$. Whereas, for measurement-only dynamics, we will have $\|\rho_{GS}\rangle\rangle = |\Omega_{meas}\rangle$. This makes it easy to calculate the purity in the different regimes:

$$\overline{\rho_A^2} \sim \begin{cases} e^{-L_A} + e^{-(L-L_A)} & (\Gamma_p = 0) \\ \text{Const.} & (\Gamma_p \to \infty) \end{cases}. \tag{4.60}$$

We notice that there is a clear difference in the order present in these two ground states signaling this transition. This comes in the form of the spin-1 z-polarization. Specifically, we expect to characterize at least one transition by examining the expectation of $(S^z)^2_{tot} = \sum_i (S^z_i)^2 \otimes \mathbb{I}_2$, which only acts on the spin-1 sector, at finite Γ_p. When the measurement rate is sufficiently high, this ground state should no longer have any z-polarization in the spin-1 sector, and at a critical rate, Γ_c^S, we expect a finite z-polarization to emerge.

Charge Sharpening Transition

Charge-sharpening occurs when a system eliminates all entanglement between different charge sectors. When measurements of local charge are infrequent, the system will eventually purify into a state comprised of elements from many charge sectors. In contrast, for sufficiently rapid measurements, the system will purify into a product state in the charge basis, where it will have a unique charge. It is still an open question whether this charge sharpening transition occurs at the same transition point as the entanglement transition.

If we wish to understand the phenomenon of charge sharpening, we must turn to another quantity that depends on the spin-1/2 space. Given the discussion above, one immediate choice would be the charge variance given in Eq. 4.21. This quantity can be cast in the double Hilbert space formalism as follows:

$$\begin{aligned}[\delta Q^2] &= [\langle Q^2\rangle_{\mathbf{m}} - \langle Q\rangle^2_{\mathbf{m}}] \\ &= \frac{\langle\langle Q\otimes Q\|(\mathcal{S}-\mathbb{I})\|\rho(t)\rangle\rangle}{\langle\langle id\|\rho(t)\rangle\rangle} \\ &= \frac{\langle\langle Q\otimes Q\|(\mathcal{S}-\mathbb{I})e^{-tH_{\text{eff,deph}}}\|\rho(0)\rangle\rangle}{\langle\langle id\|e^{-tH_{\text{eff,deph}}}\|\rho(0)\rangle\rangle}.\end{aligned} \tag{4.61}$$

This quantity was shown to distinguish the different regimes for charge sharpening. And again, we can check that there is truly a distinction for ground states in our two extreme regimes. Repeating the analysis above, we find

$$[\delta Q^2] = \frac{\langle\langle Q\otimes Q\|(\mathcal{S}-\mathbb{I})\|\rho_{GS}\rangle\rangle}{\langle\langle id\|\rho_{GS}\rangle\rangle} = \begin{cases}\text{Cost.} & (\Gamma_p = 0)\\ 0 & (\Gamma_p\to\infty)\end{cases}. \tag{4.62}$$

Note that, due to the $(\mathcal{S}-\mathbb{I})$ factor, $[\delta Q^2]$ must vanish in the area-law phase since it is symmetric under replica permutation. Thus, this transition must occur within the volume-law phase or at the entanglement transition itself. Further, if the ground state resides in a single charge sector of charge, m, $\|\rho_{GS}\rangle\rangle = \|P_m\otimes P_m\rangle\rangle$, the numerator will vanish because

$$\langle\langle Q\otimes Q\|(\mathcal{S}-\mathbb{I})\|P_m\otimes P_m\rangle\rangle = \text{Tr}[Q^2P_m] - \text{Tr}[QP_m]^2 = m^2 - m^2 = 0. \tag{4.63}$$

We can identify a similar order parameter to distinguish the ground states in these extreme regimes. And indeed, there is a difference in their orders in the spin-1/2 sectors. These phases are distinguished by spin-1/2 charge fluctuations between $\mathbb{I}_3\otimes\sigma_0^z$ and $\mathbb{I}_3\otimes\sigma_x^z$. Again, we focus on the two ground states in extreme limits. In the measurement-only limit, there is no correlation between local spin-1/2 configurations. In the absence of measurements, there will be perfect, constant correlation between spin-1/2 components at arbitrary distances. This is reminiscent of the different scaling predicted in Eq. 4.22 for similar charge fluctuations.

Spectral Signatures

In the limits of pure measurement or pure unitary dynamics, one can distinguish between both area-law and volume law phases, and charge-sharp and charge-fuzzy phases using the

doubled Hilbert space formalism. However, the characterization of the different phases is general, and expected to hold for finite measurement rate, Γ_p. Further, following, [130], these phases should be distinguishable by the timescales for purification and for disentangling charge sectors. In principle, these timescales should be derivable from the low-energy spectrum of $H_{\text{eff,deph}}$, and it is conjectured that the different orders present should correspond to different spectral features, such as the relative size of different excitation gaps.[13]

4.3.3 Discussion and Outlook

As in Ch. 2, we note that the Doubled Hilbert Space framework is strictly more general than any Haar-averaging description, applying to systems of arbitrary symmetric interactions and local Hilbert space dimension without recourse to ancilla degrees of freedom. Further, this framework with ready extensions to systems with non-Abelian symmetries, long-range interactions, multipole symmetries and more. Further, in the case of dynamics preserving a U(1) symmetry, this model grounds these insights about dynamical timescales in a familiar physical picture through a dual description of specific excitations within a familiar equilibrium system.

Finally, there is an additional and immediate benefit to this perspective. By uncovering a systematic way to restrict to the low-energy subspace of a system's dynamics, one may readily simulate behavior in this regime for massively reduced computational costs.

This doubled Hilbert space formalism presents fertile soil for the exploration of generic properties of dynamical systems. Much as with pure unitary evolution, we hope to extend the analysis of U(1)-symmetric systems to those with multipole symmetries, Krylov-resolved dynamics, and long-range interactions. In addition, we hope to investigate the dynamical transitions and properties of different metrics, such as the entanglement negativity, which has a simple expression in terms of state permutations[148]. Extending further, this paradigm seems to present insights into the classification of topological orders in mixed state systems, and has already been used to diagnose SPT order in systems with decoherence using a generalization of strange correlators[138] and to characterize decoherence transitions in systems with topological order[149].

Nomenclature for Chapter 4

Selected Abbreviations

OTOC Out-of-time-ordered correlator
MIPT Measurement-induced phase transition
MRC Monitored Random Circuit
SPT Symmetry protected topological order
SET Symmetry enhanced topological order
SSB Spontaneous Symmetry Breaking

[13] This is the subject of a forthcoming work: O Ogunnaike, JY Lee, R Lohar (2024), *Filling-resolved Replica SSB*, Manuscript in preparation

Variables

H_{eff} The effective Hamiltonian on k-copies, accounting for both unitary dynamics and measurement, $H_{\text{eff}} = HH_{\mathcal{L}}^{(k)} + H_{\mathcal{M}}$

$S^{(n)}(\rho)$ The n'th moment of Rényi entanglement entropy

$[\delta Q^2]$ The charge variance after circuit and trajectory averaging

Γ_p The rate of measurement in H_{eff}

Chapter 5

Conclusion

In this dissertation, we have reviewed a number of effects of symmetry in dynamical quantum many-body systems through the doubled Hilbert space perspective. This approach allowed us to employ techniques from equilibrium quantum theory. Doing so, we were able to unite a number of results and predict some new phenomena using the same, intuitive framework. In particular, it was shown that the behavior of late-time autocorrelation functions in thermalizing systems with symmetry constraints could be understood by examining the low-energy spectrum of an effective Hamiltonian, $H_{\mathcal{L}}$, living in the doubled Hilbert space and derived from Lindbladian system dynamics, $\mathcal{L}[\cdot]$.

This study demonstrated that conventional discrete symmetries produced a gapped spectrum for $H_{\mathcal{L}}$, resulting in little difference from systems with no symmetry other than the presence of dynamically disconnected symmetry sectors. In contrast, the presence of continuous symmetries produced gappless goldstone modes in the spectrum of $H_{\mathcal{L}}$, resulting in diffusive charge transport at late times and regardless of the Abelian or non-Abelian nature of the underlying symmetry. Next, it was shown that systems with m'th-order multipole symmetries *typically* displayed subdifusive charge transport with a dynamical exponent, $z = 2m + 2$. The phenomena of Hilbert space fragmentation in such multipole-conserving systems was explained through the appearance of an exponentially ground state degeneracy for $H_{\mathcal{L}}$, and novel Krylov-resolved dynamics with anomalously low dynamical exponents, $z = 2(m - p + 1)$ were proposed and numerically verified for Krlov sectors with bounded p'th-order multipole fluctuations. Finally, it was shown that long-range interactions, $h \sim \frac{1}{r^\alpha}$ in d dimension that conserve m'th-order multipole moments could result in three distinct charge dynamics with dynamical exponent, $2m$, $2(m+\alpha)-d$, and $2m+2$, depending on the locality of the interactions as defined by α.

Finally, This framework was shown to generalize to systems with coherent dynamics and measurements by including multiple system copies. In the latter case, it was shown that one may explain the entanglement transition as a replica symmetry breaking transition relating the exchange operations between system copies. Further, it was proposed that a charge sharpening transition should appear as a similar symmetry-breaking transition involving the continuous symmetries of the different copies.

This study demonstrates the potency of this double Hilbert space framework, providing a qualitative understanding both familiar and novel universal properties of dynamical phenomena in the language of equilibrium physics.

Appendix A

Appendix

Included below is a list of papers published during my time at MIT:

1. **O. Ogunnaike**, J. Feldmeier, J.Y. Lee
   Unifying Emergent Hydrodynamics and Lindbladian Low Energy Spectra across Symmetries, Constraints, and Long-Range Interactions , Phys. Rev. Lett. 131, 220403
2. Z. Dong, **O. Ogunnaike**, L. Levitov
   Collective excitations in chiral Stoner magnets,Phys. Rev. Lett. 130 (20), 206701, Editor's Suggestion
3. Z. Dong, M. Davydova, **O. Ogunnaike**, L. Levitov
   Isospin-and momentum-polarized orders in bilayer graphene, Phys. Rev. B 107, 075108
4. Sophie Fisher, **O. Ogunnaike***, L. Levitov
   Three-Body Bound States of Quantum Particles: Higher Stability Through Braiding, Phys. Rev. A 109, 043323

References

[1] Aristotle Translated with introduction, commentary, Note on Recent Work, and and revised Bibliography by W. Charlton. *Physics*. Clarendon Aristotle Series. Oxford, New York: Oxford University Press, Mar. 1984. ISBN: 978-0-19-872026-3.

[2] Christian Gross and Immanuel Bloch. "Quantum simulations with ultracold atoms in optical lattices". In: *Science* 357.6355 (Sept. 2017). Publisher: American Association for the Advancement of Science, pp. 995–1001. DOI: 10.1126/science.aal3837. URL: https://www.science.org/doi/10.1126/science.aal3837.

[3] Marcos Rigol, Vanja Dunjko, and Maxim Olshanii. "Thermalization and its mechanism for generic isolated quantum systems". en. In: *Nature* 452.7189 (Apr. 2008). Publisher: Nature Publishing Group, pp. 854–858. ISSN: 1476-4687. DOI: 10.1038/nature06838. URL: https://www.nature.com/articles/nature06838.

[4] Florian SchÃ€fer, Takeshi Fukuhara, Seiji Sugawa, Yosuke Takasu, and Yoshiro Takahashi. "Tools for quantum simulation with ultracold atoms in optical lattices". In: *Nature Reviews Physics* 2.8 (July 2020). arXiv:2006.06120 [cond-mat], pp. 411–425. ISSN: 2522-5820. DOI: 10.1038/s42254-020-0195-3. URL: http://arxiv.org/abs/2006.06120.

[5] Hannes Bernien et al. "Probing many-body dynamics on a 51-atom quantum simulator". en. In: *Nature* 551.7682 (Nov. 2017). Publisher: Nature Publishing Group, pp. 579–584. ISSN: 1476-4687. DOI: 10.1038/nature24622. URL: https://www.nature.com/articles/nature24622.

[6] Antoine Browaeys and Thierry Lahaye. "Many-Body Physics with Individually-Controlled Rydberg Atoms". In: *Nature Physics* 16.2 (Feb. 2020). arXiv:2002.07413 [cond-mat, physics:physics, physics:quant-ph], pp. 132–142. ISSN: 1745-2473, 1745-2481. DOI: 10.1038/s41567-019-0733-z. URL: http://arxiv.org/abs/2002.07413.

[7] R. Blatt and C. F. Roos. "Quantum simulations with trapped ions". en. In: *Nature Physics* 8.4 (Apr. 2012). Publisher: Nature Publishing Group, pp. 277–284. ISSN: 1745-2481. DOI: 10.1038/nphys2252. URL: https://www.nature.com/articles/nphys2252.

[8] R. Islam, C. Senko, W. C. Campbell, S. Korenblit, J. Smith, A. Lee, E. E. Edwards, C.-C. J. Wang, J. K. Freericks, and C. Monroe. "Emergence and Frustration of Magnetic Order with Variable-Range Interactions in a Trapped Ion Quantum Simulator". In: *Science* 340.6132 (May 2013). arXiv:1210.0142 [cond-mat, physics:quant-ph], pp. 583–587. ISSN: 0036-8075, 1095-9203. DOI: 10.1126/science.1232296. URL: http://arxiv.org/abs/1210.0142.

[9] Joseph W. Britton, Brian C. Sawyer, Adam C. Keith, C.-C. Joseph Wang, James K. Freericks, Hermann Uys, Michael J. Biercuk, and John J. Bollinger. "Engineered 2D Ising interactions on a trapped-ion quantum simulator with hundreds of spins". In: *Nature* 484.7395 (Apr. 2012). arXiv:1204.5789 [cond-mat, physics:physics, physics:quant-ph], pp. 489–492. ISSN: 0028-0836, 1476-4687. DOI: 10.1038/nature10981. URL: http://arxiv.org/abs/1204.5789.

[10] Adam M. Kaufman, M. Eric Tai, Alexander Lukin, Matthew Rispoli, Robert Schittko, Philipp M. Preiss, and Markus Greiner. "Quantum thermalization through entanglement in an isolated many-body system". In: *Science* 353.6301 (Aug. 2016). Publisher: American Association for the Advancement of Science, pp. 794–800. DOI: 10.1126/science.aaf6725. URL: https://www.science.org/doi/10.1126/science.aaf6725.

[11] Patricia Mendoza-MÃ©ndez, Leticia LÃ³pez-Flores, Alejandro Vizcarra-RendÃ³n, Luis E. SÃ¡nchez-DÃaz, and Magdaleno Medina-Noyola. "Generalized Langevin equation for tracer diffusion in atomic liquids". In: *Physica A: Statistical Mechanics and its Applications* 394 (Jan. 2014), pp. 1–16. ISSN: 0378-4371. DOI: 10.1016/j.physa.2013.09.061. URL: https://www.sciencedirect.com/science/article/pii/S0378437113009382.

[12] L. Boltzmann. "Weitere Studien uber das Wärmegleichgewicht unter Gasmolekulen". In: *Sitzungsberichte Akademie der Wissenschaften* 66 (1872), pp. 275–370. URL: https://doi.org/10.1142/9781848161337_0015.

[13] Takashi Mori, Tatsuhiko N. Ikeda, Eriko Kaminishi, and Masahito Ueda. "Thermalization and prethermalization in isolated quantum systems: a theoretical overview". In: *Journal of Physics B: Atomic, Molecular and Optical Physics* 51.11 (June 2018). arXiv:1712.08790 [cond-mat, physics:quant-ph], p. 112001. ISSN: 0953-4075, 1361-6455. DOI: 10.1088/1361-6455/aabcdf. URL: http://arxiv.org/abs/1712.08790.

[14] M. Toda, M. Toda, N. Saito, R. Kubo, and N. Saito. *Statistical Physics I: Equilibrium Statistical Mechanics*. Springer Series in Solid-State Sciences. Springer Berlin Heidelberg, 2012. ISBN: 978-3-642-58134-2. URL: https://books.google.com/books?id=uWbvCAAAQBAJ.

[15] R. Balescu. *Equilibrium and Nonequilibrium Statistical Mechanics*. Wiley, 1975. URL: https://books.google.com/books?id=MwHNwgEACAAJ.

[16] Joel L. Lebowitz and Oliver Penrose. “Modern ergodic theory”. In: *Physics Today* 26.2 (Feb. 1973). _eprint: https://pubs.aip.org/physicstoday/article-pdf/26/2/23/8276421/23_1_online.pdf, pp. 23–29. ISSN: 0031-9228. DOI: 10.1063/1.3127948. URL: https://doi.org/10.1063/1.3127948.

[17] David Ruelle. “Resonances of chaotic dynamical systems”. In: *Physical Review Letters* 56.5 (Feb. 1986). Publisher: American Physical Society, pp. 405–407. DOI: 10.1103/PhysRevLett.56.405. URL: https://link.aps.org/doi/10.1103/PhysRevLett.56.405.

[18] David Ruelle. “Locating resonances for AxiomA dynamical systems”. en. In: *Journal of Statistical Physics* 44.3 (Aug. 1986), pp. 281–292. ISSN: 1572-9613. DOI: 10.1007/BF01011300. URL: https://doi.org/10.1007/BF01011300.

[19] Michael A. Nielsen and Isaac L. Chuang. *Quantum Computation and Quantum Information: 10th Anniversary Edition*. en. ISBN: 9780511976667 Publisher: Cambridge University Press. Dec. 2010. DOI: 10.1017/CBO9780511976667. URL: https://www.cambridge.org/highereducation/books/quantum-computation-and-quantum-information/01E10196D0A682A6AEFFEA52D53BE9AE.

[20] Bruno Bertini, Pavel Kos, and TomaÅŸ Prosen. “Entanglement Spreading in a Minimal Model of Maximal Many-Body Quantum Chaos”. In: *Physical Review X* 9.2 (May 2019). Publisher: American Physical Society, p. 021033. DOI: 10.1103/PhysRevX.9.021033. URL: https://link.aps.org/doi/10.1103/PhysRevX.9.021033.

[21] Sheldon Goldstein, Joel L. Lebowitz, Roderich Tumulka, and Nino ZanghÃ¬. “Canonical Typicality”. In: *Physical Review Letters* 96.5 (Feb. 2006). Publisher: American Physical Society, p. 050403. DOI: 10.1103/PhysRevLett.96.050403. URL: https://link.aps.org/doi/10.1103/PhysRevLett.96.050403.

[22] Peter Reimann. “Foundation of Statistical Mechanics under Experimentally Realistic Conditions”. In: *Physical Review Letters* 101.19 (Nov. 2008). Publisher: American Physical Society, p. 190403. DOI: 10.1103/PhysRevLett.101.190403. URL: https://link.aps.org/doi/10.1103/PhysRevLett.101.190403.

[23] Hal Tasaki. “From Quantum Dynamics to the Canonical Distribution: General Picture and a Rigorous Example”. In: *Physical Review Letters* 80.7 (Feb. 1998). Publisher: American Physical Society, pp. 1373–1376. DOI: 10.1103/PhysRevLett.80.1373. URL: https://link.aps.org/doi/10.1103/PhysRevLett.80.1373.

[24] John von Neumann. “Proof of the Ergodic Theorem and the H-Theorem in Quantum Mechanics”. In: *The European Physical Journal H* 35.2 (Nov. 2010). arXiv:1003.2133 [cond-mat, physics:physics, physics:quant-ph], pp. 201–237. ISSN: 2102-6459, 2102-6467. DOI: 10.1140/epjh/e2010-00008-5. URL: http://arxiv.org/abs/1003.2133.

[25] Giulio Biroli, Corinna Kollath, and Andreas M. LÃ€uchli. “Effect of Rare Fluctuations on the Thermalization of Isolated Quantum Systems”. In: *Physical Review Letters* 105.25 (Dec. 2010). Publisher: American Physical Society, p. 250401. DOI: 10.1103/PhysRevLett.105.250401. URL: https://link.aps.org/doi/10.1103/PhysRevLett.105.250401.

[26] Eugene P. Wigner. “Characteristic Vectors of Bordered Matrices With Infinite Dimensions”. In: *Annals of Mathematics* 62.3 (1955). Publisher: Annals of Mathematics, pp. 548–564. ISSN: 0003-486X. DOI: 10.2307/1970079. URL: https://www.jstor.org/stable/1970079.

[27] M. L. Mehta. *Random matrices*. Third edition. Pure and applied mathematics (Academic Press) ; Amsterdam ; San Diego, CA : Elsevier/Academic Press, 2004. ISBN: 978-0-12-088409-4.

[28] Luca D’Alessio, Yariv Kafri, Anatoli Polkovnikov, and Marcos Rigol. “From Quantum Chaos and Eigenstate Thermalization to Statistical Mechanics and Thermodynamics”. In: *Advances in Physics* 65.3 (May 2016). arXiv:1509.06411 [cond-mat, physics:quant-ph], pp. 239–362. ISSN: 0001-8732, 1460-6976. DOI: 10.1080/00018732.2016.1198134. URL: http://arxiv.org/abs/1509.06411.

[29] Eiki Iyoda, Kazuya Kaneko, and Takahiro Sagawa. “Fluctuation Theorem for Many-Body Pure Quantum States”. In: *Physical Review Letters* 119.10 (Sept. 2017). Publisher: American Physical Society, p. 100601. DOI: 10.1103/PhysRevLett.119.100601. URL: https://link.aps.org/doi/10.1103/PhysRevLett.119.100601.

[30] Takashi Mori and Naoto Shiraishi. “Thermalization without eigenstate thermalization hypothesis after a quantum quench”. In: *Physical Review E* 96.2 (Aug. 2017). Publisher: American Physical Society, p. 022153. DOI: 10.1103/PhysRevE.96.022153. URL: https://link.aps.org/doi/10.1103/PhysRevE.96.022153.

[31] Naoto Shiraishi and Takashi Mori. “Systematic Construction of Counterexamples to the Eigenstate Thermalization Hypothesis”. In: *Physical Review Letters* 119.3 (July 2017). Publisher: American Physical Society, p. 030601. DOI: 10.1103/PhysRevLett.119.030601. URL: https://link.aps.org/doi/10.1103/PhysRevLett.119.030601.

[32] Marcos Rigol. “Breakdown of Thermalization in Finite One-Dimensional Systems”. In: *Physical Review Letters* 103.10 (Sept. 2009). Publisher: American Physical Society, p. 100403. DOI: 10.1103/PhysRevLett.103.100403. URL: https://link.aps.org/doi/10.1103/PhysRevLett.103.100403.

[33] Rahul Nandkishore and David A. Huse. “Many-Body Localization and Thermalization in Quantum Statistical Mechanics”. en. In: *Annual Review of Condensed Matter Physics* 6.Volume 6, 2015 (Mar. 2015). Publisher: Annual Reviews, pp. 15–38. ISSN: 1947-5454, 1947-5462. DOI: 10.1146/annurev-conmatphys-031214-014726. URL:

https://www.annualreviews.org/content/journals/10.1146/annurev-conmatphys-031214-014726.

[34] David A. Huse, Rahul Nandkishore, and Vadim Oganesyan. "Phenomenology of fully many-body-localized systems". In: *Physical Review B* 90.17 (Nov. 2014). Publisher: American Physical Society, p. 174202. DOI: 10.1103/PhysRevB.90.174202. URL: https://link.aps.org/doi/10.1103/PhysRevB.90.174202.

[35] Maksym Serbyn, Z. Papić, and Dmitry A. Abanin. "Local Conservation Laws and the Structure of the Many-Body Localized States". In: *Physical Review Letters* 111.12 (Sept. 2013). Publisher: American Physical Society, p. 127201. DOI: 10.1103/PhysRevLett.111.127201. URL: https://link.aps.org/doi/10.1103/PhysRevLett.111.127201.

[36] Pablo Sala, Tibor Rakovszky, Ruben Verresen, Michael Knap, and Frank Pollmann. "Ergodicity Breaking Arising from Hilbert Space Fragmentation in Dipole-Conserving Hamiltonians". In: *Physical Review X* 10.1 (Feb. 2020). Publisher: American Physical Society, p. 011047. DOI: 10.1103/PhysRevX.10.011047. URL: https://link.aps.org/doi/10.1103/PhysRevX.10.011047.

[37] Vedika Khemani, Michael Hermele, and Rahul Nandkishore. "Localization from Hilbert space shattering: From theory to physical realizations". In: *Physical Review B* 101.17 (May 2020). Publisher: American Physical Society, p. 174204. DOI: 10.1103/PhysRevB.101.174204. URL: https://link.aps.org/doi/10.1103/PhysRevB.101.174204.

[38] Shriya Pai, Michael Pretko, and Rahul M. Nandkishore. "Localization in Fractonic Random Circuits". In: *Physical Review X* 9.2 (Apr. 2019). Publisher: American Physical Society, p. 021003. DOI: 10.1103/PhysRevX.9.021003. URL: https://link.aps.org/doi/10.1103/PhysRevX.9.021003.

[39] Luca D'Alessio, Yariv Kafri, Anatoli Polkovnikov, and Marcos Rigol. "From quantum chaos and eigenstate thermalization to statistical mechanics and thermodynamics". In: *Advances in Physics* 65.3 (2016), pp. 239–362. DOI: 10.1080/00018732.2016.1198134. eprint: https://doi.org/10.1080/00018732.2016.1198134. URL: https://doi.org/10.1080/00018732.2016.1198134.

[40] Chaitanya Murthy, Arman Babakhani, Fernando Iniguez, Mark Srednicki, and Nicole Yunger Halpern. "Non-Abelian Eigenstate Thermalization Hypothesis". In: *Physical Review Letters* 130.14 (Apr. 2023). Publisher: American Physical Society, p. 140402. DOI: 10.1103/PhysRevLett.130.140402. URL: https://link.aps.org/doi/10.1103/PhysRevLett.130.140402.

[41] C. J. Turner, A. A. Michailidis, D. A. Abanin, M. Serbyn, and Z. Papić. "Weak ergodicity breaking from quantum many-body scars". en. In: *Nature Physics* 14.7 (July 2018). Publisher: Nature Publishing Group, pp. 745–749. ISSN: 1745-2481. DOI: 10.1038/s41567-018-0137-5. URL: https://www.nature.com/articles/s41567-018-0137-5.

[42] Paola Ruggiero, Vincenzo Alba, and Pasquale Calabrese. "Entanglement negativity in random spin chains". In: *Physical Review B* 94.3 (July 2016). Publisher: American Physical Society, p. 035152. DOI: 10.1103/PhysRevB.94.035152. URL: https://link.aps.org/doi/10.1103/PhysRevB.94.035152.

[43] Philipp Hyllus, Wieslaw Laskowski, Roland Krischek, Christian Schwemmer, Witlef Wieczorek, Harald Weinfurter, Luca Pezzé, and Augusto Smerzi. "Fisher information and multiparticle entanglement". In: *Physical Review A* 85.2 (Feb. 2012). Publisher: American Physical Society, p. 022321. DOI: 10.1103/PhysRevA.85.022321. URL: https://link.aps.org/doi/10.1103/PhysRevA.85.022321.

[44] Vedika Khemani, Ashvin Vishwanath, and David A. Huse. "Operator Spreading and the Emergence of Dissipative Hydrodynamics under Unitary Evolution with Conservation Laws". In: *Phys. Rev. X* 8 (3 Sept. 2018), p. 031057. DOI: 10.1103/PhysRevX.8.031057. URL: https://link.aps.org/doi/10.1103/PhysRevX.8.031057.

[45] Wen Wei Ho and Dmitry A. Abanin. "Entanglement dynamics in quantum many-body systems". In: *Physical Review B* 95.9 (Mar. 2017). Publisher: American Physical Society, p. 094302. DOI: 10.1103/PhysRevB.95.094302. URL: https://link.aps.org/doi/10.1103/PhysRevB.95.094302.

[46] T. Langen, R. Geiger, M. Kuhnert, B. Rauer, and J. Schmiedmayer. "Local emergence of thermal correlations in an isolated quantum many-body system". en. In: *Nature Physics* 9.10 (Oct. 2013). Publisher: Nature Publishing Group, pp. 640–643. ISSN: 1745-2481. DOI: 10.1038/nphys2739. URL: https://www.nature.com/articles/nphys2739.

[47] Elliott H. Lieb and Derek W. Robinson. "The finite group velocity of quantum spin systems". en. In: *Communications in Mathematical Physics* 28.3 (Sept. 1972), pp. 251–257. ISSN: 1432-0916. DOI: 10.1007/BF01645779. URL: https://doi.org/10.1007/BF01645779.

[48] Marc Cheneau, Peter Barmettler, Dario Poletti, Manuel Endres, Peter Schauß, Takeshi Fukuhara, Christian Gross, Immanuel Bloch, Corinna Kollath, and Stefan Kuhr. "Light-cone-like spreading of correlations in a quantum many-body system". en. In: *Nature* 481.7382 (Jan. 2012). Publisher: Nature Publishing Group, pp. 484–487. ISSN: 1476-4687. DOI: 10.1038/nature10748. URL: https://www.nature.com/articles/nature10748.

[49] Philip Richerme, Zhe-Xuan Gong, Aaron Lee, Crystal Senko, Jacob Smith, Michael Foss-Feig, Spyridon Michalakis, Alexey V. Gorshkov, and Christopher Monroe. "Non-local propagation of correlations in quantum systems with long-range interactions". en. In: *Nature* 511.7508 (July 2014). Publisher: Nature Publishing Group, pp. 198–201. ISSN: 1476-4687. DOI: 10.1038/nature13450. URL: https://www.nature.com/articles/nature13450.

[50] Brian Swingle. "Unscrambling the physics of out-of-time-order correlators". en. In: *Nature Physics* 14.10 (Oct. 2018). Publisher: Nature Publishing Group, pp. 988–990. ISSN: 1745-2481. DOI: 10.1038/s41567-018-0295-5. URL: https://www.nature.com/articles/s41567-018-0295-5.

[51] Juan Maldacena, Stephen H. Shenker, and Douglas Stanford. "A bound on chaos". In: *Journal of High Energy Physics* 2016.8 (Aug. 2016). arXiv:1503.01409 [cond-mat, physics:hep-th, physics:nlin, physics:quant-ph], p. 106. ISSN: 1029-8479. DOI: 10.1007/JHEP08(2016)106. URL: http://arxiv.org/abs/1503.01409.

[52] Anatoly I. Larkin and Yu. N. Ovchinnikov. "Quasiclassical Method in the Theory of Superconductivity". In: *Journal of Experimental and Theoretical Physics* (1969). URL: https://api.semanticscholar.org/CorpusID:117608877.

[53] Thomas Schuster. "Many-Body Quantum Information Dynamics". en. PhD thesis. UC Berkeley, 2022. URL: https://escholarship.org/uc/item/2694w4p8.

[54] Beni Yoshida and Norman Y. Yao. "Disentangling Scrambling and Decoherence via Quantum Teleportation". In: *Physical Review X* 9.1 (Jan. 2019). Publisher: American Physical Society, p. 011006. DOI: 10.1103/PhysRevX.9.011006. URL: https://link.aps.org/doi/10.1103/PhysRevX.9.011006.

[55] R. van Leeuwen, N.E. Dahlen, G. Stefanucci, C.-O. Almbladh, and U. von Barth. "Introduction to the Keldysh Formalism". en. In: *Time-Dependent Density Functional Theory*. Ed. by Miguel A.L. Marques, Carsten A. Ullrich, Fernando Nogueira, Angel Rubio, Kieron Burke, and Eberhard K. U. Gross. Berlin, Heidelberg: Springer, 2006, pp. 33–59. ISBN: 978-3-540-35426-0. DOI: 10.1007/3-540-35426-3_3. URL: https://doi.org/10.1007/3-540-35426-3_3.

[56] Heinz-Peter Breuer and Francesco Petruccione. *The Theory of Open Quantum Systems*. Oxford, New York: Oxford University Press, Mar. 2007. ISBN: 978-0-19-921390-0.

[57] Alioscia Hamma, Siddhartha Santra, and Paolo Zanardi. "Quantum Entanglement in Random Physical States". In: *Physical Review Letters* 109.4 (July 2012). Publisher: American Physical Society, p. 040502. DOI: 10.1103/PhysRevLett.109.040502. URL: https://link.aps.org/doi/10.1103/PhysRevLett.109.040502.

[58] C.W. von Keyserlingk, Tibor Rakovszky, Frank Pollmann, and S.L. Sondhi. "Operator Hydrodynamics, OTOCs, and Entanglement Growth in Systems without Conservation Laws". In: *Physical Review X* 8.2 (Apr. 2018). Publisher: American Physical Society, p. 021013. DOI: 10.1103/PhysRevX.8.021013. URL: https://link.aps.org/doi/10.1103/PhysRevX.8.021013.

[59] Adam Nahum, Sagar Vijay, and Jeongwan Haah. "Operator Spreading in Random Unitary Circuits". In: *Physical Review X* 8.2 (Apr. 2018). Publisher: American Physical Society, p. 021014. DOI: 10.1103/PhysRevX.8.021014. URL: https://link.aps.org/doi/10.1103/PhysRevX.8.021014.

[60] Adam Nahum, Jonathan Ruhman, Sagar Vijay, and Jeongwan Haah. "Quantum Entanglement Growth under Random Unitary Dynamics". In: *Physical Review X* 7.3 (July 2017). Publisher: American Physical Society, p. 031016. DOI: 10.1103/PhysRevX.7.031016. URL: https://link.aps.org/doi/10.1103/PhysRevX.7.031016.

[61] Matthew P. A. Fisher, Vedika Khemani, Adam Nahum, and Sagar Vijay. "Random Quantum Circuits". In: *Annual Review of Condensed Matter Physics* 14.1 (Mar. 2023). arXiv:2207.14280 [cond-mat, physics:quant-ph], pp. 335–379. ISSN: 1947-5454, 1947-5462. DOI: 10.1146/annurev-conmatphys-031720-030658. URL: http://arxiv.org/abs/2207.14280.

[62] Vedika Khemani, Ashvin Vishwanath, and David A. Huse. "Operator Spreading and the Emergence of Dissipative Hydrodynamics under Unitary Evolution with Conservation Laws". In: *Physical Review X* 8.3 (Sept. 2018). ISSN: 2160-3308. DOI: 10.1103/physrevx.8.031057. URL: http://dx.doi.org/10.1103/PhysRevX.8.031057.

[63] Don Weingarten. "Asymptotic behavior of group integrals in the limit of infinite rank". In: *Journal of Mathematical Physics* 19.5 (May 1978), pp. 999–1001. ISSN: 0022-2488. DOI: 10.1063/1.523807. URL: https://doi.org/10.1063/1.523807.

[64] C. W. von Keyserlingk, Tibor Rakovszky, Frank Pollmann, and S. L. Sondhi. "Operator Hydrodynamics, OTOCs, and Entanglement Growth in Systems without Conservation Laws". In: *Phys. Rev. X* 8 (2 Apr. 2018), p. 021013. DOI: 10.1103/PhysRevX.8.021013. URL: https://link.aps.org/doi/10.1103/PhysRevX.8.021013.

[65] Tibor Rakovszky, Frank Pollmann, and C. W. von Keyserlingk. "Diffusive Hydrodynamics of Out-of-Time-Ordered Correlators with Charge Conservation". In: *Phys. Rev. X* 8 (3 Sept. 2018), p. 031058. DOI: 10.1103/PhysRevX.8.031058. URL: https://link.aps.org/doi/10.1103/PhysRevX.8.031058.

[66] Man-Duen Choi. "Completely positive linear maps on complex matrices". In: *Linear Algebra and its Applications* 10.3 (1975), pp. 285–290. ISSN: 0024-3795. DOI: https://doi.org/10.1016/0024-3795(75)90075-0. URL: https://www.sciencedirect.com/science/article/pii/0024379575900750.

[67] A. Jamiołkowski. "Linear transformations which preserve trace and positive semidefiniteness of operators". In: *Reports on Mathematical Physics* 3.4 (1972), pp. 275–278. ISSN: 0034-4877. DOI: https://doi.org/10.1016/0034-4877(72)90011-0. URL: https://www.sciencedirect.com/science/article/pii/0034487772900110.

[68] Haruki Watanabe. "Counting Rules of Nambu-Goldstone Modes". In: *Annual Review of Condensed Matter Physics* 11.1 (Mar. 2020). arXiv:1904.00569 [cond-mat, physics:hep-ph, physics:hep-th, physics:physics], pp. 169–187. ISSN: 1947-5454, 1947-5462. DOI: 10.1146/annurev-conmatphys-031119-050644. URL: http://arxiv.org/abs/1904.00569.

[69] C. Kittel and P. McEuen. *Introduction to Solid State Physics*. Wiley, 2018. ISBN: 978-1-119-45416-8.

[70] R. P. Feynman. "Atomic Theory of the λ Transition in Helium". In: *Phys. Rev.* 91 (6 Sept. 1953), pp. 1291–1301. DOI: 10.1103/PhysRev.91.1291. URL: https://link.aps.org/doi/10.1103/PhysRev.91.1291.

[71] R. P. Feynman. "Atomic Theory of the Two-Fluid Model of Liquid Helium". In: *Phys. Rev.* 94 (2 Apr. 1954), pp. 262–277. DOI: 10.1103/PhysRev.94.262. URL: https://link.aps.org/doi/10.1103/PhysRev.94.262.

[72] S. M. Girvin, A. H. MacDonald, and P. M. Platzman. "Magneto-roton theory of collective excitations in the fractional quantum Hall effect". In: *Phys. Rev. B* 33 (4 Feb. 1986), pp. 2481–2494. DOI: 10.1103/PhysRevB.33.2481. URL: https://link.aps.org/doi/10.1103/PhysRevB.33.2481.

[73] Stefan Knabe. "Energy gaps and elementary excitations for certain VBS-quantum antiferromagnets". en. In: *Journal of Statistical Physics* 52.3 (Aug. 1988), pp. 627–638. ISSN: 1572-9613. DOI: 10.1007/BF01019721. URL: https://doi.org/10.1007/BF01019721.

[74] Anurag Anshu. "Improved local spectral gap thresholds for lattices of finite size". In: *Physical Review B* 101.16 (Apr. 2020). Publisher: American Physical Society, p. 165104. DOI: 10.1103/PhysRevB.101.165104. URL: https://link.aps.org/doi/10.1103/PhysRevB.101.165104.

[75] David Gosset and Evgeny Mozgunov. "Local gap threshold for frustration-free spin systems". In: *Journal of Mathematical Physics* 57.9 (Sept. 2016), p. 091901. ISSN: 0022-2488. DOI: 10.1063/1.4962337. URL: https://doi.org/10.1063/1.4962337.

[76] Haruki Watanabe, Hosho Katsura, and Jong Yeon Lee. *Spontaneous breaking of U(1) symmetry at zero temperature in one dimension*. arXiv:2310.16881 [cond-mat, physics:quant-ph]. Dec. 2023. DOI: 10.48550/arXiv.2310.16881. URL: http://arxiv.org/abs/2310.16881.

[77] Yoshimasa Hidaka and Yuki Minami. "Spontaneous symmetry breaking and Nambu-Goldstone modes in open classical and quantum systems". In: *Progress of Theoretical and Experimental Physics* 2020.3 (Mar. 2020). arXiv:1907.08241 [cond-mat, physics:hep-ph, physics:hep-th], 033A01. ISSN: 2050-3911. DOI: 10.1093/ptep/ptaa005. URL: http://arxiv.org/abs/1907.08241.

[78] Claudio Castelnovo, Claudio Chamon, Christopher Mudry, and Pierre Pujol. "From quantum mechanics to classical statistical physics: Generalized Rokhsar-Kivelson Hamiltonians and the "Stochastic Matrix Form" decomposition". In: *Annals of Physics* 318.2 (Aug. 2005), pp. 316–344. ISSN: 0003-4916. DOI: 10.1016/j.aop.2005.01.006. URL: https://www.sciencedirect.com/science/article/pii/S0003491605000096.

[79] Z. Papić. "Weak Ergodicity Breaking Through the Lens of Quantum Entanglement". In: *Entanglement in Spin Chains: From Theory to Quantum Technology Applications*. Ed. by A. Bayat, S. Bose, and H. Johannesson. Quantum Science and Technology. © 2022 The Author(s), under exclusive license to Springer Nature Switzerland AG. This version of the chapter has been accepted for publication, after peer review (when applicable) and is subject to Springer Nature?s AM terms of use

(https://www.springernature.com/gp/open-research/policies/accepted-manuscript-terms), but is not the Version of Record and does not reflect post-acceptance improvements, or any corrections. The Version of Record is available online at: https://doi.org/10.1007/978-3-031-03998-0_13. Springer, Apr. 2022, pp. 341–395. URL: https://eprints.whiterose.ac.uk/181168/.

[80] Anushya Chandran, Thomas Iadecola, Vedika Khemani, and Roderich Moessner. "Quantum Many-Body Scars: A Quasiparticle Perspective". In: *Annual Review of Condensed Matter Physics* 14.1 (Mar. 2023). arXiv:2206.11528 [cond-mat, physics:quant-ph], pp. 443–469. ISSN: 1947-5454, 1947-5462. DOI: 10.1146/annurev-conmatphys-031620-101617. URL: http://arxiv.org/abs/2206.11528.

[81] Sanjay Moudgalya, B. Andrei Bernevig, and Nicolas Regnault. "Quantum Many-Body Scars and Hilbert Space Fragmentation: A Review of Exact Results". In: *Reports on Progress in Physics* 85.8 (Aug. 2022). arXiv:2109.00548 [cond-mat, physics:quant-ph], p. 086501. ISSN: 0034-4885, 1361-6633. DOI: 10.1088/1361-6633/ac73a0. URL: http://arxiv.org/abs/2109.00548.

[82] Zlatko Papić'. *Weak ergodicity breaking through the lens of quantum entanglement*. arXiv:2108.03460 [cond-mat]. Aug. 2021. DOI: 10.48550/arXiv.2108.03460. URL: http://arxiv.org/abs/2108.03460.

[83] Sanjay Moudgalya and Olexei I. Motrunich. "Hilbert Space Fragmentation and Commutant Algebras". In: *Phys. Rev. X* 12 (1 Mar. 2022), p. 011050. DOI: 10.1103/PhysRevX.12.011050. URL: https://link.aps.org/doi/10.1103/PhysRevX.12.011050.

[84] Sanjay Moudgalya and Olexei I. Motrunich. *Exhaustive Characterization of Quantum Many-Body Scars using Commutant Algebras*. arXiv:2209.03377 [cond-mat, physics:math-ph, physics:quant-ph]. Dec. 2023. DOI: 10.48550/arXiv.2209.03377. URL: http://arxiv.org/abs/2209.03377.

[85] Sanjay Moudgalya and Olexei I. Motrunich. "Numerical Methods for Detecting Symmetries and Commutant Algebras". In: *Physical Review B* 107.22 (June 2023). arXiv:2302.03028 [cond-mat, physics:quant-ph], p. 224312. ISSN: 2469-9950, 2469-9969. DOI: 10.1103/PhysRevB.107.224312. URL: http://arxiv.org/abs/2302.03028.

[86] R. M. Nandkishore and M. Hermele. "Fractons". In: *Annual Review of Condensed Matter Physics* 10.1 (2019), pp. 295–313. DOI: 10.1146/annurev-conmatphys-031218-013604.

[87] M. Pretko, X. Chen, and Y. You. "Fracton phases of matter". In: *International Journal of Modern Physics A* 35.06 (Feb. 2020), p. 2030003. ISSN: 1793-656X. DOI: 10.1142/s0217751x20300033. URL: http://dx.doi.org/10.1142/S0217751X20300033.

[88] C. Chamon. "Quantum Glassiness in Strongly Correlated Clean Systems: An Example of Topological Overprotection". In: *Phys. Rev. Lett.* 94 (4 Jan. 2005), p. 040402. DOI: 10.1103/PhysRevLett.94.040402. URL: https://link.aps.org/doi/10.1103/PhysRevLett.94.040402.

[89] Jeongwan Haah. "Local stabilizer codes in three dimensions without string logical operators". In: *Phys. Rev. A* 83 (4 Apr. 2011), p. 042330. DOI: 10.1103/PhysRevA.83.042330. URL: https://link.aps.org/doi/10.1103/PhysRevA.83.042330.

[90] B. Yoshida. "Exotic topological order in fractal spin liquids". In: *Phys. Rev. B* 88 (12 Sept. 2013), p. 125122. DOI: 10.1103/PhysRevB.88.125122. URL: https://link.aps.org/doi/10.1103/PhysRevB.88.125122.

[91] S. Vijay, J. Haah, and L. Fu. "A new kind of topological quantum order: A dimensional hierarchy of quasiparticles built from stationary excitations". In: *Phys. Rev. B* 92 (23 Dec. 2015), p. 235136. DOI: 10.1103/PhysRevB.92.235136. URL: https://link.aps.org/doi/10.1103/PhysRevB.92.235136.

[92] M. Pretko and L. Radzihovsky. "Fracton-Elasticity Duality". In: *Phys. Rev. Lett.* 120 (19 May 2018), p. 195301. DOI: 10.1103/PhysRevLett.120.195301. URL: https://link.aps.org/doi/10.1103/PhysRevLett.120.195301.

[93] M. Pretko. "Subdimensional particle structure of higher rank $U(1)$ spin liquids". In: *Phys. Rev. B* 95 (11 Mar. 2017), p. 115139. DOI: 10.1103/PhysRevB.95.115139. URL: https://link.aps.org/doi/10.1103/PhysRevB.95.115139.

[94] M. Pretko. "The fracton gauge principle". In: *Phys. Rev. B* 98 (11 Sept. 2018), p. 115134. DOI: 10.1103/PhysRevB.98.115134. URL: https://link.aps.org/doi/10.1103/PhysRevB.98.115134.

[95] Andrey Gromov, Andrew Lucas, and Rahul M Nandkishore. "Fracton hydrodynamics". In: *Physical Review Research* 2.3 (2020), p. 033124.

[96] Johannes Feldmeier, Pablo Sala, Giuseppe De Tomasi, Frank Pollmann, and Michael Knap. "Anomalous diffusion in dipole-and higher-moment-conserving systems". In: *Physical Review Letters* 125.24 (2020), p. 245303.

[97] Alan Morningstar, Vedika Khemani, and David A Huse. "Kinetically constrained freezing transition in a dipole-conserving system". In: *Physical Review B* 101.21 (2020), p. 214205.

[98] Elmer Guardado-Sanchez, Alan Morningstar, Benjamin M Spar, Peter T Brown, David A Huse, and Waseem S Bakr. "Subdiffusion and heat transport in a tilted two-dimensional Fermi-Hubbard system". In: *Physical Review X* 10.1 (2020), p. 011042.

[99] J. Iaconis, A. Lucas, and R. Nandkishore. "Multipole conservation laws and subdiffusion in any dimension". In: *Phys. Rev. E* 103 (2 Feb. 2021), p. 022142. DOI: 10.1103/PhysRevE.103.022142. URL: https://link.aps.org/doi/10.1103/PhysRevE.103.022142.

[100] Hansveer Singh, Brayden A. Ware, Romain Vasseur, and Aaron J. Friedman. "Subdiffusion and Many-Body Quantum Chaos with Kinetic Constraints". In: *Physical Review Letters* 127.23 (Dec. 2021). DOI: 10.1103/physrevlett.127.230602. URL: https://doi.org/10.1103%5C%2Fphysrevlett.127.230602.

[101] Pablo Sala, Tibor Rakovszky, Ruben Verresen, Michael Knap, and Frank Pollmann. "Ergodicity Breaking Arising from Hilbert Space Fragmentation in Dipole-Conserving Hamiltonians". In: *Phys. Rev. X* 10 (1 Feb. 2020), p. 011047. DOI: 10.1103/PhysRevX.10.011047. URL: https://link.aps.org/doi/10.1103/PhysRevX.10.011047.

[102] Vedika Khemani, Michael Hermele, and Rahul Nandkishore. "Localization from Hilbert space shattering: From theory to physical realizations". In: *Phys. Rev. B* 101 (17 May 2020), p. 174204. DOI: 10.1103/PhysRevB.101.174204. URL: https://link.aps.org/doi/10.1103/PhysRevB.101.174204.

[103] Sanjay Moudgalya, Abhinav Prem, David A. Huse, and Amos Chan. "Spectral statistics in constrained many-body quantum chaotic systems". In: *Physical Review Research* 3.2 (June 2021). arXiv:2009.11863 [cond-mat, physics:quant-ph], p. 023176. ISSN: 2643-1564. DOI: 10.1103/PhysRevResearch.3.023176. URL: http://arxiv.org/abs/2009.11863.

[104] Tibor Rakovszky, Pablo Sala, Ruben Verresen, Michael Knap, and Frank Pollmann. "Statistical localization: From strong fragmentation to strong edge modes". In: *Phys. Rev. B* 101 (12 Mar. 2020), p. 125126. DOI: 10.1103/PhysRevB.101.125126. URL: https://link.aps.org/doi/10.1103/PhysRevB.101.125126.

[105] Sanjay Moudgalya, Abhinav Prem, David A. Huse, and Amos Chan. "Spectral statistics in constrained many-body quantum chaotic systems". In: *Phys. Rev. Res.* 3 (2 June 2021), p. 023176. DOI: 10.1103/PhysRevResearch.3.023176. URL: https://link.aps.org/doi/10.1103/PhysRevResearch.3.023176.

[106] Xiaozhou Feng and Brian Skinner. "Hilbert space fragmentation produces an effective attraction between fractons". In: *Phys. Rev. Res.* 4 (1 Jan. 2022), p. 013053. DOI: 10.1103/PhysRevResearch.4.013053. URL: https://link.aps.org/doi/10.1103/PhysRevResearch.4.013053.

[107] Philip Zechmann, Ehud Altman, Michael Knap, and Johannes Feldmeier. "Fractonic Luttinger Liquids and Supersolids in a Constrained Bose-Hubbard Model". In: *arXiv preprint arXiv:2210.11072* (2022).

[108] Sanjay Moudgalya and Olexei I. Motrunich. *Symmetries as Ground States of Local Superoperators*. arXiv:2309.15167 [cond-mat, physics:hep-th, physics:math-ph, physics:quant-ph]. Dec. 2023. DOI: 10.48550/arXiv.2309.15167. URL: http://arxiv.org/abs/2309.15167.

[109] J. Iaconis, S. Vijay, and R. Nandkishore. "Anomalous subdiffusion from subsystem symmetries". In: *Phys. Rev. B* 100 (21 Dec. 2019), p. 214301. DOI: 10.1103/PhysRevB.100.214301. URL: https://link.aps.org/doi/10.1103/PhysRevB.100.214301.

[110] Eduardo Fradkin and Steven Kivelson. "Short range resonating valence bond theories and superconductivity". In: *Modern Physics Letters B* 4.03 (1990), pp. 225–232.

[111] R. Moessner, S. L. Sondhi, and Eduardo Fradkin. "Short-ranged resonating valence bond physics, quantum dimer models, and Ising gauge theories". In: *Phys. Rev. B* 65 (2 Dec. 2001), p. 024504. DOI: 10.1103/PhysRevB.65.024504. URL: https://link.aps.org/doi/10.1103/PhysRevB.65.024504.

[112] D Horn. "Finite matrix models with continuous local gauge invariance". In: *Physics Letters B* 100.2 (1981), pp. 149–151.

[113] Peter Orland and Daniel Rohrlich. "Lattice gauge magnets: Local isospin from spin". In: *Nuclear Physics B* 338.3 (1990), pp. 647–672.

[114] Shailesh Chandrasekharan and U-J Wiese. "Quantum link models: A discrete approach to gauge theories". In: *Nuclear Physics B* 492.1-2 (1997), pp. 455–471.

[115] Alexander Schuckert, Izabella Lovas, and Michael Knap. "Nonlocal emergent hydrodynamics in a long-range quantum spin system". In: *Phys. Rev. B* 101 (2 Jan. 2020), 020416(R). DOI: 10.1103/PhysRevB.101.020416. URL: https://link.aps.org/doi/10.1103/PhysRevB.101.020416.

[116] M. K. Joshi, F. Kranzl, A. Schuckert, I. Lovas, C. Maier, R. Blatt, M. Knap, and C. F. Roos. "Observing emergent hydrodynamics in a long-range quantum magnet". In: *Science* 376.6594 (2022), pp. 720–724. DOI: 10.1126/science.abk2400. URL: https://www.science.org/doi/abs/10.1126/science.abk2400.

[117] Xiaolong Deng, Ivan Khaymovich, and Alexander L. Burin. *Superdiffusion in random two dimensional system with ubiquitous long-range hopping*. 2022. arXiv: 2205.14715 [cond-mat.dis-nn].

[118] Olumakinde Ogunnaike, Johannes Feldmeier, and Jong Yeon Lee. "Unifying Emergent Hydrodynamics and Lindbladian Low-Energy Spectra across Symmetries, Constraints, and Long-Range Interactions". In: *Physical Review Letters* 131.22 (Nov. 2023). Publisher: American Physical Society, p. 220403. DOI: 10.1103/PhysRevLett.131.220403. URL: https://link.aps.org/doi/10.1103/PhysRevLett.131.220403.

[119] Zongping Gong and Ryusuke Hamazaki. "Bounds in Nonequilibrium Quantum Dynamics". In: *International Journal of Modern Physics B* 36.31 (Dec. 2022). arXiv:2202.02011 [cond-mat, physics:math-ph, physics:quant-ph], p. 2230007. ISSN: 0217-9792, 1793-6578. DOI: 10.1142/S0217979222300079. URL: http://arxiv.org/abs/2202.02011.

[120] Takashi Mori and Tatsuhiko Shirai. "Resolving a Discrepancy between Liouvillian Gap and Relaxation Time in Boundary-Dissipated Quantum Many-Body Systems". In: *Physical Review Letters* 125.23 (Dec. 2020). Publisher: American Physical Society, p. 230604. DOI: 10.1103/PhysRevLett.125.230604. URL: https://link.aps.org/doi/10.1103/PhysRevLett.125.230604.

[121] Taiki Haga, Masaya Nakagawa, Ryusuke Hamazaki, and Masahito Ueda. "Liouvillian Skin Effect: Slowing Down of Relaxation Processes without Gap Closing". In: *Physical Review Letters* 127.7 (Aug. 2021). Publisher: American Physical Society, p. 070402. DOI: 10.1103/PhysRevLett.127.070402. URL: https://link.aps.org/doi/10.1103/PhysRevLett.127.070402.

[122] Michael J. Kastoryano and Jens Eisert. "Rapid mixing implies exponential decay of correlations". In: *Journal of Mathematical Physics* 54.10 (Oct. 2013). arXiv:1303.6304 [math-ph, physics:quant-ph], p. 102201. ISSN: 0022-2488, 1089-7658. DOI: 10.1063/1.4822481. URL: http://arxiv.org/abs/1303.6304.

[123] Eric Vernier. "Mixing times and cutoffs in open quadratic fermionic systems". en. In: *SciPost Physics* 9.4 (Oct. 2020), p. 049. ISSN: 2542-4653. DOI: 10.21468/SciPostPhys.9.4.049. URL: https://scipost.org/SciPostPhys.9.4.049.

[124] Michael J. Kastoryano, David Reeb, and Michael M. Wolf. "A Cutoff Phenomenon for Quantum Markov Chains". In: *Journal of Physics A: Mathematical and Theoretical* 45.7 (Feb. 2012). arXiv:1111.2123 [math-ph, physics:quant-ph], p. 075307. ISSN: 1751-8113, 1751-8121. DOI: 10.1088/1751-8113/45/7/075307. URL: http://arxiv.org/abs/1111.2123.

[125] Tibor Rakovszky, Sarang Gopalakrishnan, and Curt von Keyserlingk. *Defining stable phases of open quantum systems*. arXiv:2308.15495 [cond-mat, physics:quant-ph]. Feb. 2024. DOI: 10.48550/arXiv.2308.15495. URL: http://arxiv.org/abs/2308.15495.

[126] Michael J. Gullans and David A. Huse. "Dynamical Purification Phase Transition Induced by Quantum Measurements". In: *Physical Review X* 10.4 (Oct. 2020). Publisher: American Physical Society, p. 041020. DOI: 10.1103/PhysRevX.10.041020. URL: https://link.aps.org/doi/10.1103/PhysRevX.10.041020.

[127] Yimu Bao, Soonwon Choi, and Ehud Altman. "Theory of the phase transition in random unitary circuits with measurements". In: *Physical Review B* 101.10 (Mar. 2020). Publisher: American Physical Society, p. 104301. DOI: 10.1103/PhysRevB.101.104301. URL: https://link.aps.org/doi/10.1103/PhysRevB.101.104301.

[128] Brian Skinner, Jonathan Ruhman, and Adam Nahum. "Measurement-Induced Phase Transitions in the Dynamics of Entanglement". In: *Physical Review X* 9.3 (July 2019). Publisher: American Physical Society, p. 031009. DOI: 10.1103/PhysRevX.9.031009. URL: https://link.aps.org/doi/10.1103/PhysRevX.9.031009.

[129] Ali Lavasani, Yahya Alavirad, and Maissam Barkeshli. "Measurement-induced topological entanglement transitions in symmetric random quantum circuits". en. In: *Nature Physics* 17.3 (Mar. 2021). Publisher: Nature Publishing Group, pp. 342–347. ISSN: 1745-2481. DOI: 10.1038/s41567-020-01112-z. URL: https://www.nature.com/articles/s41567-020-01112-z.

[130] Utkarsh Agrawal, Aidan Zabalo, Kun Chen, Justin H. Wilson, Andrew C. Potter, J.H. Pixley, Sarang Gopalakrishnan, and Romain Vasseur. "Entanglement and Charge-Sharpening Transitions in U(1) Symmetric Monitored Quantum Circuits". In: *Physical Review X* 12.4 (Oct. 2022). Publisher: American Physical Society, p. 041002. DOI: 10.1103/PhysRevX.12.041002. URL: https://link.aps.org/doi/10.1103/PhysRevX.12.041002.

[131] Fergus Barratt, Utkarsh Agrawal, Sarang Gopalakrishnan, David A. Huse, Romain Vasseur, and Andrew C. Potter. "Field Theory of Charge Sharpening in Symmetric Monitored Quantum Circuits". In: *Physical Review Letters* 129.12 (Sept. 2022). Publisher: American Physical Society, p. 120604. DOI: 10.1103/PhysRevLett.129.120604. URL: https://link.aps.org/doi/10.1103/PhysRevLett.129.120604.

[132] Patrick Hayden, Sepehr Nezami, Xiao-Liang Qi, Nathaniel Thomas, Michael Walter, and Zhao Yang. "Holographic duality from random tensor networks". en. In: *Journal of High Energy Physics* 2016.11 (Nov. 2016), p. 9. ISSN: 1029-8479. DOI: 10.1007/JHEP11(2016)009. URL: https://doi.org/10.1007/JHEP11(2016)009.

[133] Romain Vasseur, Andrew C. Potter, Yi-Zhuang You, and Andreas W. W. Ludwig. "Entanglement transitions from holographic random tensor networks". In: *Physical Review B* 100.13 (Oct. 2019). Publisher: American Physical Society, p. 134203. DOI: 10.1103/PhysRevB.100.134203. URL: https://link.aps.org/doi/10.1103/PhysRevB.100.134203.

[134] Tianci Zhou and Adam Nahum. "Emergent statistical mechanics of entanglement in random unitary circuits". In: *Physical Review B* 99.17 (May 2019). Publisher: American Physical Society, p. 174205. DOI: 10.1103/PhysRevB.99.174205. URL: https://link.aps.org/doi/10.1103/PhysRevB.99.174205.

[135] Andrew C. Potter and Romain Vasseur. "Entanglement Dynamics in Hybrid Quantum Circuits". en. In: *Entanglement in Spin Chains: From Theory to Quantum Technology Applications*. Ed. by Abolfazl Bayat, Sougato Bose, and Henrik Johannesson. Cham: Springer International Publishing, 2022, pp. 211–249. ISBN: 978-3-031-03998-0. DOI: 10.1007/978-3-031-03998-0_9. URL: https://doi.org/10.1007/978-3-031-03998-0_9.

[136] Yimu Bao, Soonwon Choi, and Ehud Altman. "Symmetry enriched phases of quantum circuits". In: *Annals of Physics* 435 (2021), p. 168618.

[137] Caroline de Groot, Alex Turzillo, and Norbert Schuch. "Symmetry Protected Topological Order in Open Quantum Systems". In: *Quantum* 6 (Nov. 2022). arXiv:2112.04483 [cond-mat, physics:quant-ph], p. 856. ISSN: 2521-327X. DOI: 10.22331/q-2022-11-10-856. URL: http://arxiv.org/abs/2112.04483.

[138] Jong Yeon Lee, Yi-Zhuang You, and Cenke Xu. *Symmetry protected topological phases under decoherence*. arXiv:2210.16323 [cond-mat, physics:quant-ph]. Feb. 2024. DOI: 10.48550/arXiv.2210.16323. URL: http://arxiv.org/abs/2210.16323.

[139] Ruochen Ma and Chong Wang. "Average Symmetry-Protected Topological Phases". In: *Physical Review X* 13.3 (Aug. 2023). Publisher: American Physical Society, p. 031016. DOI: 10.1103/PhysRevX.13.031016. URL: https://link.aps.org/doi/10.1103/PhysRevX.13.031016.

[140] Yaodong Li, Xiao Chen, and Matthew P. A. Fisher. "Measurement-driven entanglement transition in hybrid quantum circuits". In: *Physical Review B* 100.13 (Oct. 2019). Publisher: American Physical Society, p. 134306. DOI: 10.1103/PhysRevB.100.134306. URL: https://link.aps.org/doi/10.1103/PhysRevB.100.134306.

[141] Matthew P.A. Fisher, Vedika Khemani, Adam Nahum, and Sagar Vijay. "Random Quantum Circuits". In: *Annual Review of Condensed Matter Physics* 14 (1 2023), null. DOI: 10.1146/annurev-conmatphys-031720-030658. URL: https://doi.org/10.1146/annurev-conmatphys-031720-030658.

[142] Aidan Zabalo, Michael J. Gullans, Justin H. Wilson, Sarang Gopalakrishnan, David A. Huse, and J. H. Pixley. "Critical properties of the measurement-induced transition in random quantum circuits". In: *Physical Review B* 101.6 (Feb. 2020). Publisher: American Physical Society, p. 060301. DOI: 10.1103/PhysRevB.101.060301. URL: https://link.aps.org/doi/10.1103/PhysRevB.101.060301.

[143] Yaodong Li, Xiao Chen, and Matthew P. A. Fisher. "Quantum Zeno effect and the many-body entanglement transition". In: *Physical Review B* 98.20 (Nov. 2018). Publisher: American Physical Society, p. 205136. DOI: 10.1103/PhysRevB.98.205136. URL: https://link.aps.org/doi/10.1103/PhysRevB.98.205136.

[144] Shayan Majidy, Utkarsh Agrawal, Sarang Gopalakrishnan, Andrew C. Potter, Romain Vasseur, and Nicole Yunger Halpern. "Critical phase and spin sharpening in SU(2)-symmetric monitored quantum circuits". In: *Physical Review B* 108.5 (Aug. 2023). Publisher: American Physical Society, p. 054307. DOI: 10.1103/PhysRevB.108.054307. URL: https://link.aps.org/doi/10.1103/PhysRevB.108.054307.

[145] Shengqi Sang and Timothy H. Hsieh. "Measurement-protected quantum phases". In: *Physical Review Research* 3.2 (June 2021). Publisher: American Physical Society, p. 023200. DOI: 10.1103/PhysRevResearch.3.023200. URL: https://link.aps.org/doi/10.1103/PhysRevResearch.3.023200.

[146] Sumner N. Hearth, Michael O. Flynn, Anushya Chandran, and Chris R. Laumann. *Unitary k-designs from random number-conserving quantum circuits*. arXiv:2306.01035 [cond-mat, physics:hep-th, physics:nlin, physics:quant-ph]. June 2023. DOI: 10.48550/arXiv.2306.01035. URL: http://arxiv.org/abs/2306.01035.

[147] Sebastian Leontica and Max McGinley. "Purification dynamics in a continuous-time hybrid quantum circuit model". In: *Physical Review B* 108.17 (Nov. 2023). Publisher: American Physical Society, p. 174308. DOI: 10.1103/PhysRevB.108.174308. URL: https://link.aps.org/doi/10.1103/PhysRevB.108.174308.

[148] Hassan Shapourian, Shang Liu, Jonah Kudler-Flam, and Ashvin Vishwanath. "Entanglement Negativity Spectrum of Random Mixed States: A Diagrammatic Approach". In: *PRX Quantum* 2.3 (Sept. 2021). Publisher: American Physical Society, p. 030347. DOI: 10.1103/PRXQuantum.2.030347. URL: https://link.aps.org/doi/10.1103/PRXQuantum.2.030347.

[149] Yimu Bao, Ruihua Fan, Ashvin Vishwanath, and Ehud Altman. *Mixed-state topological order and the errorfield double formulation of decoherence-induced transitions*. arXiv:2301.05687 [cond-mat, physics:quant-ph]. Jan. 2023. DOI: 10.48550/arXiv.2301.05687. URL: http://arxiv.org/abs/2301.05687.